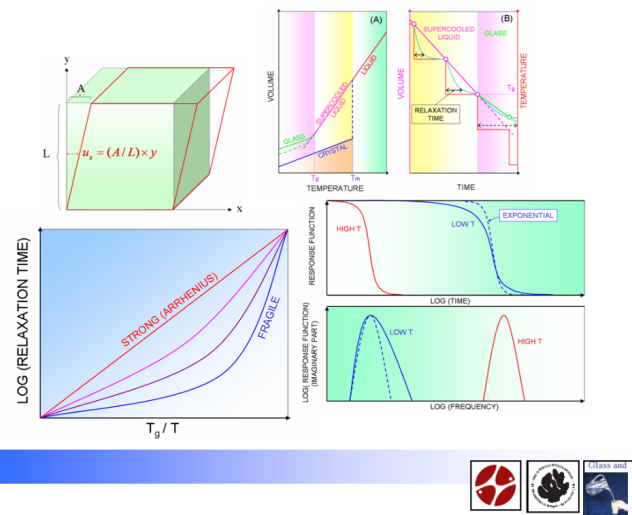


phd thesis

Experimental Studies of Supercooled Liquids, Gels and Glasses

*Dynamic Correlation Lengths and Off-Equilibrium
Dynamics*



Claudio Maggi

Supervisor: Jeppe C. Dyre

*Danish National Research Foundation Centre "Glass and Time",
IMFUFA, Department of Science, Systems and Models,
Roskilde University, Denmark*

May 10, 2010

Experimental Studies of Supercooled Liquids, Gels and Glasses - Dynamic Correlation Lengths and Off-Equilibrium Dynamics

Ph.D. afhandling af Claudio Maggi, indleveret d. 29. april, 2010.

Dansk abstract:

Afhandlingen består af en engelsksproget tekst på 114 sider samt 5 videnskabelige artikler. Hovedfokus er på undersøgelser af underafkølede væskers, gelers og glassers dynamik.

To af artiklerne præsenterer målinger af det frekvens-afhængige shear modul vha PSG-teknikken udviklet af "Glas og Tid" gruppen. I den første artikel præsenteres målinger på fem seje væsker tæt på deres glasovergang. Analysen af data inkluderer en karakterisering af temperaturafhængigheden af relaxationstiden, såvel som af relaxationsfunktionens form. Disse målinger gør det muligt at teste shoving modellen som knytter den strukturelle relaxationstid til højfrekvens shear modulet. I den anden PSG artikel præsenteres målinger af det dynamiske shear modul på to monoalkoholer. Disse målinger sammenlignes med dielektriske målinger på de samme væsker og under identiske eksperimentelle forhold. Artiklen konkluderer at de karakteristiske Debye-processer, som dominerer det dielektriske respons af monoalkoholer, ikke kan observeres i shear modulet. Denne mekaniske responsfunktion har altså kun bidrag fra den strukturelle relaxation, et resultat som er konsistent med resultater fra dynamisk lysspredning og fra kalorimetri (kapitel 2).

Dynamikken af geler og glasser som er ude af ligevægt studeres i to artikler, dels eksperimentelle og dels teoretiske (via computer-simuleringer). Depolariseret dynamisk lysspredning blev benyttet til at studere en geldannende kolloid-opløsning ude af ligevægt. Der blev også foretaget Kerr-effekt målinger på dette system. Kombinationen af disse to teknikker gør det muligt at vise, at fluktuations-dissipations (FD) teoremet er brudt og at beregne den effektive temperatur af systemet. Disse resultater præsenteres og diskuteres i kapitel 3A, hvor resultaterne af computer-simuleringer af brud på FD-teoremet også diskuteres. Sidstnævnte resultater refererer til et standard model-system som bringes ud af ligevægt ved hurtig afkøling og/eller en hurtig densitetsstigning. Det vises at hvordan egenskaberne af modelsystemet - som dog deles med hele klassen af "strongly correlating liquids" - medfører at den effektive temperatur efter et hop mellem to tilstande kun afhænger af slutdensiteten. Det vises endvidere hvordan man for denne klasse af væsker ud fra en enkelt off-equilibrium simulering kan forudsige den effektive temperatur for en glas produceret ved et vilkårligt densitets/temperatur - hop (kapitel 4).

Dynamisk heterogenitet af dynamik, både i og uden for ligevægt, diskuteres i kapitel 5. Ny shear målinger præsenteres ud fra hvilke den dynamiske korrelationslængde kan bestemmes som beskrevet i en af de fem publikationer (hvor en 4-punkts korrelator beregnes via en eksperimentelt lettere tilgængelig 3-punkts korrelator). Sammenligning med 4-punkts korrelatorerne fra dielektriske målinger viser at antallet af dynamisk korrelede molekyler generelt er lidt forskellig fra den tilsvarende størrelse beregnet ud fra målinger af shear modulet. Analysen viser imidlertid også, at de to karakteristiske korrelationsvolumener er proportionale i deres stigning når temperaturen sænkes.

Kapitel 5 diskuterer endvidere et nyt eksperiment som gør det muligt direkte at måle 4-punkts susceptibiliteten ved at kombinere forskellige lysspredningsteknikker. I kapitel 6 præsenteres en ny model som forbinder de frekvensafhængige shear og dielektriske responsfunktioner, en model som bygger på antagelsen af dynamisk heterogenitet.

Abstract

This PhD thesis is accompanied by a number of papers whose main focus is the investigation of the dynamics of supercooled liquids, gels and glasses. Moreover new theoretical and experimental results are presented.

Two of the articles presented report frequency-resolved (broad-band) shear-mechanical measurements acquired via a unique technique developed by our group (the piezo-shear-gauge (PSG) method). In one of these we measure the dynamic shear modulus of five glass-forming liquids close to the glass transition temperature. The analysis includes a characterization of the temperature-evolution of the relaxation time of the mechanical response and of its shape. The measurements of the dynamic shear modulus allow for a test of the shoving model that links the structural relaxation time to the infinite-frequency shear-modulus. In the second work employing the PSG method the dynamic shear-modulus of two monohydroxy molecular liquids (monoalcohols) is determined. These measurements are compared with dielectric-spectroscopy measurements performed on the same liquids and in the same experimental conditions. The findings of this work indicate that the additional Debye-process (that dominates the dielectric response of these monoalcohols) can not be detected in the frequency-resolved shear-modulus. This mechanical response function displays indeed only a clear structural relaxation in agreement with dynamic light scattering and calorimetric measurements. These results are illustrated and expanded in Chapter 2.

The off-equilibrium dynamics of gels and glasses was also subject of investigations as it can be found in the other companion articles. These studies have been carried by means of experiments and computer simulations. An off-equilibrium gel-forming colloidal solution is studied combining depolarized dynamic light scattering measurements and Kerr-effect response measurements. The combined use of these two measurements allow one to determine whether the fluctuation-dissipation theorem is violated out of equilibrium and what is the effective temperature associated with this non-equilibrium condition. The findings of this work are presented in Chapter 3. A computer simulation study of the violation of theorem is also presented. This is done for a widely studied a model glass-former taken out of equilibrium via fast cooling and/or densification. It is shown how the special properties of this liquid (shared by the entire class of strongly correlating liquids) imply that the effective temperature depends only on the final density of the off-equilibrium jump. In addition it is shown how only for these liquids a single off-equilibrium simulation allows one to predict the effective temperature of any glass produced by an arbitrary density/temperature jump. This work is illustrated and expanded by new findings in Chapter 4.

The dynamic heterogeneity of the glassy dynamics in and out of equilibrium was studied as a further subject. Additional shear-modulus measurements were studied extracting the characteristic dynamic correlation volumes associated with this mechanical relaxation. A separate paper was dedicated to this analysis. The estimation of the four-point correlator reported in this work is based on some approximation schemes that allow one to quantify this via a more accessible three-point susceptibility. A careful comparison of this quantity obtained by means of dielectric measurements reveals that the number of dynamically correlated molecules estimated is generally slightly different for the shear and dielectric response. Nevertheless the analysis indicates that these characteristic correlation volumes grow proportionally as the temperature is lowered. These results are presented in Chapter 5 where we also illustrate a new experiment for the direct measurement of the four-point susceptibility obtained by combined dynamic light scattering techniques. In Chapter 6 we present a new model for the connection of the shear and the dielectric response accounting for the presence of the dynamic heterogeneities.

Acknowledgements

This Ph.D. was financed by the Danish National Research Foundation Center for Viscous Liquids Dynamics *Glass and Time*. The works presented in this thesis received a deep benefit from the interaction with a number of scientists.

We thank the members of the glass group for the technical help and the daily discussion: J. Papini, D. Gundermann, T. Hecksher, N. Gnan, A. Nielsen, I. H. Pedersen, T. Rasmussen, E. H. Larsen, P. Olsen, K. Høffding, H. Larsen, B. Igarashi, N. Saglanmak, B. Jakobsen, N. P. Bailey, K. Niss, S. Toxværd, T. B. Schrøder, T. Christensen, N. B. Olsen, and J. C. Dyre.

I have performed the measurements reported in Paper I and wrote the article under the supervision of B. Jakobsen, T. Christensen, N. B. Olsen and J. C. Dyre. I thank U. Buchenau and G. P. Johari for the interesting comments on the results of this work.

I have performed some of the measurements reported in Paper II and contributed to write the article. This was done under the supervision of B. Jakobsen, T. Christensen and J. C. Dyre. We wish to thank R. Bergman for the interesting discussion about the findings reported in Paper II.

The experiment described in Paper III was set up and used by me to obtain the measurements under the supervision of R. Di Leonardo and G. Ruocco. I wrote the paper in collaboration with G. Ruocco and J. C. Dyre. I thank G. Diezemann for the stimulating discussion on Paper III.

Together with N. Gnan I have planned the study of the effective temperature reported in Paper IV. N. Gnan performed the Monte-Carlo simulations. The manuscript was written by me and N. Gnan in collaboration with T. B. Schrøder and J. C. Dyre. I would like to thank G. Biroli, W. Kob, J. Kurchan, S. Franz and R. Jack for the useful discussion and comments on Paper IV. I especially thank L. Berthier for kindly instructing us about his method used in Paper IV. I have found the correlation between the violation factor and the glassy non-ergodicity factor described in Chapter 4. I thank L. Leuzzi for the interesting discussion about this.

I had the idea of comparing the shear and dielectric multi-point susceptibilities reported in Paper V. I have written the article under the supervision of B. Jakobsen, and J. C. Dyre. We acknowledge C. Alba-Simionesco, C. Dalle-Ferrier, S. Capaccioli and F. Zamponi for the useful comments and insights on Paper V.

I have designed the experiment for the direct measurement of the four-point susceptibility described in Chapter 5. I thank R. Di Leonardo, G. Ruocco for the useful advice and discussion for the realization of this experiment. I thank L. Cipelletti and L. Berthier for the interesting comments and questions about the experiment.

I have cast the new model for the connection between shear and dielectric response described in Chapter 6. I thank in particular B. Jakobsen and N. B. Olsen for the discussion on this.

Contents

Abstract in Danish	iii
Contents	vii
1 Introduction	1
1.1 Dynamic Glass Transition and Relaxation Time	1
1.2 Fragility and Stretched Relaxation	1
1.3 Linear Response and Fluctuation-Dissipation Theorem	4
1.4 Heterogeneous Dynamics	5
2 Equilibrium Shear-Mechanical Response of Several Glass-Formers	7
2.1 Shear-Mechanical Response	7
2.2 Features of The Mechanical Relaxation in Five Supercooled Liquids	8
2.3 Mechanical Relaxation and Dielectric Relaxation in Two Monoalcohols	14
3 An Experimental Study of The Off-Equilibrium Fluctuation-Dissipation Relation	19
3.1 Generalized Fluctuation-Dissipation Relation	19
3.2 An Experimental Study of The Off-Equilibrium Fluctuation-Dissipation Relation	22
3.3 Experimental Details	24
3.3.1 Dynamic light scattering of cylindrically symmetric macromolecules	24
3.3.2 Filtering the VV contribution to the depolarized light scattering	26
3.3.3 Roto-translational decoupling and separation of timescales	28
3.3.4 Linearity check for the response function	29
3.3.5 Experimental set-up	30
4 Computer Simulation Studies of The Off-Equilibrium Fluctuation-Dissipation Relation	33
4.1 Density-Scaling Effective Temperature in Strongly Correlating Liquids	33
4.1.1 Simulation details	36
4.1.2 Equilibrium and off-equilibrium energy landscape in strongly correlating liquids	40

4.1.3	A correlation between the non-ergodicity factor and the violation factor	42
5	Experimental Studies of The Heterogeneous Dynamics	47
5.1	Multi-Point Susceptibilities	47
5.1.1	The three-point susceptibility	53
5.2	Comparing Shear and Dielectric Dynamical Fluctuations	56
5.3	A Direct Experimental Measurement of The Four-Point Susceptibility	60
5.3.1	Homodyne and heterodyne photon-correlation spectroscopy	62
5.3.2	Measurement of the four-point susceptibility by combined PCS techniques	68
6	Heterogeneous Modeling of The Connection between Shear and Dielectric Relaxation	79
6.1	The Failure of The Stokes-Einstein Relation	79
6.2	An Analogy between The GDB Model and The SER	82
6.3	The Modified GDB model	88
7	Outlook	101
7.1	Shear-Mechanical Beta Relaxation	101
7.2	Experimental Studies of the Off-Equilibrium Dynamics	101
7.3	Numerical Studies of the Off-Equilibrium Dynamics	102
7.4	Experimental Investigation of The Multi-Point Susceptibilities .	102
7.5	Modeling The Connection of Shear and Dielectric Response . .	103
	Bibliography	105
	Bibliography	105
	Papers	119
Paper I	121
Paper II	127
Paper III	135
Paper IV	141
Paper V	145

Chapter 1

Introduction

This chapter contains a very brief introduction to the phenomenology of supercooled liquids and glasses. Illustrating shortly these basic concepts we also mention the main subjects of investigation of the thesis. A number of excellent and far more detailed reviews [1, 2, 3, 4, 5, 6] have inspired this introductory chapter.

1.1 Dynamic Glass Transition and Relaxation Time

Let us imagine to cool a liquid and to measure its volume (Figure 1.1(A)). The liquid will contract as we lower the temperature. This process can be thought as a time series of small steps in temperature followed by little changes in volume (Figure 1.1(B)). After each temperature change the liquid's volume will take a given time to reach its new equilibrium state. Naturally the lower is the temperature the longer will be this relaxation time needed by the liquid to re-equilibrate. Equally expected there will be a temperature T_g low enough at which the liquid cannot equilibrate before the next temperature down-step. At this temperature, where the relaxation time is of the order of the cooling rate, the liquid falls out of the equilibrium and the glass is formed.

In this cooling process the liquid passes the melting temperature T_m below which it might crystallize. However if the cooling-rate is high enough crystal formation can be avoided and the liquid is said to be supercooled. This can be done keeping the liquid in the supercooled equilibrium state that is metastable with respect to the crystal the latter having lower free-energy.

It is clear that the glass-transition temperature defined here depends on the cooling rate: if we cool the liquid slower we get a lower T_g . Conventionally T_g is also defined as the temperature where the relaxation time reaches an arbitrary large value (typically this is 10^2 or 10^3 s).

1.2 Fragility and Stretched Relaxation

The relaxation time τ grows differently for different liquids as they are cooled. Some liquids indeed show a relaxation time that increases exponentially with the inverse temperature:

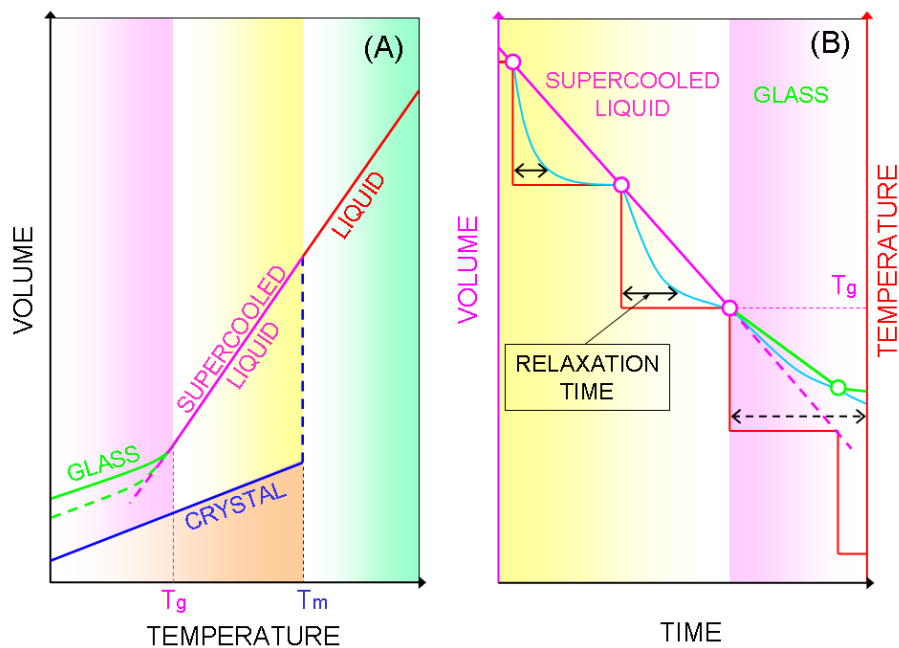


Figure 1.1: Sketch of the phenomenology of the glass transition as seen by measuring the volume[7] of the liquid upon cooling. (A) shows the behavior of the liquid's volume as the temperature is lowered and the crystallization at T_m is avoided. Below T_m the liquid is supercooled and when the relaxation time reaches a value of the order of the cooling rate at T_g the glass transition occurs. If the cooling is slower T_g is lower (dashed green line). As shown in (B) the cooling process can be imagined as a series of temperature steps in time (red line). At each step the volume as to re-equilibrate to the new volume in a given relaxation time (blue line). The equilibrium volume obtained after each temperature-step is represented by circles. The characteristic relaxation time grows as T is lowered when the it is comparable with the inverse cooling rate the following cooling step acts on an non-equilibrated system and the glass is formed.

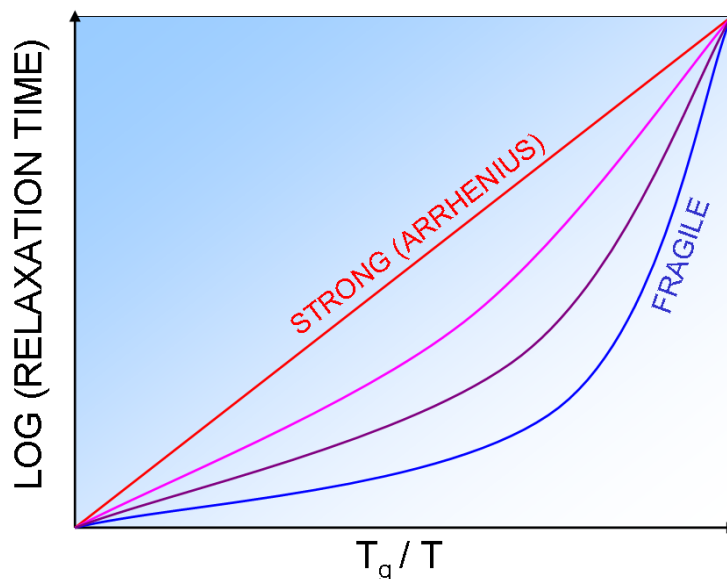


Figure 1.2: Sketch of the behavior of the logarithm of the relaxation time as a function of the inverse temperature (Agell's plot). This plot underlines the differences between strong liquids following (Equation (1.1)) with constant E and fragile liquids showing a steeper increase of relaxation time upon cooling.

$$\tau = \tau_0 \exp\left(\frac{E}{k_B T}\right) \quad (1.1)$$

where $\tau_0 \simeq 10^{-14}$ s is the high temperature limit of the relaxation time and E is the activation energy. The liquids showing the Arrhenius temperature dependence of the relaxation time (Equation (1.1)) are also called strong liquids, examples of liquids belonging to this class are SiO_2 (ordinary silica glass) and GeO_2 . Other liquids (like toluene or o-terphenyl) display instead a much steeper increase of the relaxation time as they are cooled. To account for this fragile behavior Equation (1.1) can be modified by making E temperature dependent letting $E = E(T)$ to be a (decreasing) function of T . The temperature dependence of the relaxation time can be characterized by the fragility [8]

$$m = \left. \frac{d \log_{10} \tau}{d(T_g/T)} \right|_{T=T_g} \quad (1.2)$$

One of the fundamental questions in glass science is which microscopic properties of a liquid determine its fragility. In the same spirit fragility has been correlated with many other properties of the supercooled liquid and of the glass [9, 10, 11, 12, 13]. Paper I, (see also Chapter 2) reports a test of the shoving model [14] connecting the relaxation time to the shear-modulus.

In addition to the relaxation time of the liquid response it is interesting also to look at its shape (Figure 1.3). The response function represents the

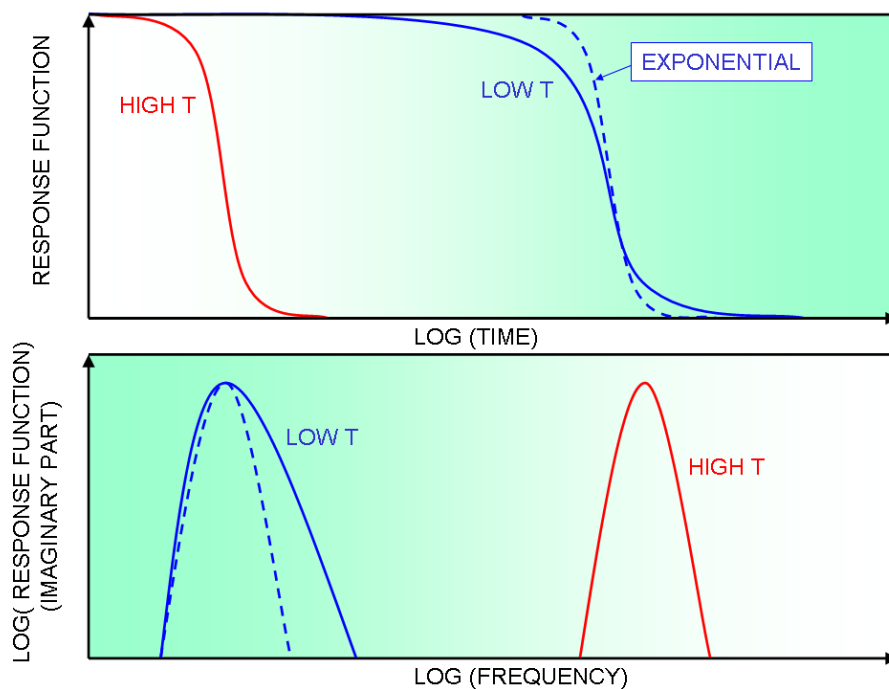


Figure 1.3: Shape of the time-dependent response function at high and low temperature (**Top**). At high temperatures the shape of the function is exponential while for the supercooled liquid the response is more stretched. This can be seen also looking at the (frequency dependent) Laplace transform of the response (**Bottom**).

time-evolution of a property of the liquid after the application of a small perturbation. This is the case of the volume relaxation after the temperature step described above, but in principle one can apply any field and measure any observable responding. The shape of the response function $\chi(t)$ in the high temperature liquid is well approximated by an exponential (Debye-relaxation)

$$\chi(t) = \exp(-t/\tau) \quad (1.3)$$

while in the supercooled state the response is generally more stretched than a simple exponential [15, 16]. A study of the non-exponential shape of the shear-mechanical response is reported in Paper I and Paper II.

1.3 Linear Response and Fluctuation-Dissipation Theorem

The concept response function intuitively introduced above can be formulated more generally within linear response theory [17, 18, 19]. Moreover the fluctuation-dissipation theorem allow us to relate the response of a system sub-

ject to a (small) external perturbation to the spontaneous fluctuations of the same system in the un-perturbed condition.

Let us imagine to monitor an observable of the system B when a small time-dependent perturbation $\epsilon(t)$ is applied. The variable B will change from its value $\langle B \rangle_0$ of the unperturbed system reacting to the external field. Assuming that the external stimulus depends on time as a Heaviside step-function applied at t' ($\epsilon(t) = \epsilon_0 \theta(t - t')$) with infinitesimal amplitude ($\epsilon_0 \rightarrow 0$) we define the response function χ as

$$\langle B(t, t') \rangle - \langle B \rangle_0 = \epsilon_0 \chi(t, t') \quad (1.4)$$

The fluctuation-dissipation theorem (FDT) establishes relationship between the response function χ of the system induced by the perturbation and its spontaneous dynamics. Assuming that the external field introduces an energy contribution to the system that is $-\epsilon A$ (where A is the variable coupled to the field), the FDT expresses the response function via the correlation function $\langle B(t)A(t') \rangle_0$ of the variables A and B at the thermodynamic equilibrium

$$k_B T \chi(t, t') = \langle B(t')A(t') \rangle_0 - \langle B(t)A(t') \rangle_0 \quad (1.5)$$

The FDT expressed in Equation (1.5) has fundamental importance in condensed-matter physics since it establishes that probing the system via an external perturbation one is actually measuring its intrinsic properties. Nevertheless the FDT is, in principle, restricted to equilibrium conditions and thus it is interesting to ask if and how it ceases to hold out of equilibrium.

As briefly illustrated above when the liquid becomes a glass it falls out of the equilibrium. This makes the off-equilibrium regime and the deviation from the FDT a major subject of study in glass-science [20, 21, 22, 23, 24]. Paper III (Chapter 3) reports an experimental investigation of the violation of the FDT in an off-equilibrium colloidal gel-forming solution. Paper IV (Chapter 4) contains a computer-simulation study of the violation of the FDT and the associated effective temperature in a special class of glasses.

1.4 Heterogeneous Dynamics

Another intriguing feature of the relaxation in a supercooled liquid is its spatial heterogeneity. The motion of the molecules of the liquid varies considerably among space as revealed by computer simulations performed well above the experimental T_g [25, 26, 27, 28]. Experimental evidences of dynamical fluctuations significantly larger than the molecules' size were also collected [29, 30, 31, 32, 33].

Multi-point correlation functions have been used intensively to characterize the spatially heterogeneous dynamics in computer simulations [25, 26, 27, 28], although measuring these quantities by direct experiments remains a major challenge. A significant advance in accessing experimentally these multi-point susceptibilities has been achieved recently [34, 35, 36]. The central idea of these works is to use the FDT to relate the three-point susceptibility to the change in any standard (two-point) response function following a change in temperature or pressure. Moreover it is shown that the three-point function can be used to approximate an even higher order correlation function, namely the

four-point susceptibility. These techniques have been used to obtain the multi-point correlation functions from a number of experimental data [37, 38] and to study in detail their temperature-dependence in comparison with the different models for the glass transition [39].

Thanks to these theoretical developments we can associate a three-point and an (approximated) four-point susceptibility to each dynamic response function measured at different temperatures. Paper V (Chapter 5) reports a systematic comparison between these high order correlation functions obtained from two different dynamical responses: the dielectric and the shear-mechanical one. In Chapter 5 we also present a new experiment capable of measuring directly the four point susceptibility in nano-particle colloidal suspensions. In Chapter 6 we introduce a new model for the direct connection of the shear and dielectric response accounting for the dynamic heterogeneity.

Chapter 2

Equilibrium Shear-Mechanical Response of Several Glass-Formers

This chapter illustrates briefly the concept of shear-mechanical relaxation and it summarizes the main findings of Paper I and Paper II. The measurements presented in these two articles are enriched here by further analysis and discussion that was not included in Paper I and Paper II.

2.1 Shear-Mechanical Response

The basic concepts defining the shear-mechanical relaxation may be sketched as follows [40, 41]. Let us imagine a small shear deformation imposed instantaneously to a cubic solid body as shown in Figure 2.1. The axial displacement u_x along x of the body from its initial position depends on the height y at which it is measured. From the construction of Figure 2.1 it is clear that $u_x = (A/L)y$. It is therefore convenient to introduce a dimensionless quantity (the strain) for characterizing the deformation $\gamma = \partial u_x / \partial y = (A/L)$. Note that for more complicated deformations of the solid $u_{xy} = \partial u_x / \partial y$ generally defines the strain tensor.

The solid reacts elastically to the imposed change of shape opposing a force. The force per unit area opposed by the solid body is the stress (tensor) σ_{xy} that defines the shear modulus G as

$$\sigma_{xy} = Gu_{xy} = G\gamma \quad (2.1)$$

In a solid σ_{xy} does not decay to zero as the time increases meaning that the system does not flow.

Allowing for the time-dependence of the shear-modulus we can describe the shear-mechanical response of a liquid. For example at high temperatures, where the relaxation is pretty exponential, we can set (Maxwell model) $G(t) = G_\infty \exp(-t/\tau)$ where G_∞ is the infinite frequency (or zero time) shear modulus. Notice again the central role of timescales defining the liquid and the glassy regimes: if the relaxation is fast the system flows and it is considered a liquid. Differently if the relaxation time is long enough one will never observe the system flowing and that will appear as a (solid) glass.

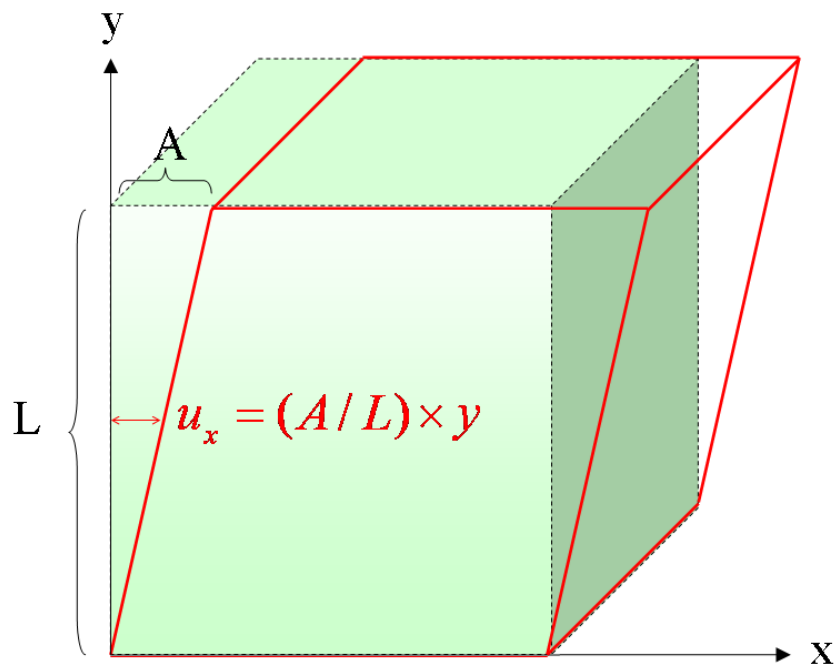


Figure 2.1: Pictorial representation of an axial (volume-preserving) deformation. The maximum displacement of the solid cubic body is $u_x = A$ located at $y = L$. This defines the strain $\gamma = \partial u_x / \partial y = (A/L)$.

2.2 Features of The Mechanical Relaxation in Five Supercooled Liquids

Paper I reported high-quality dynamic shear-modulus measurements for five glass-forming liquids. The full names of the liquids studied and the abbreviations used are reported in Table 2.1. These measurements¹ were obtained by the *piezoelectric shear-modulus gauge* (PSG) method that allow one to measure the frequency-resolved (complex) shear-modulus ($G = G' + iG''$) of supercooled liquids in a wide dynamical range spanning from 10^{-3} Hz to 10 kHz. All technical details about the PSG technique and the experimental set-up used for the measurements can be found in Ref.s [42, 43, 44].

These broad-band shear-mechanical measurements allow one to characterize the temperature evolution of the relaxation time of the shear response. A simple way of defining the relaxation time is by locating the maximum G''_{\max} of the mechanical loss $G''(\omega)$ (imaginary part) as shown in Figure 2.2. Once the angular frequency ω_{\max} corresponding to this maximum is found, the relaxation time τ is computed as $\tau = \omega_{\max}^{-1}$. Plotting τ as a function of the inverse temperature as in Figure 2.3, we can appreciate the significant increase of the shear-mechanical relaxation time upon cooling. Figure 2.3 also shows fits of

¹All the shear-mechanical data reported in Paper I are available in the “Glass and Time: Data Repository” found online at <http://glass.ruc.dk/data>.

Features of The Mechanical Relaxation in Five Supercooled Liquids

Liquid	Abbreviation	T_g [K]	m	(clear) β -process
pentaphenyltrimethyltrisiloxane	DC705	227.5	117.6	no
dibutyl phthalate	DBP	175.4	91.8	yes
diethyl phthalate	DEP	180.2	89.1	yes
1,2-propanediol	-	162.5	62.4	no
m-touluidine	-	182.9	110.9	yes

Table 2.1: Names and abbreviations of the liquids studied in Paper I. The glass transition temperature T_g and the fragility m are calculated from the fits with the VFT equation (2.3). The table also reports if the liquids shows or not a clear Johari-Goldstein β relaxation.

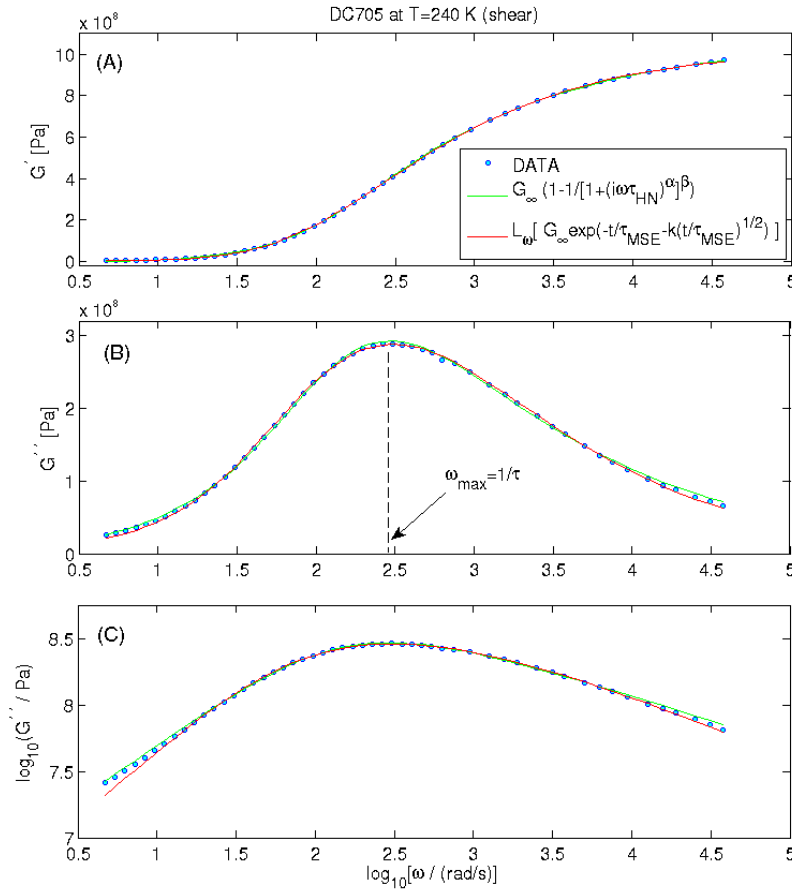


Figure 2.2: Shear-mechanical response of DC705 at $T = 240$ K. In (A) and (B), respectively, the real (G') and imaginary part (G'') are plotted as a function of $\log_{10}(\omega)$. The vertical dashed line in (B) locates the maximum of the loss of the shear modulus, the corresponding inverse ω_{\max} defines the relaxation time. The full lines are fits with the functions (2.4) (green) and (2.5) (red). (C) shows the quality of the fits on a double-log scale.

2. EQUILIBRIUM SHEAR-MECHANICAL RESPONSE OF SEVERAL GLASS-FORMERS

the shear relaxation times with two frequently used fitting functions. One is the Avramov equation [45, 46, 47, 48, 49, 50] (full lines in Figure 2.3)

$$\tau(T) = \tau_0 \exp\left(\frac{B}{T^n}\right) \quad (2.2)$$

The other is the Vogel-Fulcher-Tammann (VFT) equation [51, 52, 53] (dashed lines in Figure 2.3)

$$\tau(T) = \tau_0 \exp\left(\frac{A}{T - T_0}\right) \quad (2.3)$$

the parameter τ_0 was fixed to $\tau_0 = 10^{-14}$ s in the fitting. This two functions were compared systematically in fitting dielectric relaxation times in a recent publication by our group [54]. In agreement with the findings of Ref. [54] the VFT equation (2.3) fits the shear relaxation data slightly better than the Avramov equation (2.2). However the difference in the quality of the fits is lower than that reported in Ref. [54] since the dynamical range of the shear measurements is narrower than that of dielectric measurements. These fits allow an easy estimation of the glass transition temperature T_g and the fragility m (see Sec. 1.2). For example from Equation (2.3) we can compute T_g (that is defined as the temperature where $\tau = \tau_g = 100$ s) as $T_g = [T_0 + A/\ln(\tau_g/\tau_0)]$ and the fragility $m = AT_g/[\ln 10(T_g - T_0)]$. The values of T_g and m computed with these formulas are listed in Table 2.1 for the five liquids studied. The marked non-Arrhenius (Sec. 1.2) behavior of the shear relaxation time of these liquids is shown in Figure 2.4 where the deviation from the Arrhenius temperature dependence is evident. Paper I reported also a test of the shoving model [14, 55, 4] for DC705 and 1,2-propanediol. This model relates directly the temperature-dependent activation energy of the supercooled liquid to the infinite frequency shear modulus.

The non-exponential form of the dynamic shear modulus is shown by Figure 2.2 for DC705 at $T = 240$ K where the shear-dynamical relaxation is fitted with two non-Debye functions: the Havriliak-Negami (HN) function [56, 57] and the modified stretched exponential (MSE) recently introduced by our group in Refs [58, 59]. The HN function can be written as follows to fit the shear response:

$$G(\omega) = G_\infty \left(1 - \frac{1}{[1 + (i\omega\tau_{HN})^\alpha]^\beta}\right) \quad (2.4)$$

where G_∞ is the infinite-frequency shear modulus, τ_{HN} is the relaxation time that is different from $\tau = \omega_{\max}^{-1}$ used above, and α and β are the stretching exponents characterizing the shape of the function. Equation (2.4) reduces to an exponential relaxation when $\alpha = 1$ and $\beta = 1$. The MSE function is easily written in the time domain for G as

$$G(t) = G_\infty \exp[-t/\tau_{MSE} - k(t/\tau_{MSE})^{1/2}] \quad (2.5)$$

to fit the data of Figure 2.2 the Laplace transform of Equation 2.5 is performed numerically (see Section 6.3 for more details). As seen from Figure 2.2 the functions (2.4) and (2.5) fit almost equally well, although the HN function has one extra fitting parameter with respect to the MSE. More precisely the HN function has two free shape parameters (α and β), while the MSE has only

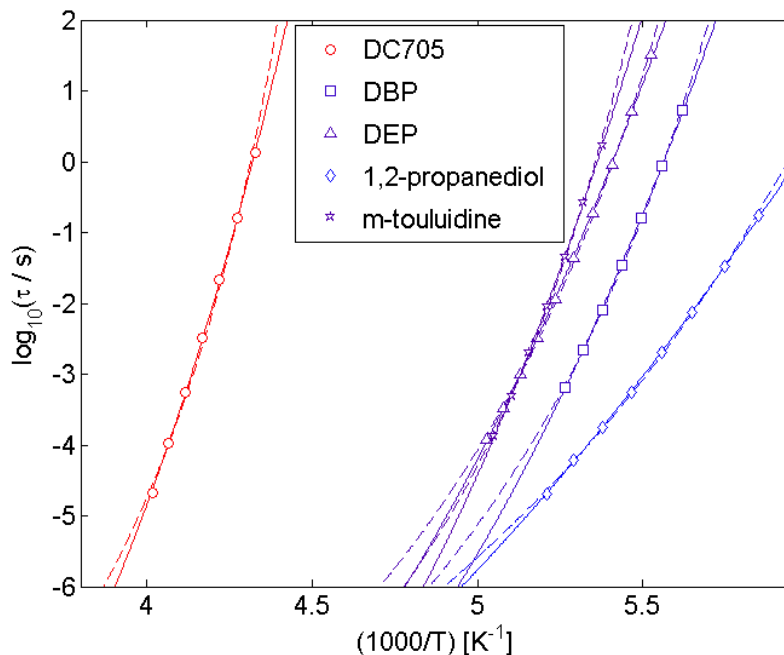


Figure 2.3: Relaxation time as a function of the inverse temperature. The full line is a fit with the Avramov equation (2.2), the dashed line represents a fit with VFT equation (2.3).

one (k), but the reduced χ^2 resulting from the fitting is only few percents lower for the function (2.4).

An alternative way of visualizing the non-exponential shape of the mechanical relaxation (not presented in Paper I) is the Nyquist plot reported in Figure 2.5 for the five liquids studied. In this graph, where G'' is reported as a function of G' , we can see the deviation from the Debye (symmetric) form of the relaxation (dashed line). Moreover Figure 2.5 reports the normalized Nyquist plots to illustrate another important feature of these relaxation, namely time-temperature superposition (TTS) [60, 61, 62, 63, 64]. If TTS holds a response function changes only its amplitude and relaxation time when temperature changes, while its shape remains unchanged. Mathematically if G obeys TTS it can generally be rewritten as $G(\omega, T) = A(T)\phi(\tau(T)\omega)$. When TTS is applies for a liquid all the response functions measured at different temperatures collapse on the same master curve in the normalized Nyquist plot of Fig 2.5. From this Figure is clear that DC705 and 1,2-propanediol show TTS to a very good degree. Differently the other liquids (DBP, DEP and m -touluidine) show a deviation from the master curve at the right end of the Nyquist plot corresponding to high frequency. The failure of TTS in these liquids at high frequency can be explained by the presence of a mechanical Johari-Goldstein β relaxation [65, 66, 67, 68, 69, 70, 64, 71, 72, 73]. As documented in detail in Paper I all the liquids displaying a rise of the shear modulus at high

2. EQUILIBRIUM SHEAR-MECHANICAL RESPONSE OF SEVERAL GLASS-FORMERS

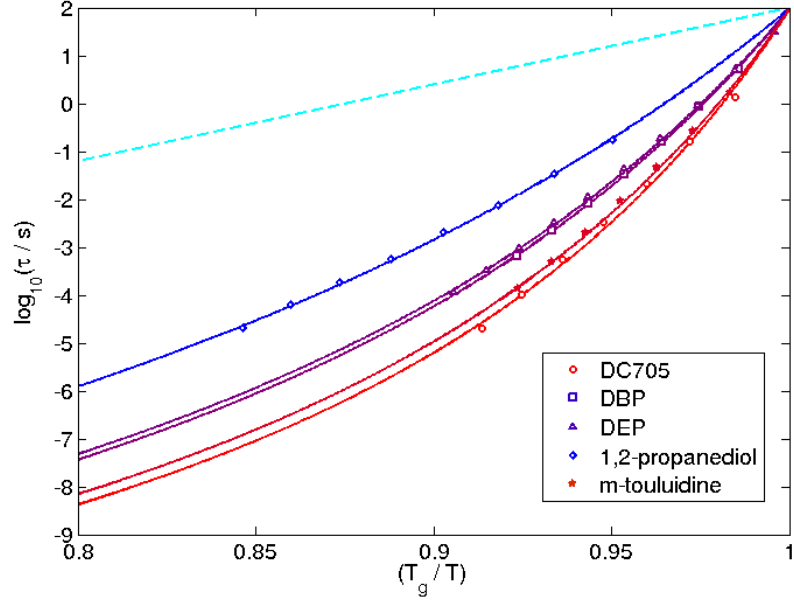


Figure 2.4: Angell's plot of the shear relaxation time and for the five liquids studied. The full lines are fits with the VFT equation(2.3). The dashed line represents the case of an Arrhenius increase of the relaxation time.

frequencies have been found to have a clear β peak in the dielectric spectra measured by other groups. Table 2.1 reports whether a liquid has or not a clear Johari-Goldstein secondary relaxation. As analysis of the shape of the shear relaxation functions Paper I contains the estimation of the minimum logarithmic slope [64, 72, 73, 74, 75, 76] of the high frequency side of the shear-mechanical response.

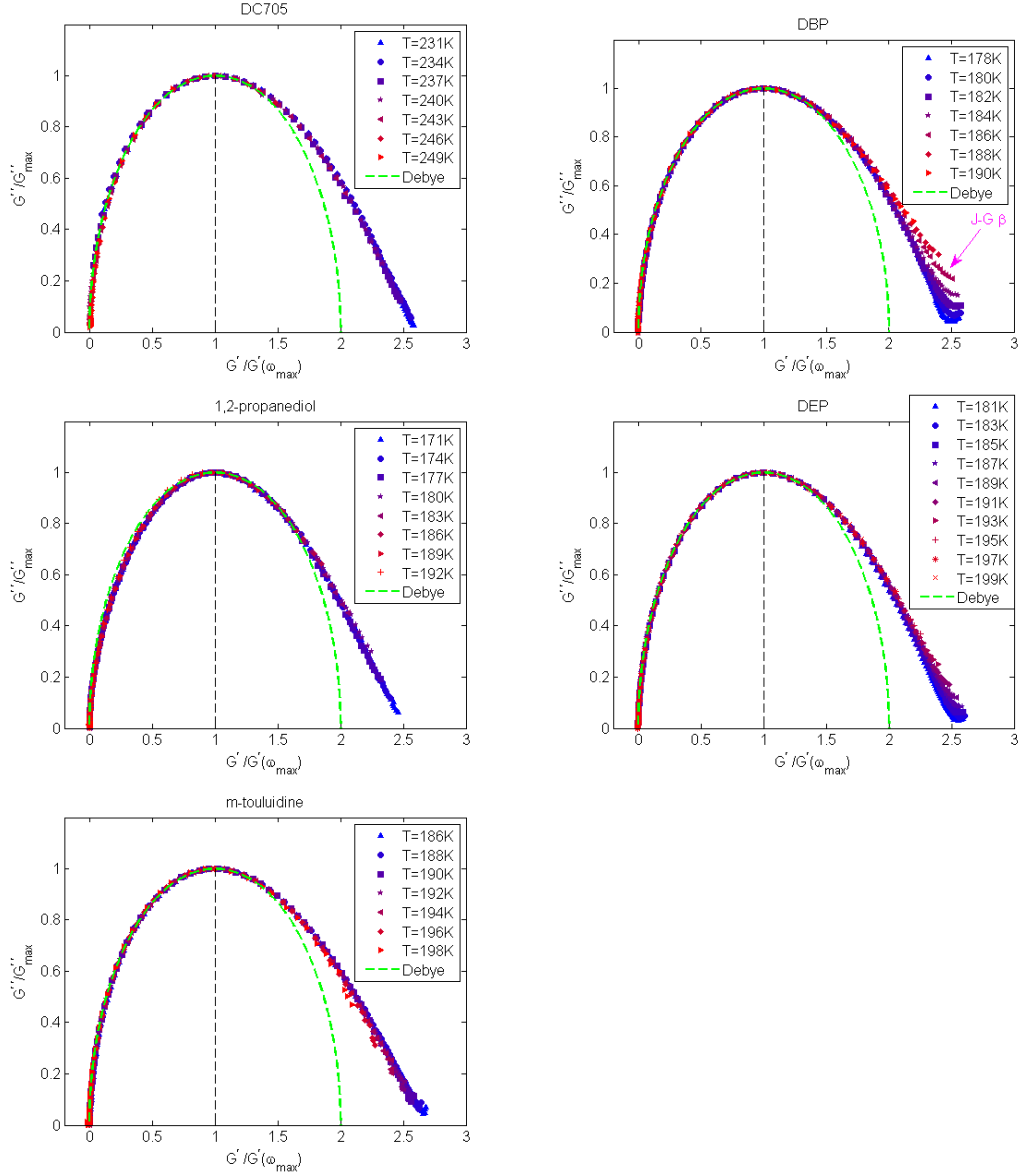


Figure 2.5: Normalized Nyquist plot of the shear-mechanical response for five glass-forming liquids at several temperatures (see legend). The real G' and the imaginary part G'' of G are normalized to their values at ω_{\max} . The frequency is a parameter in these plots, the left end of the plot corresponds to low frequencies while the right end corresponds to high frequencies. The dashed line is the Nyquist plot corresponding to an exponential shear relaxation (i.e. Equation (2.4) with $\alpha = 1$ and $\beta = 1$). If TTS is obeyed the data at different temperatures collapse on the same master curve. This is the case of DC705 and 1,2-propanediol.

2. EQUILIBRIUM SHEAR-MECHANICAL RESPONSE OF SEVERAL GLASS-FORMERS

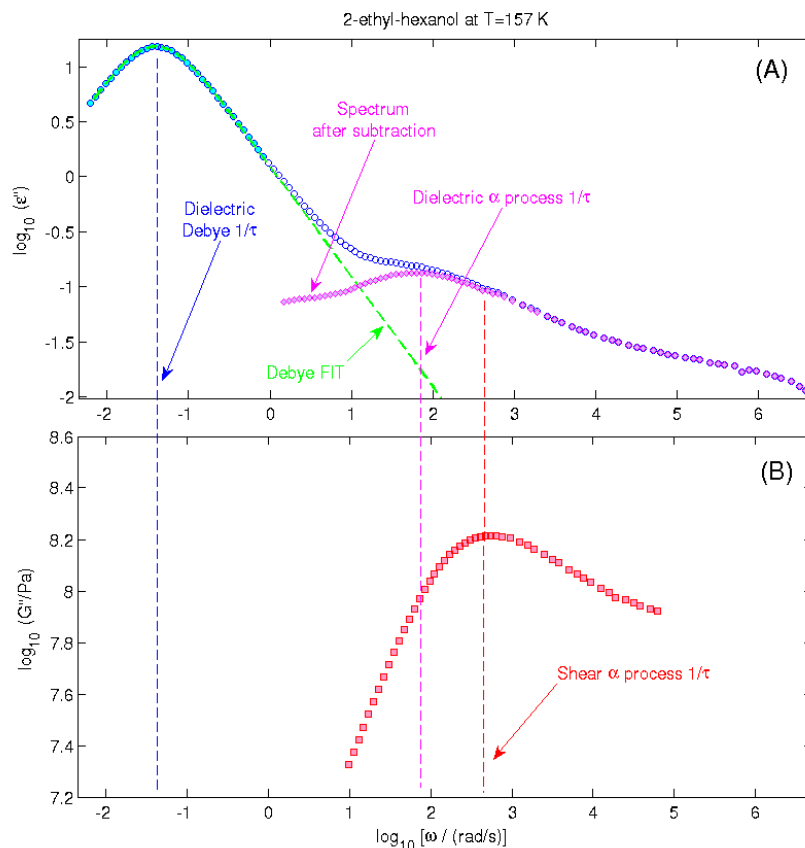


Figure 2.6: **(A)** Imaginary part ϵ'' of the dielectric susceptibility ϵ as a function of ω (circles) for . The filled circles are the points fitted with a Debye relaxation Equation (2.6). The fitting function (dashed line) is subtracted from the full spectrum and the structural α relaxation time is associated with the peak of the resulting points (diamonds). The vertical lines indicate the positions of the peaks. **(B)** Imaginary part G'' of the shear modulus G as a function of ω (squares). The mechanical spectrum is dominated by a mechanical α process with evidence of an intense β activity at high frequency. The vertical line indicates the position of the α peak.

2.3 Mechanical Relaxation and Dielectric Relaxation in Two Monoalcohols

Paper II presents frequency-resolved dielectric and shear-mechanical measurements of two supercooled monohydroxy liquids (monoalcohols): 2-butanol and 2-ethyl-1-hexanol. The particular feature of monoalcohols is that they exhibit an intense Debye-like relaxation dominating the dielectric susceptibility [77, 78]. In addition the dielectric spectra of this liquid show a standard α relaxation [79, 80, 81] and a Johari-Goldstain β process [65]. Figure 2.6.A

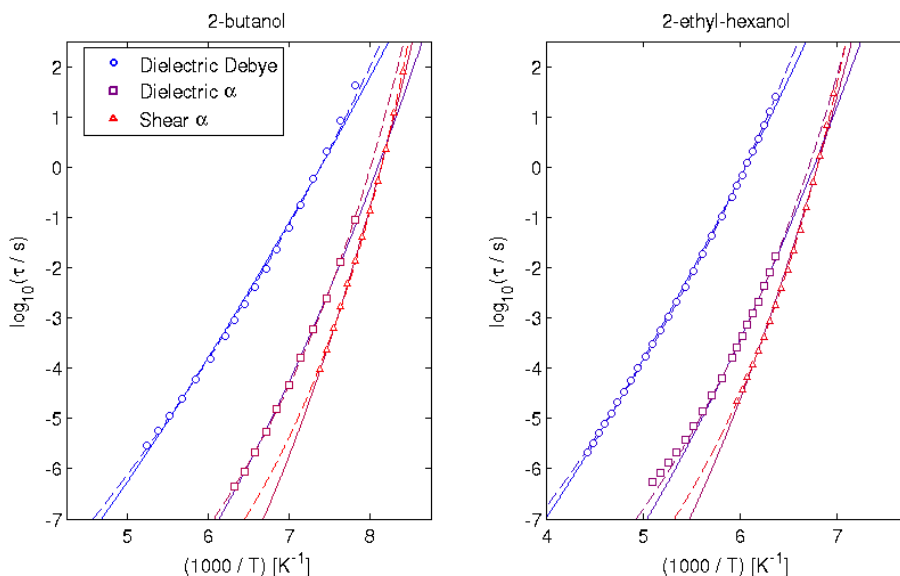


Figure 2.7: Relaxation time as a function of the inverse temperature. The full line is a fit with the Avramov equation (2.2), the dashed line represents a fit with VFT equation (2.3).

shows an example of the measured dielectric susceptibility ϵ . In Figure 2.6.A ϵ'' (imaginary part) is plotted as a function of frequency for 2-ethyl-1-hexanol at $T = 157$ K. Figure 2.6.A also illustrates the procedure followed in Paper II to extract the peak position of the structural α dielectric process. A fit of the points close to the Debye peak is performed with the Debye function

$$\epsilon = \epsilon_{\infty} + \frac{\Delta\epsilon}{1 + i\tau\omega} \quad (2.6)$$

This fitting function is then subtracted from the full spectrum and the peak of the resulting dielectric loss is identified as the dielectric α relaxation time.

As seen in Figure 2.6.(B) our shear measurements show that the Debye process is not seen in the mechanical relaxation. The measured mechanical spectrum is featured by a clear (non-Debye) α process and the rise of G'' at high frequency hints for the presence of a mechanical β relaxation². This findings are in agreement with a number of different measurements like calorimetry, photon-correlation spectroscopy and ultrasonic mechanical measurements (See Ref.s 7-19 of Paper II). These experiments did not reveal any clear signature of the Debye process as seen in dielectrics.

Our results show clearly that the shear and dielectric α relaxation times at the same temperature are found within the same decade as seen in Figure 2.7 (see also the vertical lines of Figure 2.6). This is in agreement with the scenario established from the comparison of dielectric and mechanical measurements carried out by our group on a number liquids: the shear-mechanical α

²See also Figure 1 in Paper II where the beta peak is fully resolved.

2. EQUILIBRIUM SHEAR-MECHANICAL RESPONSE OF SEVERAL GLASS-FORMERS

	2-butanol	2-ethyl-1-hexanol
T_g [K] (dielectric Debye)	125.0	153.9
T_g [K] (dielectric α)	119.9	142.3
T_g [K] (shear α)	118.9	142.0
m (dielectric Debye)	27.5	31.0
m (dielectric α)	55.1	48.4
m (shear α)	67.7	63.8

Table 2.2: Properties of the shear-mechanical and dielectric relaxation of the two monoalcohols studied in Paper II. The glass transition temperature T_g and the fragility m are calculated from the fits with the VFT equation (2.3) of the relaxation times of the various processes.

relaxation is always faster than the dielectric one, but they are usually not separated by more than a factor ten [72, 73]. Differently the dielectric Debye process is separated by about a factor 10^3 from the mechanical α relaxation both in 2-butanol and 2-ethyl-1-hexanol. As done in Sec. 2.2 we show in Figure 2.7 the fits of the relaxation times of the different process (dielectric-Debye, dielectric α and shear α) with Avramov equation (2.3) and the VFT equation (2.3).

The glass transition temperatures and the fragilities of the processes estimated with the VFT fits are reported in Table 2.2. The estimated glass transition temperatures are very close for the shear and dielectric α relaxation times, while for the Debye process T_g is significantly higher. Moreover fragility obtained for the Debye process is lower than the one estimated for the dielectric and shear α relaxation times. This can be seen also in the Angell plot of Figure 2.8, where the less fragile behavior of the Debye relaxation time is evident. In Figure we show the (normalized) Nyquist plot of the dielectric and shear-mechanical response. A comparison with a Debye fitting shows clearly the good agreement of the dielectric response with Equation (2.6) while the shear-mechanical spectra show a very clear non-Debye form.

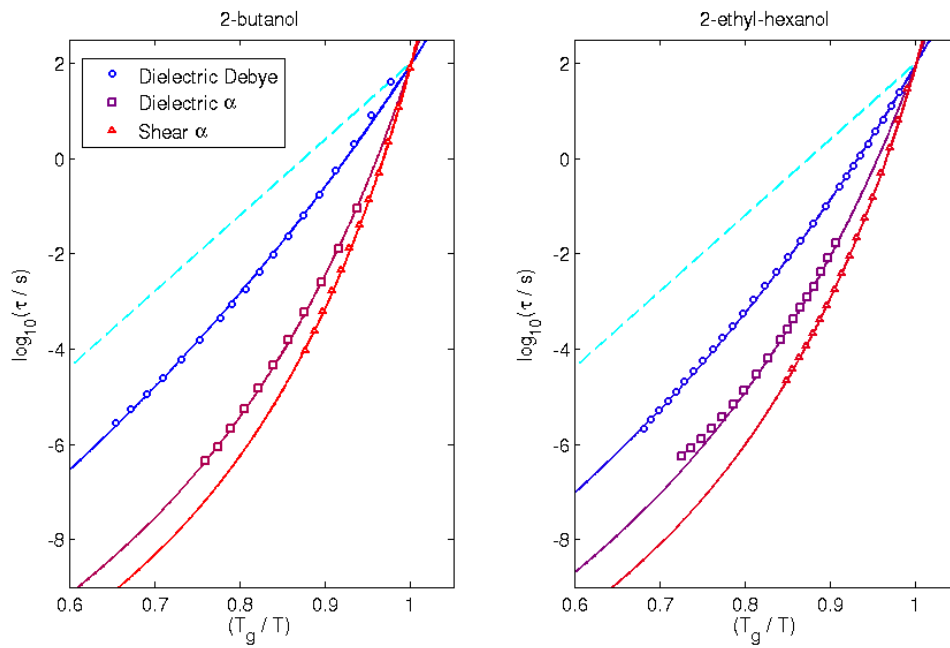


Figure 2.8: Angell plot of the dielectric relaxation time and of the shear-mechanical relaxation time for two monoalcohols. The full lines are fits with the VFT equation(2.3). The dashed line represents the case of an Arrhenius increase of the relaxation time.

2. EQUILIBRIUM SHEAR-MECHANICAL RESPONSE OF SEVERAL GLASS-FORMERS

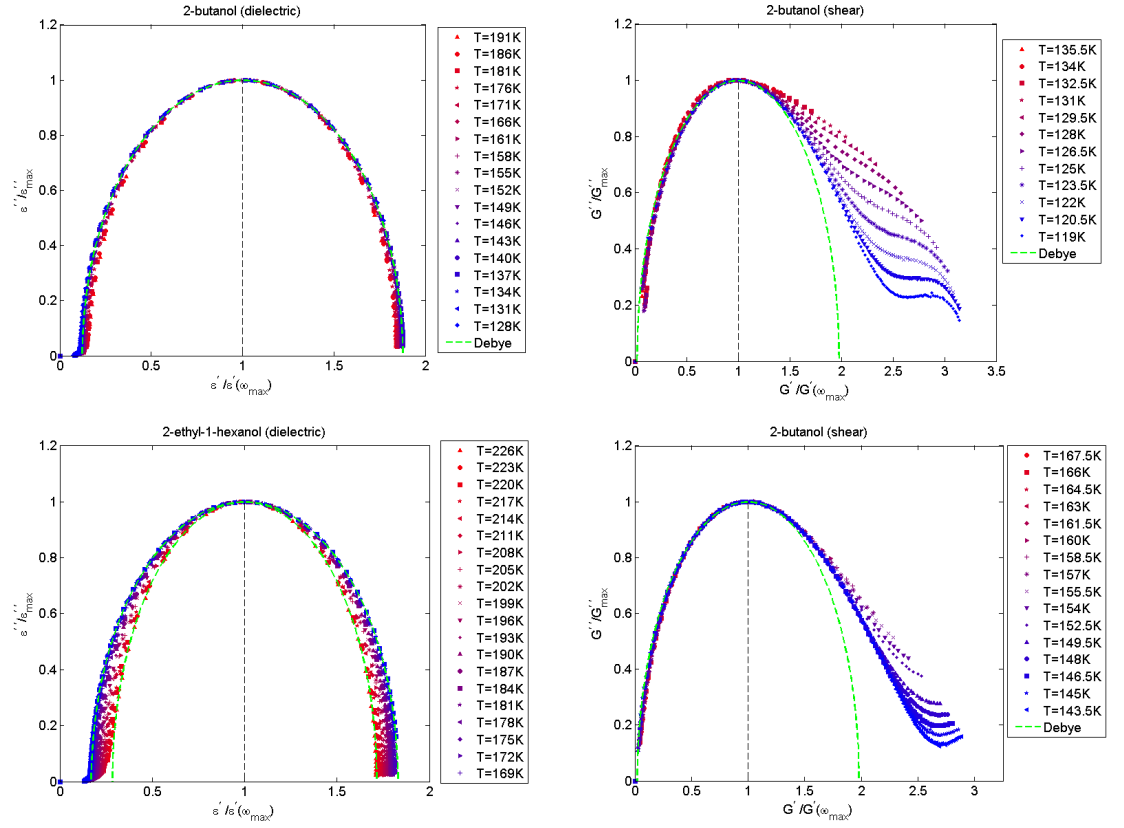


Figure 2.9: Normalized Nyquist plot of the dielectric (left) and of the shear-mechanical response (right) for the two monoalcohols studied in Paper II. The dominating Debye relaxation of the dielectric data is fitted with Equation (2.6) (dashed line).

Chapter 3

An Experimental Study of The Off-Equilibrium Fluctuation-Dissipation Relation

In this chapter we briefly illustrate the generalized fluctuation dissipation relation (FDR), moreover we summarize shortly the main findings of the experiment described in Paper III reporting many experimental details. The experiment (Paper III) investigates the FDR in a gel-forming colloidal suspension by the combination of two different dynamic light scattering techniques.

3.1 Generalized Fluctuation-Dissipation Relation

As mentioned in Sec. 1.3 an interesting problem in glass science is the characterization of the off-equilibrium glassy state obtained by quickly cooling the supercooled liquid. Within this context it is important to understand the relationship between the fundamental quantities describing the dynamics of a many-body system: the correlation function and the response function. We recall briefly here the FDR proposed for glassy systems by J. Kurchan and L. F. Cugliandolo [20, 21, 22, 23]. Let us start by casting the equilibrium FDT [17, 18, 19] in its differential form (compare with Equation (1.5) in Sec. 1.3)

$$T\partial_t\chi(t,t') = -\partial_{t'}C(t,t') \quad (3.1)$$

Where χ is the response function and C is the correlation function as defined in Sec. 1.3. At the equilibrium these functions satisfy time translational invariance (TTI), i.e. they are function of the time-difference ($t - t'$) only ($C = C(t - t')$ and $\chi = \chi(t - t')$).

Let us imagine now to cool instantaneously our equilibrium liquid to a very low temperature. In this process the liquid falls out of equilibrium being unable to equilibrate to the new temperature within our observation time-scale. This regime is called physical aging regime and in this the correlation and the response function do not obey TTI. In the off-equilibrium condition described above the FDT can be generalized to the FDR introducing the violation factor $X(t,t')$ in the expression (3.1) as

3. AN EXPERIMENTAL STUDY OF THE OFF-EQUILIBRIUM
FLUCTUATION-DISSIPATION RELATION

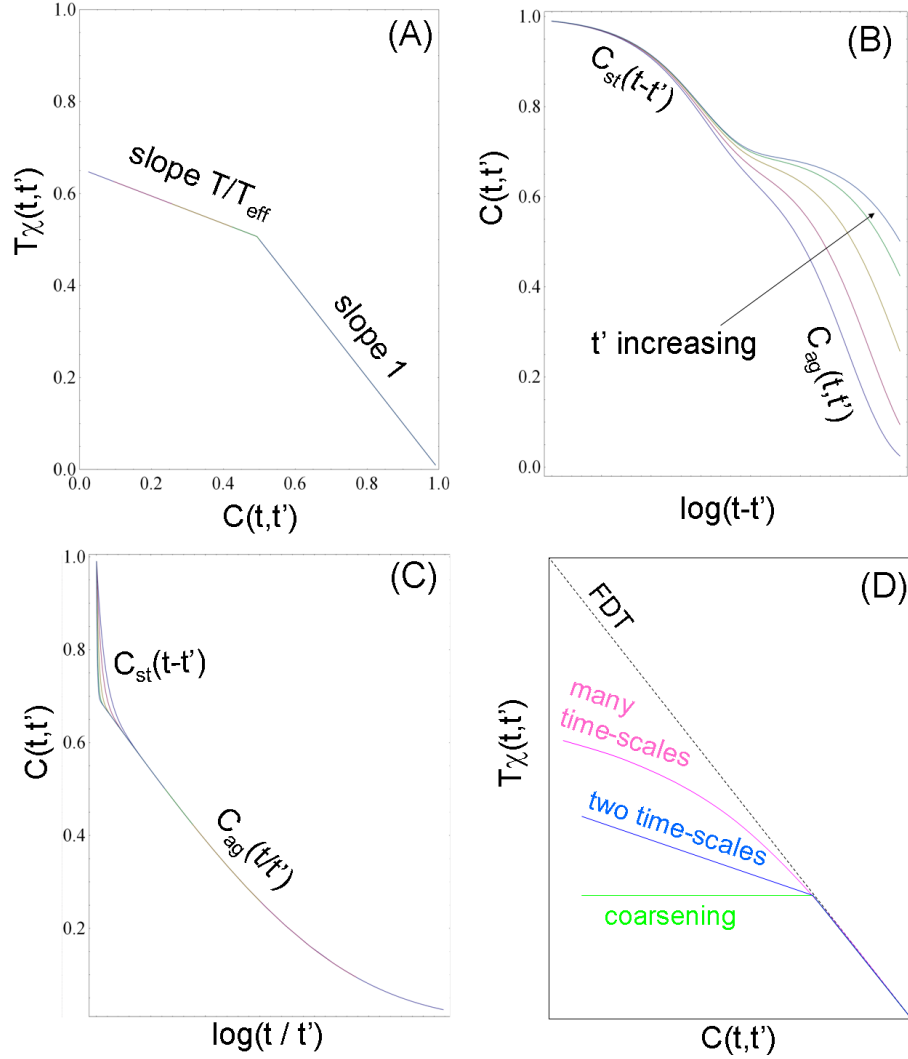


Figure 3.1: **(A)** Sketch of the FD-plot for an out of equilibrium structural glassy system. The two slopes define the bath temperature at which the fast dynamics is in equilibrium and the effective temperature for the slow structural rearrangements. **(B)** Aging of the correlation function and decomposition in a short times stationary part $C_{\text{st}}(t-t')$ and a long times aging part $C_{\text{ag}}(t, t')$. **(C)** Scaling of the slow aging component of the correlation function $C_{\text{ag}}(t, t')$ in the full-scaling case $C_{\text{ag}} = C_{\text{ag}}(t/t')$. **(D)** Various scenarios of the FDR violations. A two-lines form of the FD-plot is found for structural glasses and some spin systems corresponding to two well separated time-scales. A curved FD-plot corresponding to many times scales is found in some spin-glasses as the SK spin-glass. A flat off-equilibrium section is found for coarsening systems, this corresponds to an infinite T_{eff} .

$$\frac{T}{X(t, t')} \partial_{t'} \chi(t, t') = -\partial_{t'} C(t, t') \quad (3.2)$$

Where $X(t, t') = 1$ when $(t - t')/t' \ll 1$, i.e. the standard FDT holds for the fast (vibrational) dynamics that equilibrates practically instantaneously to the new temperature; while $X(t, t') < 1$ when $(t - t')/t' \gg 1$ i.e. the FDT is violated by the (off-equilibrium) slow structural rearrangements. Moreover it is assumed that in for long time-scales $(t - t')/t' \gg 1$ the violation factor depends on the times t and t' only through C , i.e. $X(t, t') = X(C(t, t'))$. Equation (3.2) suggests to define an effective temperature for the slow structural dynamics as

$$T_{\text{eff}} = \frac{T}{X(t, t')} (> T) \quad (3.3)$$

when $(t - t')/t' \gg 1$, meaning that the slow dynamics behaves as if it were thermalized at the (higher) temperature T_{eff} . From the experimental and the computational point of view is more convenient to work with the integrated responses and correlation rather than with the time derivatives appearing directly in the FDR (Equation (3.2)). What is usually done in practice is to build a parametric FD-plot reporting $\chi(t, t')$ as function of $C(t, t')$. This has the typical form composed by two lines as shown Figure 3.1(A). Since we can rewrite $X = \partial T \chi(t, t') / \partial C(t, t')$ the violation factor is estimated as the inverse slope of the FD-plot. Knowing the violation factor we can estimate the effective temperature (Equation (3.3)).

This scenario was found to apply remarkably well in analytically solvable models for the glassy dynamics and simulations of some spin-glasses and structural glasses [82, 83, 84, 20, 85], at least in the limit in which both t and t' are large enough. Consistently with the two-step behavior of T_{eff} described above in these systems the dynamic correlation function can be divided in a stationary term C_{st} plus an aging term C_{ag} as follows (see Figure 3.1(B))

$$C(t, t') = C_{\text{st}}(t - t') + C_{\text{ag}}(t, t') \quad (3.4)$$

In a structural glass this decomposition corresponds to the separation between the fast vibrational dynamics and the slow structural dynamics. The same decomposition is possible for the off-equilibrium response $\chi(t, t')$. The stationary components of the dynamic functions, i.e. $C_{\text{st}}(t - t')$ and $\chi_{\text{st}}(t - t')$, satisfy TTI and the FDT as if they were at the equilibrium at the quenching temperature T . Differently the aging functions $C_{\text{ag}}(t, t')$ and $\chi_{\text{ag}}(t, t')$ age and their decay becomes slower as the aging times increases. These functions violate the TTI and the FDT. Moreover a full-aging scenario is found in these numerical and theoretical works in which C_{ag} simply scales as $C_{\text{ag}}(t, t') = C_{\text{ag}}(t/t')$ (see Figure 3.1(C)). The same scaling is found for the response $\chi_{\text{ag}}(t, t') = \chi_{\text{ag}}(t/t')$. In this case is the relaxation time τ of the aging functions grows as the aging time $\tau \sim t'$ and is also obvious that if $X = X(C)$.

Although the full-aging picture illustrated above is found in many mean-field glassy models and in numerical simulations of structural glasses there are cases where deviations from the full aging are evident. Noticeable examples of this are found in theoretical and simulation studies of coarsening systems and spin-glass systems with a more complicated free-energy landscape. This is important to stress since the aging process of the colloidal suspension in Paper III

is very different from the full-aging scenario described above. In the experiment we find that the relevant time scale defining whether the FDT is violated or not is not simply the aging time t_w , but rather the aging-time dependent relaxation time of the correlation function $\tau(t_w)$. It is interesting to notice also that some systems exhibit an FDT violation qualitatively different from the one depicted above [20]. Some spin systems as the Sherrington-Kirkpatrick (SK) spin-glass show an infinite series of relaxation time-scales with a broad spectrum of effective temperatures associated. In these cases the FD-plot has a curved form as shown in Figure 3.1(D). Moreover in models where the cooling induces a coarsening process the off-equilibrium part of the FD-plot is flat (see Figure 3.1(D)), a feature that is associated with an infinite effective temperature.

3.2 An Experimental Study of The Off-Equilibrium Fluctuation-Dissipation Relation

Although several theoretical and computer simulation studies of the FDR can be found in literature [82, 83, 84, 85, 86, 87, 88], few experiments were performed so far. This kind of experiment constitutes a major experimental challenge, since one has to measure simultaneously the correlation function and the response function. Moreover one has to obtain these measurements after an extremely fast cooling process of the sample.

Despite fluctuations are notoriously difficult to measure, the magnetization fluctuations together with the response to the external magnetic field were measured in some spin-glasses [89, 90, 91]. Unfortunately these experiments were restricted to time-scales $(t - t')/t' \lesssim 1$ and did not detect any systematic deviation from the FDT. Later on a clear FDT violation was measured in an experiment performed on an insulating spin glass [92]. Nevertheless the effective temperature measured from these violations was found to be much higher than the initial equilibrium temperature at which the samples were kept before the quench, making difficult the interpretation of the effective temperature.

Even more puzzling results were found in structural systems. The FDR was studied in glassy glycerol by combined voltage noise and resonance measurements [93]. Surprisingly the FDT was found to be significantly violated also in the time regime where $(t - t')/t' \ll 1$. Similar results were also found in a polymer glass (polycarbonate) with an effective temperature orders of magnitude higher than the bath temperature [94].

Paper III studied the FDR in an aging colloidal solution of Laponite. Laponite is a synthetic clay intensively studied for its intricate dynamical and structural behavior [95, 96, 97, 98, 99, 100, 101] and its numerous applications [102, 103, 104]. Several features of these colloidal suspensions make them particularly suitable for studying their off-equilibrium dynamics. These colloids are found to age spontaneously after the preparation at room temperature and pressure (without requiring any fast cooling procedure) toward an arrested state. The suspension is easily prepared by stirring vigorously (purified) water with the addition of the Laponite powder. The aging process of the colloidal solution proceeds very slowly ranging from several hours to days depending on the concentration of the colloid in the solvent.

In the experiment described in Paper III a low concentration solution of Laponite was chosen to have a very slow aging process and to obtain several

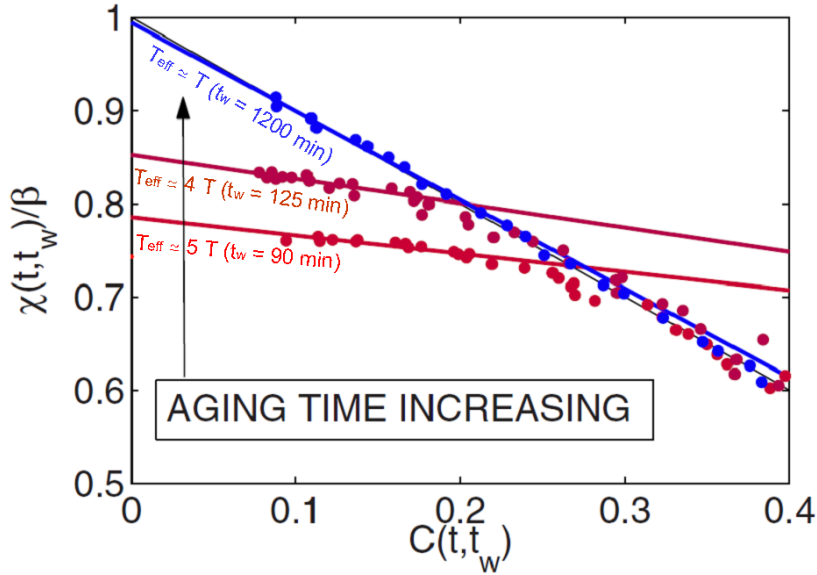


Figure 3.2: FD plot (response function vs correlation function) for a low concentration Laponite solution in aging (see Paper III and the Auxiliary Material for Paper IV). The violation of the FDT is clearly seen for short aging times. This is located at timescales of the order of the relaxation time. The violations found to decrease as the aging time increases recovering the standard FDT at the longest aging time.

measurement of the correlation function and the response function during aging. The correlation function of the spontaneous fluctuations is easily accessible in colloids by dynamic light scattering. The experiment made use of depolarized dynamic light scattering measurements combined with DC Kerr-effect response measurements (see the following Section for the experimental details). This combination of experiments allowed for the comparison of the correlation and response functions in the aging process. A clear violation of the FDT was observed at short aging times and at timescales of the order of the relaxation time of the (aging) correlation function (see Figure 3.2). At these short aging times an effective temperature about five times higher than the bath temperature was measured. The intensity of the violation was found to decrease systematically as the aging proceeds re-obtaining the FDT at the longest aging time. It is worth to notice that a number of other experiments (employing different techniques) have investigated the FDR in aging colloidal solutions of Laponite so far. The conflicting results of these experiments are summarized in Sec. I of Paper III. Nevertheless the experiment of Paper III is the only one in the literature where the measurements are specifically sensitive to the dynamics of the Laponite colloidal particles. It is interesting to add to the discussion of Paper III the findings of a recent experimental work [105] employing time-dependent nonlinear optical absorption measurements and polarized dynamic

light scattering measurements for the study of aging Laponite solutions. In this work some indirect evidence of the FDT violation was found in qualitative agreement with the results of Paper III.

The intrinsic difficulty of the measurements required and the unclear results reported so far have not decreased the experimental effort in studying the violations of the FDT and the effective temperature in various systems. Indeed the FDR was investigated recently in a liquid crystal at the electric-field driven (nematic) phase transition [106]. Very recently the violation of the FDT was measured in a quenched polymer (polyvinyl acetate) by electric force microscopy techniques [107].

3.3 Experimental Details

In this Section we provide an accurate analysis of the main experimental and conceptual problems we have found in the realization of the experiment of Paper III. In Sec.3.3.1 we recall some basic dynamic light scattering theory specialized for the case of cylindrical macromolecules in solution. This is needed to discuss in detail the assumption that the depolarized component of the scattered light is a function of the colloids reorientation angles only (Sec.3.3.2 and 3.3.3). This special assumption is accompanied by the results of some preliminary tests. We discuss in Sec.3.3.4 the birefringence measurement and the test performed to ensure that the response function is linear in the applied external field. In Sec. 3.3.5 we report all the important technical details about the experiment performed.

3.3.1 Dynamic light scattering of cylindrically symmetric macromolecules

In Paper III we claim to be able to measure the correlation function of the rotations of the Laponite colloidal particles (or macromolecules). We will see in the following sections that this conclusion is very reasonable if we have a rather good filtering of the polarized contribution to the depolarized scattered light and if we have decoupling between rotation and translation motions of the Laponite particle suspended in the solution. We also provide experimental tests to verify the approximations we make.

We start recalling some basic dynamic light scattering theory regarding the time-correlation function being this the dynamic quantity measured in photon-correlation spectroscopy (PCS) [108, 109, 110, 111]. This is done in the case of the polarized and depolarized components of the scattered electric field. In a light scattering experiment a polarized laser beam (with wavelength λ) is directed to the sample and the scattered light at a given angle is collected selecting its polarization. The wavevectors of the incoming beam and of the detected field (\mathbf{k}_i and \mathbf{k}_f) define the scattering plane and the scattering vector as $\mathbf{k} = \mathbf{k}_f - \mathbf{k}_i$. The propagation vectors \mathbf{k}_i and \mathbf{k}_f form the scattering angle ϑ that determine the modulus of the exchanged wavevector $|\mathbf{k}| = k = 4\pi n \sin(\vartheta/2)/\lambda$, n being the refraction index of the scattering medium.

The orientations of the polarization vectors respect to the scattering plane define the scattering geometry. If the initial and the final polarization vectors (\mathbf{n}_i and \mathbf{n}_f) are both perpendicular to the scattering plane we select the so

called VV scattering geometry, while, if \mathbf{n}_i and \mathbf{n}_f are respectively perpendicular and parallel to it, we have the VH scattering geometry.

We consider a sample consisting of macromolecules suspended in a solution where the significant fluctuations of the scattered field are due to the macromolecules and not to the solvent molecules. We furthermore assume that the colloidal particles are non-spherical, but they have a cylindrical symmetry. This is the case of Laponite particles since, when dissolved in water, the Laponite particle assumes the form of a flat cylinder with a diameter of 25 nm and a thickness of about 1 nm. If the mentioned assumptions apply we can find that the correlation function of the scattered electromagnetic field in the VV and VH scattering geometry are respectively proportional to

$$I_{VV}(\mathbf{k}, \tau) = \alpha^2 \left\langle \sum_i e^{-i\mathbf{k}\cdot\mathbf{r}_i(0)} \sum_j e^{i\mathbf{k}\cdot\mathbf{r}_j(\tau)} \right\rangle + \frac{4}{3} I_{VH}(\mathbf{k}, \tau) \quad (3.5)$$

$$I_{VH}(\mathbf{k}, \tau) =$$

$$\frac{\beta^2}{15} \left\langle \sum_i \{e^{-i\mathbf{k}\cdot\mathbf{r}_i(0)} P_2[\cos(\theta_i(0))]\} \sum_j \{e^{i\mathbf{k}\cdot\mathbf{r}_j(\tau)} P_2[\cos(\theta_j(\tau))]\} \right\rangle \quad (3.6)$$

In Eqs. (3.5) and (3.6) α and β are the isotropic and anisotropic parts of optical polarizability tensor, $\mathbf{r}_i(\tau)$ is the position of the center of mass of the i -th particle at the time τ , $\theta_i(\tau)$ is the angle that the symmetry axis of the i -th macromolecule forms with the vertical coordinated axis at the time τ , P_2 is the second order Legendre polynomial ($P_2(x) = (3x^2 - 1)/2$), and the sums are extended over all the particles contained in the scattering volume. Note that α and β are given by $\alpha = (\alpha_{\parallel} + 2\alpha_{\perp})/3$ and $\beta = (\alpha_{\parallel} - \alpha_{\perp})$ where $\alpha_{\parallel}, \alpha_{\perp}$ are the components of the polarizability tensor α . This tensor is diagonal in the molecule-fixed reference frame with the z axis that lies along the molecule's symmetry axis. Note that in the following we will set

$$F(\mathbf{k}, \tau) = \left\langle \sum_i e^{-i\mathbf{k}\cdot\mathbf{r}_i(0)} \sum_j e^{i\mathbf{k}\cdot\mathbf{r}_j(t)} \right\rangle$$

that is proportional to the intermediate scattering function.

We remark that, in our experiment, we use the Gaussian approximation to obtain the scattered field autocorrelation function. This establishes a relationship between correlation function I the field component E and the correlation function $I^{(2)}$ of its intensity $|E|^2$ that is

$$I^{(2)}(\tau) = \langle |E(0)|^2 |E(\tau)|^2 \rangle = [\langle |E|^2 \rangle]^2 + [\langle E^*(0)E(\tau) \rangle]^2 = |I(0)|^2 + |I(\tau)|^2$$

$I^{(2)}$ and I are respectively called homodyne and heterodyne correlation function. This approximation holds if the scattered field is the result of the superposition of many independent stochastic contributions (see Chapter 5):

$$E(\tau) = \sum_n E_n(\tau)$$

3. AN EXPERIMENTAL STUDY OF THE OFF-EQUILIBRIUM FLUCTUATION-DISSIPATION RELATION

In this way $I^{(2)}$ is determined by I .

In the following we will focus our attention on the normalized auto-correlation functions

$$g(\tau) = \frac{\langle E^*(0)E(\tau) \rangle}{\langle |E|^2 \rangle}$$

$$g^{(2)}(\tau) = \frac{\langle |E(0)|^2 |E(\tau)|^2 \rangle}{\langle |E|^2 \rangle^2}$$

so that the Gaussian approximation is

$$g^{(2)}(\tau) = 1 + |g(\tau)|^2$$

Note that, in actual experiments, one has that the previous equation becomes

$$g^{(2)}(\tau) = 1 + \sigma |g(\tau)|^2 \quad (3.7)$$

where $\sigma < 1$ is an instrumental coherence factor (also called dynamical contrast factor) that depends mainly on the number of coherence areas exposed on the detector's photosensitive area.

3.3.2 Filtering the VV contribution to the depolarized light scattering

Eqs. (3.5) and (3.6) apply when the polarization selection of the scattered light is perfect. In actual experiments one has polarizer filter with a finite rejection factor. The rejection factor f is defined considering the ratio between the intensities I_V and I_H detected after filtering a linearly polarized beam set in parallel and orthogonally to the polarizer axis: $f = I_H/I_V$. We can take in to account the finite value of f approximating the measured correlation functions \tilde{I} as

$$\tilde{I}_{VV}(\mathbf{k}, \tau) \simeq (1 - 2f^{1/2})\alpha^2 F(\mathbf{k}, \tau) + \frac{4}{3}(1 - f^{1/2}/2)I_{VH}(\mathbf{k}, \tau) \quad (3.8)$$

$$\tilde{I}_{VH}(\mathbf{k}, \tau) \simeq 2f^{1/2}\alpha^2 F(\mathbf{k}, \tau) + \frac{4}{3}(3/4 - f^{1/2}/2)I_{VH}(\mathbf{k}, \tau) \quad (3.9)$$

The correction in Equation (3.8) can be neglected in our experiment since we use the best filter available (with $f < 10^{-7}$) to select the scattered light reducing \tilde{I}_{VV} to I_{VV} . On the other hand (3.9) becomes equal to (3.6) only if $2f^{1/2}\alpha^2 \ll 4\beta^2/45$ (or equivalently if the depolarization ratio $r = \beta^2/(15\alpha^2) \gg (3/2)f^{1/2}$). This simply means that only if the polarizer can efficiently depress the polarized component of the scattered wave we have

$$\tilde{I}_{VH} = I_{VH} \quad (3.10)$$

Note that if, contrarily, the polarization ratio is

$$r \sim f^{1/2} \quad (3.11)$$

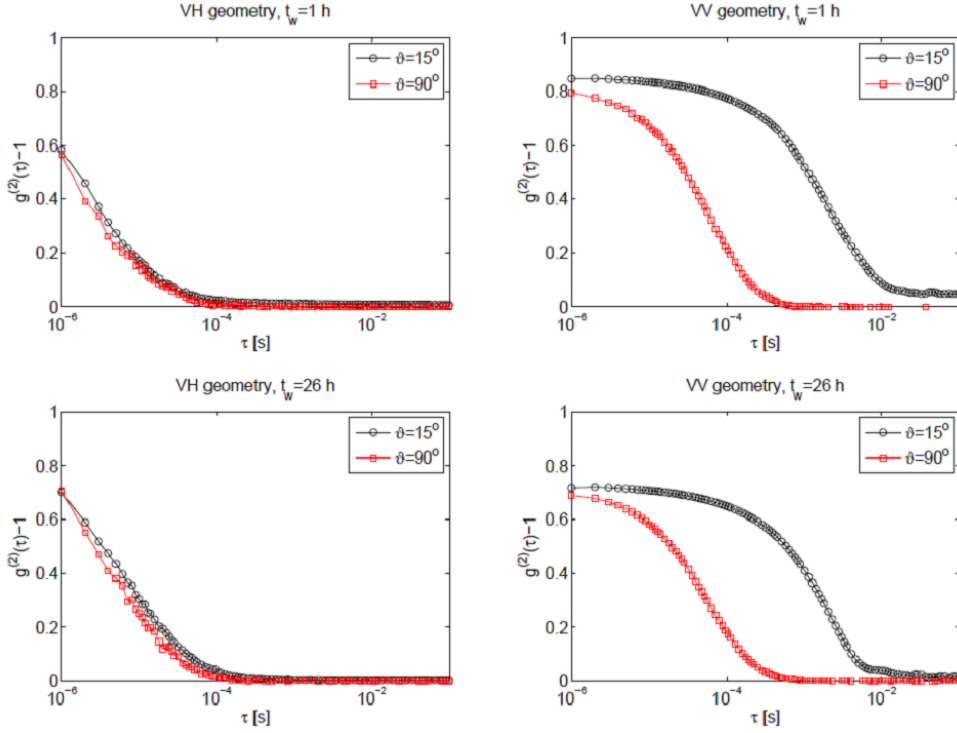


Figure 3.3: VH (left) and VV (right) correlation functions measured at two different angles and at different aging times. Note that the VH correlation function does not depend on the scattering angle ϑ while the VV function does.

there must be a dependence of \tilde{I}_{VH} on \mathbf{k} (and therefore on the scattering angle ϑ) introduced by the term $\alpha^2 F(\mathbf{k}, \tau)$.

We have carried out preliminary tests for our experiment to check if the depolarized time-correlation function shows any significant dependence on the scattering angle. We have measured the correlation functions $g_{VH}^{(2)}$ and $g_{VV}^{(2)}$ at two different scattering angles for Laponite aqueous sample. The sample has a 1 % Laponite weight fraction as the one used in the FDT experiment. The VV geometry and the VH geometry correlation functions have been measured at the scattering angles $\vartheta = 15^\circ, 90^\circ$ and at different aging times. This change in ϑ makes k vary, approximately, of a factor 5. The results are shown in Figure 3.3. As it can be clearly seen the VH correlation function does not depend on \mathbf{k} while the VV function does. The relative difference between the $\vartheta = 15^\circ$ VH function and the $\vartheta = 90^\circ$ VH function is always below the 10 %. We can state that the term $F(\mathbf{k}, \tau)$ in (3.9) is efficiently eliminated by the polarizer giving $\tilde{I}_{VH} = I_{VH}$. Furthermore the \mathbf{k} -dependence is not found in $I_{VH}(\mathbf{k}, \tau)$. This means that that the function g_{VV} is dependent on \mathbf{k} only through $F(\mathbf{k}, \tau)$. The remarkable fact that g_{VH} is independent on the exchanged wavevector will be interpreted in the next Section leading to the result that the VH correlation function is the correlation function of a rotational variable only.

3.3.3 Roto-translational decoupling and separation of timescales

In general a colloidal particle suspended in a solvent moves accordingly to a Brownian motion. Thermal fluctuations in the solvent often push the particle some direction so that its center of mass moves experiencing the random force and the solvent friction. The particle can also rotate in a similar manner since an instantaneous torque can act on it.

If we assume that these rotational and translational motions of the colloidal particle are uncorrelated over appreciable long times. The average defining the scattering functions can be rewritten in a simplified way, if we set.

$$\langle e^{-i\mathbf{k}\cdot\mathbf{r}_j(0)} P_2(\theta_i(\tau)) \rangle = \langle e^{-i\mathbf{k}\cdot\mathbf{r}_j(0)} \rangle \langle P_2(\theta_i(\tau)) \rangle = 0$$

we have that Eqs. (3.5) and (3.6) reduce to

$$I_{VV}(\mathbf{k}, \tau) = F(\mathbf{k}, \tau) \left[\alpha^2 + \frac{4}{45} \beta^2 \langle A(0)A(\tau) \rangle \right] \quad (3.12)$$

$$I_{VH}(\mathbf{k}, \tau) = \frac{\beta^2}{15} \langle A(0)A(\tau) \rangle F(\mathbf{k}, \tau) \quad (3.13)$$

where we have defined $A(\tau) = \sum_i P_2(\theta_i(\tau))$. Note that, to obtain this equations, we do not have to assume that the two are not correlated at all, but only on the timescales (μs - ms) and the length-scales ($q^{-1}(\simeq \lambda) \simeq 500 \text{ nm}$) probed in our experiment. We can clearly see that this approximation separates the function $F(\mathbf{k}, \tau)$ (containing the information about the translation of the colloidal particle) from $\langle A(0)A(\tau) \rangle$ (that is related to the rotation of its symmetry axes) in the VH function. In this way the \mathbf{k} dependence is extracted from the angular correlation function.

When the rotational and the translational relaxation processes are uncorrelated they likely take place on different timescales. If we assume that the characteristic time for the rotational relaxation is much smaller than the characteristic time of the translational one we have that

$$I_{VV}(\mathbf{k}, \tau) \simeq \alpha^2 F(\mathbf{k}, \tau) + \frac{4\beta^2}{45} \langle A(0)A(\tau) \rangle \quad (3.14)$$

$$I_{VH}(\mathbf{k}, \tau) \simeq \frac{\beta^2}{15} \langle A(0)A(\tau) \rangle \quad (3.15)$$

Note that if this approximation is valid the relaxation time of the function I_{VV} is approximately given by the (\mathbf{k} -dependent) relaxation time of $F(\mathbf{k}, \tau)$. An easy consistency check of this approximations can be done verifying if the relaxation times are well separated. A rough estimation of the relaxation time τ_r is given by (twice) the time at which the function $g^{(2)} - 1$ reaches the value σ/e (see Equation (3.7)). This corresponds to model the heterodyne relaxation as a simple exponential, assuming that the factor σ depends weakly on the polarization. In this way σ can be found from the short-time value of g_{VV} : $\sigma \simeq g_{VV}^{(2)}(1\mu\text{s}) - 1$. This estimate gives for the functions g_{VH} and g_{VV} the relaxation times $\tau_{VV} = 120\mu\text{s}$ and $\tau_{VH} = 8\mu\text{s}$ (see Figure 3.3). This is compatible with the results of Ref. (Laura Zulian) in which the (integrated)

relaxation time of the VV correlation function, for a low concentration Laponite solution, is estimated to be around 200 μs at the beginning of its aging process.

In summary we can state that the VH scattering correlation function is, at very good approximation, the correlation function of the angular variable $A(\tau)$ only. This conclusion can be obtained assuming that: (i) The polarized contribution to the VH scattering can be neglected since the rejection factor of the polarizer is high enough. (ii) The rotational and translational motions are not coupled and the rotational characteristic time is much shorter than the translational one. These approximations have been checked with preliminary experimental tests covering the aging time interval studied in the FDT experiment.

3.3.4 Linearity check for the response function

When performing an experiment that measures a response function one should be careful that the response is a linear response. If the field acting on the system is too intense, linear response theory does not apply and the FDT is not satisfied. Being aware of this fact one has to be sure of measuring a linear response when he needs to check if the FDT is violated. In a response experiment we measure the change in dynamic variable induced by an external field. If linear response theory applies the change in the observable A is proportional to the external force. We can thus write that

$$\langle A(\tau) \rangle \propto F\chi(\tau)$$

where F is the external force and $\chi(\tau)$ is the response function associated with the variable A .

In the experiment of Paper III we apply an external electric field to the colloidal solution to measure the induced birefringence. The sample is sandwiched between two plane electrodes contained in a cell provided with windows (Kerr cell) (see Sec. 3.3.5). The quantity we can measure, with the proper optical set-up, is the dynamic birefringence $\delta n(\tau)$ that is proportional to the average of angular variable introduced in Sec.3.3.3 in presence of the external field

$$\delta n(\tau) \propto \langle A(\tau) \rangle$$

The change in A induced by the external field can be rewritten in terms of a response function and of the external perturbation. In our case the Kerr-effect response is proportional to the intensity of the applied electric field. The anisotropic colloidal particle under the effect of the field develops an induced dipole, this interacts itself with the field. It can be shown very easily [112, 113, 114] that the energy contribution introduced by the external electric field is given by $-E_0^2 A(\tau)$, where E_0 . This means that, if the response is linear, the average change in A is proportional to the square of the field modulus:

$$\langle A(\tau) \rangle \propto E_0^2 \chi(\tau) \tag{3.16}$$

This linearity can be checked easily in our experiment since we can monitor the voltage applied to the cell. Indeed the Kerr cell is nothing but a planar capacitor so that the applied voltage is proportional to the field: $E_0^2 \propto V_0^2$. We tested the validity of Equation 3.16 varying the voltage applied to the Kerr

3. AN EXPERIMENTAL STUDY OF THE OFF-EQUILIBRIUM FLUCTUATION-DISSIPATION RELATION

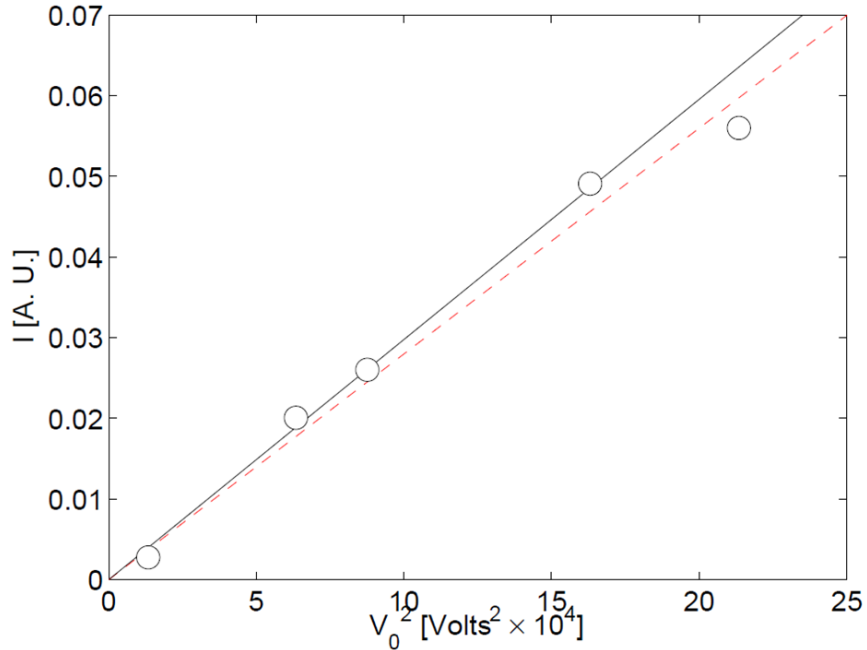


Figure 3.4: Intensity of the birefringence response at $\tau = 1$ ms as a function of the applied voltage. The measurement are performed at the beginning of the aging process of the colloidal solution $t_w \simeq 2$ hours. This preliminary test for the FDT experiment provides a value for the applied field at which the response is a linear response.

cell and measuring the intensity of the induced birefringence at $\tau = 1$ ms. The tests were performed on a Laponite sample at the same concentration of the one used for the FDT experiment and at the beginning of the aging process ($t_w \simeq 2$ hours) where the violation of the theorem is more intense. These data are reported in Figure 3.4, where we can see that a small deviation from linearity is present when $V_0 \simeq 400$ Volts. The FDT experiment has then been carried out in the linear regime for the response, at an applied voltage of 250 Volts.

3.3.5 Experimental set-up

The experiment is designed to give the PCS measurement and the Kerr-effect measurement on the same sample (see Figure 3.5).

The same laser is used as a probe of the spontaneous fluctuations of the orientation dynamics and also as a probe of the induced birefringence when performing the Kerr-effect measurement. This is a mono-mode DPSS green laser ($\lambda = 532$ nm) with a 100 mW power output. The initial polarization of the light produced is 1:100 and the beam is additionally polarized with a standard-grade Glan-Thompson polarizer (P1) with rejection factor $f < 10^{-5}$. The angle that the polarization axis of P1 forms with the vertical (respect to

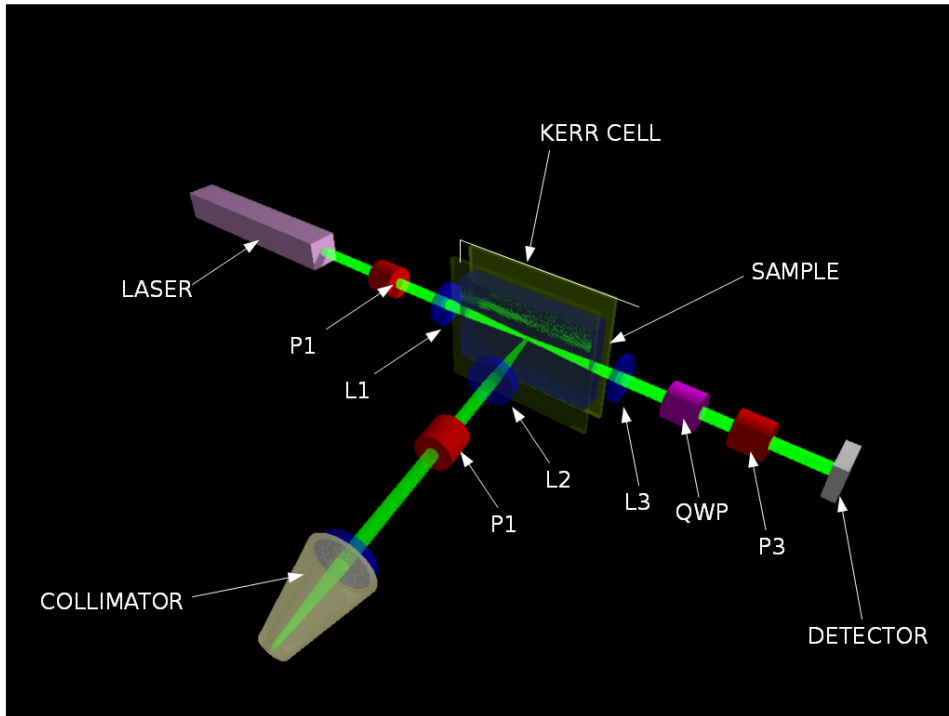


Figure 3.5: Sketch of the experimental set-up. The laser radiation ($\lambda=532$ nm) is polarized by the polarizer P1 and focused by the lens L1 at the center of the cell containing the sample. The scattered light is collected by the lens L2 and selected by the polarizer P2 (orthogonal to P1). A photomultiplier tube (PMT) detects the scattered photons. When no electric pulse is applied to the cell, the output of the PMT is acquired by a computer equipped with a custom digital correlator, this measures and stores the correlation function. The Kerr cell containing the sample is provided by two electrodes connected to a source of amplified electric pulses. The forward-scattered light (rotated by the electrically stimulated sample) is collected by the lens L3 and passes through a quarter-wave plate (QWP) and the polarizer P3 (orthogonal to P1). The transmitted light is detected by a photodiode connected to a digital oscilloscope. This is triggered to the source of electric pulse measuring and storing the Kerr-response function.

3. AN EXPERIMENTAL STUDY OF THE OFF-EQUILIBRIUM FLUCTUATION-DISSIPATION RELATION

the scattering plane) is 30° . The angles for the axis of the polarizers P1 and P3 and the quarter-wave plate (QWP) are selected to maximize the birefringence response [112, 113, 114].

The polarized laser-light is directed to the Kerr-cell by a lens L1 having the focus placed at the center of the cell. The cell is composed by a PVC envelope containing the two plane copper-electrodes (dimensions $4 \times 50 \times 135$ mm) and its provided by glass windows on three sides to let the light pass through. The sample is sandwiched between the two electrodes. Note that one of the electrodes has small hole (5 mm diameter) to allow the light scattered at 90° to pass through.

The voltage is applied to the electrodes by means of a gated RF amplifier connected to a wave generator providing the sinusoidal voltage oscillating at a frequency around 10 MHz. Note that this high frequency component of the applied electric field is not seen by the rotating colloidal discs responding to the square of the applied electric field and having characteristic relaxation time much larger than this inverse frequency. Note also that it is important to use an high-frequency oscillating field in order to suppresses the ionic conduction in the solution that would be present if a static DC field was used. The maximum duration of the high-voltage pulses is restricted to 1 ms.

When the amplifier is activated the response measurement is performed. The light transmitted by medium is collected by the lens L3 having its focus in the center of the cell (coinciding with the focus of L1). This light beam passes through a quarter-wave plate (QWP) set with its principal axis vertical and the analyzer P3 with its polarization forming an angle of 45° with the vertical. P3 is a standard-grade Glan-Thompson polarizer with rejection factor $f < 10^{-5}$. The analyzed light is then measured with an high-speed Si detector whose output is amplified by a custom-built amplifier with a 20 dB gain. This detector is triggered with the RF amplifier. The time-dependent output voltage of the Si detector is measured and stored by means of a digital oscilloscope. It can be shown easily [112, 113, 114] that, with this optical set-up, the intensity of the light detected is proportional to the induced birefringence δn introduced in Sec. 3.3.4. Each response function has been efficiently measured averaging it for approximatively 10 min.

When the electric pulses are not provided to the cell the PCS measurement at a 90° scattering angle are performed. The light is collected by the lens L2 with its focus coinciding with the focus of L1. The scattered electromagnetic wave passes through the analyzer P2 that is an high-quality Glan-Thompson polarizer with rejection factor $f < 10^{-7}$. The polarization axis of P2 is set horizontally respect to the scattering plane. The selected radiation is then collected by a collimator. This directs the light to an optical fiber connected to it that delivers the photons to a photo-multiplier-tube (PMT). The PMT (approx. 300 dark counts) produces a digital output that is acquired by a National Instruments card and processed by the software package *PhotonLab*¹ performing real-time multi-tau autocorrelation. The correlation function are averaged approximatively for 20 min and stored in a computer.

¹*PhotonLab* is a Python extension for the acquisition and analysis of photon counts developed by R. Di Leonardo

Chapter 4

Computer Simulation Studies of The Off-Equilibrium Fluctuation-Dissipation Relation

This chapter summarizes and expands the results of Paper IV. The simulations of Paper IV are focused on the study the FDR, and the related effective temperature, in a special class of liquids. We review the main features of these liquids that characterize their out of equilibrium behavior and the properties of the effective temperature. Moreover we present additional analysis showing some intriguing analogies with spin-glass systems.

4.1 Density-Scaling Effective Temperature in Strongly Correlating Liquids

In Paper IV the FDR is studied in computer simulations applying new theoretical concepts introduced by our group (see Ref.s [115, 116, 117, 118, 119, 120]). These works identified and characterized a class of liquids, named strongly correlating liquids (SCLs), having strong correlation between the instantaneous equilibrium fluctuations of potential energy and virial (at fixed density ρ and temperature T)

$$\Delta W(t) \simeq \gamma \Delta U(t) \quad (4.1)$$

where $W/V = p - Nk_B T/V$ is the configurational (excess) component of the pressure of the liquid system (the virial), and $\Delta U(t) = U(t) - \langle U \rangle$ and $\Delta W(t) = W(t) - \langle W \rangle$ are, respectively, the fluctuations of potential energy and virial. The fundamental property (4.1) can be equivalently expressed by the correlation coefficient between ΔW and ΔU that is close to unity, i.e.

$$\frac{\langle \Delta U(t) \Delta W(t) \rangle}{\sqrt{\langle [\Delta U(t)]^2 \rangle \langle [\Delta W(t)]^2 \rangle}} \simeq 1 \quad (4.2)$$

The validity of the properties (4.1) and (4.2) can be explained by the fact that the pair interaction potential $v_{\text{SCL}}(r)$ of a SCL is very well approximated by an inverse power law potential plus a linear term of the form (see Ref. [118])

$$v_{\text{SCL}}(r) \simeq Ar^{-3\gamma} + Br + C \quad (4.3)$$

where r is the interparticle distance. This implies that a SCL acquires many (but not all) of the scaling properties of systems interacting via inverse power law potential (soft spheres). SCLs include van der Waals liquids like Lennard-Jones type liquids but not, e.g., hydrogen-bonding liquids.

The numerical work of Paper IV illustrate why for SCLs the effective temperature depends only on final density of the glass produce by any cooling and/or compression procedure applied to an equilibrium liquid (see Figure 4.1). This result is a consequence of the existence of isomorphs in the phase digram of SCLs (the concept of isomorphs was introduced in Ref. [120]). The isomorphic line in the (T, ρ) plane is defined by the density scaling equation $\rho^\gamma/T = \text{const}$ and jumping along this line (by changing T and ρ) takes the system instantaneously at the equilibrium. Moreover two transformations bringing the system from two initial states (T_1, ρ_1) and (T_2, ρ_2) that are isomorphs ($\rho_1^\gamma/T_1 = \rho_2^\gamma/T_2$) to the same final state (T_3, ρ_3) show an identical aging behavior. In particular these two transformations must have the same (aging) correlation and response function and, therefore, the same violation factor and the same effective temperature. In practice for each crunch (instantaneous density increase) it exists a quench (instantaneous temperature decrease) with an identical aging pattern. This explains the findings of a previous work [84] on the FDR in which it was found that T_{eff} depends only on the final density for the single-component Lennard-Jones model liquid. These results must hold for all SCLs, and in Paper IV they are verified accurately for the Kob-Andersen binary Lennard-Jones (KABLJ) liquid [121, 122, 123] that belongs to the SCL class. In this article it is also shown a specific counter-example, i.e. the monatomic Lennard-Jones Gaussian liquid (MLJG) [124] (that is not a SCL), for which T_{eff} does not depend only on the final density.

Using another property of SCLs it is also shown that the effective temperature obeys a density-scaling equation

$$\frac{\rho^\gamma}{T_{\text{eff}}} = \text{const} \quad (4.4)$$

This follows from the fact that two jumps $(T_1, \rho_1) \rightarrow (T_2, \rho_2)$ and $(T_3, \rho_3) \rightarrow (T_4, \rho_4)$ between mutually isomorphs states, i.e. with $\rho_1^\gamma/T_1 = \rho_3^\gamma/T_3$ and $\rho_2^\gamma/T_2 = \rho_4^\gamma/T_4$, have identical reduced-unit dynamics and therefore identical scaled (see the next Section for more details) $T\chi(t, t')$ and $C(t, t')$. When this is the case we have the same violation factor in the two jumps $X_2 = X_4$, and Equation (4.4) follows simply by plugging $T_2 = T_{\text{eff}2}X_2$ and $T_4 = T_{\text{eff}4}X_4$ into the equation $\rho_2^\gamma/T_2 = \rho_4^\gamma/T_4$.

The validity of Equation (4.4) can be extended beyond jumps involving only two isomorphs lines. This can be done if we add to the property illustrated above the fact that T_{eff} is independent from the initial and final states if the system is a rapidly relaxing liquid in the initial state and if the system is taken in a very viscous regime by the jump into the final state (T_2, ρ_2) . These extreme transformations in which T_{eff} is well defined independently on the particular initial and final (T, ρ) might be synthetically expressed as $(\rho_1^\gamma/T_1 \sim 0) \rightarrow (\rho_2^\gamma/T_2 \sim \infty)$. Under these conditions Equation (4.4) is valid to a very

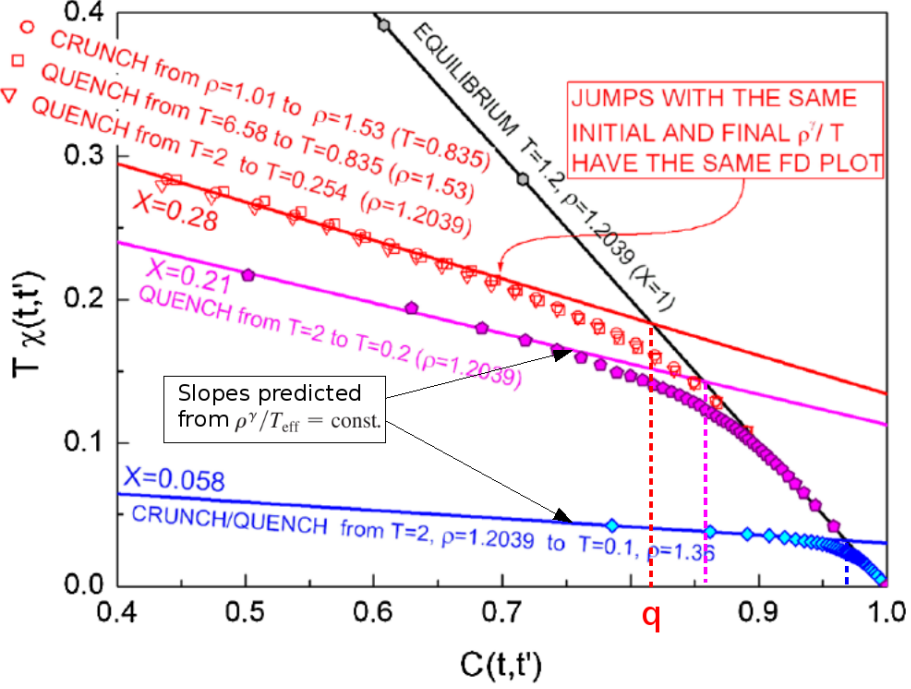


Figure 4.1: FD plot for the KABLJ in various quenches and/or crunches (see Paper IV and Sec. 4.1.1). All FD-plots have fixed $t = 10^4$ (MC steps) and t' varying from 10^3 to 10^4 . All functions plotted here have the same reduced \mathbf{k} -vector with respect to the final density of (○) and the same reduced microscopic time (see Sec. 4.1.1). In the crunch (○) we set $|\mathbf{k}| = 7.81$ corresponding to the reduced \mathbf{k} -vector $|\tilde{\mathbf{k}}| = 6.78$ (see Sec. 4.1.1 for details). The crunch (○) overlaps very well with the quench (◻) that takes the system from an initial state isomorphic to the one of the crunch to the same final state. Note also the good superposition of the additional quench (▽) that takes the system from a state isomorphic to the initial state of (○) to a state isomorphic to the final one of (○). The full lines have the slopes predicted from the density scaling relation Equation (4.4) for $T_{\text{eff}} = T/X$, adjusted only by a vertical shift to fit the data ($-X$ is the slope of the FD-plot at long times). The procedure followed to extract the characteristic value q of C at which the FDT is violated is shown by the vertical dashed lines. This is defined as the intersection between the full lines predicted for the long-timescales FD-plot and the equilibrium FDT line. As it is seen X and q appear to be correlated (see Sec. 4.1.3).

good approximation for any glass produced by an arbitrary densification and/or cooling of the SCL system.

As discussed in Paper IV the implication of this scenario is that the effective temperature of any SCL-glass, resulting from an arbitrary density and/or temperature jump, can be predicted from a single out-of-equilibrium simulation providing the value of γ and of the constant appearing in Equation (4.4).

4.1.1 Simulation details

The SCL systems studied in Paper IV is a binary mixture (80:20) of 1000 particles interacting via Kob-Andersen Lennard-Jones potential. Simulations are performed in the canonical (NVT) ensemble using the Metropolis Monte Carlo (MC) algorithm [125, 126]. Simulation parameters are taken from Ref.s [121, 122, 123]. The observables A and B considered for studying the FDR are

$$A_{\mathbf{k}}(t) = \frac{1}{N} \sum_{j=1}^N \eta_j \cos[\mathbf{k} \cdot \mathbf{r}_j(t)] \quad (4.5)$$

and

$$B_{\mathbf{k}}(t) = 2 \sum_{j=1}^N \eta_j \cos[\mathbf{k} \cdot \mathbf{r}_j(t)] \quad (4.6)$$

where $\mathbf{r}_j(t)$ is the position of the j th particle at time t , \mathbf{k} is the exchanged wavevector, η_j is a bimodal random variable with zero mean assuming the values ± 1 , and the sum is extended to all the N particles of the system (both species). With this choice of variables the correlation function C is the self intermediate scattering function that may also be rewritten as

$$C(t, t') = \langle A_{\mathbf{k}}(t) B_{\mathbf{k}}(t') \rangle = \frac{1}{N} \sum_{j=1}^N \langle \cos[\mathbf{k} \cdot (\mathbf{r}_j(t) - \mathbf{r}_j(t'))] \rangle \quad (4.7)$$

The integrated linear response function $\chi(t, t')$ is the variation of the variable $A_{\mathbf{k}}$ to the infinitesimal field h (coupled to $B_{\mathbf{k}}$) that introduces an energy contribution $-hB_{\mathbf{k}}$. If the field h depends on time as a delta function $h = h\delta(t - t')$ the response function can be rewritten as

$$\chi(t, t') = \int_{t'}^t dt'' \left. \frac{\partial \langle A_{\mathbf{k}}(t) \rangle}{\partial h(t'')} \right|_{h \rightarrow 0} \quad (4.8)$$

In Paper IV we refer often to the reduced-units dynamics. The correct reduced units for the Newtonian dynamics and for the Brownian dynamics were reviewed in Ref. [120]. For the MC dynamics the reduced length is given by $\tilde{l} = \rho^{1/3}l$. This defines the reduced k-vector $\tilde{\mathbf{k}} = \rho^{-1/3}\mathbf{k}$ implying that, given a wave-vector \mathbf{k}_1 at density ρ_1 , the k-vector with equivalent $\tilde{\mathbf{k}}$ at density ρ_2 is $\mathbf{k}_2 = (\rho_2/\rho_1)^{1/3}\mathbf{k}_1$. The microscopic time τ in the MC dynamics is set by the maximum random step attempted by the particle δ_{\max} , i.e. $\tau = \tau(\delta_{\max})$. This is fixed to minimize the relaxation time of the (equilibrium) correlation function at a given intermediate T and ρ (we set δ_{\max} at the same value chosen in Ref.s [122, 123], minimizing the decay-time of C at $T = 0.75$ and $\rho = 1.2$). It follows that two MC simulations (performed at ρ_1 and ρ_2 respectively) have the

same reduced time $\tilde{\tau}$ if $\tilde{\delta}_{\max}$ is the same, that is when $\delta_{\max 2} = (\rho_1/\rho_2)^{1/3}\delta_{\max 1}$. However note that this is a minor adjustment of δ_{\max} : in the density range explored (in our simulations ρ varies from 1 to 1.53) δ_{\max} changes at most 15%.

The response function is computed without applying the perturbing field following the new method introduced by L. Berthier in Ref. [123] for MC simulations of liquid systems. To illustrate the method let us recall that in a MC simulation [125, 126] we start from the system having a configuration $\{\mathbf{r}^N\}_t$ at time t given by the position of each of the N particles

$$\{\mathbf{r}^N\}_t = \{\mathbf{r}_1(t), \dots, \mathbf{r}_N(t)\} \quad (4.9)$$

To probe the phase space statistically a new random configuration $\{\mathbf{r}^N\}'_t$ is proposed. The acceptance rate of this move, indicated by $\mathcal{A}(\{\mathbf{r}^N\}_t \rightarrow \{\mathbf{r}^N\}'_t)$, is set by the energy difference of the configurations $\{\mathbf{r}^N\}_t$ and $\{\mathbf{r}^N\}'_t$ according to the Metropolis rule [125, 126].

The system might assume the trial configuration at the next time-step $t+1$, i.e. $\{\mathbf{r}^N\}_{t+1} = \{\mathbf{r}^N\}'_t$, or remain in the previous configuration, $\{\mathbf{r}^N\}_{t+1} = \{\mathbf{r}^N\}_t$, depending on the acceptance rate \mathcal{A} . This defines the transition probability W as

$$W(\{\mathbf{r}^N\}_t \rightarrow \{\mathbf{r}^N\}_{t+1}) = \begin{cases} \mathcal{A}(\{\mathbf{r}^N\}_t \rightarrow \{\mathbf{r}^N\}'_t) \\ \text{if } \{\mathbf{r}^N\}_{t+1} = \{\mathbf{r}^N\}'_t \\ \\ 1 - \mathcal{A}(\{\mathbf{r}^N\}_t \rightarrow \{\mathbf{r}^N\}'_t) \\ \text{if } \{\mathbf{r}^N\}_{t+1} = \{\mathbf{r}^N\}_t \end{cases} \quad (4.10)$$

The probability $\mathcal{P}_\alpha(t' \rightarrow t)$ that the system follows a specific trajectory α taking it from the configuration $\{\mathbf{r}^N\}_{t'}^\alpha$ at time t' to the configuration $\{\mathbf{r}^N\}_t^\alpha$ at time t is given by the combined transition probabilities W , i.e.

$$\mathcal{P}_\alpha(t' \rightarrow t) = \prod_{t''=t'}^{t-1} W(\{\mathbf{r}^N\}_{t''}^\alpha \rightarrow \{\mathbf{r}^N\}_{t''+1}^\alpha) \quad (4.11)$$

An average quantity in the MC simulation is given by the average over all the M sampled trajectories weighted by their probability so that the correlation function (4.7) becomes

$$C(t, t') = \langle A_{\mathbf{k}}(t)B_{\mathbf{k}}(t') \rangle = \frac{1}{M} \sum_{\alpha=1}^M \mathcal{P}_\alpha(t' \rightarrow t) A_{\mathbf{k}}(\{\mathbf{r}^N\}_t^\alpha) B_{\mathbf{k}}(\{\mathbf{r}^N\}_{t'}^\alpha) \quad (4.12)$$

Similarly the response function (4.8) of the variable $A_{\mathbf{k}}$ can be rewritten as

$$\chi(t, t') = \frac{\partial}{\partial h} \left[\frac{1}{M} \sum_{\alpha=1}^M \mathcal{P}_\alpha(t' \rightarrow t) A_{\mathbf{k}}(\{\mathbf{r}^N\}_t^\alpha) \right]_{h \rightarrow 0} \quad (4.13)$$

were the probabilities are now affected by the infinitesimal field h .

4. COMPUTER SIMULATION STUDIES OF THE OFF-EQUILIBRIUM
FLUCTUATION-DISSIPATION RELATION

The method proposed in Ref. [123] is based on the idea of taking the derivative of Equation (4.13) inside the sum in order to differentiate and take the limit $h \rightarrow 0$ before computing the average. In this way we will be able to compute the response function without actually including the external-field contribution $-hB_{\mathbf{k}}$ into the energy of the system. To show this in practice we rewrite the probability of Equation (4.11) using the identity $x = \exp[\ln(x)]$ as

$$\mathcal{P}_\alpha(t' \rightarrow t) = \exp \left[\sum_{t''=t'}^{t-1} \ln \left[W(\{\mathbf{r}^N\}_{t''}^\alpha \rightarrow \{\mathbf{r}^N\}_{t''+1}^\alpha) \right] \right] \quad (4.14)$$

If we take the derivative with respect to h of Equation (4.14) we get

$$\frac{\partial}{\partial h} \mathcal{P}_\alpha(t' \rightarrow t) = \sum_{t''=t'}^{t-1} \frac{\partial}{\partial h} \ln \left[W(\{\mathbf{r}^N\}_{t''}^\alpha \rightarrow \{\mathbf{r}^N\}_{t''+1}^\alpha) \right] \mathcal{P}_\alpha(t' \rightarrow t) \quad (4.15)$$

Using Equation (4.15) into Equation (4.13) we obtain

$$\begin{aligned} \chi(t, t') = & \\ & \frac{1}{M} \sum_{\alpha=1}^M \mathcal{P}_\alpha(t' \rightarrow t) A_{\mathbf{k}}(\{\mathbf{r}^N\}_t^\alpha) \times \\ & \sum_{t''=t'}^{t-1} \left[\frac{\partial}{\partial h} \ln \left[W(\{\mathbf{r}^N\}_{t''}^\alpha \rightarrow \{\mathbf{r}^N\}_{t''+1}^\alpha) \right] \right]_{h \rightarrow 0} \end{aligned} \quad (4.16)$$

Notice that the limit $h \rightarrow 0$ has been taken for all the terms in Equation (4.16) so that the probability $\mathcal{P}^\alpha(t' \rightarrow t)$ has reduced to the un-perturbed one. Introducing the quantity

$$R(t' \rightarrow t) = \sum_{t''=t'}^{t-1} \left[\frac{\partial}{\partial h} \ln \left[W(\{\mathbf{r}^N\}_{t''}^\alpha \rightarrow \{\mathbf{r}^N\}_{t''+1}^\alpha) \right] \right]_{h \rightarrow 0} \quad (4.17)$$

Equation (4.16) that can be rewritten in the simpler form

$$\chi(t, t') = \langle A_{\mathbf{k}}(t) R(t' \rightarrow t) \rangle \quad (4.18)$$

that is now an average on the un-perturbed trajectories.

As we have shown the issue of computing $\chi(t, t')$ has been reduced to the simpler task of obtaining the function $R(t' \rightarrow t)$ that is composed by the derivative of the logarithms of the transition probabilities (Equation (4.18)) with $h \rightarrow 0$. To do this practically in a MC-Metropolis simulation we can proceed examining the transition probabilities in all the possible situations. In the case the trial configuration $\{\mathbf{r}^N\}'_t$ is accepted (i.e. $\{\mathbf{r}^N\}_{t+1} = \{\mathbf{r}^N\}'_t$) we have

$$\begin{aligned}
 W(\{\mathbf{r}^N\}_t \rightarrow \{\mathbf{r}^N\}_{t+1}) = \\
 \exp \left[-\frac{1}{T} [U(\{\mathbf{r}^N\}_{t+1}) - hB(\{\mathbf{r}^N\}_{t+1}) + \right. \\
 \left. - U(\{\mathbf{r}^N\}_t) + hB(\{\mathbf{r}^N\}_t)] \right] \quad (4.19)
 \end{aligned}$$

when

$$U(\{\mathbf{r}^N\}_{t+1}) - hB(\{\mathbf{r}^N\}_{t+1}) - U(\{\mathbf{r}^N\}_t) + hB(\{\mathbf{r}^N\}_t) > 0 \quad (4.20)$$

and

$$W(\{\mathbf{r}^N\}_t \rightarrow \{\mathbf{r}^N\}_{t+1}) = 1 \quad (4.21)$$

when

$$U(\{\mathbf{r}^N\}_{t+1}) - hB(\{\mathbf{r}^N\}_{t+1}) - U(\{\mathbf{r}^N\}_t) + hB(\{\mathbf{r}^N\}_t) \leq 0 \quad (4.22)$$

According to these Equations we have that the needed derivatives are given by

$$\frac{\partial}{\partial h} \ln [W(\{\mathbf{r}^N\}_t \rightarrow \{\mathbf{r}^N\}_{t+1})]_{h \rightarrow 0} = \frac{1}{T} [B(\{\mathbf{r}^N\}_{t+1}) - B(\{\mathbf{r}^N\}_t)] \quad (4.23)$$

when $U(\{\mathbf{r}^N\}_{t+1}) - U(\{\mathbf{r}^N\}_t) > 0$, or when $U(\{\mathbf{r}^N\}_{t+1}) - U(\{\mathbf{r}^N\}_t) = 0$ and $B(\{\mathbf{r}^N\}_{t+1}) - B(\{\mathbf{r}^N\}_t) < 0$. Differently we have that

$$\frac{\partial}{\partial h} \ln [W(\{\mathbf{r}^N\}_t \rightarrow \{\mathbf{r}^N\}_{t+1})]_{h \rightarrow 0} = 0 \quad (4.24)$$

when $U(\{\mathbf{r}^N\}_{t+1}) - U(\{\mathbf{r}^N\}_t) < 0$, or when $U(\{\mathbf{r}^N\}_{t+1}) - U(\{\mathbf{r}^N\}_t) = 0$ and $B(\{\mathbf{r}^N\}_{t+1}) - B(\{\mathbf{r}^N\}_t) \geq 0$.

The last case to consider is when the trial configuration is rejected. When this happens the configuration remains the same $\{\mathbf{r}^N\}_{t+1} = \{\mathbf{r}^N\}_t \neq \{\mathbf{r}^N\}'_t$ and the transition probability is $1 - W(\{\mathbf{r}^N\}_t \rightarrow \{\mathbf{r}^N\}_{t+1})$, where W is given by Equation (4.19) having $\{\mathbf{r}^N\}_{t+1}$ replaced by $\{\mathbf{r}^N\}'_t$ in the expression. In this situation we have

$$\begin{aligned}
 \frac{\partial}{\partial h} \ln [W(\{\mathbf{r}^N\}_t \rightarrow \{\mathbf{r}^N\}_{t+1})]_{h \rightarrow 0} = \\
 \left(\frac{1}{T} \right) \frac{B(\{\mathbf{r}^N\}'_t) - B(\{\mathbf{r}^N\}_t)}{1 - \exp [U(\{\mathbf{r}^N\}'_t) - U(\{\mathbf{r}^N\}_t)]} \quad (4.25)
 \end{aligned}$$

Concluding by computing the Equations (4.23), (4.24) and (4.25) we can calculate the response function without applying the external field as proposed in Ref. [123]. This method, used in Paper IV, provides a great simplification since one does not have to run many preliminary simulations to check the linearity of the response function in the field (see also Section 3.3.4).

4.1.2 Equilibrium and off-equilibrium energy landscape in strongly correlating liquids

Studying in detail the off-equilibrium dynamics of the SCL we have investigated the relationship between the inherent state (IS) energy [127, 128, 129] and the effective temperature by additional simulations. While the fast vibrational dynamics is associated with the rapid oscillations of the system in a potential energy minimum, the transitions between ISs correspond to the slow structural rearrangements. This schematic division suggests that the effective temperature measured from the FDR individuates the typical basins visited during aging as it was originally suggested by F. Sciortino and P. Tartaglia in Ref. [129].

To test these ideas we have calculated the off-equilibrium average IS energy $\langle e_{\text{IS}}(t) \rangle$ for a number of off-equilibrium jumps at long times ($t = 10^4$ MC steps), and in the same simulation we have obtained the effective temperature T_{eff} from the FDR. After T_{eff} is determined in the off-equilibrium simulation, we have simulated the system at the equilibrium at $T = T_{\text{eff}}$ and we have computed the equilibrium average IS energy $\langle e_{\text{IS}} \rangle_{T=T_{\text{eff}}}$. In Figure 4.2 we show $\langle e_{\text{IS}} \rangle_{T=T_{\text{eff}}}$ as a function of $\langle e_{\text{IS}}(t) \rangle$. As it can be seen from Figure 4.2 the equilibrium and the off-equilibrium IS energies are found to coincide to a very good approximation, i.e.

$$\langle e_{\text{IS}} \rangle_{T=T_{\text{eff}}} = \langle e_{\text{IS}}(t) \rangle \quad (4.26)$$

This means that for the SCL system T_{eff} indicates which part of the potential energy landscape is visited during the aging with respect to the equilibrium states. In contrast (see Figure 4.2), this interpretation is clearly not valid (Equation (4.26) does not apply) for the (non-SCL) MLJG system, confirming the idea that SCLs have simpler glassy behavior than liquids in general.

The correspondence between the equilibrium and off-equilibrium ISs suggests that a SCL system has to follow a precise aging pattern during the thermalization. This route to the dynamical arrest is restricted to the same ISs that the system visits by a series of infinitesimal changes of temperature (at fixed volume) taking the liquid from the initial IS to the IS in which it remains trapped during aging. So far we have found no clear way to obtain this aging property directly from the constitutive properties of the SCLs (Equations (4.1), (4.2), (4.3)).

Moreover these considerations do not clarify why an aging non-SCL system visits ISs that it would not probe at the equilibrium. In this case it is interesting to consider that by simply quenching a non-SCL system this might be avoiding an equilibrium liquid-to-liquid transition [130, 131, 132, 133, 134, 135]. This idea has to be confirmed more accurately by comparing the structure of an aging and of an equilibrium non-SCL system as the MLJG liquid. Nevertheless this scenario may be understood qualitatively considering the typical behavior

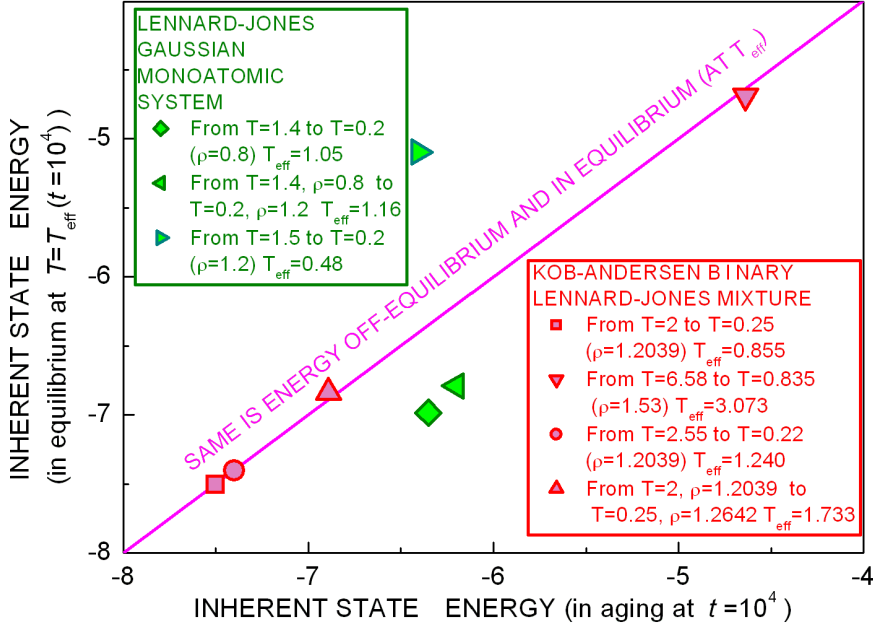


Figure 4.2: Comparison between the (average) equilibrium inherent states energy (at $T = T_{\text{eff}}(t)$) and the off-equilibrium inherent states energy (at time t) in several jumps in the glass (see legend). For the KABLJ systems (red symbols) these two quantities coincide, indicating that the aging system at t visits the same inherent states of the system in equilibrium at the temperature $T = T_{\text{eff}}(t)$ given by the FDR. This is clearly not the case for the MLJG systems (green symbols). The energy values of the MLJG are scaled by a factor 2.5 for an easier comparison with the KABLJ energies.

of the structure of water or silicon upon cooling. These systems are non-SCL systems as discussed in Ref.s [117, 120] and they shows clearly the emergence of a very open and empty structure at low temperatures promoted by the formation of a large number directional bonds. It reasonable to imagine that the formation of this structured liquid requires the system to be annealed at some temperature that is low enough to favor the new structure. If such a complicated liquid were taken out of the equilibrium by a sudden temperature decrease starting from high temperature the different structure could still be the favored one, but the significant rearrangements required to form it would be highly suppressed. Note that this possible scenario is qualitatively analogous to the description of an avoided crystallization leading to a stable supercooled-liquid regime [136, 137, 138, 6]. In practice we could think that the equilibrium non-SCL system at $T = T_{\text{eff}}$ is very different from the aging system since the latter did not have time to perform the transition to the new liquid phase. This picture would qualitatively explain why the off-equilibrium system is visiting some ISs that are un-accessible at the equilibrium. Furthermore this scenario

suggests to allow density to change in order to obtain an equilibrium system structurally more similar to the aging one defining in this way some sort of effective density. One can imagine that, in the case of water, by restricting the liquid in smaller volumes (obtaining a higher pressure) we could suppress the open structure creating an equilibrium system that has a short-range order more similar to the one of the quenched system (at large volume). Certainly more work is needed to clarify these issues and computer simulations might open the way to a new series of studies.

4.1.3 A correlation between the non-ergodicity factor and the violation factor

The results of Paper IV, summarized at the beginning of Sec. 4.1, focused mainly on the FDT violation factor and the effective temperature. Another interesting feature to consider is the value of the correlation function $C(t, t')$ at which the standard FDT is violated. This parameter represents off-equilibrium non-ergodicity factor of the structural glass. To define sharply the characteristic value q of C at which the FDT is violated we can proceed as follows (as it is shown in Figure 4.1). First we fit the points of the FD-plot corresponding to long time-scales $(t - t')/t' \gg 1$ with a straight line (the slope of this line defines the violation factor X), then we identify the intersection of this line with the FDT line (the abscissa of this intersection point defines q). Notice that this is the same approach used in Paper III to define q .

It is quite clear from Figure 4.1 that if X is lower the deviation from the FDT appears at values of $C(t, t')$ closer to the unity. On a more general ground we already know, from the properties of SCLs illustrated in the previous Section, that the violation factor is a function only of the final state of the transformation. Mathematically speaking we have that $X = X(\rho_2^\gamma/T_2)$, when $(\rho_1^\gamma/T_1 \sim 0) \rightarrow (\rho_2^\gamma/T_2 \sim \infty)$. In particular if we plug the definition $T_{\text{eff}} = T/X$ (Equations (3.3)) into Equation (4.4) we obtain

$$X(\rho^\gamma/T) = \text{const} \frac{T}{\rho^\gamma} \quad (4.27)$$

where we have dropped the index 2 since it is clear that from now on we refer only to the final state of the off-equilibrium jump.

As stated in Sec. 4.1 jumping between mutually isomorphic states gives the same scaled $T\chi(t, t')$ and $C(t, t')$ and therefore the same q . Moreover it is found that whenever Equation (4.4) applies we have that also q depends only on the scaling parameter of the final state ρ^γ/T . This can be appreciated from Figure 4.3 that reports the values of q and X for a number of jumps in the glass not only involving initial and final state points that are mutually isomorphic. From this Figure it is clear that, to a very good approximation, each value q corresponds to a single value of $X = X(\rho^\gamma/T)$ leading us to conclude that $q = q(\rho^\gamma/T)$. As we did for X we can state that the non-ergodic factor q depends only on the final scaling parameter but, unfortunately, we do not know a priori the functional form of $q(\rho^\gamma/T)$. Differently we know that X is given by the simple Equation (4.27).

It is intriguing to notice that a very similar situation, where X and q are functions of the same thermodynamic parameter, is found in those spin systems with quenched disorder exhibiting the so called one-step replica-breaking

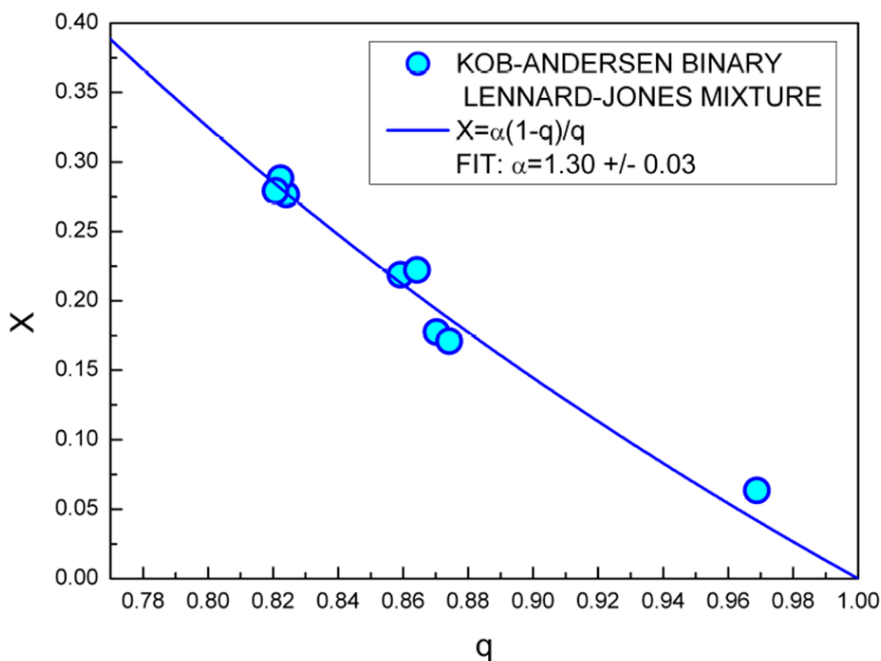


Figure 4.3: Violation factor as a function of the non-ergodicity factor in the off-equilibrium simulations of the KABLJ for a number of off-equilibrium temperature and/or density jumps not only involving initial and final state points that are mutually isomorphic. Notice that, to a very good approximation, each value q corresponds to a single value of $X = X(\rho^\gamma/T)$, indicating also $q = q(\rho^\gamma/T)$. The full line is a fit with the Equation (4.30) similar to (4.30) describing the connection between q and X in the p -spin spherical model.

(1-RSB) scenario [139, 140, 141, 142, 143, 144, 145]. More generally these spin-systems have a number of properties in common with structural supercooled liquids and glasses. For example they show a two step-relaxation in the equilibrium correlation function and a two time-scales violation of the FDT as found in structural glasses. Moreover some of their thermodynamic observables, as the specific heat, show a temperature behavior similar to the one found in supercooled structural systems. These analogies were noticed by Kirkpatrick, Thirumalai and Wolynes in a series of works [146, 147, 148] and led to the formulation of the Random First Order Transition Theory of the glass transition [149, 150, 151, 152].

An important spin-glass model belonging to the 1-RSB class is the spherical p -spin model [153, 154, 20, 144, 145], since its statics and dynamics can be solved exactly. This model is defined by the Hamiltonian:

$$H = - \sum_{1 \leq i_1 < \dots < i_p \leq N} J_{i_1 \dots i_p} S_{i_1} \dots S_{i_p} \quad (4.28)$$

where the S_i are N continuous spins interacting in groups of p elements via

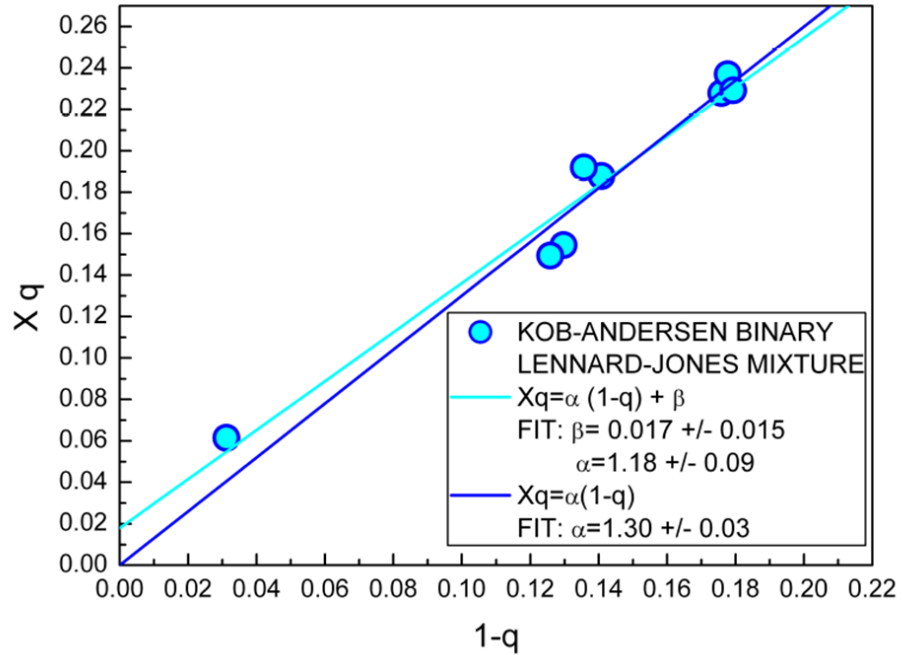


Figure 4.4: Xq plotted as function of $(1 - q)$. The full lines are fits with Equation (4.31) and (4.31) (parameters from the off-equilibrium simulations of the KABLJ). Notice that the fitting function (4.32) has an intercept compatible with zero.

the random couplings $J_{i_1..i_p}$. These couplings are distributed according to a Gaussian with variance equal to $(J^2 p! N^{1-p}/2)$. A final requirement of the model is that the spins satisfy the global constraint $\sum_i S_i^2 = N$. The dynamics of this model can be solved exactly at the equilibrium obtaining a two-step relaxation for the spin-spin correlation function [154, 145]. Out of equilibrium it can be shown that a FDR with the same form of Equation (3.2) holds [154, 144]. Finally it can be proved [154, 144] that the value of the spin-spin correlation function q at which the FDT is violated and the violation factor X are related by the following equation

$$X = \frac{(p-2)(1-q)}{q} \quad (4.29)$$

It turns out that an equation similar to Equation (4.29) can be used to describe the bound between X and q observed for the KABLJ liquid illustrated above. The function relating X to q in the KABLJ can be well fitted by a function of the form (see Figure 4.3)

$$X = \alpha \frac{1-q}{q} \quad (4.30)$$

where α is a free fitting parameter. To test further the quality of the function (4.30) in describing the correlation between X and q we fit the quantity Xq as a function of $(1 - q)$ with a straight line forced to pass through zero and a straight line with free intercept (see Figure 4.4). This corresponds to fit with the two functions

$$Xq = \alpha(1 - q) \tag{4.31}$$

and

$$Xq = \alpha(1 - q) + \beta \tag{4.32}$$

As seen from Figure 4.4 the fitting function (4.32) has a intercept compatible with zero, making the simpler Equation (4.31) preferable for fitting. It has also to be noticed that, if Equation (4.31) applies well, from a single out of equilibrium jump we can not only predict the effective temperature but the full FD-plot. Indeed from a single quench simulation we can obtain γ , the constant of Equation (4.27) as $\text{const} = X\rho^\gamma/T$, and the parameter α of Equation (4.31) as $\alpha = Xq/(1 - q)$. Once these values are obtained from a single off-equilibrium simulation, we can predict X and q by using Equation (4.27) $X = \text{const} T/\rho^\gamma$ and

$$q(\rho^\gamma/T) = \frac{\alpha(\rho^\gamma/T)}{\alpha(\rho^\gamma/T) + \text{const}} \tag{4.33}$$

The FD-plots predicted from Equations (4.27) and (4.33) are illustrated in Figure 4.5 (colored surface). In Figure 4.5 the prediction is compared with three FD-plots corresponding to off-equilibrium jumps to states with well separated ρ^γ/T .

Perhaps it is interesting to consider more in detail the qualitative physical meaning of an equation of the kind (4.29)-(4.30) [154, 145, 144]. To do this we recall that the phase space of the p -spin model can be uniquely partitioned in ergodic sub-components (states) separated by free-energy barriers diverging in the thermodynamic limit. When the spin-system is taken out of equilibrium by a quench below the dynamic transition temperature T_d it remains trapped for ever in some of these states with higher energy than the final equilibrium state. In this context the parameter q represents the overlap between configuration belonging to same state for one single realization of the disordered couplings J . Qualitatively speaking q quantifies the similarity between two different spin configurations belonging to the same free-energy basin that have evolved for a large, but finite, time. Notice that $q = 1$ if we consider the overlap between two copies of the same configuration. Alternatively $1 - q$ can be interpreted as a measurement of the characteristic size of the sub-component of the phase space, i.e. a large q indicates that the configurations of a single portion of phase space are very close to each other meaning that the component is, in some sense, small. On the other hand $1 - X$ is the probability that two randomly chosen configurations belong to the same component of the phase space, and therefore that they have overlap q . This means that, if X is small, the trapping states for the off-equilibrium dynamics have small degeneracy (i.e. they have small configurational entropy), so that there is an high probability that two configurations fall in the same state. Contrarily if X is large the

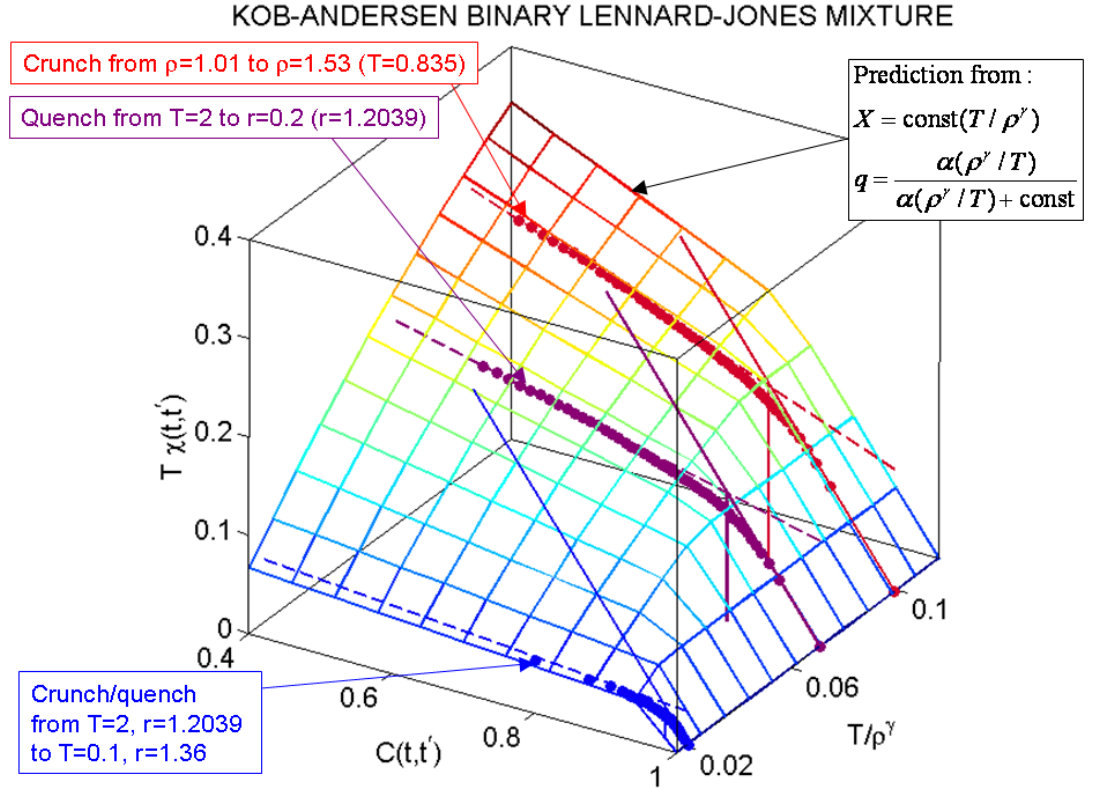


Figure 4.5: Three-dimensional FD-plots for the KABLJ. The surface is predicted via Equations (4.27) and (4.33). This is compared with three FD-plots corresponding to off-equilibrium jumps to states with well separated ρ^γ/T .

off-equilibrium states have large multiplicity and it is un-probable that two configurations belong to the same state.

According to these considerations Equation (4.29) gives us a qualitative description of the topological properties of the free-energy landscape of the p -spin model. In particular it tells us that if those trapping states dominating the off-equilibrium dynamics are small (and with high overlap) they are few, differently if those states are large (and with small overlap) they are many. At this point is natural to ask if the same qualitative correlation between X and q seen for the KABLJ glass is telling us that a similar structure of the landscape is present in this liquid system. This would be interesting to study in more detail, especially using the frequently employed mapping between the states and potential energy minima in structural supercooled liquids and glasses mentioned above [127, 128, 129].

Chapter 5

Experimental Studies of The Heterogeneous Dynamics

This Chapter is dedicated to the study of the heterogeneous dynamics. We start by giving some useful definitions of the multi-point susceptibilities. Moreover we review the relationships linking the three-point susceptibility to the temperature-induced change in a standard correlation function. We illustrate the main findings of Paper V based on these theoretical developments. Finally we present a new experiment capable of measuring directly the four-point susceptibility in systems of nano-particles.

5.1 Multi-Point Susceptibilities

As mentioned in Section 1.4 an interesting feature of the structural dynamics of supercooled and glassy systems is its spatial heterogeneity. Qualitatively speaking this corresponds to say that some of the atoms (or of the molecules) constituting the liquid system move very differently from the average on the timescale of the structural relaxation. The existence of this heterogeneous motion imply a that the dynamics fluctuates considerably among space also meaning that the molecular motions are correlated. The situation is captured very clearly by computer simulations as seen in Figure 5.1(A) and (B). In this Figure we show the displacement vector-field

$$\Delta \mathbf{r}_j(t \simeq \tau_\alpha) = \mathbf{r}_j(t \simeq \tau_\alpha) - \mathbf{r}_j(0)$$

of the particles for the KABLJ liquid (see Section 4.1.1) after a time comparable to the structural relaxation time. The system is simulated by MC dynamics at density $\rho = 1.2$ and temperature $T = 0.42$. As it is seen from Figure 5.1(A) a large number of particles in left-upper corner of the simulation box has much larger displacement than the rest of the particles. This can be seen even more clearly in Figure 5.1(B) where a slice of the 3D box has been reproduced. This shows a rather heterogeneous displacement field evidenced by the coloring.

Computer simulations have easy access to the study of this scenario, although they are restricted to short time-scales of few hundreds of nanoseconds. In this context multi-point susceptibilities have been use very often to statistically characterize the heterogeneous dynamics [25, 26, 27, 28]. To fix the ideas let us consider a standard (two-point) correlation function C [17, 18, 19]

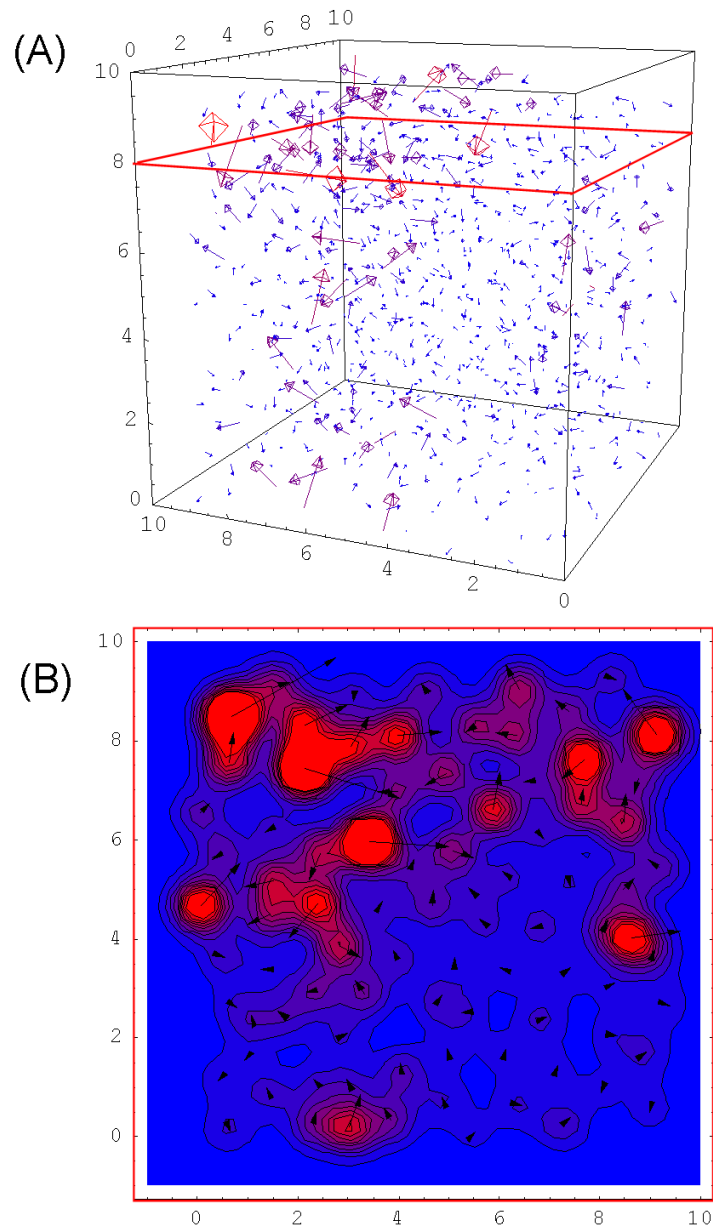


Figure 5.1: **(A)** displacement field of the particles of a Kob-Andersen Binary Lennard Jones liquid simulated for a time of the order of the relaxation time at $T \simeq 0.42$ and $\rho = 1.2$. The heterogeneous motion is clearly seen as a group of particles in left-upper corner of the simulation box having a much larger displacement than the average. The plane evidenced by the red lines indicates the slice of the box reproduced in **(B)** this is taken at height $z \simeq 8$. **(B)** shows the displacement field of this slice when projected on the horizontal plane (vectors). The coloring is produced by smoothing a function that associates to the position of each particle at $t = 0$ a color close to red if the displacement is high and close to blue if the displacement is low.

(see also Section 1.3 and 4.1.1) of the fluctuations of the variable A at the equilibrium

$$C(t) = \langle \mathcal{C}(0, t) \rangle = \langle \delta A(t) \delta A(0) \rangle \quad (5.1)$$

where and $\mathcal{C}(0, t) = \delta A(t) \delta A(0)$ and $\delta A(t) = A(t) - \langle A \rangle$ is the instantaneous fluctuation of the observable A . As illustrated in Section 1.3 and 4.1.1 the correlation function $C(t)$ represents the statistical quantity describing the spontaneous dynamics of a many-body system.

From the qualitative description of the heterogeneities given above, it is clear that when the dynamics is heterogeneous one expects large deviations of the molecular motions from the average and, consequently, large fluctuations of the de-correlations from the average correlation function (5.1). It is therefore natural to associate the heterogeneity with the fluctuations of the whole correlation function around its average value by defining a four-point susceptibility $\chi_4(t)$ as the variance of the function $C(t)$

$$\chi_4(t) = N \left[\langle [\delta A(t) \delta A(0)]^2 \rangle - \langle \delta A(t) \delta A(0) \rangle^2 \right] \quad (5.2)$$

that may be rewritten more synthetically as

$$\chi_4(t) = N \left[\langle \mathcal{C}^2(0, t) \rangle - \langle \mathcal{C}(0, t) \rangle^2 \right] = N \langle [\delta \mathcal{C}(0, t)]^2 \rangle \quad (5.3)$$

where N is the number of particles of the system and $\delta \mathcal{C}(0, t) = \mathcal{C}(0, t) - \langle \mathcal{C}(0, t) \rangle$. Note that multiplying the variance $\langle [\delta \mathcal{C}(0, t)]^2 \rangle$ by the factor N is needed in order to promote $\chi_4(t)$ to be an intensive (system's size independent) quantity that can be associated with a well defined spatial extent of the dynamical correlations. This is because a properly normalized auto-correlation function is also an intensive (dynamic) quantity. This is the case, for example, of the self-intermediate scattering function defined in Section 4.1.1. For this reason the fluctuations of the correlation function are expected to decrease as

$$\langle [\delta \mathcal{C}(0, t)]^2 \rangle \sim \frac{1}{N} \quad (5.4)$$

in the thermodynamic limit. The situation is completely analogous to the more familiar case of an intensive static quantity [17, 18, 19]. In general the variance $\langle (\delta \mathcal{O})^2 \rangle$ of any intensive observable \mathcal{O} decreases when the system's size grows as

$$\langle (\delta \mathcal{O})^2 \rangle \sim \frac{1}{N} \quad (5.5)$$

while its average stays constant ($\langle \mathcal{O} \rangle \sim \text{const}$) as N grows. This gives the usual small fluctuations, with respect to the average values, in the thermodynamic limit¹

$$\frac{\langle (\delta \mathcal{O})^2 \rangle}{\langle \mathcal{O} \rangle^2} \sim \frac{1}{N} \quad (5.6)$$

¹Notice that small fluctuations are expected also for an extensive variable ($\langle \mathcal{O} \rangle \sim N$) whose variance grows linearly with the system's size $\langle (\delta \mathcal{O})^2 \rangle \sim N$, giving $\langle (\delta \mathcal{O})^2 \rangle / \langle \mathcal{O} \rangle^2 \sim N^{-1}$ in the thermodynamic limit.

It is instructive to consider more in detail the reason why the dynamic variance of Equations (5.2) and (5.3) contains informations about the spatial correlations. To illustrate this let us start by a simpler case considering which spatial correlations are involved in the standard correlation function $C(t)$. For doing this we rewrite the instantaneous value of the variable A as a space-average of instantaneous local contributions $a(\mathbf{r}, t)$ as follows

$$A(t) = \frac{1}{V} \int d^3\mathbf{r} a(\mathbf{r}, t) \quad (5.7)$$

and therefore

$$\delta A(t) = \frac{1}{V} \int d^3\mathbf{r} \delta a(\mathbf{r}, t) = \frac{1}{V} \int d^3\mathbf{r} a(\mathbf{r}, t) - \langle A \rangle \quad (5.8)$$

where V is the system's volume and we have introduced the local fluctuation $\delta a(\mathbf{r}, t)$. Inserting the definition (5.8) in the correlation function (5.1) we obtain

$$C(t) = \left\langle \frac{1}{V} \int d^3\mathbf{r} \delta a(\mathbf{r}, t) \frac{1}{V} \int d^3\mathbf{r}' \delta a(\mathbf{r}', 0) \right\rangle \quad (5.9)$$

Using the translational invariance Equation (5.9) can be rewritten also as

$$C(t) = \left\langle \frac{1}{V} \int d^3\mathbf{r} \delta a(\mathbf{r}, t) \delta a(\mathbf{0}, 0) \right\rangle \quad (5.10)$$

Equations (5.9) and (5.10) show how the standard correlation function $C(t)$ correlates only the fluctuations of the variable a belonging to two points in space ($\mathbf{0}$ and \mathbf{r}) clarifying why we often refer to $C(t)$ as a two-point susceptibility.

Similarly to what we have done with $C(t)$, we can obtain an expression for $\chi_4(t)$ showing explicitly its spatial dependence. To do this let us introduce the local correlation of fluctuations

$$c(\mathbf{r}, 0, t) = \delta a(\mathbf{r}, t) \delta a(\mathbf{0}, 0) \quad (5.11)$$

that can be used to write Equation (5.10) in a more compact way

$$C(t) = \left\langle \frac{1}{V} \int d^3\mathbf{r} c(\mathbf{r}, 0, t) \right\rangle \quad (5.12)$$

By comparing Equation (5.12) with Equation (5.1) it is clear that we can rewrite the function $\mathcal{C}(0, t)$ appearing also in Equation (5.3) as

$$\mathcal{C}(0, t) = \frac{1}{V} \int d^3\mathbf{r} c(\mathbf{r}, 0, t) \quad (5.13)$$

and

$$\delta \mathcal{C}(0, t) = \frac{1}{V} \int d^3\mathbf{r} \delta c(\mathbf{r}, 0, t) = \frac{1}{V} \int d^3\mathbf{r} c(\mathbf{r}, 0, t) - \langle \mathcal{C}(0, t) \rangle \quad (5.14)$$

where we have defined the local fluctuation $\delta c(\mathbf{r}, 0, t)$ of the (local) correlation in complete analogy with Equation (5.8). By inserting Equation (5.14) in Equation (5.3) we have that $\chi_4(t)$ is rewritten as

$$\chi_4(t) = N \left\langle \frac{1}{V} \int d^3\mathbf{r} \delta c(\mathbf{r}, 0, t) \frac{1}{V} \int d^3\mathbf{r}' \delta c(\mathbf{r}', 0, t) \right\rangle \quad (5.15)$$

Equation (5.15) shows clearly how $\chi_4(t)$ correlates two functions $\delta c(\mathbf{r}, 0, t)$ that by themselves involve two points in space motivating the name four-point susceptibility given to $\chi_4(t)$. Equation (5.15) can be simplified by assuming translational invariance to obtain

$$\chi_4(t) = \rho \left\langle \int d^3\mathbf{r} \delta c(\mathbf{r}, 0, t) \delta c(\mathbf{0}, 0, t) \right\rangle \quad (5.16)$$

where $\rho = N/V$ is the density of the system.

The typical non-monotonic behavior of $\chi_4(t)$ is clearly seen in computer simulations of supercooled model-liquids. In Figure 5.2 we show the $\chi_4(t)$ obtained in the Monte-Carlo computer simulation of the Kob-Andersen binary Lennard-Jones mixture (see Section 4.1.1). Moreover $\chi_4(t)$ is found to grow in amplitude as the temperature decreases and its peak shifts to longer times [34, 35, 36]. The four-point susceptibility of Figure 5.2(B) is computed by the variance of the self-intermediate scattering function shown in Figure 5.2(A). By comparing Figure 5.2(A) and (B) it is clear that the four point susceptibility reaches its maximum $\max_t \{\chi_4(t)\}$ approximatively in correspondence of the relaxation time of the correlation function, i.e. at $t \simeq \tau_\alpha$.

At this point it also is worthy to notice that when the correlation function $C(t)$ considered for obtaining $\chi_4(t)$ is properly normalized (and therefore adimensional) we can interpret $\chi_4(t)$ as a (dynamic) number of molecules whose dynamics is correlated. In particular the maximum $\max_t \{\chi_4(t)\} \simeq \chi_4(t = \tau_\alpha)$ is taken as the characteristic number of molecules whose dynamics is correlated [34, 37, 38, 39]

$$N_{\text{corr}} = \max_t \{\chi_4(t)\} \quad (5.17)$$

When the correct normalization is needed we can simply replace fluctuation of the variable $\delta A(t)$ appearing in the Equations above with the normalized fluctuation $\delta \hat{A}(t)$ defined as

$$\delta \hat{A}(t) = \frac{\delta A(t)}{\sqrt{\langle (\delta A)^2 \rangle}} \quad (5.18)$$

This corresponds to divide the (non-normalized) correlation function $C(0, t)$ by the constant

$$\langle C(0, 0) \rangle = C(0) \quad (5.19)$$

in this way the correlation function $\langle \hat{C}(0, t) \rangle = \langle C(0, t) \rangle / C(0)$ is normalized to the unity for $t = 0$. Alternatively we can divide $\chi_4(t)$ by the factor

$$\langle (\delta A)^2 \rangle^2 = \langle C(0, 0) \rangle^2 = C(0)^2 \quad (5.20)$$

The self-intermediate scattering function considered above is an example of a well normalized (adimensional) correlation function, so that its maximum amplitude can be readily taken as the characteristic number of molecules whose dynamics is correlated (see Figure 5.2(B))

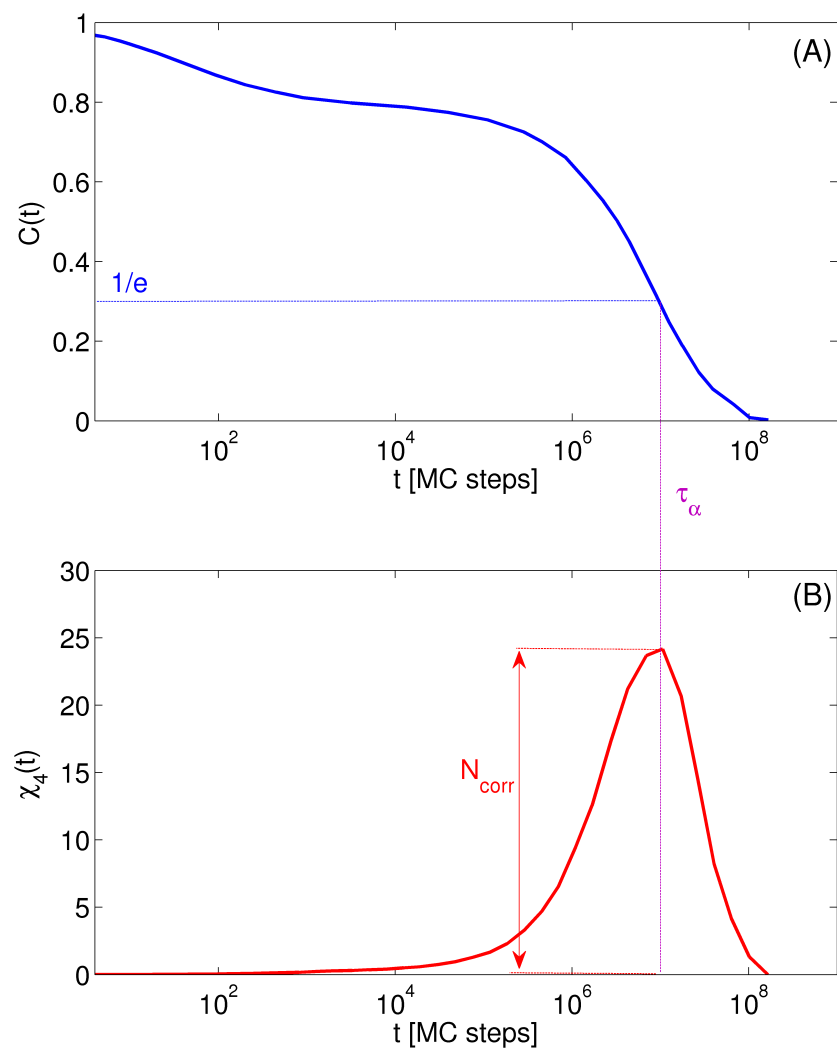


Figure 5.2: **(A)** Self-intermediate scattering function for the KABLJ system at $\rho = 1.2$ and $T = 0.42$ (see Section 4.1.1). The relaxation time τ_α can be roughly defined as the value of t at which the correlation function reaches the value $1/e$. **(B)** Four point susceptibility $\chi_4(t)$ corresponding to the same simulation of **(A)**. Notice that $\chi_4(t)$ reaches a maximum at $t \simeq \tau_\alpha$. This maximum can be taken as the characteristic number of molecules whose dynamic is correlated.

5.1.1 The three-point susceptibility

So far we have considered $\chi_4(t)$ and its very informative content about the spatial correlations of the dynamics. Nevertheless another class of slightly simpler multi-point susceptibilities can be studied and this turns out to be more easily accessible by experiments. These are the three-point susceptibilities defined as

$$\chi_3(t) = N[\langle \mathcal{C}(0, t)B(0) \rangle - \langle \mathcal{C}(0, t) \rangle \langle B \rangle] = N \langle \delta \mathcal{C}(0, t) \delta B(0) \rangle \quad (5.21)$$

that is the correlation between the fluctuation of the variable B at time $t = 0$ and the fluctuation of the dynamic function $\mathcal{C}(0, t)$. As done above we can express the spatial dependence of the function (5.21) just by plugging into Equation (5.21) the Equations (5.8) and (5.14) obtaining

$$\chi_3(t) = N \left\langle \frac{1}{V} \int d^3\mathbf{r} \delta c(\mathbf{r}, 0, t) \frac{1}{V} \int d^3\mathbf{r}' \delta b(\mathbf{r}', 0) \right\rangle \quad (5.22)$$

As seen from Equation (5.22) the three-point susceptibility embodies the correlation between a one-point quantity $\delta b(\mathbf{r}, 0)$ and a two-point (dynamic) quantity $\delta c(\mathbf{r}, 0, t)$. Again the Equation (5.22) is simplified by using translational invariance

$$\chi_3(t) = \rho \left\langle \int d^3\mathbf{r} \delta c(\mathbf{r}, 0, t) \delta b(\mathbf{0}, 0) \right\rangle \quad (5.23)$$

The physical meaning of the three-point susceptibility and the way to its experimental determination become clear if one specifies the variable B contained in the function. To do this we must consider the fluctuation of the variable coupled to a temperature change, i.e. the proper thermodynamic potential of the ensemble. This is the energy in the NVT ensemble, or the enthalpy in the NPT ensemble. In the following we restrict our considerations to the NPT ensemble that is relevant for experiments. To this purpose we recall that that the total enthalpy H_{tot} is an extensive quantity being that defined as

$$H_{\text{tot}} = E_{\text{tot}} + pV \quad (5.24)$$

where E_{tot} is the total internal energy and p is the constant pressure of the system. As we did for $\chi_4(t)$ we want $\chi_3(t)$ to be an intensive variable, so we will consider the instantaneous enthalpy per particle

$$H(t) = \frac{H_{\text{tot}}(t)}{N} \quad (5.25)$$

The variance of H , i.e. $\langle (\delta H)^2 \rangle$, is conveniently expressed by using the fluctuation-dissipation theorem (FDT) as [155, 34, 35, 36, 37]

$$N \langle (\delta H)^2 \rangle = k_B T^2 c_p \quad (5.26)$$

where c_p is the specific heat per particle at constant pressure. Notice again that the multiplying factor N is needed in order to have an intensive specific heat. Indeed the enthalpy per particle is intensive and its variance decreases as $\langle (\delta H)^2 \rangle \sim N^{-1}$ in the thermodynamic limit (see Equations (5.5) and (5.6)).

Replacing the variable B in Equation (5.21) with the enthalpy per particle H of Equation (5.25) we get

$$\chi_3(t) = N \langle \delta \mathcal{C}(0, t) \delta H(0) \rangle \quad (5.27)$$

This quantity represents the correlation between an enthalpy fluctuation and the fluctuation of the dynamic correlation function and it tells us how a change of the thermodynamic potential influences the dynamics. The typical form of the function $\chi_3(t)$ is very similar to the one of $\chi_4(t)$ with a non-monotonic behavior displaying a maximum in correspondence of $t \simeq \tau_\alpha$ (see Figure 5.2(B)). Moreover $\chi_3(t)$ grows in amplitude and its peak shifts to longer times as the temperature decreases. As we did for $\chi_4(t)$ we notice that we can associate to the maximum amplitude of $\chi_3(t)$ the characteristic number $N_{\text{corr}T}$ of molecules whose dynamics is correlated to an enthalpy fluctuation. To do this, assuming that $\mathcal{C}(0, t)$ is already properly normalized, we just need to divide the fluctuations of H by the factor $\sqrt{k_B c_p T}$ that is the characteristic amplitude of the fluctuation of the enthalpy per particle (see also Equation (5.18)). In this way we obtain a correctly normalized (adimensional) $\chi_3(t)$ and therefore

$$N_{\text{corr}T} = \frac{\max_t \{|\chi_3(t)|\}}{\sqrt{k_B c_p T}} \quad (5.28)$$

notice that the absolute value is taken in order to have a positive $N_{\text{corr}T}$.

To understand how the function (5.27) can be obtained in experiments we must use again the FDT. Let us write first the standard FDT for the change in a generic variable $\langle \mathcal{O} \rangle$ induced by a temperature change

$$\frac{\partial \langle \mathcal{O} \rangle}{\partial T} = N \frac{\langle \delta \mathcal{O} \delta H \rangle}{k_B T^2} \quad (5.29)$$

that consistently gives Equation (5.26) if we set $\mathcal{O} = H$. In analogy we can write a (dynamic) FDT for the induced change χ_T in the correlation function

$$\chi_T(t) = \frac{\partial \langle \mathcal{C}(0, t) \rangle}{\partial T} = N \frac{\langle \delta \mathcal{C}(0, t) \delta H(0) \rangle}{k_B T^2} \quad (5.30)$$

If we now use Equation (5.27) into Equation (5.30) we get

$$\chi_3(t) = k_B T^2 \chi_T(t) \quad (5.31)$$

For the $N_{\text{corr}T}$ of Equation (5.28) we have

$$N_{\text{corr}T} = \sqrt{\frac{k_B}{c_p}} T \max_t \{|\chi_T(t)|\} \quad (5.32)$$

As we can see from Equation (5.31) and Equation (5.30) the problem of measuring the complicated three-point susceptibility has been reduced to measuring the temperature-step induced change in the standard (two-point) correlation function $C(t)$. This is a major simplification since $C(t)$ at different temperatures is, in fact, the quantity that is practically measured in any dynamic experiment. More precisely what we usually measure by dynamical experiments

is the frequency-resolved linear response function as the dielectric susceptibility $\epsilon(\omega)$ or the shear modulus $G(\omega)$ (see Chapter 2). All the results given above apply also for these complex responses. In practice we can substitute $C(t)$ with a generic two-point response function $\chi(\omega)$ that is re-writable as a space integral (as it is $C(t)$ in Equation (5.10)) and that is properly normalized. Conventionally we use a normalized function of the form [34, 37, 38]

$$\tilde{\chi}(\omega) = \frac{\chi(\omega) - \chi(\infty)}{\chi(0) - \chi(\infty)} \quad (5.33)$$

and we consider its real part when replacing $C(t)$ in the Equations above. Following this approach we obtain a frequency-resolved three-point susceptibility

$$\chi_3(\omega, T) = k_B T^2 \chi_T(\omega, T) = k_B T^2 \frac{\partial \tilde{\chi}'(\omega, T)}{\partial T} \quad (5.34)$$

where the prime stands for the real part and now we have indicated the temperature dependence of the functions. In the Equation (5.34) we have also defined

$$\chi_T(\omega, T) = \frac{\partial \tilde{\chi}'(\omega, T)}{\partial T} \quad (5.35)$$

The last interesting thing to consider is that there is a precise link between $\chi_3(t)$ and $\chi_4(t)$. This is easily understood if we notice that, while $\chi_4(t) = N \langle [\delta \mathcal{C}(0, t)]^2 \rangle$ has the form of a variance, $\chi_3(t) = N \langle \delta \mathcal{C}(0, t) \delta H(0) \rangle$ is the covariance of $\mathcal{C}(0, t)$ and $H(0)$. This allow us to use the Cauchy-Schwartz inequality [156, 157] to write that

$$[\langle \delta \mathcal{C}(0, t) \delta H(0) \rangle]^2 \leq \langle [\delta \mathcal{C}(0, t)]^2 \rangle \langle (\delta H)^2 \rangle \quad (5.36)$$

Using Equations (5.30), (5.26) and (5.3) into the inequality (5.36) we obtain

$$\chi_4(t) \geq \frac{k_B}{c_p} T^2 \chi_T^2(t) \quad (5.37)$$

As seen from Equation (5.37) the experimentally accessible function $\chi_T(t)$ does not only gives us the information about the three-point correlations (Equation (5.31)), but it also provides a rigorous lower bound for the more complicated four-point susceptibility $\chi_4(t)$.

It also important to notice few more facts about the connection between $\chi_4(t)$ and $\chi_T(t)$. First the two functions show the same qualitative form with a peak at $t \simeq \tau_\alpha$ as mentioned above. Secondly computer simulations have shown that the the difference between the left-hand side and the right-hand side of the inequality (5.37) is high at high temperature, but it reduces rapidly as the temperature decreases giving

$$\chi_4(t) \simeq \frac{k_B}{c_p} T^2 \chi_T^2(t) \quad (5.38)$$

at the lowest temperatures that are usually reached in simulations [34, 35, 36]. This suggests that at those very low temperatures explored in experiments the quantity $\frac{k_B}{c_p} T^2 \chi_T^2(t)$ can be used as an even better approximation of $\chi_4(t)$. Moreover it is interesting to notice that within the mode-coupling theory it

can be shown that the amplitude of $\chi_4(t)$ and $\chi_T(t)$ diverge at the MCT temperature T_c . In the MCT theoretical framework the two functions diverge as $\chi_4(t) \sim \chi_T^2(t) \sim (T/T_c - 1)^{-1/2}$. Finally we stress that assuming the validity of the approximation (5.38) corresponds to assume that the fluctuations in the dynamical correlation function are mainly caused by the enthalpy fluctuations. From Equation (5.38) we also have that

$$N_{\text{corr}} \simeq N_{\text{corr}T}^2 \quad (5.39)$$

5.2 Comparing Shear and Dielectric Dynamical Fluctuations

From the very general discussion reported in the previous Section we can state that we can associate a tree-point susceptibility to each properly normalized dynamic (two-point) quantity measured as a function of temperature. This also allow us to estimate the a characteristic number of molecules whose dynamics is correlated to the enthalpy fluctuations for each measurable dynamic function. Moreover each three-point susceptibility may be used to approximate the corresponding four-point susceptibility.

These observations naturally lead to ask what is the relationship between the spatial extent of the dynamical correlations belonging to different probes and why a specific dynamic function may embody dynamical correlations larger or smaller than another. Furthermore one could ask if an observable-independent (unique) dynamical correlation volume can be defined in some way. To answer these questions from the experimental point of view it is important to have access to different temperature-dependent dynamical measurements performed on the same liquid. The only comparison of the three-point susceptibilities obtained from different measurements reported in the literature is, to our knowledge, the one found in Ref. [37] and it is restricted to a single liquid. All the other studies of the experimentally-determined three-point susceptibility have focused on data obtained by a single technique, i.e. dielectric spectroscopy for molecular supercooled liquids and dynamic light scattering for concentrated colloidal suspension [34, 38, 39].

Ref. [37] reported the comparison of the three-point susceptibility for *m*-toluidine obtained from coherent quasi-elastic neutron scattering, dielectric spectroscopy and photon-correlation spectroscopy (PCS). The amplitude of $\chi_3(t)$ corresponding to neutron scattering measurement was found to be low as expected since these measurements are restricted to short relaxation times (approximately below 10 ns). The amplitudes of $\chi_3(t)$ were also obtained from dielectrics and PCS over an overlapping temperature range in which the relaxation time of the two measured functions varied by about two decades (approximately from 10^{-2} to 1 sec). The $\chi_3(t)$ computed from these two data-sets were found to have different absolute values. Moreover their temperature-dependence was found to be quite different: the amplitude of the dielectric $\chi_3(t)$ was found to grow sensibly faster than the amplitude of the PCS $\chi_3(t)$ upon cooling.

To address this fundamental issue more exhaustively we have compared the multi-point susceptibility extracted from dielectric and shear-mechanical measurements. Paper V reports a systematic comparison of the multi-point

susceptibilities computed from the measurements of $G(\omega, T)$ and $\epsilon(\omega, T)$ for seven glass-formers. The supercooled systems studied are the following: triphenylethylene (TPE), tetramethyltetraphenyl-trisiloxane (DC704), polyphenyl ether (PPE), perhydrosqualene (squalane), polybutadiene (PB20), decahydroisoquinoline (DHIQ), and tripropylene glycol (TPG). DC704, TPE, PPE, squalane and DHIQ are molecular van der Waals bonded liquids, TPG has hydrogen bonds, and PB20 is a polymer with molecular weight of 5000 g/mol. The original shear-mechanical and dielectric measurements² performed on these glass-formers were presented and studied in detail by our group in Ref.s [71, 72, 73]. It is important to stress that the shear-mechanical measurements and the dielectric measurements are performed in the same cryostat upon identical experimental conditions eliminating many sources of errors that could influence the data comparison. Moreover our mechanical measurements offer a very wide frequency range to compare the shear modulus with the dielectric susceptibility. Indeed the PSG technique allow us to measure the dynamic shear modulus in a frequency range spanning from 10 KHz to 1 mHz.

From the study of Ref.s [71, 72] it emerged a clear picture of the features of the shear-modulus and the dielectric response. The relaxation time of the dynamic shear modulus is generally shorter than the relaxation time of the dielectric susceptibility at the same temperature T . Moreover the shear response function and the dielectric response function are found to have slightly different shapes in general. Nevertheless, to a good approximation the shear and dielectric characteristic alpha relaxation, τ_G and τ_ϵ , times grow proportionally upon cooling, i.e.

$$\tau_G(T) \propto \tau_\epsilon(T) \quad (5.40)$$

As discussed in detail in Ref.s [71, 72] those liquids that do not show any clear Johari-Goldstain beta relaxation have a temperature-independent shape to a very good approximation. This feature is referred as time-temperature superposition (TTS), and it is found to hold to a very good degree in the temperature-frequency range explored both for the shear and the dielectric response functions. For those liquids that have a clear beta-relaxation the alpha relaxations in the shear and dielectric spectrum seem to approach a temperature independent shape as the temperature is lowered. This scenario has been studied in detail in Ref. [76] in which a vast amount of dielectric measurements was analyzed confirming that the alpha process progressively approaches a TTS form as the temperature is lowered and it becomes well separated in frequency from the secondary beta process. This last observation suggests to assume that TTS holds for the individual structural alpha relaxation in shear and dielectric spectra (as done in Paper V) and that the failure of TTS in the full spectra may be rationalized as a superposition of the alpha process with the secondary process having different temperature-dependences.

In Paper V we show how these well established properties seen in experiments imply some precise relationships between the shear and dielectric four-point susceptibilities. First we show that the shear and dielectric four-point susceptibilities have their peaks located at slightly different frequencies at the

²All the shear-mechanical and dielectric data analyzed in Paper V are available in the ‘‘Glass and Time: Data Repository’’ found online at <http://glass.ruc.dk/data>.

same temperature. In particular the shear $\chi_4(\omega, T)$ must have its peak located at higher frequencies than the dielectric one. Moreover we show how the dielectric and mechanical four-point susceptibilities have, generally, also different shapes depending on the shape of the functions $G(\omega, T)$ and $\epsilon(\omega, T)$. We illustrate also that the absolute values of the amplitudes of the four-point susceptibilities (i.e. the N_{corr}^s) are different. Nevertheless the shear and dielectric N_{corr}^s grow proportionally to each other as the temperature is lowered

$$N_{\text{corr}}^G(T) \propto N_{\text{corr}}^\epsilon(T) \quad (5.41)$$

The similarity of the shapes of the normalized response functions $\tilde{G}(\omega, T)$ and $\tilde{\epsilon}(\omega, T)$ sets the proportionality constant between $N_{\text{corr}}^G(T)$ and $N_{\text{corr}}^\epsilon(T)$. To be precise if the two response functions have very similar stretching parameters we have

$$\frac{N_{\text{corr}}^\epsilon(T)}{N_{\text{corr}}^G(T)} \simeq 1 \quad (5.42)$$

while if the shear $\tilde{G}(\omega, T)$ is broader than the dielectric $\tilde{\epsilon}(\omega, T)$ we have

$$\frac{N_{\text{corr}}^\epsilon(T)}{N_{\text{corr}}^G(T)} > 1 \quad (5.43)$$

The ratio $N_{\text{corr}}^\epsilon(T)/N_{\text{corr}}^G(T)$ is shown in Figure 5.3. As it seen from this Figure the ratio stays constant to a good approximation for all glass-formers as the temperature decreases and the relaxation time grows several orders of magnitudes. Moreover the multiplicative factor between the absolute values of $N_{\text{corr}}^\epsilon(T)$ and $N_{\text{corr}}^G(T)$ is of order one being $0.5 \lesssim N_{\text{corr}}^\epsilon(T)/N_{\text{corr}}^G(T) \lesssim 2$. This points out that, although a unique N_{corr} can not be probably defined, the same physical mechanism is leading the growth of the shear and dielectric dynamical correlations upon cooling.

These findings can be rationalized mathematically by considering the form assumed by the function $\chi_T(\omega)$ when we specify the form of the normalized response function $\tilde{\chi}(\omega, T)$. Let us first analyze the simple case of a Debye frequency-dependent (normalized) response

$$\tilde{\chi}(\omega, T) = \frac{1}{1 + i\omega\tau(T)} \quad (5.44)$$

This function is properly normalized ($\tilde{\chi}(0, T) = 1$ and $\tilde{\chi}(\infty, T) = 0$) and it depends on time only through the relaxation time $\tau(T)$ (TTS applies). The $\chi_T(\omega, T)$ corresponding to $\tilde{\chi}(\omega, T)$ is given by the temperature derivative of its real part

$$\chi_T(\omega, T) = \frac{\partial \tilde{\chi}'(\omega, T)}{\partial T} = \frac{-2\omega^2\tau(T)}{(1 + \omega^2\tau^2(T))^2} \frac{\partial \tau(T)}{\partial T} \quad (5.45)$$

This function has its maximum in ω exactly at $\omega = 1/\tau(T)$. Evaluating Equation (5.45) at the maximum we obtain from Equation (5.32)

$$N_{\text{corr}T}(T) = \frac{1}{2} \sqrt{\frac{k_B}{c_p}} \left| \frac{\partial \ln \tau(T)}{\partial \ln T} \right| \quad (5.46)$$

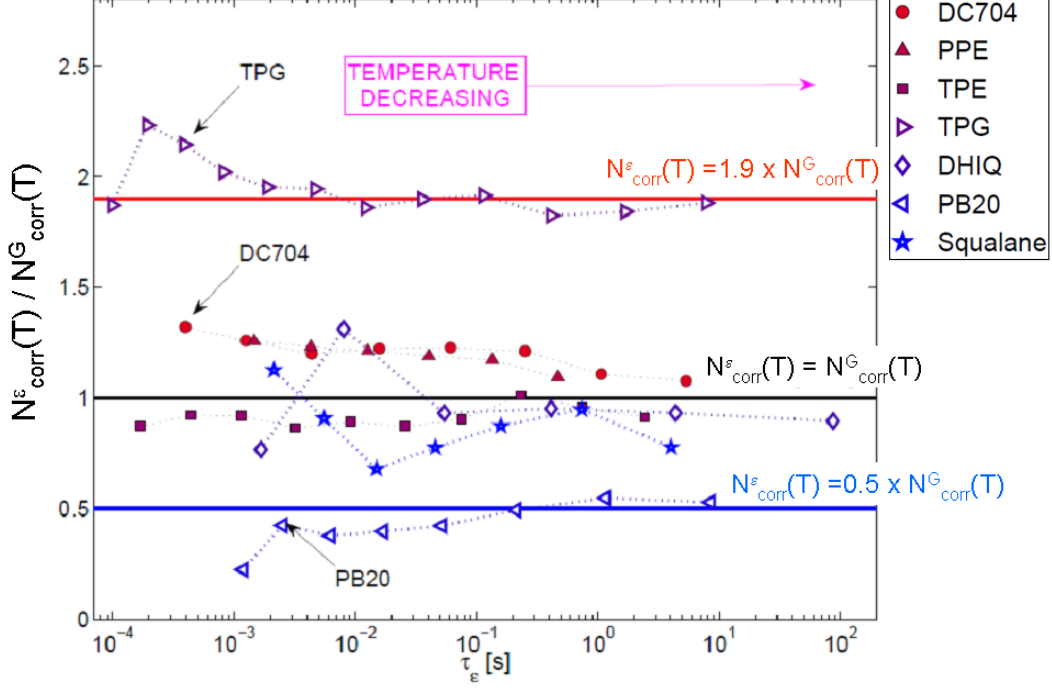


Figure 5.3: Ratio between the characteristic numbers of dynamically correlated molecules in the dielectric and in the shear relaxation for seven glass-formers (see legend). This ratio is plotted as a function of the dielectric relaxation time. $N_{\text{corr}}^\epsilon(T)/N_{\text{corr}}^G(T)$ stays constant to a good approximation for all glass-formers as the temperature decreases and the relaxation time grows several orders of magnitudes.

As seen from the previous Equation we have that if TTS applies $N_{\text{corr}T}$ is directly proportional to the change of the relaxation time upon cooling given by the term $|\partial \ln \tau(T)/\partial \ln T|$. This result is very general, indeed for any normalized function obeying TTS, i.e.

$$\tilde{\chi}(\omega, T) = \tilde{\chi}(\omega \tau(T)) \quad (5.47)$$

we have, to a very good approximation, that

$$N_{\text{corr}T}(T) = \sqrt{\frac{k_B}{c_p}} \left| f(1) \frac{\partial \ln \tau(T)}{\partial \ln T} \right| \quad (5.48)$$

In the previous Equation we have used

$$f(1) = \left. \frac{\partial \tilde{\chi}'(x)}{\partial x} \right|_{x=1} \quad (5.49)$$

where we have set $x = \omega\tau(T)$. The function $f(1)$ does depend on the stretching but once that is fixed (TTS applies) $f(1)$ is just constant factor. For example for a normalized Havriliak-Negami function

$$\tilde{\chi}(\omega, T) = \frac{1}{[1 + (i\omega\tau(T))^{\alpha}]^{\beta}} \quad (5.50)$$

we have

$$f(1) = -\alpha\beta \operatorname{Re} \left[\frac{i^{\alpha}}{(1 + i^{\alpha})^{1+\beta}} \right] \quad (5.51)$$

as discussed in Paper V.

When the shear and dielectric relaxation times grow proportionally upon cooling (Equation (5.40)) we have also

$$\left| \frac{\partial \ln \tau_{\epsilon}(T)}{\partial \ln T} \right| \simeq \left| \frac{\partial \ln \tau_G(T)}{\partial \ln T} \right| \quad (5.52)$$

although we may have

$$f_{\epsilon}(1) \neq f_G(1) \quad (5.53)$$

since we have, in general, different stretching for $\tilde{G}(\omega\tau_G(T))$ and for $\tilde{\epsilon}(\omega\tau_{\epsilon}(T))$. This lead us to conclude that

$$\frac{N_{\text{corr}}^{\epsilon}(T)}{N_{\text{corr}}^G(T)} \simeq \left[\frac{N_{\text{corr}T}^{\epsilon}(T)}{N_{\text{corr}T}^G(T)} \right]^2 \simeq \left[\frac{f_{\epsilon}(1)}{f_G(1)} \right]^2 = \text{const} \quad (5.54)$$

where we have used Equation (5.39). From the Equation above it is clear that the proportionality factor is closer to the unity for the $N_{\text{corr}T}$ s than for the N_{corr} s. This is shown in Figure 5.4 where it can be seen that $0.7 \lesssim N_{\text{corr}T}^{\epsilon}(T)/N_{\text{corr}T}^G(T) \lesssim 1.4$.

In conclusion we want to underline that recent measurements performed by our group seems to confirm this scenario for several other dynamic relaxation function. In addition to the shear and dielectric measurements dynamic specific heat [158, 159], bulk modulus [160] and thermal expansivity [161] measurements have been done using the same cryostat. These have shown the proportional growth of the relaxation times of each of this functions upon cooling. Moreover TTS seems to be obeyed by all of these dynamic quantities to a good degree. This study involving many different kind of measurements have been performed so far only on a single liquid (DC704). Nevertheless these findings indicate a scenario for the dynamical correlations in which their growth is determined by a unique physical phenomenon showing the same temperature behavior among the different dynamic susceptibilities.

5.3 A Direct Experimental Measurement of The Four-Point Susceptibility

In the previous Sections we have illustrated and used an indirect (and approximated) approach to the estimation of the four-point susceptibility. This is allowed by two fundamental conditions: the system under study it is at the thermodynamic equilibrium, so that we can rely on the fluctuation-dissipation

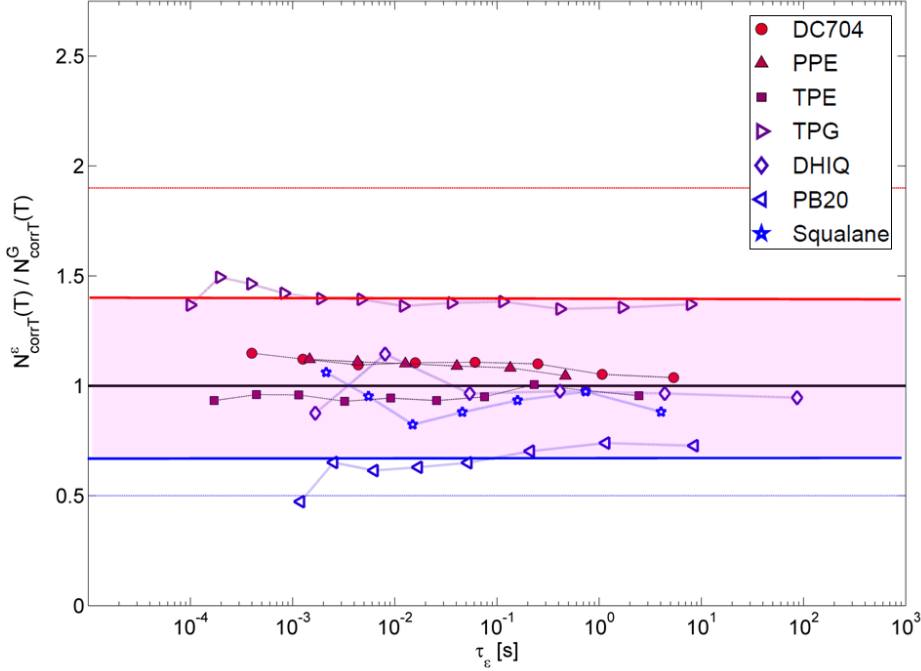


Figure 5.4: Ratio between the characteristic numbers of dynamically correlated molecules to the enthalpy fluctuations in the dielectric and in the shear relaxation for seven glass-formers (see legend). This ratio is plotted as a function of the dielectric relaxation time. $N_{\text{corr}T}^{\epsilon}(T)/N_{\text{corr}T}^G(T)$ stays constant to a good approximation for all glass-formers as the temperature decreases and the relaxation time grows several orders of magnitudes. The shaded area emphasizes that $N_{\text{corr}T}^{\epsilon}(T)/N_{\text{corr}T}^G(T)$ is closer to the unity than $N_{\text{corr}}^{\epsilon}(T)/N_{\text{corr}}^G(T)$.

theorem, and the source of the fluctuations in the dynamic correlation or response function is mainly the fluctuations in the enthalpy. When these two requirements are not matched by the physical system under study we need a direct measurement of the fluctuations of the correlation or the response function to measure the four-point susceptibility.

Certainly if one can measure the position of the particles of the system as a function of time the four-point susceptibility can be readily obtained as it is done in computer simulations. This can be done via optical microscopy techniques for colloidal systems whose particles are large enough to be resolved (see for example Ref. [32]). In the following we illustrate a new experiment capable of measuring directly the four-point susceptibility without resolving the positions of the individual particles. The experiment employs two different dynamic light scattering techniques combining heterodyne and homodyne photon-correlation spectroscopy (PCS). Furthermore in the experiment we use small scattering volumes to enhance the dynamical fluctuations. We perform this experiment on an aging low concentration colloidal solution of Laponite (see also Section 3.2) reporting the measured four-point susceptibility. This

colloidal suspension is the ideal candidate for such an experiment for several of its features. First the indirect approach to the determination of $\chi_4(t)$ discussed in the Sections above is not applicable. This is because this colloidal system is out of equilibrium and we can not use on the FDT. Moreover we do not know a priori if there is a static quantity whose fluctuations are the major source of fluctuations in the dynamic correlation function measured (as the enthalpy in supercooled liquids). In addition the Laponite colloidal particles suspended in water are too small to be resolved by standard microscopy techniques. Indeed the Laponite colloidal particle dissolved in water has the form of flat cylinder with a thickness of about 1 nm and a radius of about 15 nm. Even if it were possible to make visible these small colloidal discs under microscope inspection by fluorescent labeling they would still be very small with respect to the standard resolution of an optical microscope on the position of a colloidal particle that is typically around 30 nm. As show in the following by our experiment the complete information on the particle positions is not needed to measure directly the four-point susceptibility. What we need to measure is more simply the difference between two distinct correlation functions. In the next Section we define these function and we illustrate how they are measured.

5.3.1 Homodyne and heterodyne photon-correlation spectroscopy

In a dynamic laser-light scattering experiment we measure the properties of the light scattered by a sample illuminated by a laser beam [108, 109, 110, 111]. The incident laser radiation and scattered radiation have their polarization selected by polarizer filters. Moreover the scattered electromagnetic wave is selected to have a precise propagation direction (see also Section 3.2). The total instantaneous amplitude of the scattered electromagnetic field $E(t)$ is given by the superposition of the electric fields $E_j(t)$ scattered by each molecule

$$E(t) = \sum_{j=1}^N E_j(t) \quad (5.55)$$

where the sum is extended to all the N molecules contained in the scattering volume. The field scattered by each molecule is given by

$$E_j(t) \propto \alpha_{if}(t) \exp[i(\mathbf{k} \cdot \mathbf{r}_j(t))] \quad (5.56)$$

where $\mathbf{r}_j(t)$ is the position of the j -th molecule at time t , \mathbf{k} is the exchanged wave-vector, and the term $\alpha_{if}(t)$ represents the component of the polarizability tensor projected along the polarization direction of the incident laser beam and the polarization direction selected for the scattered wave.

In a homodyne PCS experiment we measure an auto-correlation function proportional to the correlation function of the intensity of the scattered electromagnetic field

$$\langle |E(0)|^2 |E(t)|^2 \rangle \quad (5.57)$$

This is the simplest PCS experiment that can be done since we only need the scattered light to impinge on the detector. The detector out-put current $i_{\text{out}}(t)$

generated by the scattered field is proportional to the intensity of the scattered field

$$i_{\text{out}}(t) \propto |E(t)|^2 \quad (5.58)$$

The correlation function of the signal $i_{\text{out}}(t)$ produced by the detector can be efficiently calculated by a correlator, i.e. a specialized electronic device designed to compute in real time the correlation function of $i_{\text{out}}(t)$, i.e.

$$\langle i_{\text{out}}(0) i_{\text{out}}(t) \rangle \propto \langle |E(0)|^2 |E(t)|^2 \rangle \quad (5.59)$$

Eliminating the unimportant constant prefactors what we considered in homodyne PCS experiments is the normalized auto-correlation function of the intensity of the scattered electromagnetic field. The normalization is performed by dividing the function by its long time limit

$$\lim_{t \rightarrow \infty} \langle i_{\text{out}}(0) i_{\text{out}}(t) \rangle = \langle i_{\text{out}} \rangle^2 \quad (5.60)$$

obtaining

$$\frac{\langle i_{\text{out}}(0) i_{\text{out}}(t) \rangle}{\langle i_{\text{out}} \rangle^2} = \frac{\langle |E(0)|^2 |E(t)|^2 \rangle}{\langle |E|^2 \rangle^2} \quad (5.61)$$

In a real experiment the amplitude fluctuating part of the correlation function of the current out-put signal is reduced because of the presence of a shot-noise term at very short t and because of the geometrical decorrelation effects of the scattered light that is produced by a source with finite extension³. Due to these phenomena what we actually measure in a PCS homodyne experiment is a dynamic correlation function of the form

$$\sigma \langle \delta i_{\text{out}}(0) \delta i_{\text{out}}(t) \rangle + \langle i_{\text{out}} \rangle^2 \quad (5.62)$$

where $\sigma = \text{const} < 1$ and where we have introduced the fluctuation of the photon-induced out-put current $\delta i_{\text{out}}(t) = i_{\text{out}}(t) - \langle i_{\text{out}} \rangle$. This results in measuring a normalized correlation function of the form

$$\sigma \frac{\langle \delta i_{\text{out}}(0) \delta i_{\text{out}}(t) \rangle}{\langle i_{\text{out}} \rangle^2} + 1 = \sigma \frac{\langle \delta |E(0)|^2 \delta |E(t)|^2 \rangle}{\langle |E|^2 \rangle^2} + 1 \quad (5.63)$$

The heterodyne method is a different PCS technique for studying the dynamics of a system via laser radiation. In this kind of experiment the field directed onto the detector is a superposition of the scattered field E and a portion of the laser field E_L (also named local oscillator in this case). If the fluctuations in the laser field are negligible and if the local oscillator field and the scattered field are statistically independent one has

$$\begin{aligned} \langle |E(0) + E_L(0)|^2 |E(t) + E_L(t)|^2 \rangle = \\ \langle |E_L|^2 \rangle^2 + 2 \langle |E_L|^2 \rangle \text{Re}[\langle E^*(0) E(t) \rangle] + \langle |E(0)|^2 |E(t)|^2 \rangle \end{aligned} \quad (5.64)$$

where the star indicates the complex conjugate. The correlation function obtained via the heterodyne method thus contains the correlation function of the

³See Chapter 4 of Ref. [108] for more details

amplitude scattered electric field differently from the homodyne correlation function that is proportional to the intensity-intensity correlation function. To obtain the most precise information on the function $\langle E^*(0)E(t) \rangle$ in a heterodyne experiment one should work in the limit $\langle |E_L|^2 \rangle \gg \langle |E|^2 \rangle$ increasing the amplitude of the second term on the right-side of Equation (5.64). The effect of having a local oscillator much more intense of the scattered filed is seen more clearly by rewriting the previous equation in the normalized form. The long time limit of the function (5.64) is given by

$$\langle |E_L|^2 \rangle^2 + \langle |E|^2 \rangle^2 \quad (5.65)$$

since $\langle E \rangle = 0$. Dividing Equation (5.64) by this term we have

$$\begin{aligned} \frac{\langle |E(0) + E_L(0)|^2 |E(t) + E_L(t)|^2 \rangle}{\langle |E_L|^2 \rangle^2 + \langle |E|^2 \rangle^2} = \\ 1 + \frac{2\langle |E_L|^2 \rangle \operatorname{Re}[\langle E^*(0)E(t) \rangle] + \langle \delta |E(0)|^2 \delta |E(t)|^2 \rangle}{\langle |E_L|^2 \rangle^2 + \langle |E|^2 \rangle^2} \end{aligned} \quad (5.66)$$

from this Equation is clear that if $\langle |E_L|^2 \rangle \gg \langle |E|^2 \rangle$ the term $\langle \delta |E(0)|^2 \delta |E(t)|^2 \rangle$ is negligible giving the ideal case of heterodyne detection

$$\begin{aligned} \frac{\langle |E(0) + E_L(0)|^2 |E(t) + E_L(t)|^2 \rangle}{\langle |E_L|^2 \rangle^2} = \\ 1 + \frac{2}{\langle |E_L|^2 \rangle} \operatorname{Re}[\langle E^*(0)E(t) \rangle] \end{aligned} \quad (5.67)$$

The considerations made above for the homodyne function about the loss of amplitude due to some experimentally unavoidable effects are valid also for the heterodyne function. In this case we will have a measured function of the form

$$\begin{aligned} \frac{\langle |E(0) + E_L(0)|^2 |E(t) + E_L(t)|^2 \rangle}{\langle |E_L|^2 \rangle^2 + \langle |E|^2 \rangle^2} = \\ 1 + \sigma \frac{2\langle |E_L|^2 \rangle \operatorname{Re}[\langle E^*(0)E(t) \rangle] + \langle \delta |E(0)|^2 \delta |E(t)|^2 \rangle}{\langle |E_L|^2 \rangle^2 + \langle |E|^2 \rangle^2} \end{aligned} \quad (5.68)$$

When doing dynamic light scattering PCS measurements one often assumes that the homodyne correlation function contains exactly the same informations of the heterodyne correlation function. This is done by assuming the validity of the Gaussian approximation. This widely used approximation works whenever the scattering volume contains many uncorrelated scattering elements. These have not to be confused with the individual scattering particles. One has to imagine the scattering volume divided in numerous sub-volumes that scatter the light in an uncorrelated way. Let us label these sub-volumes with the index $\alpha = 1, \dots, M$. The particles within an individual volume α may move and scatter the radiation in a correlated way. Nevertheless a large amount of particles

contained in the other sub-volumes that are far away from α will move and scatter the incoming wave independently. When this is the case the total scattering field $E = \sum_{\alpha=1}^M E_\alpha$ is the superposition of many independent stochastic contributions. In this situation, as prescribed by the central limit theorem, the total field $E(t)$ becomes a stochastic variable with Gaussian distribution independently on the original distributions of the variables E_α . We recall that for a real variable x following a Gaussian distribution with width w we have

$$\mathcal{P}(x) = \frac{\exp[-x^2/(2w^2)]}{w\sqrt{2\pi}} \quad (5.69)$$

and therefore

$$\begin{aligned} \langle x^2 \rangle &= \int dx \mathcal{P}(x) x^2 = w^2 \\ \langle x^4 \rangle &= \int dx \mathcal{P}(x) x^4 = 3w^4 \end{aligned} \quad (5.70)$$

so there is a relationship between the second and fourth moment of the distribution

$$\langle x^4 \rangle = 3 [\langle x^2 \rangle]^2 \quad (5.71)$$

For a complex Gaussian variable $z = x + iy$ (as it is the scattered field E) we have in analogy with the equations above

$$\begin{aligned} \mathcal{P}(z) &= \frac{\exp[-|z|^2/(2w^2)]}{2\pi w^2} \\ \int dy \int dx \mathcal{P}(z) |z|^2 &= 2w^2 \\ \int dy \int dx \mathcal{P}(z) |z|^4 &= 8w^4 \end{aligned} \quad (5.72)$$

so the relationship between the second and fourth moment of the distribution becomes

$$\langle |z|^4 \rangle = 2 |\langle |z|^2 \rangle|^2 \quad (5.73)$$

When the scattered field E is a Gaussian variable we can write a static relation between the first and second moment identical to Equation (5.73)

$$\langle |E|^4 \rangle = 2 |\langle |E|^2 \rangle|^2 \quad (5.74)$$

This can be generalized to the dynamic case just by assuming that both $E(0)$ and $E(t)$ are Gaussian variables obtaining

$$\langle |E(0)|^2 |E(t)|^2 \rangle = |\langle |E|^2 \rangle|^2 + |\langle E^*(0)E(t) \rangle|^2 \quad (5.75)$$

that consistently gives back Equation (5.74) if we set $t = 0$. The Gaussian approximation (5.75) tells us that if the scattering volume contains many correlation volumes the heterodyne measurement giving the function $\langle E^*(0)E(t) \rangle$ gives the same informations of the homodyne measurement giving the function $\langle |E(0)|^2 |E(t)|^2 \rangle$. It is important to notice that if normalize Equation (5.75) and we rewrite it as

$$\frac{\langle |E(0)|^2 |E(t)|^2 \rangle}{|\langle |E|^2 \rangle|^2} - \frac{|\langle E^*(0)E(t) \rangle|^2}{|\langle |E|^2 \rangle|^2} = 1 \quad (5.76)$$

the right end side of this Equation has exactly the form of the four-point susceptibility given by Equation (5.2). This is telling us that if we have many uncorrelated sub-volumes in the scattering volume our four-point susceptibility will reduce to a trivial constant factor independently on the finite size of the correlations. On the other hand if the size of the scattering volume is not infinitely large with respect to the spatial extent of the correlation between nearby sub-volumes a time-dependent deviation from the Gaussian approximation is expected and this gives directly the four-point susceptibility. In practice the experimental determination of $\chi_4(t)$ can be translated in the search for a deviation from the Gaussian approximation. In this case is essential to have a small scattering volume so that the deviation is not not infinitesimal and undetectable.

The simplest case in which the Gaussian approximation applies is when we perform the homodyne experiments on very diluted colloidal suspensions. In this case the fact that the scattering volume contains many uncorrelated scattering elements coincides with the fact that the scattering volume contains many independent scattering colloidal particles. Nevertheless this is a particular case and one should not forget that the Gaussian approximation has more general validity as discussed above. Moreover one can consider that in some cases, even if we have extremely diluted suspension, we might obtain different informations from homodyne and heterodyne experiments. To illustrate this let us consider first the case of a very diluted colloidal solution composed of large spherical particles diluted in a molecular solvent. In this case the heterodyne field-field correlation function can be derived assuming that the diffusion equation describes the density fluctuations

$$\frac{\partial}{\partial t}\rho(\mathbf{r},t) = D\nabla^2\rho(\mathbf{r},t) \quad (5.77)$$

where the $\rho(\mathbf{r},t) = \sum_{j=1}^N \delta(\mathbf{r} - \mathbf{r}_j(t))$ is the density field and D is the diffusion coefficient. If the scattering colloidal particle is spherical the polarizability of the colloidal particle is just a unitary tensor multiplied by a constant (see Equation (5.56)). In this case the electric field is directly proportional to the spatial Fourier transform of the fluctuations of the density field $E(t) \propto \sum_{j=1}^N \exp[i\mathbf{k} \cdot \mathbf{r}_j(t)]$. This allow us to write a Fourier-transformed diffusion equation for E from Equation (5.77)

$$\frac{\partial}{\partial t}E(t) = -k^2DE(t) \quad (5.78)$$

where $k = |\mathbf{k}|$. Equation (5.78) can be rewritten as an equation for the heterodyne correlation function $\langle E^*(0)E(t) \rangle$ just by multiplying both sides by the term $E^*(0)$ and taking the average

$$\frac{\partial}{\partial t}\langle E^*(0)E(t) \rangle = -k^2D\langle E^*(0)E(t) \rangle \quad (5.79)$$

Equation (5.79) can be easily solved with the boundary condition

$$\langle E^*(0)E(0) \rangle \propto \left\langle \sum_{j=1}^N \exp[i\mathbf{k} \cdot (\mathbf{r}_j(0) - \mathbf{r}_j(0))] \right\rangle = \langle N \rangle \quad (5.80)$$

where $\langle N \rangle$ is the average number of particles contained in the scattering volume. Note that to obtain Equation (5.80) we have neglected all the cross-particle terms since the solution is infinitely diluted and different particles are completely uncorrelated. The solution of Equations (5.79)-(5.80) is

$$\langle E^*(0)E(t) \rangle \propto \langle N \rangle \exp(-k^2 Dt) \quad (5.81)$$

In this case the Gaussian approximation (5.75) obviously applies so that we can write

$$\langle |E(0)|^2 |E(t)|^2 \rangle \propto \langle N \rangle^2 + \langle N \rangle^2 \exp(-2k^2 Dt) \quad (5.82)$$

Notice that the quantity $\tau = (2k^2 D)^{-1}$ is the relaxation time of the correlation function. All those experiments that use homodyne PCS to measure the size of the colloidal particles, proteins or macromolecules diluted in a solvent are based on Equation (5.82). This is done by using the Einstein FDT relating the diffusion constant D to the friction constant ζ

$$D = \frac{k_B T}{\zeta} \quad (5.83)$$

Moreover the friction constant can be expressed via the Stokes approximation in the case of stick-boundary conditions

$$\zeta = 6\pi\eta R \quad (5.84)$$

where η is the viscosity of the solvent and R is the radius of the colloidal particle. In this way one first measures the relaxation time τ of the homodyne correlation function and then extracts the radius of the particles as $R = \tau k^2 k_B T / (3\pi\eta)$. Notice that in this case there would be no advantage in measuring the heterodyne function since that would give the same information about the particle's radius.

A slightly different situation in which the two functions give a different result is when a uniform motion of the particles is present in the solution. This is the case of the electrophoretic experiments in which an external electric field accelerates in some direction the diluted ionic colloids (macroions). In other experiments we can accelerate the solvent for example by centrifugation driving the colloids to their terminal velocity. These cases in which the diluted colloids are driven by a uniform velocity field \mathbf{V} can be described by adding a drift term to the diffusion equation

$$\frac{\partial}{\partial t} \rho(\mathbf{r}, t) + \mathbf{V} \cdot \nabla \rho(\mathbf{r}, t) = D \nabla^2 \rho(\mathbf{r}, t) \quad (5.85)$$

From the driven diffusion Equation (5.85) we obtain the following expression for the field-field correlation function

$$\langle E(0)^* E(t) \rangle \propto \langle N \rangle \exp(i\mathbf{k} \cdot \mathbf{V}t) \exp(-k^2 Dt) \quad (5.86)$$

At this point we have to recall that in the heterodyne detection we measure the real part of $\langle E(0)^* E(t) \rangle$ (see Equations (5.66) and (5.67)) so that the resulting function will be

$$\text{Re}[\langle E(0)^* E(t) \rangle] \propto \langle N \rangle \cos(\mathbf{k} \cdot \mathbf{V}t) \exp(-k^2 Dt) \quad (5.87)$$

This means that we observe oscillations in the heterodyne function carrying informations about the velocity field. The difference between the homodyne and heterodyne detection is clear in this case, although the Gaussian approximation is still valid and it still gives Equation (5.82) just by inserting Equation (5.86) into (5.75). In practice the homodyne measurement is insensitive to the uniform velocity field while the heterodyne is not. In this context it is important to notice that also a gravity field, driving the sedimentation of the colloids, could induce a drift term in the diffusion equation. Nevertheless, if the exchanged wavevector lies on the horizontal plane, the product $\mathbf{k} \cdot \mathbf{V}$ is close to zero since the gravity-induced velocity field is vertical. In this scattering geometry the term $\cos(\mathbf{k} \cdot \mathbf{V}t)$ is close to the unity perturbing very little the heterodyne function from its diffusive behavior so that Equation (5.87) reduces to Equation (5.81).

Another interesting case, in which the homodyne and heterodyne measurements give qualitatively different results, is when we have considerable fluctuations in the number of particles contained in the scattering volume. This fluctuations may affect the homodyne function also in the simple case of a very dilute solutions whose density fluctuations are described by the diffusion Equation (5.81). When this happens the intensity-intensity correlation function may be rewritten as

$$\langle |E(0)|^2 |E(t)|^2 \rangle \propto \langle N \rangle^2 + \langle N \rangle^2 \exp(-2k^2Dt) + \langle \delta N(0)\delta N(t) \rangle \quad (5.88)$$

where $\delta N(t) = N(t) - \langle N \rangle$ is the fluctuation of the number of particles contained in the scattering volume. The particular form of the time-dependent function $\langle \delta N(0)\delta N(t) \rangle$ depends on the specific geometry of the scattering volume. Nevertheless it can be shown that the amplitude of the extra term $\langle \delta N(0)\delta N(t) \rangle$ is of the order of $\langle N \rangle$, i.e.

$$\langle \delta N(0)\delta N(t) \rangle = \langle N \rangle n(t) \quad (5.89)$$

where $n(t=0) = 1$ and $n(t \rightarrow \infty) = 0$. It is important to notice that the first two terms at the right-hand side of Equation (5.88) obey the Gaussian approximation while the last term represent a deviation from the Gaussian behavior. If we rewrite Equation (5.88) in the normalized form

$$\frac{\langle |E(0)|^2 |E(t)|^2 \rangle}{\langle |E|^2 \rangle^2} = 1 + \exp(-2k^2Dt) + \langle N \rangle^{-1} n(t) \quad (5.90)$$

we can see that if we have a large enough scattering volume (and a large $\langle N \rangle$) the extra term can be neglected with respect to first two.

5.3.2 Measurement of the four-point susceptibility by combined PCS techniques

In the previous Section we have illustrated the heterodyne and the homodyne PCS methods and we have presented two simple cases in which the two functions give different informations. If we want to use the two techniques combined to measure the four-point susceptibility we have to design an experiment in which we can perform both measurements. This is done by setting-up the experiment depicted in Figure 5.5.

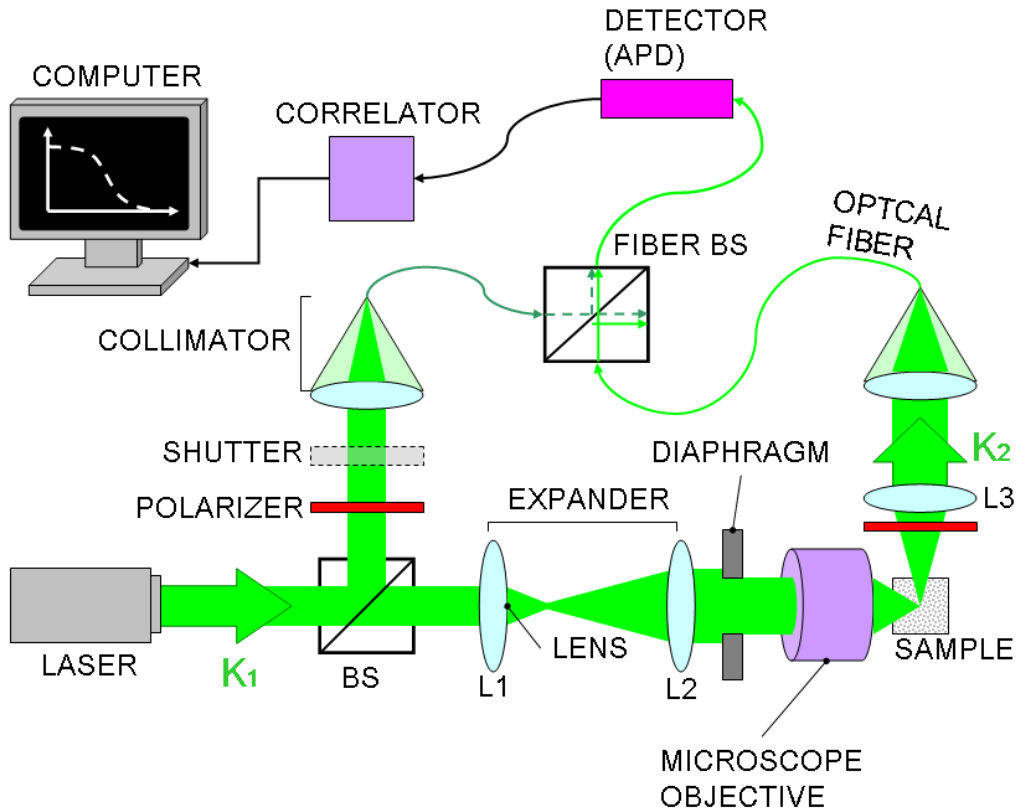


Figure 5.5: Experimental set-up for the combined measurement of the heterodyne and of homodyne correlation function with a small scattering volume. If the shutter is open the laser field is mixed with the scattered radiation by the built-in fiber BS and delivered to the detector. In this case the heterodyne function is measured. If the shutter is closed the homodyne measurement is performed. The laser beam is focused onto the sample by a microscope objective. The scattered electromagnetic wave is collected by a lens and directed to the optical fiber system.

In this experiment we use a probe light beam produced by an ultra-stable, mono-mode DPSS laser with power out-put up to 300 mW. This is a green laser ($\lambda = 532$ nm) vertically polarized with a polarization ratio better than $2 \times 10^2:1$. The laser light is split by a beam-splitter cube (BS) that divides the beam in components with equal intensity. One of the components is directed to the sample and the other one is collected by a collimator and used as a local oscillator for the heterodyne measurement. When the homodyne measurement is performed an automatic shutter blocks the local oscillator. The portion of the laser probe directed to the colloidal sample is first expanded by a couple of lenses (L1 and L2) and then focused by a microscope objective. The focal lengths of the lenses are chosen to illuminate the entire aperture of the microscope objective that has a diameter of 20 mm. An iris diaphragm is used to eliminate the light arriving outside the border of the microscope objective. The objective is an infinity-corrected Olympus imaging objective with $10\times$ magnification. This has an effective focal length of 18 mm and a working distance of 10.6 mm. The beam is focused at the center of the cuvette containing the sample. This is an optical-quality quartz cuvette with flat surfaces. The scattered light at an angle $\vartheta \simeq 90^\circ$ is selected by a polarizer and collected by a lens (L3) that directs the radiation to the collimator. The lens L3 is chosen to have a short focal length for 35 mm and is placed with its focal point coinciding with the objective focal point. The collimator has focal length of 15 mm and it focuses the beam onto an optical fiber that delivers the scattered light to the detector. The optical fiber is a monomode optical fiber optimized for the green radiation, this is connected directly to an built-in BS cube. In this way, when the shutter is open, the electromagnetic field of the local oscillator is superimposed to the scattered electromagnetic field and this total field to the detector. Differently when the shutter is closed only the scattered electromagnetic wave arrives to the detector. The detector used is an avalanche photodiode (APD) with high quantum efficiency (about 60 % at $\lambda \simeq 532$ nm) and with a wide linear response range. A number of absorptive filters are used in the experiment in order to obtain the desired intensity of the scattered light and of the local oscillator. The current out-put of the APD is received by a correlator that performs fast multi-tau correlation of the signal. The correlation function computed by this device is stored in a computer.

Knowing the size of the beam and the focal lengths of the optics we can estimate the size of the scattering volume. This can be done assuming that the monomode laser beam is a Gaussian beam [162, 163, 164] propagating along the z direction. The intensity of this beam is distributed according to a Gaussian function

$$I(x, y, z) = \frac{I_0}{\pi w^2(z)} \exp[-2(x^2 + y^2)/w^2(z)] \quad (5.91)$$

where $w(z)$ is the waist of the beam and I_0 is the total intensity of the beam. When a Gaussian beam of waist w arrives on a lens, with focal length ϕ , this is focused into a beam with smaller waist. In this case the function $w(z)$ can be expressed as

$$w(z) = w_1 \sqrt{1 + \left(\frac{\lambda z}{\pi w_1^2}\right)^2} \quad (5.92)$$

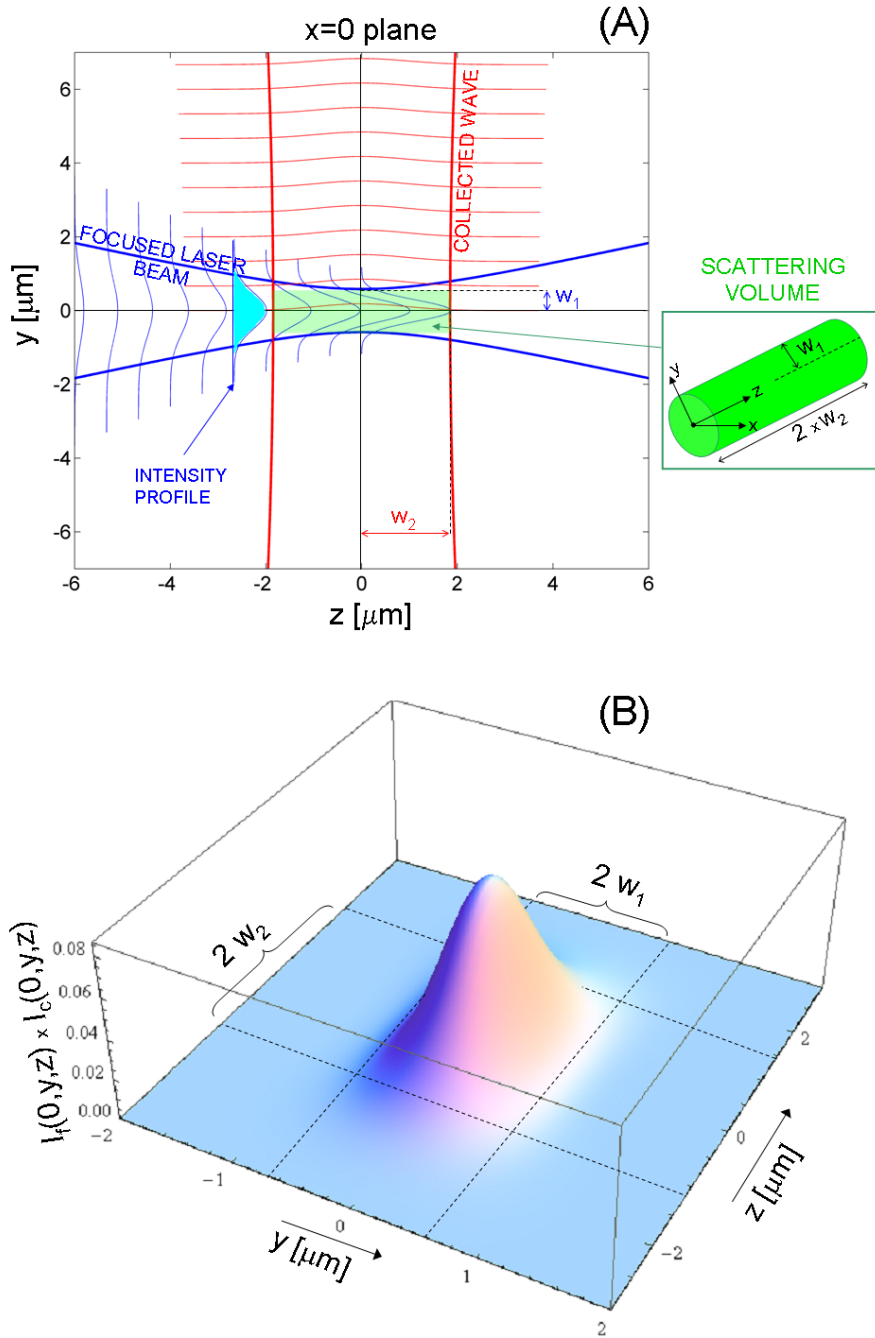


Figure 5.6: (A) Geometry of the focused and of the collected beam in the experiment projected on the plane $x = 0$. The beams are considered to be Gaussian with minimum waist w_1 and w_2 and the intersection between the two defines a cylindrical volume that can be taken as the scattering volume. Almost 90 % of the collected scattered light is emitted by this volume. (B) Modulated intensity profile on the $x = 0$ plane, as it seen the significant contribution of the intensity comes from the volume defined by w_1 and w_2 .

where $w_1 \simeq 2.44 \times \lambda \phi / w$ and the origin of the z axis is now set at the focal point of the lens (see Figure 5.6(A)). For the laser beam focused by the microscope objective we have $w \simeq 20$ mm and $w_1 \simeq 0.58 \mu\text{m}$. As it is seen it is essential to work with an expanded beam and with an objective with short focal length in order to have a small beam waist and therefore a small scattering volume. The geometry of the beam defined by the collecting optics can be evaluated in a similar way assuming that a Gaussian beam propagates into the monomode optical fiber. The waist of this beam is set by the diameter of the inner core of the fiber that is about $1.6 \mu\text{m}$. The collected beam is thus defined by Equations (5.91) and (5.92) with a waist $w_2 \simeq 1.85 \mu\text{m}$. In the scattering geometry of our experiment the collected electromagnetic wave propagates along the y direction, i.e. orthogonally with respect to the focused laser beam with an intensity distribution

$$I_c(x, y, z) = \frac{I_0}{\pi w^2(y)} \exp[-2(x^2 + z^2)/w^2(y)] \quad (5.93)$$

The scattering volume can be defined by weighting the illuminated portion of the sample by the superposition of the focused I_f and the collected intensity fields $I_f(x, y, x) \times I_c(x, y, x)$, where I_f is given by Equation (5.91). Integrating this multiplication of functions it can be shown that almost the 90 % of the collected scattered intensity is emitted by a cylinder with radius equal to $w_1 = 0.58 \mu\text{m}$ and height $2 \times w_2 \simeq 3.7 \mu\text{m}$ centered at the intersection between the focused laser beam and of the collecting beam (see Figure 5.6(B)). These estimates can be used as the dimensions of the scattering volume.

The experimental set-up described above allows for the alternated measurement of the heterodyne and the homodyne correlation functions during the aging process of the sample. Notice that in principle we should measure the two functions simultaneously, but in practice they can be measured in alternated way since the aging process of the sample is very slow and one can average over many measurements of each function. The experiment is performed by averaging the homodyne correlation function for 5 min, and successively averaging the heterodyne function for 5 min synchronizing the measurements with the shutter opening. This loop is repeated continuously for an aging time up to five days for the sample studied. As detailed in the previous Section the auto-correlation functions measured in the heterodyne mode is

$$g^{(1)}(t, t_w) = 1 + \sigma_1 \frac{2\langle |E_L|^2 \rangle \text{Re}[\langle E^*(t_w)E(t) \rangle] + \langle \delta |E(t_w)|^2 \delta |E(t)|^2 \rangle}{\langle |E_L|^2 \rangle^2 + \langle |E(t_w)|^2 \rangle^2} \quad (5.94)$$

where now we indicate the two times t and t_w since the system is aging. The average long-time value $\langle |E(t_w)|^2 \rangle$ is now the intensity averaged over a time much longer than the relaxation time but much shorter than the time needed to observe a change in the correlation function. To be as close as possible to the ideal heterodyne detection we want to work in the condition $\langle |E_L|^2 \rangle \gg \langle |E(t_w)|^2 \rangle$. This is done using several attenuating filters to obtain the intensities $\langle |E_L|^2 \rangle \simeq 8 \times 10^5$ counts/sec and $\langle |E(t_w)|^2 \rangle \simeq 25 \times 10^3$ counts/sec. Moreover we average a number of measured heterodyne functions (each averaged for 5 min) in different aging-time intervals. This is made possible by the fact that the aging is very slow, although at short aging times we can average over a larger

number of measurements than at long aging times. This is because the aging speeds up at longer aging times. In practice we have that the relaxation time of the functions grow faster at longer the aging times. However we can define properly these aging time sectors by setting a maximum variance allowed for each of this averaged functions. We chose this to be below 10^{-4} and, as we will see, the deviation from the Gaussian approximation observed is significantly larger than that. In the homodyne mode the function measured is

$$g^{(2)}(t, t_w) = 1 + \sigma_2 \frac{\langle \delta|E(t_w)|^2 \delta|E(t)|^2 \rangle}{\langle |E(t_w)|^2 \rangle^2} \quad (5.95)$$

Restricting the aging time interval in which the homodyne function is averaged to the same used for the heterodyne function we can obtain also for this function a variance smaller than 10^{-4} .

For correctly interpreting the experimental data some extra assumptions are needed. For the heterodyne function we assume that no significant uniform motion of the colloids takes place along the exchanged wavevector. As discusses in Section 5.3.1 this would give a complex field-field correlation function whose real part is oscillating. This assumption corresponds to say that the correlation function $\langle E^*(t_w)E(t) \rangle$ is a real function

$$\langle E^*(t_w)E(t) \rangle = \text{Re}[\langle E^*(t_w)E(t) \rangle] \quad (5.96)$$

However we notice that a uniform motion that could be present in the sample is the one driven by the gravity force acting on the colloids. Is such a precipitation process were present we should observe sedimentation at the bottom of the cuvette. In the overall aging time in which our sample is studied we see no evidence of sedimentation. The sample remains homogeneously clear with no increase of scattered light from the lower part of the cuvette. Moreover as discussed in Section 5.3.1 even if an extremely small gravity drift were present in the dynamics of the system the correlation function would not be affected by that since the velocity filed would be orthogonal to the exchanged wave-vector.

In addition to this we assume that the Gaussian approximation holds at $(t - t_w) = 0$. This is needed in order to normalize the homodyne function. Indeed what we measure is the correlation function of the intensity fluctuations up to a factor σ_2 (see Equation (5.95)). If deviations from the Gaussian approximation are expected one can not be sure a priori that

$$\frac{\langle \delta|E(t_w)|^2 \delta|E(t_w)|^2 \rangle}{\langle |E(t_w)|^2 \rangle^2} = 1 \quad (5.97)$$

The situation is different for the field-field correlation function, although also $\langle E(t_w)^*E(t) \rangle$ is measured up to a multiplicative factor σ_1 . This is because the field-field function has to be normalized to the unity by definition

$$\frac{\langle E(t_w)^*E(t_w) \rangle}{\langle |E(t_w)|^2 \rangle} = 1 \quad (5.98)$$

If we rewrite the function $\langle \delta|E(t_w)|^2 \delta|E(t)|^2 \rangle$ via the contributions of the individual particles (via Equations (5.55) and (5.55)) we see that this assumption corresponds to the fact that the full correlation function is dominated by the auto-correlations of the same particles and that cross-particles correlations average to zero at $(t - t_w) = 0$. Notice also that this assumption is consistent

with the findings of computer simulations of equilibrium glassy systems on the four-point susceptibility (see for example Ref. [27]).

Finally we assume that the fluctuations of the number of molecules contained in the scattering volume are negligible. As we have seen in Section 5.3.1 these fluctuations are expected to affect the normalized homodyne function with an additional decaying function of amplitude $\langle N \rangle^{-1}$. The average number $\langle N \rangle$ of Laponite colloidal discs contained in the scattering volume can be estimated knowing the concentration weight C_w of the sample. This is defined as the ratio between the mass of the Laponite powder M_L and the total mass of the sample (composed by the Laponite and a mass of water $M_{\text{H}_2\text{O}}$)

$$C_w = \frac{M_L}{M_{\text{H}_2\text{O}} + M_L} \quad (5.99)$$

From this Equation we can obtain the number of Laponite particles per unit volume. To do this we must express the mass of the Laponite contained in the sample as the sum of the masses of the N_{tot} colloidal discs each having volume v and mass density ρ_L^m

$$M_L = \rho_L^m N_{\text{tot}} v \quad (5.100)$$

The density of the dry Laponite powder is 2.3 g/cm^3 and the volume of each nano-particle is given by $v = \pi r^2 h$ where $r = 15 \text{ nm}$ is the radius of the colloidal disc and $h = 1 \text{ nm}$ is its thickness. Using Equation (5.100) into Equation (5.99) after some algebra we get the number density of the Laponite particles ρ_L as

$$\rho_L = \frac{C_w \rho_{\text{H}_2\text{O}}^m}{v(\rho_L^m - C_w \rho_L^m + C_w \rho_{\text{H}_2\text{O}}^m)} \quad (5.101)$$

where $\rho_{\text{H}_2\text{O}}^m = 1 \text{ g/cm}^3$ is the mass density of water. Multiplying ρ_L by the scattering volume estimated above we get an estimate of the average number of particles contained in the scattering volume for the sample used in our experiment that has low concentration $C_w \simeq 1.1 \times 10^{-2}$

$$\langle N \rangle = \rho_L (\pi w_1^2 2w_2) \simeq 2.7 \times 10^4 \quad (5.102)$$

Now we can see that the term disturbing the normalized homodyne function is of the order $\langle N \rangle^{-1} \simeq 3.7 \times 10^{-5}$ that is smaller than the maximum allowed variance on $g^{(1)}(t, t_w)$ and $g^{(2)}(t, t_w)$ that is 10^{-4} . Assuming that this term can be neglected is consistent with the precision that we have imposed to the measurements. Moreover as we will see the observed deviation from the Gaussian approximation is significantly larger than $\langle N \rangle^{-1}$.

Summarizing, following the assumptions illustrated above, we obtain the normalized intensity-intensity correlation function from the measured homodyne function $g^{(2)}(t, t_w)$ (see Equation (5.95)) normalized to the unity. The field-field correlation function is found from the measured heterodyne function $g^{(1)}(t, t_w)$ by inverting Equation (5.94) and normalizing the obtained function to the unity. The two functions measured at three well separated aging times for are reported in Figure 5.7(A). The evolution of the correlation functions is evident and, as the system ages, the functions have longer relaxation time. As it is seen these functions overlap very well at short aging times while at large aging times the two are slightly separated. This signals the failure of

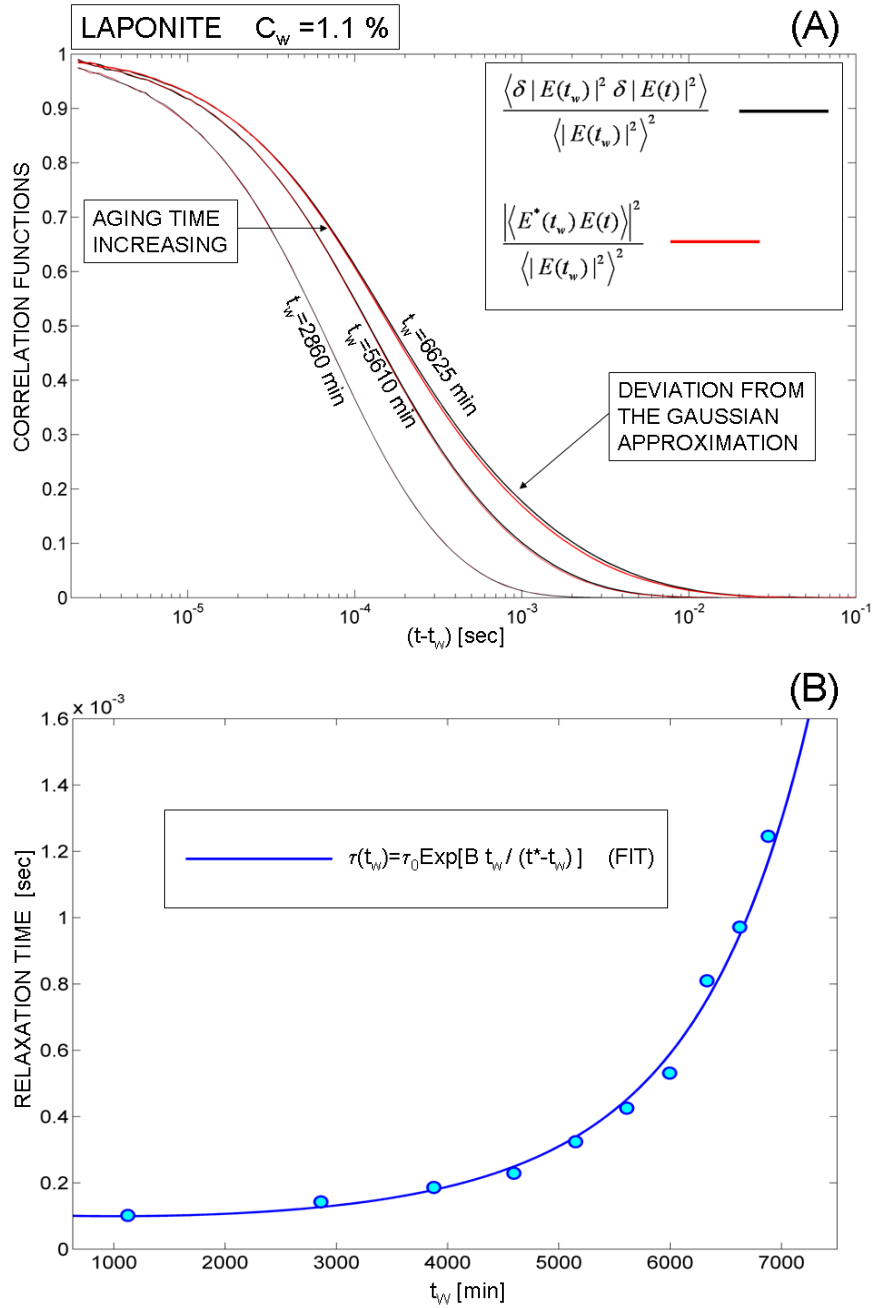


Figure 5.7: **(A)** Normalized intensity-intensity (black) and field-field (red) correlation function at three well separated aging times for a Laponite sample with $C_w = 1.1 \times 10^{-2}$. As it seen the aging functions are well overlapped at short aging times while at the longest aging time a small but clear separation between the functions is observed signaling a failure of the Gaussian approximation. **(B)** Aging relaxation time defined as the integral of the intensity-intensity correlation function (Equation (5.103)). A function of the form $\tau(t_w) = \tau_0 \exp[Bt_w/(t^* - t_w)]$ fits well the growth of the relaxation time in aging.

the Gaussian approximation and the emergence of a non-trivial high-order correlation. The relaxation time grows as the aging time increases as shown in Figure 5.7(B). Since the correlation functions are very stretched is convenient to define the aging relaxation time $\tau(t_w)$ as the integral of the function

$$\tau(t_w) = \int_0^\infty d(t - t_w) \frac{\langle \delta |E(t_w)|^2 \delta |E(t)|^2 \rangle}{\langle |E(t_w)|^2 \rangle^2} \quad (5.103)$$

This is found to grow faster than exponentially with the aging time confirming the findings of previous works (see for example Ref. [99]). A function of the form $\tau(t_w) = \tau_0 \exp[Bt_w/(t^* - t_w)]$ describes well the growth of the relaxation time in aging.

The aging four-point susceptibility is computed as

$$\chi_4(t, t_w) = \frac{\langle \delta |E(t_w)|^2 \delta |E(t)|^2 \rangle}{\langle |E(t_w)|^2 \rangle^2} - \frac{\langle \delta |E(t_w)|^2 \delta E(t_w) \rangle}{\langle |E(t_w)|^2 \rangle^2} \quad (5.104)$$

where we have removed the unimportant constant factor one appearing in the Gaussian limit. $\chi_4(t, t_w)$ is shown in Figure 5.8(A). As it is seen this grows in amplitude and its peak shifts to longer times as the aging time increases. We find a systematic increase of the amplitude of the four-point susceptibility with the aging time. In Figure 5.8(B) we show the amplitude of the four-point susceptibility $\chi_4^{\max}(t_w) = \max_{(t-t_w)} \{\chi_4(t, t_w)\}$ as a function of the aging time. From the findings of computer simulations and experiments on $\chi_3(t)$ for equilibrium supercooled liquids we expect a slow growth of the amplitude of χ_4 with the relaxation time of the system $\chi_4 \sim \log(\tau)$. For this reason we have fitted $\chi_4^{\max}(t_w)$ with a function of the form $\chi_4^{\max}(t_w) = A + Bt_w/(t - t_w)$ and, as we can see in Figure 5.8(B), this captures the trend of the data. When a well defined peak is found in $\chi_4(t, t_w)$ we can identify its characteristic time τ_{\max} . This is found to grow as the aging time increases following closely the relaxation time τ as shown in the inset of Figure 5.8(B).

In conclusion our experiment shows that is possible to observe a deviation from the Gaussian approximation and therefore a growing four-point susceptibility in aging. The experiment is performed on an out of equilibrium suspension of colloidal nano-particles for which the approximation schemes valid at the equilibrium for supercooled liquids are not applicable. Furthermore the direct imaging of the particles is not possible because of their extremely small dimensions. Nevertheless we are able to access χ_4 by measuring two correlation functions in a small scattering volume. It is important to notice that our approach does not require to confine the liquid in a small volume inducing surface effects that would irremediably change the dynamical properties of the system studied with respect to its bulk dynamics. In our experiment is the probe laser beam that reduces to the desired size. The dimensions of the scattering volume that can be reached with visible light are restricted to the micron range. This suggests that a similar approach could be followed for measuring the four-point susceptibility in molecular supercooled liquids and glasses by using nano-focused X-rays. In the recent years major advances have been made in X-ray optics making possible to obtain beams with a waist down to 10 nm (see for example Ref. [165]). This seems a promising route to follow in the study of the complex dynamics of supercooled liquids and glasses.

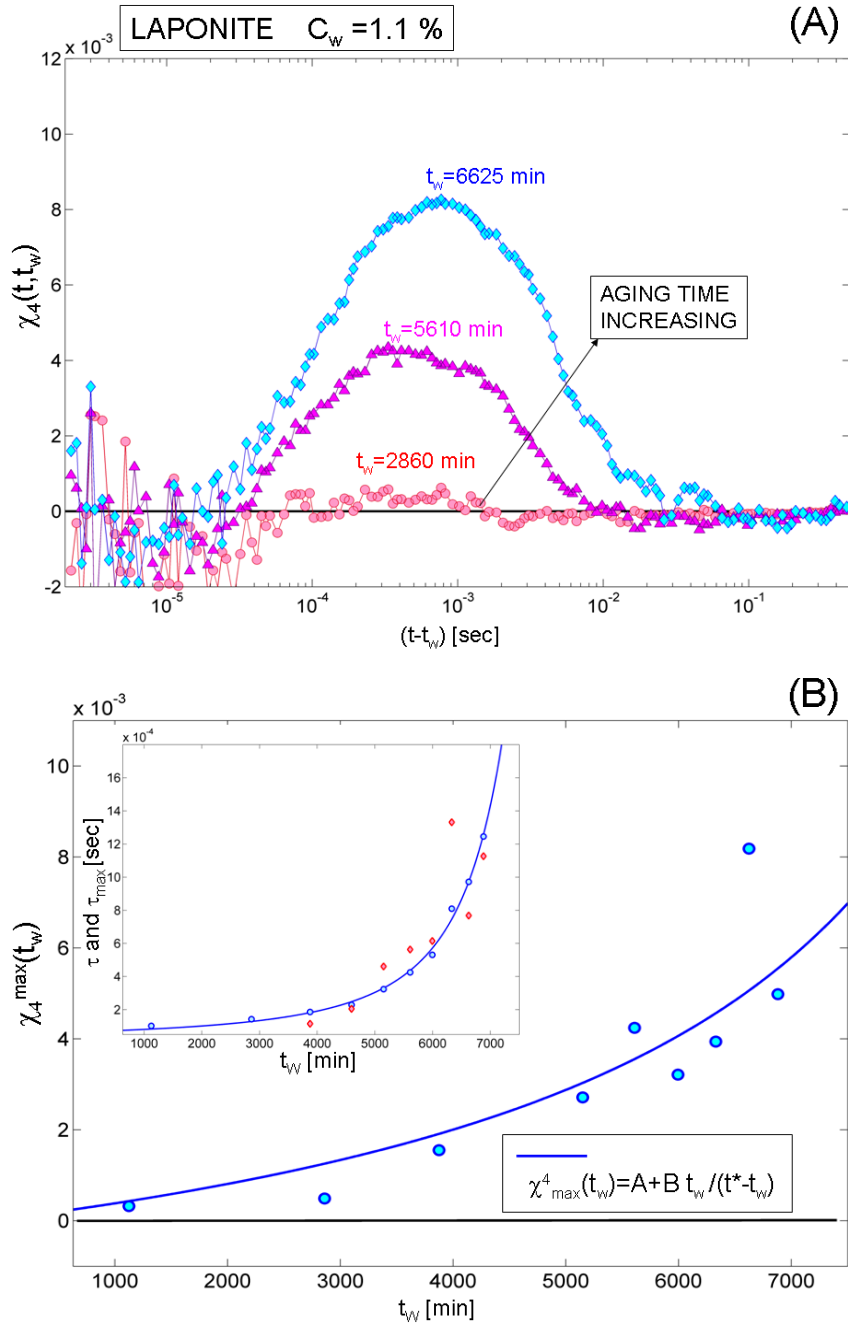


Figure 5.8: (A) Four-point susceptibility computed via Equation (5.104) at three well separated aging times for a Laponite sample with $C_w = 1.1 \times 10^{-2}$. The function grows in amplitude and its peak shifts to longer times as the aging time increases. (B) Amplitude of the function $\chi_4(t, t_w)$ as function of the aging time (main panel). The function $\chi_4^{\max}(t_w) = A + B t_w / (t^* - t_w)$ is used for fitting the data. In the inset we show the relaxation time of the system τ (circles) compared with the characteristic peak position τ_{\max} of $\chi_4(t, t_w)$ (diamonds). τ_{\max} and τ grow very similarly as the aging time increases.

Chapter 6

Heterogeneous Modeling of The Connection between Shear and Dielectric Relaxation

In this chapter we present a new model for connecting directly the shear and dielectric relaxation. This is done by introducing a modification into the Gemant-DiMarzio-Bishop (GDB) model accounting for the heterogeneous dynamics. We start by showing that an analogy exists between the break-down of the Stokes-Einstein relation (SER) and the failure of the GDB model. Following this line we introduce the new model and we compare it to the experimental data.

6.1 The Failure of The Stokes-Einstein Relation

As shown in Section 5.3.1 we can model the density relaxation by a diffusion equation in the case of a large macromolecule moving in a molecular solvent. It turns out that a Fickian diffusion equation can be used to describe reasonably well the density fluctuations for a molecular liquid system at high temperature. However this approach fails in a supercooled liquid. In particular the SER connecting the viscosity η and the diffusion coefficient D ceases to be valid as we cool a molecular liquid into the supercooled regime. To fix the ideas let us rewrite the SER as in Section 5.3.1

$$D(T) = \frac{k_B T}{6\pi\eta(T)R} \quad (6.1)$$

where R is the radius of the diffusing molecule and now we have expressed the diffusion coefficient and the viscosity as functions of the temperature T . We recall that for obtaining Equation (6.1) from the diffusion equation we have used the FDT and the Stokes law. Apart from the unimportant constant factors of Equation (6.1) the SER establishes a proportionality relationship between the diffusion constant and the viscosity

$$D(T) \propto \frac{T}{\eta(T)} \quad (6.2)$$

6. HETEROGENEOUS MODELING OF THE CONNECTION BETWEEN SHEAR AND DIELECTRIC RELAXATION

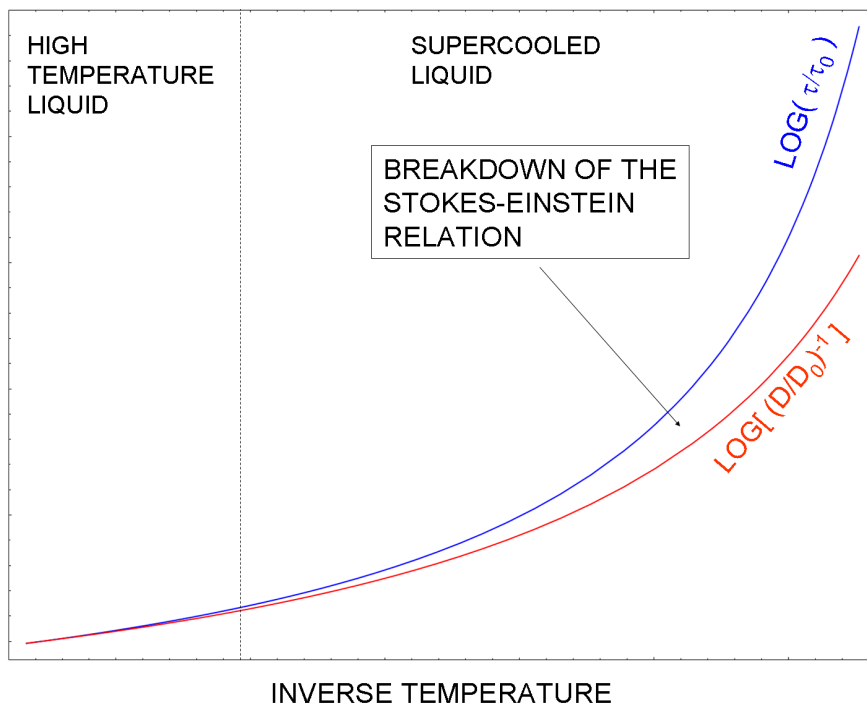


Figure 6.1: Sketch of the break-down of the SER in the supercooled regime. This can be seen as a failure of the proportionality between the diffusion constant and the inverse relaxation time of the system. In this illustration the relaxation time and the diffusion coefficient are normalized to their high temperature limit values (τ_0 and D_0 respectively). In the high temperature state the SER holds but in the supercooled regime the inverse diffusion coefficient becomes orders of magnitudes smaller than the relaxation time. For actual measurements see Ref. [168] where the inverse diffusion constant separates of about two decades from the relaxation time in o-terphenyl when $\tau \sim 1$ s.

It was clearly established by experiments that Equation (6.2) is significantly violated in supercooled liquids (see Ref.s [166, 167, 168, 30, 6]). As we cool the system into the supercooled phase we find that the diffusion coefficient is orders of magnitudes larger than the inverse viscosity, i.e. $D \gg T/\eta$. This means that while the structural rearrangements needed to relax an elastic deformation are deeply suppressed the diffusion of the molecules is still surprisingly active. Moreover the break-down of the SER has been related to the heterogeneous dynamics by several authors. In particular a very clear and simple argument supporting this link has been provided in Ref. [168] (see also Ref.s [30, 6]).

To illustrate this connection let us first rewrite Equation (6.2) as an equation relating the diffusion coefficient to the structural relaxation time of the liquid system. To do this we recall that at high temperature the shear relaxation is well described by an exponential function with relaxation time τ , i.e. $G(t) = G_\infty \exp(-t/\tau)$ (see Section 2.1). The viscosity is defined as the time-integral of the shear-modulus so that we obtain the Maxwell formula

$$\eta = \int_0^\infty dt G(t) = G_\infty \tau \quad (6.3)$$

If we use Equation (6.3) into (6.2) we have

$$D(T) \propto \frac{T}{G_\infty(T) \tau(T)} \quad (6.4)$$

We can neglect the weak temperature dependences of the terms T and $G_\infty(T)$ in Equation (6.4) to write the approximate proportionality relation

$$D(T) \propto \frac{1}{\tau(T)} \quad (6.5)$$

At some low temperature the SER breaks down and a clear deviation from Equation (6.5) is observed [168] as sketched in Figure 6.1. To establish a link between this phenomenon and the heterogeneous dynamics we consider the simple case in which we have two relaxation times τ_1 and τ_2 in the system that are well separated $\tau_2 \gg \tau_1$. This is an oversimplified scenario for the heterogeneous dynamics in which we imagine to have a group of particles moving fast, having short relaxation time τ_1 , and a group of slow particles with long relaxation time τ_2 . Although the SER (6.5) applies for the individual groups 1 and 2 giving $D_1 \propto \tau_1^{-1}$ and $D_2 \propto \tau_2^{-1}$, we have that the average diffusion constant \bar{D} is dominated by the fast dynamics

$$\bar{D} \propto \overline{\left(\frac{1}{\tau}\right)} = \frac{1}{2}(\tau_1^{-1} + \tau_2^{-1}) \simeq \tau_1^{-1}/2 \quad (6.6)$$

where we have assumed to have fast and slow particles in equal number. On the contrary the average relaxation time is mainly determined by the relaxation time of the slow particles since

$$\bar{\tau} = \frac{1}{2}(\tau_1 + \tau_2) \simeq \tau_2/2 \quad (6.7)$$

In this trivial example the presence of separated relaxation times accounts for the failure of the SER when this is applied to the average diffusion constant and the average relaxation time giving

$$\bar{D} \propto \tau_1^{-1}/2 \gg \frac{1}{\bar{\tau}} \simeq \tau_2^{-1}/2 \quad (6.8)$$

More generally we have that the SER fails at low temperatures since the dynamics becomes heterogeneous leading to a broad distribution of relaxation times $\mathcal{P}(\tau)$. This means that the diffusion constant will be dominated by the contributions of the relaxation time distribution at short τ while the relaxation time is determined by the tail of $\mathcal{P}(\tau)$ at long relaxation times giving $\bar{D} \gg 1/\bar{\tau}$. As we will see in the following a similar situation is found when we apply the GDB model connecting dielectric and shear mechanical relaxation to relaxation functions with broad relaxation-time distributions. To explain this point more in detail we briefly illustrate the model in the next Section.

6.2 An Analogy between The GDB Model and The SER

The GDB model establishes a connection between the dynamic shear modulus and the dynamic dielectric response (see Ref.s [169, 170, 71, 73] for the studies on the model reported so far). Thanks to the high quality shear modulus measurements obtained with the piezo-shear gauge (PSG) technique¹ combined with dielectric measurements it was possible to study in detail the GDB model. This was done in Ref.s [71, 73] in which the model was tested on a set of dielectric and shear mechanical measurements. In these works it was shown that the GDB model has several predictions that are correct on a qualitative level. For example the model predicts that the shear loss-peak frequency has to be higher than the dielectric loss-peak frequency. Moreover the model predicts that the beta relaxation has to be more intense in the dynamic shear-modulus than it is in the dielectric susceptibility. On the other hand the model was found to be very limited on a more quantitative ground. In Ref.s [71, 73] it was shown how to compute the shear-response using the model provided as input the measured dielectric spectrum. It was shown that this predicted mechanical spectrum had a moderate or poor agreement with the measured spectrum depending on the liquid considered.

The GDB model provides a link between the shear modulus and rotational polarization coefficient α_r . This is defined as the constant relating the average molecular dipole moment of the system $\langle \mu \rangle$ to the average local electric field \mathbf{E}_d

$$\langle \mu \rangle = \alpha_r \mathbf{E}_d \quad (6.9)$$

The GDB model is based on the assumption that the rotational dynamics of the molecular dipoles is described by a generalized diffusion equation. In this model one considers the orientational probability density $f(\theta)$. The quantity $f(\theta')d\theta$ is probability that the permanent dipole of a molecule has an orientation angle between θ' and $\theta' + d\theta$ with respect to some laboratory fixed reference frame. The equation describing the time-evolution of $f(\theta, t)$ has the form of an integro-differential equation

$$\begin{aligned} \frac{\partial f}{\partial t} = \frac{1}{\sin \theta} \frac{\partial}{\partial \theta} \left[\sin \theta \left(\int_{-\infty}^t dt' \frac{\partial f}{\partial \theta} \Big|_{t'} D(t-t') \right. \right. \\ \left. \left. - f \int_{-\infty}^t dt' V(t-t') M(t') \right) \right] \end{aligned} \quad (6.10)$$

where D is a generalized (time-dependent) rotational diffusion coefficient, V is the angular mobility memory function that is coupled to the torque $M = -\mu E_d \sin \theta$ produced by the local electric field \mathbf{E}_d . The first term on the right hand side of Equation (6.10) represents a generalized diffusion term while the second term embodies the response to the external electric field. These two terms can be related using the FDT giving

$$D(t) = k_B T V(t) \quad (6.11)$$

¹See also Chapter 2.

Using Equation (6.11) we can solve Equation (6.10), to first order, in the case of an oscillating electric field $\mathbf{E}_d(t) = \mathbf{E}_d \exp(i\omega t)$ obtaining the following expression for the rotational polarization coefficient

$$\alpha_r(\omega) = \frac{\mu^2}{3k_B T [1 + i\omega (V(\omega) 2K_B T)^{-1}]} \quad (6.12)$$

Moreover we can express V via a generalized rotational Stokes law as follows

$$V(\omega) = \frac{1}{8\pi\eta(\omega)R^3} \quad (6.13)$$

where $\eta(\omega)$ is the frequency-dependent viscosity and R is the molecular radius. If we use Equation (6.13) in (6.12) we obtain the following expression for $\alpha_r(\omega)$

$$\alpha_r(\omega) = \frac{\mu^2}{3k_B T [1 + 4\pi R^3 i\omega \eta(\omega) (k_B T)^{-1}]} \quad (6.14)$$

Using the general definition of viscosity (Equation (6.3)) we can relate the frequency-dependent viscosity to the frequency-dependent shear modulus

$$i\omega \eta(\omega) = G(\omega) \quad (6.15)$$

Using Equation (6.15) in (6.14) we get

$$\alpha_r(\omega) = \frac{\mu^2}{3k_B T [1 + 4\pi R^3 G(\omega) (k_B T)^{-1}]} \quad (6.16)$$

Having obtained a relation connecting the rotational polarization coefficient to the shear modulus (Equation (6.16)) now we need to relate α_r to the measured dielectric susceptibility ϵ . Following Ref.s [71, 73] we use the Clausius Mossotti approximation [171, 172, 173]

$$\frac{\epsilon(\omega) - 1}{\epsilon(\omega) + 2} = \frac{\rho_d [\alpha_r(\omega) + \alpha_i]}{3\epsilon_0} \quad (6.17)$$

where $\epsilon(\omega)$ is the frequency-dependent dielectric susceptibility, ρ_d is the number of dipoles per unit volume, ϵ_0 is the vacuum dielectric constant and α_i is the molecular induced polarization coefficient accounting for the electronic distribution distortion of the molecule caused by the electric field. α_i is related to the refractive index n in the high frequency limit in which $\alpha_r(\omega \rightarrow \infty) = 0$

$$\frac{n^2 - 1}{n^2 + 2} = \frac{\rho_d \alpha_i}{3\epsilon_0} \quad (6.18)$$

If we use Equations (6.17) and (6.18) into (6.16) and we rearrange the expression we obtain

$$\frac{\epsilon(\omega) - n^2}{\epsilon(0) - n^2} = \frac{1}{1 + (4\pi R^3) (k_B T)^{-1} [\epsilon(0) + 2] (n^2 + 2)^{-1} G(\omega)} \quad (6.19)$$

where $\epsilon(0)$ is the low frequency limit of the dielectric susceptibility $\epsilon(0) = \epsilon(\omega \rightarrow 0)$. Equation (6.19) can be inverted to obtain $G(\omega)$ as a function of $\epsilon(\omega)$

$$G(\omega) = \frac{k_B T}{4\pi R^3} \left[\frac{n^2 + 2}{\epsilon(0) + 2} \right] \left[\frac{\epsilon(0) - n^2}{\epsilon(\omega) - n^2} - 1 \right] = A \left[\frac{\epsilon(0) - n^2}{\epsilon(\omega) - n^2} - 1 \right] \quad (6.20)$$

where we have defined $A = (n^2 + 2)/(\epsilon(0) + 2)$. Except for the multiplicative frequency-independent term A determining the amplitude of $G(\omega)$, the GDB model given by Equation (6.20) predicts the relaxation time of the shear modulus and its shape from the measured dielectric susceptibility. This prediction is, in principle, parameter-free if the refraction index n is known. However accurate measurements of the refractive index are not generally available in the literature at low temperatures. In Ref.s [71, 73] it was discussed, and confirmed by some measurements, that some physical bounds can be set for $n(T)$. In particular we can state that the refractive index is bounded from below by the value of n at room temperature T_{room} that is more easily measured, i.e. $n(T) \geq n(T_{\text{room}})$. Moreover n^2 , that is related to the polarizability of the medium at optical frequencies, is smaller than the asymptotic value of the dielectric susceptibility ϵ_∞ seen in the frequency range spanned by our dielectric measurements limited to $\nu \simeq 1$ MHz. Using these bounds together we have that

$$n^2(T_{\text{room}}) \leq n^2(T) \leq \epsilon_\infty(T) \quad (6.21)$$

In practice we can use the model as a one-parameter prediction for the normalized $G(\omega)$, having measured $\epsilon(\omega)$, where the single free parameter n is strictly bounded by the inequality (6.21).

To understand better how the GDB model acts and in which sense it is similar to the SER we start by applying the model to a dielectric Debye-like relaxation. To this purpose let us consider a dielectric susceptibility of the form

$$\epsilon(\omega) = \epsilon_\infty + \frac{\Delta\epsilon}{1 + i\omega\tau} \quad (6.22)$$

where $\Delta\epsilon$ is the amplitude of the dielectric susceptibility and ϵ_∞ is its high frequency plateau that is $\epsilon_\infty \geq n^2$ according to the inequality (6.21). If we plug Equation (6.22) into the GDB model (6.20) after some algebra we obtain

$$G(\omega) = \left(\frac{A \Delta\epsilon}{\epsilon_\infty - n^2} \right) \frac{i\omega\tau[\Delta\epsilon/(\Delta\epsilon + \epsilon_\infty - n^2)]}{1 + i\omega\tau[\Delta\epsilon/(\Delta\epsilon + \epsilon_\infty - n^2)]} \quad (6.23)$$

If we absorb all the frequency-independent terms in the constant A' and if we introduce the modified relaxation time

$$\tilde{\tau} = \tau[\Delta\epsilon/(\Delta\epsilon + \epsilon_\infty - n^2)] \quad (6.24)$$

we can rewrite Equation (6.23) more compactly

$$G(\omega) = A' \frac{i\omega\tilde{\tau}}{1 + i\omega\tilde{\tau}} \quad (6.25)$$

This example shows that the GDB model maps a dielectric Debye relaxation into a shear Debye-like relaxation, as sketched in Figure 6.2(A) and (B). Indeed Equation (6.25) describes a Debye relaxation for $G(\omega)$. Notice that the multiplicative term $i\omega\tilde{\tau}$ gives the right behavior to the real part of $G(\omega)$ that

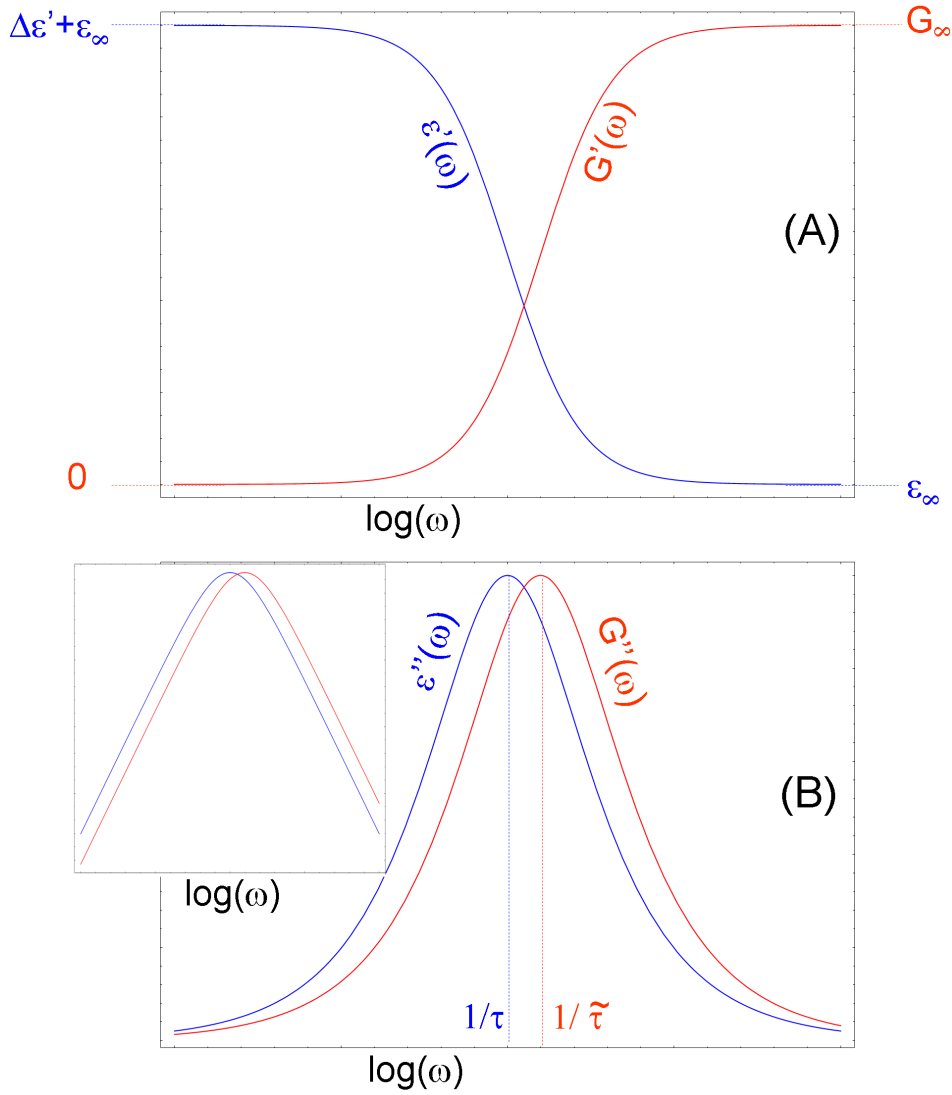


Figure 6.2: Illustration of the application of the GDB model (6.20) to a Debye dielectric relaxation $\epsilon(\omega)$ (Equation (6.22)) predicting a Debye shear relaxation. (A) shows the real parts of $\epsilon(\omega)$ (blue) and $G(\omega)$ (red). (B) shows the imaginary parts of $\epsilon(\omega)$ (blue) and $G(\omega)$ (red), the inset of (B) shows the imaginary parts in a double log-scale. As its seen the predicted dynamic shear modulus has shorter relaxation time then the dielectric susceptibility $\tilde{\tau} < \tau$.

6. HETEROGENEOUS MODELING OF THE CONNECTION BETWEEN SHEAR AND DIELECTRIC RELAXATION

approaches G_∞ at high frequency and goes to zero at low frequency. Moreover the predicted shear modulus has a relaxation time shorter than the dielectric susceptibility $\tilde{\tau} < \tau$ since $\Delta\epsilon/(\Delta\epsilon + \epsilon_\infty - n^2) < 1$.

In order to show in which sense the model is analogous to the SER we must take into account what happens if we apply the GDB model in a heterogeneous situation. As done in Section 6.1 we consider an oversimplified heterogeneous scenario in which we have a group of fast rotating dipoles and a group of slow dipoles in the system. Moreover we assume that the dielectric susceptibility of the fast dipoles is Debye-like and has relaxation time τ_1 . Similarly we assume that the slow dipoles have a Debye-like susceptibility with relaxation time τ_2 . As done in the previous Section we consider the case of well separated relaxation times $\tau_2 \gg \tau_1$. The overall dielectric spectrum will be given by

$$\epsilon(\omega) = \epsilon_\infty + \frac{\Delta\epsilon}{2} [\tilde{\epsilon}_1(\omega) + \tilde{\epsilon}_2(\omega)] = \epsilon_\infty + \frac{\Delta\epsilon}{2} \left(\frac{1}{1 + i\omega\tau_1} + \frac{1}{1 + i\omega\tau_2} \right) \quad (6.26)$$

where we have assumed to have fast and slow dipoles in equal number. In Equation (6.26) we have introduced the normalized susceptibilities $\tilde{\epsilon}_1(\omega) = (1 + i\omega\tau_1)^{-1}$ and $\tilde{\epsilon}_2(\omega) = (1 + i\omega\tau_2)^{-1}$. The dynamic shear modulus obtained by applying the GDB model to the dielectric spectrum (6.26) is

$$G(\omega) = A \left[\frac{\Delta\epsilon + \epsilon_\infty - n^2}{(\Delta\epsilon/2)[\tilde{\epsilon}_1(\omega) + \tilde{\epsilon}_2(\omega)] + \epsilon_\infty - n^2} - 1 \right] \quad (6.27)$$

To understand qualitatively what happens to the predicted mechanical spectrum $G(\omega)$ is convenient to consider the behavior of the functions $\tilde{\epsilon}_1(\omega)$ and $\tilde{\epsilon}_2(\omega)$ at different frequencies. At low frequencies of the order of $\omega \simeq \tau_2^{-1} \ll \tau_1^{-1}$ the function $\tilde{\epsilon}_1(\omega)$ reaches its plateau value and is practically constant $\tilde{\epsilon}_1(\omega \simeq \tau_2^{-1}) \simeq 1$ giving

$$G_2(\omega) = G(\omega \simeq \tau_2^{-1}) \simeq A \left[\frac{\Delta\epsilon + \epsilon_\infty - n^2}{(\Delta\epsilon/2)[1 + \tilde{\epsilon}_2(\omega)] + \epsilon_\infty - n^2} - 1 \right] \quad (6.28)$$

Contrarily at high frequencies $\omega \simeq \tau_1^{-1} \gg \tau_2^{-1}$ the function $\tilde{\epsilon}_2(\omega)$ decays to zero $\tilde{\epsilon}_2(\omega \simeq \tau_2^{-1}) \simeq 0$ giving

$$G_1(\omega) = G(\omega \simeq \tau_1^{-1}) \simeq A \left[\frac{\Delta\epsilon + \epsilon_\infty - n^2}{(\Delta\epsilon/2)\tilde{\epsilon}_1(\omega) + \epsilon_\infty - n^2} - 1 \right] \quad (6.29)$$

Since the denominator of Equation (6.28) is larger than the one of Equation (6.29) we have that

$$\text{Re}[G_1(\omega)] > \text{Re}[G_2(\omega)] \quad (6.30)$$

the same inequality holds for the imaginary part. The situation is sketched in Figure 6.3(A) and (B). Moreover the balance between the high and low-frequency parts of $G(\omega)$ is set by the value of the amplitude $\Delta\epsilon$ with respect to the term $(\epsilon_\infty - n^2)$. If $\Delta\epsilon$ is large compared to $(\epsilon_\infty - n^2)$ the computed $G(\omega)$ is largely dominated by its high-frequency components. Contrarily if the

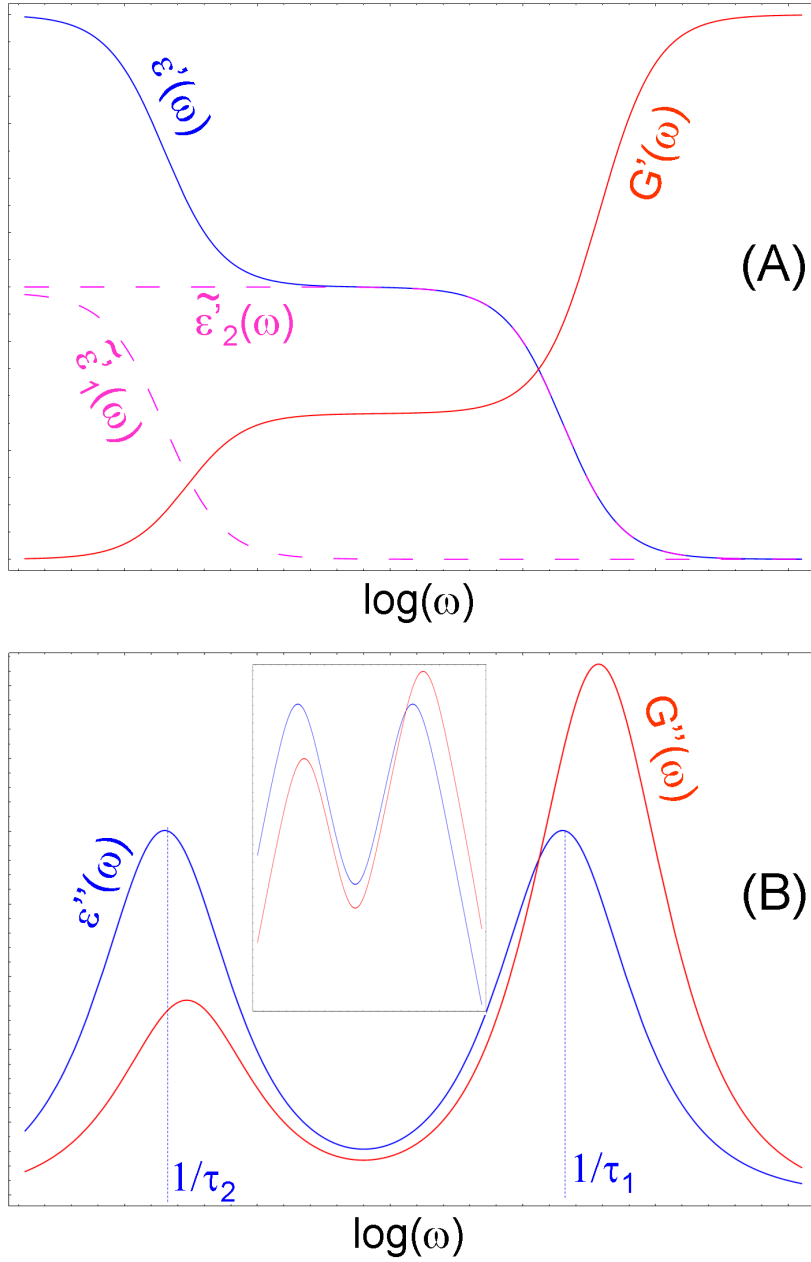


Figure 6.3: Illustration of the application of the GDB model (6.20) to a dielectric relaxation $\epsilon(\omega)$ composed by two Debye relaxations with well separated relaxation times (Equation (6.26)). (A) shows the real parts of $\epsilon(\omega)$ (blue) and $G(\omega)$ (red). The dashed lines represent the real parts of the Debye functions $\tilde{\epsilon}_1$ and $\tilde{\epsilon}_2$ composing $\epsilon(\omega)$. (B) shows the imaginary parts of $\epsilon(\omega)$ (blue) and $G(\omega)$ (red), the inset of (B) shows the imaginary parts in a double log-scale. As its seen in predicted $G(\omega)$ the high-frequency part is enhanced with respect to the low frequency part.

dielectric susceptibility has small $\Delta\epsilon$ the amplitude of the high frequency component in $G(\omega)$ will be only a little larger than the amplitude of its component at low frequencies.

What we have found in general is that the high-frequency contribution to $G(\omega)$, coming from the fast relaxing dipoles, is enhanced with respect to the low-frequency one determined by the slow dipoles, similarly to the case of the diffusion that is enhanced by the fast particles. In other words, when we apply the GDB model to an heterogeneous dielectric relaxation, the shear modulus receives a larger contribution from the fast components of the relaxation-time spectrum of the dielectric response, pretty much as the diffusion constant D in the SER that is dominated by the short relaxation times. From a more general point of view this results is not so surprising since the GDB model is built on the same fundamental assumptions that lead to the SER. Indeed for obtaining the GDB model and the SER we assume that a diffusion equations determines the dynamics of the interesting relaxing quantity. Moreover we use the FDT to relate the mobility or the friction to the diffusion. Finally we use a Stokes law to connect the friction or the mobility to the viscosity.

This approach seems interesting especially because when we predict $G(\omega)$ from the measured dielectric response via the GDB model we often obtain a $G(\omega)$ that is too broad with respect to the actually measured dynamic shear-modulus, as we will shown in the next Section (see also the discussion in Ref.s [71, 73]). Moreover this unwanted broadening is seen mainly at high frequencies suggesting that, somehow, we are not weighting correctly the components of the heterogeneous dielectric spectrum. In the next Section we introduce a new version of the GDB model that is built to account for this problem.

6.3 The Modified GDB model

The modified GDB (GDBM) model is based on the idea that the correct dynamic shear modulus is obtained by applying the original GDB model to the individual components of the dielectric spectrum. For the sake of clarity we use a more compact notation from now on indicating the GDB model (6.20) as an operator $\mathcal{M}_G[\dots]$ acting on the dielectric susceptibility $\epsilon(\omega)$ to give the dynamic shear modulus $G(\omega)$

$$G(\omega) = \mathcal{M}_G[\epsilon(\omega)] \quad (6.31)$$

In the same way we indicate the GDBM model as an operator $\mathcal{M}_{GM}[\dots]$. Now we can imagine that an heterogeneous supercooled liquid system has an overall dielectric response $\epsilon(\omega)$ that is the sum of many components $\epsilon_\alpha(\omega)$, i.e. $\epsilon(\omega) = \sum_\alpha \epsilon_\alpha(\omega)$. This correspond to assume an heterogeneous scenario in which we have many sub-regions in the liquid system relaxing in different ways. The GDBM model is defined by the application of the GDB model on the individual terms of $\epsilon(\omega)$

$$G(\omega) = \mathcal{M}_{GM}[\epsilon(\omega)] = \sum_\alpha \mathcal{M}_G[\epsilon_\alpha(\omega)] \quad (6.32)$$

Notice that it is already clear that the two models (6.31) and (6.32) will generally give a different $G(\omega)$. This is because the operator \mathcal{M}_G is non-linear

in its argument $\epsilon(\omega)$ and therefore it does not commute with the sum giving $\sum_{\alpha} \mathcal{M}_{\text{G}}[\epsilon_{\alpha}(\omega)] \neq \mathcal{M}_{\text{G}}[\sum_{\alpha} \epsilon_{\alpha}(\omega)]$.

To use in practice the GDBM model one has to make some additional assumptions on the components $\epsilon_{\alpha}(\omega)$ forming the dielectric spectrum. Indeed, in principle, these terms may have different relaxation time, shape and amplitude that are not known a priori. To overcome this issue we will assume that the non-Debye shape of the dielectric spectrum is the result of the superposition of many Debye-like processes that correspond to the relaxations in the sub-volumes of the system. Notice that this approach it is often referred has the heterogeneous explanation for the stretching of the response function in supercooled liquids and it is at the basis of the interpretation of dielectric hole-burning experiments [174, 30, 6]. In contrast the homogeneous explanation assumes that the relaxation function of the system is intrinsically non-Debye with no connection to the spatially varying dynamics. The validity of these scenarios was quite debated in the literature (see Ref.s [175, 176, 177, 30]). In this respect we know now that supercooled liquids do have a spatial fluctuations in the dynamics, and that these can be characterized by the multi-point susceptibilities as confirmed by many numerical works and some experimental studies (see the discussion in Chapter 5). It is therefore reasonable to expect that these spatial heterogeneities in the dynamics contribute significantly to the stretching of the response functions of a supercooled liquid. Moreover, for applying practically the GDBM model, it is very convenient to use the heterogeneous interpretation of the non-Debye dielectric relaxation. Indeed, following this assumption, we can rewrite the dielectric susceptibility as follows

$$\epsilon(\omega) = \int_0^{\infty} d\tau' \mathcal{P}(\tau') \left(\epsilon_{\infty} + \frac{\Delta\epsilon}{1 + i\omega\tau'} \right) \quad (6.33)$$

where $\mathcal{P}(\tau')$ is the normalized ($\int_0^{\infty} d\tau' \mathcal{P}(\tau') = 1$) spatial distribution of relaxation times. Notice also that by writing Equation (6.33) we are making a further simplification since we assuming that the amplitude $\Delta\epsilon$ and the baseline ϵ_{∞} of $\epsilon(\omega)$ do not fluctuate being these constants independent on τ' . With this decomposition the GDBM model (6.31) can be rewritten as

$$G(\omega) = \mathcal{M}_{\text{GM}}[\epsilon(\omega)] = \int_0^{\infty} d\tau' \mathcal{P}(\tau') \mathcal{M}_{\text{G}} \left[\epsilon_{\infty} + \frac{\Delta\epsilon}{1 + i\omega\tau'} \right] \quad (6.34)$$

Here we see again an analogy with the SER. In the GDBM model indeed we assume that the GDB model works when applied to the individual Debye components of $\epsilon(\omega)$, as we assume that the SER still works for the individual relaxation times of fast and slow particles but not for the overall relaxation of the system (see Section 6.1). Notice also that by using the GDBM model (6.34) we are assuming that the shear and dielectric response have the same relaxation time spectrum a part from a scaling factor. The shear relaxation time spectrum is scaled by the factor $\Delta\epsilon/(\Delta\epsilon + \epsilon_{\infty} - n^2) < 1$ introduced in Equation (6.24) with respect to the dielectric one.

For illustrating the GDBM model at work we consider first the simple heterogeneous scenario introduced in the previous Section in which two Debye-like relaxation functions compose the dielectric susceptibility. In this case we can rewrite Equation (6.26) as

$$\epsilon(\omega) = \int_0^\infty d\tau' [\delta(\tau' - \tau_1)/2 + \delta(\tau' - \tau_2)/2] \left(\epsilon_\infty + \frac{\Delta\epsilon}{1 + i\omega\tau'} \right) \quad (6.35)$$

where $\delta(x)$ is the Dirac delta function. Using the GDBM model (6.34) on the spectrum (6.35) we obtain

$$\begin{aligned} G(\omega) &= \int_0^\infty d\tau' [\delta(\tau' - \tau_1)/2 + \delta(\tau' - \tau_2)/2] A' \left(\frac{i\omega\tau' s}{1 + i\omega\tau' s} \right) \\ &= \frac{A'}{2} \left(\frac{i\omega\tau_1 s}{1 + i\omega\tau_1 s} + \frac{i\omega\tau_2 s}{1 + i\omega\tau_2 s} \right) \end{aligned} \quad (6.36)$$

where we have used Equation (6.25) and we have introduced the scaling factor for the relaxation time $s = [\Delta\epsilon/(\Delta\epsilon + \epsilon_\infty - n^2)]$. As we can see now the two Debye dielectric components are mapped into two Debye-like components in the shear spectrum with the same amplitude (see Figure 6.4(A) and (B)). In the GDBM model the two Debye dielectric elements in $\epsilon(\omega)$ contribute equally to $G(\omega)$, differently from the GDB model in which the high-frequency part of the mechanical relaxation spectrum is enhanced (see Figure 6.3).

Now we want to apply the GDBM model to some experimentally measured $\epsilon(\omega)$ and check its quality in predicting $G(\omega)$ with respect to the GDB model. For obtaining the distribution of relaxation times $\mathcal{P}(\tau)$ of the dielectric susceptibility (Equation (6.33)) we fit the measured $\epsilon(\omega)$ with a Laplace-transformed modified stretched exponential function (MSE) [58, 59]. Notice that the time-resolved MSE dielectric susceptibility is (see also Section 2.2)

$$\begin{aligned} \epsilon_{\text{MSE}}(t) &= \epsilon_\infty - \Delta\epsilon \exp[-t/\tau_0 - k(t/\tau_0)^{1/2}] \\ &= \int_0^\infty d\tau \mathcal{P}_{\text{MSE}}(\tau) [\epsilon_\infty - \Delta\epsilon \exp(-t/\tau)] \end{aligned} \quad (6.37)$$

where τ_0 is the longest relaxation time and k is the shape parameter of the MSE function. The relaxation time distribution \mathcal{P}_{MSE} defining the MSE function is given by [178]

$$\mathcal{P}_{\text{MSE}}(\tau) = \frac{1}{\mathcal{N}} \frac{\tau_0 \Theta(\tau_0 - \tau)}{2\tau(\tau_0 - \tau)} \exp\left[\frac{-k\tau}{\tau_0 - \tau}\right] \sqrt{\frac{k\tau}{\pi(\tau_0 - \tau)}} \quad (6.38)$$

where $\Theta(x)$ is the Heaviside step function, and \mathcal{N} is the normalization factor

$$\mathcal{N} = \int_0^{\tau_0} d\tau \frac{\tau_0}{2\tau(\tau_0 - \tau)} \exp\left[\frac{-k\tau}{\tau_0 - \tau}\right] \sqrt{\frac{k\tau}{\pi(\tau_0 - \tau)}} \quad (6.39)$$

Since the Laplace transform is a linear operation we have that $\epsilon_{\text{MSE}}(\omega)$ can be expressed, as in Equation (6.33), as follows

$$\epsilon_{\text{MSE}}(\omega) = \int_0^\infty d\tau \mathcal{P}_{\text{MSE}}(\tau) \left(\epsilon_\infty + \frac{\Delta\epsilon}{1 + i\omega\tau} \right) \quad (6.40)$$

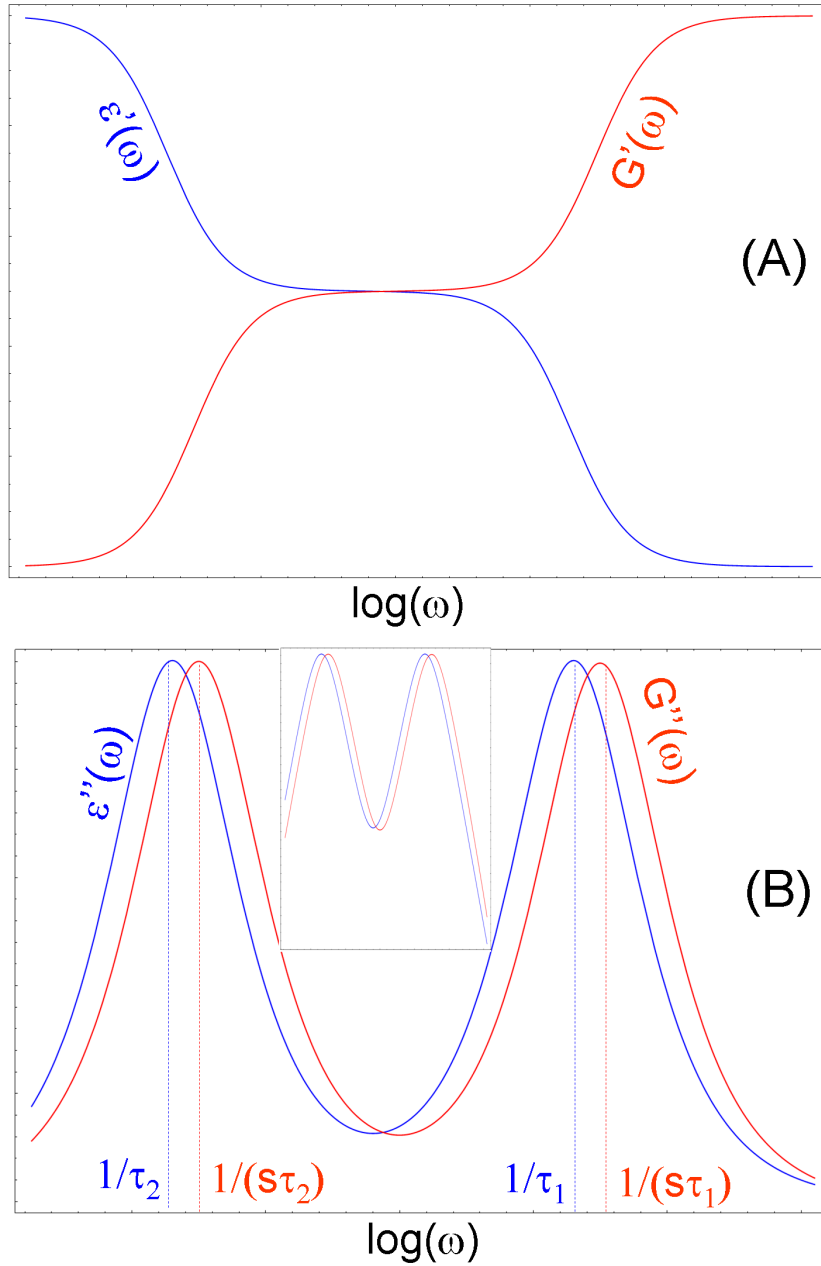


Figure 6.4: Illustration of the application of the GDBM model (6.34) to a dielectric relaxation $\epsilon(\omega)$ composed by two Debye relaxations with well separated relaxation times (Equation (6.35)). (A) shows the real parts of $\epsilon(\omega)$ (blue) and $G(\omega)$ (red). (B) shows the imaginary parts of $\epsilon(\omega)$ (blue) and $G(\omega)$ (red), the inset of (B) shows the imaginary parts in a double log-scale. As its seen the $G(\omega)$ predicted by the GDBM receive an equal contribution form the high-frequency and from the low-frequency part of the dielectric spectrum, differently from the prediction of the GDB model in which the high-frequency part is enhanced (see Figure 6.3).

Using Equation (6.40) represents also a valid numerical approach for fitting the measured frequency-resolved dielectric susceptibility. This can be done easily by converting the integral (6.40) into a discrete sum in order to evaluate $\epsilon_{\text{MSE}}(\omega)$ and by fitting the experimental $\epsilon(\omega)$ with respect to the parameters ϵ_∞ , $\Delta\epsilon$, k and τ_0 . Notice that a similar method could be used for fitting the data in the frequency domain with a generic stretched exponential (KWW) function $\epsilon_{\text{KWW}}(t) = \epsilon_\infty - \Delta\epsilon \exp[-(t/\tau_0)^\beta]$. However the KWW function is much harder to integrate numerically in order to obtain $\epsilon_{\text{KWW}}(\omega)$. This is because its $\mathcal{P}_{\text{KWW}}(\tau)$ contains an extra integral of an additional parameter (see Ref. [178]). Moreover the integral defining $\epsilon_{\text{MSE}}(\omega)$ is bounded between zero and τ_0 by the function $\Theta(\tau_0 - \tau)$ contained in $\mathcal{P}_{\text{MSE}}(\tau)$ making the computation particularly convenient. Differently when we integrate the function $\epsilon_{\text{KWW}}(\omega)$ we should consider a wide domain for τ since $\mathcal{P}_{\text{KWW}}(\tau)$ decreases slowly as $\tau \rightarrow \infty$, with no sharp cut-off, slowing down considerably the numerical integration.

We start by comparing the GDBM model and GDB model applied on the dielectric response of two liquids: tetramethyltetraphenyltrisiloxane (DC704) and polyphenyl ether (PPE). The dielectric and shear measurements performed by our group on these liquids were presented in Ref.s [71, 73, 72]. Here we focus on the ability of the two models in predicting the shape of $G(\omega)$ so we will consider in the dielectric and shear relaxation functions at one single temperature close to T_g . As discussed in Ref.s [71, 73, 72] indeed time-temperature superposition applies for the dielectric and mechanical alpha processes of DC704 and PPE in the frequency/temperature range accessible by our dielectric and shear measurements. Therefore we expect that the quality of the models in giving the right shape of $G(\omega)$ does not change too much considering some other temperature in the experimentally accessible range.

In Figure 6.5(A) and (B) we show the measured real and imaginary part of the dielectric susceptibility of DC704 at $T = 219.5$ K ($T_g = 211$ K) fitted by the MSE function (6.40). As it can be seen the MSE function fits excellently the experimental dielectric data. In Figure 6.5(B) and (C) we report the measured dynamic shear modulus (real and imaginary part) of DC704 at $T = 219.5$ K and we compare it with the predictions of the GDB and of the GDBM models. The amplitude of the predicted $G(\omega)$ is scaled to match the G_∞ of the measured shear modulus. Moreover we adjust the parameter n for predicted $G(\omega)$ compatibly with the inequality (6.21) (see Table 6.3). As it can be seen from Figure 6.5 the original GDB works quite well for DC704 as found also in Ref.s [71, 73], although the predicted $G(\omega)$ is a little too broad compared to the measured one. Differently the GDBM model predicts a $G(\omega)$ with a narrower shape that is more similar to the one of the measured $G(\omega)$. This situation is somehow expected since the the amplitude of the dielectric response of DC704 is not too large compared to the factor $(\epsilon_\infty - n^2)$. This implies that the high-frequency components of $G(\omega)$ predicted by the GDB model are not enhanced too much with respect to its low-frequency components as discussed in the previous Section.

The situation is quite different for PPE. In Figure 6.6(A) and (B) we show the measured real and imaginary part of the dielectric susceptibility of PPE at $T = 256.0$ K ($T_g = 245$ K) fitted by the MSE function (6.40). Again the MSE function fits very well the measured $\epsilon(\omega)$. In Figure 6.6(B) and (C) we report the measured dynamic shear modulus (real and imaginary part) of PPE at $T = 256.0$ K and we compare it with the predictions of the GDB and of the

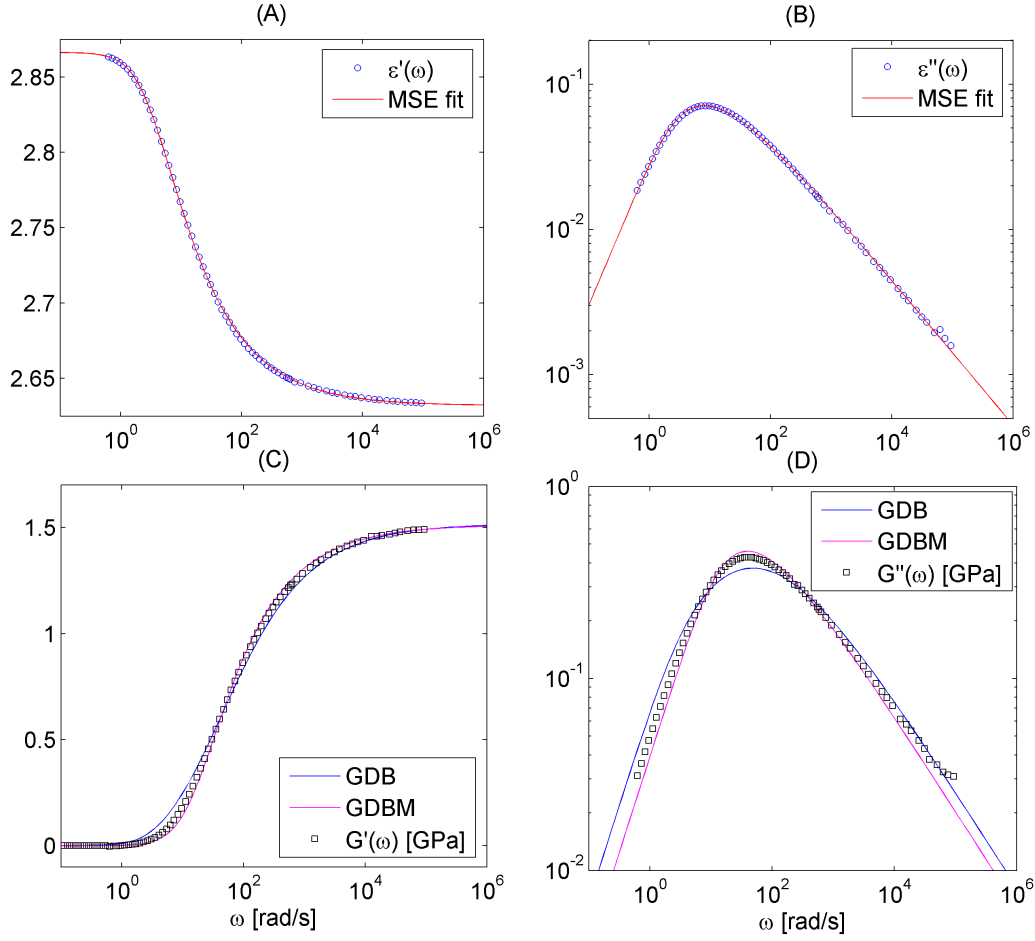


Figure 6.5: (A) and (B) show, respectively, the real and the imaginary parts (circles) of the measured dielectric response of DC704 at $T = 219.5$ K ($T_g = 211$ K). The red line is the fitting MSE function (6.40). (C) and (D) show, respectively, the real and the imaginary parts of the measured dynamic shear modulus of DC704 at $T = 219.5$ K (squares). The blue line is the $G(\omega)$ predicted by the GDB model, the purple line is the $G(\omega)$ predicted by the GDBM model.

Liquid	T_g [K]	$n^2(T_{\text{room}})$	$n^2(T)$ (GDB)	$n^2(T)$ (GDBM)	$\epsilon_\infty(T)$
DC704 (at $T = 219.5$ K)	211	2.430	2.502	2.572	2.632
PPE (at $T = 256$ K)	245	2.659	2.7	2.7	2.932
TPG (at $T = 194.0$ K)	190	2.085	2.1	2.1	2.826

Table 6.1: Value of the parameter $n(T)$ adjusted for the GDB model and the GDBM model. The $n(T)$ is chosen compatibly with the inequality (6.21). The values of n at room temperature are taken from Ref.s [71, 73, 72]. The value of $\epsilon_\infty(T)$ is determined by the fitting.

6. HETEROGENEOUS MODELING OF THE CONNECTION BETWEEN SHEAR AND DIELECTRIC RELAXATION

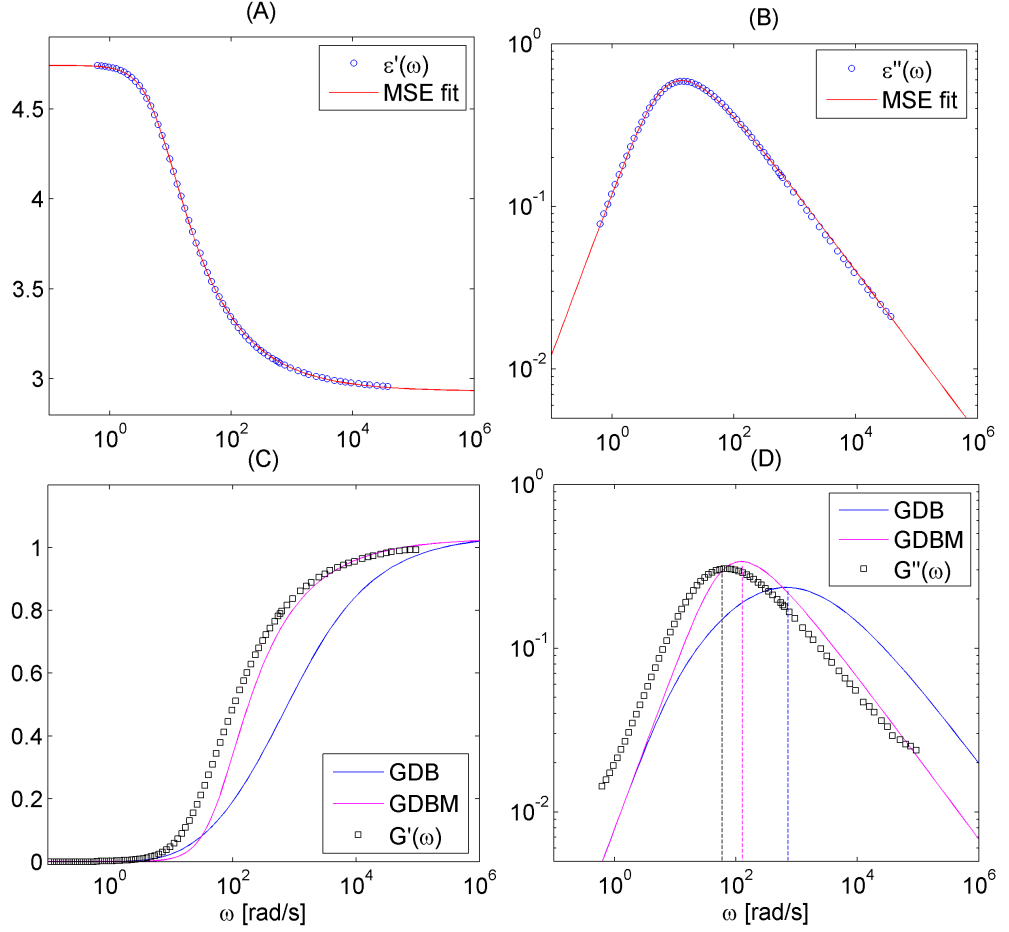


Figure 6.6: **(A)** and **(B)** show, respectively, the real and the imaginary parts (circles) of the measured dielectric response of PPE at $T = 256.0$ K ($T_g = 245$ K). The red line is the fitting MSE function (6.40). **(C)** and **(D)** show, respectively, the real and the imaginary parts of the measured dynamic shear modulus of PPE at $T = 256.0$ K (squares). The blue line is the $G(\omega)$ predicted by the GDB model, the purple line is the $G(\omega)$ predicted by the GDBM model. The vertical dashed lines indicates the shear loss peak positions of the measured $G(\omega)$ and of the $G(\omega)$ predicted by the models.

GDBM models. The amplitudes of the two predicted $G(\omega)$ and the values of n are set as in the case of DC704 (see Table 6.3). For PPE $\Delta\epsilon$ is quite large and the GDB model predicts a completely deformed mechanical spectrum that is dominated by its high-frequency components. The loss peak position predicted by the GDB model is more than an order of magnitude larger than the measured one. Differently the GDBM model seems to weight correctly the components of the spectrum giving a $G(\omega)$ with a shape extremely similar to the measured one. The loss peak position of the $G(\omega)$ obtained from the GDBM model is still not matching perfectly with the measured one. However the shear loss peak position predicted by the GDBM model is only about a factor two larger than the measured one.

Now we consider the application of the models to a liquid having a beta relaxation. Notice that in this case the single MSE function is not enough to describe the dielectric spectrum. To efficiently fit the full dielectric response of a supercooled liquid showing a beta process we can use a linear combination of a MSE function and a Cole-Cole (CC) function $\epsilon_{CC}(\omega)$ [179, 180] (see also Ref. [58]). This fitting function may be conveniently written as

$$\epsilon(\omega) = \epsilon_{\infty} + \Delta\epsilon \left[\left(\int_0^{\infty} d\tau' \mathcal{P}_{\text{MSE}}(\tau') \frac{1-a}{1+i\omega\tau'} \right) + a \tilde{\epsilon}_{\text{CC}}(\omega) \right] \quad (6.41)$$

where $0 \leq a \leq 1$ sets the relative amplitude of the alpha and the beta process and the (normalized) CC function is given by the expression

$$\tilde{\epsilon}_{\text{CC}}(\omega) = \frac{1}{1 + (i\omega\tau_{\beta})^{\alpha}} \quad (6.42)$$

where τ_{β} indicates the characteristic relaxation time of the secondary process and α is the shape parameter.

Notice that at this point we could apply the GDBM model in two alternative ways depending on how we treat the non-Debye shape of the beta process. Indeed we may assume that the heterogeneous explanation applies also for the stretching of the beta relaxation and that its non-Debye shape is the result of the superposition of many Debye-like processes. In this case the GDBM model applies on the Debye components of the dielectric spectrum belonging both to the alpha and the beta relaxation. For the sake of clarity we will refer to this first version of the model with the acronym GDBM1. Mathematically we will indicate the GDBM1 model as an operator $\mathcal{M}_{\text{GM1}}[\dots]$. The GDBM1 model can be written as

$$G(\omega) = \mathcal{M}_{\text{GM1}}[\epsilon(\omega)] = \int_0^{\infty} d\tau' \mathcal{P}_{\text{TOT}}(\tau') \mathcal{M}_{\text{G}} \left[\epsilon_{\infty} + \frac{\Delta\epsilon}{1+i\omega\tau'} \right] \quad (6.43)$$

where

$$\mathcal{P}_{\text{TOT}}(\tau) = (1-a) \mathcal{P}_{\text{MSE}}(\tau) + a \mathcal{P}_{\text{CC}}(\tau) \quad (6.44)$$

In Equation (6.44) $\mathcal{P}_{\text{MSE}}(\tau)$ is the relaxation time distribution of the MSE function (Equation (6.38)) and $\mathcal{P}_{\text{CC}}(\tau)$ is the relaxation time distribution of the CC function [178]

$$\mathcal{P}_{CC}(\tau) = \frac{1}{2\pi\tau} \left(\frac{\sin(\pi\alpha)}{\cosh[\alpha \ln(\tau/\tau_\beta)] + \cos(\pi\alpha)} \right) \quad (6.45)$$

The parameter a in Equation (6.44) determines the relative amplitude of the MSE function and of the CC function contributing to the overall $\epsilon(\omega)$ (as in Equation (6.41)), with the bound $0 \leq a \leq 1$ ensuring the normalization.

The other way of applying the GDBM model, when a beta process is present, is by assuming that the secondary relaxation is homogeneously stretched. This corresponds to assume that the beta process is intrinsically non-Debye and it is not the result of the superposition of many Debye-like processes. Although this assumption might seem somehow weird it can be justified qualitatively as follows. We should keep in mind that the relaxation time τ_α of the alpha process grows rapidly upon cooling increasing (at least) in an Arrhenius way. On the other hand the beta relaxation time τ_β generally has a much weaker temperature dependence and, in most cases, it is even difficult to see any clear change of τ_β in the entire supercooled equilibrium phase (see Ref. [181]). In Section 5.1.1 we have seen that the typical size of the spatial fluctuations of a dynamic response function can be approximated by the simple formula $N_{\text{corr}} \simeq (k_B/c_p)f^2|\partial \ln \tau/\partial \ln T|^2$ where c_p is the specific heat per particle at constant pressure, τ is the relaxation time of the function and f is a constant multiplicative factor of order one. With this expression we can roughly estimate the characteristic amplitude of the dynamic fluctuations in the response function on the timescale of the relaxation time. If we apply this idea separately to the alpha and to the beta relaxations as two independent processes, we immediately realize that the amplitude of the spatial fluctuations of the beta dynamics is practically insignificant with respect to the typical amplitude of the fluctuations of the alpha relaxation. In particular this is the case close to T_g where the alpha relaxation time grows sharply (especially for fragile liquids) giving $|\partial \ln \tau_\alpha/\partial \ln T|^2 \gg |\partial \ln \tau_\beta/\partial \ln T|^2$. This qualitative argument supports the idea that the beta relaxation is intrinsically non-Debye since its spatial fluctuations are negligible with respect to those characterizing the structural alpha process. Following this suggestion we can rewrite the GDBM model, differently from the GDBM1 model (6.43), with the operator \mathcal{M}_G acting on the decomposed alpha process and on the (non decomposed) beta relaxation. We will refer to this second version of the GDBM model with the acronym GDBM2 and we will indicate the GDBM2 model as an operator $\mathcal{M}_{\text{GM2}}[\dots]$. The GDBM2 model can be formally written as

$$\begin{aligned} G(\omega) &= \mathcal{M}_{\text{GM2}}[\epsilon(\omega)] \\ &= \int_0^\infty d\tau' \mathcal{P}_{\text{MSE}}(\tau') \mathcal{M}_G \left[\epsilon_\infty + \Delta\epsilon \left(\frac{1-a}{1+i\omega\tau'} + \frac{a}{1+(i\omega\tau_\beta)^\alpha} \right) \right] \end{aligned} \quad (6.46)$$

Let us now see how the GBD, GDBM1 and GDBM2 models work in predicting $G(\omega)$ from a measured dielectric spectrum showing a clear beta relaxation. For doing this we consider the dielectric and mechanical measurement on tripropylene glycol (TPG) presented in Ref.s [71, 73, 72]. We apply the models to a measurement of $\epsilon(\omega)$ close to $T_g = 190$ K where the alpha and beta

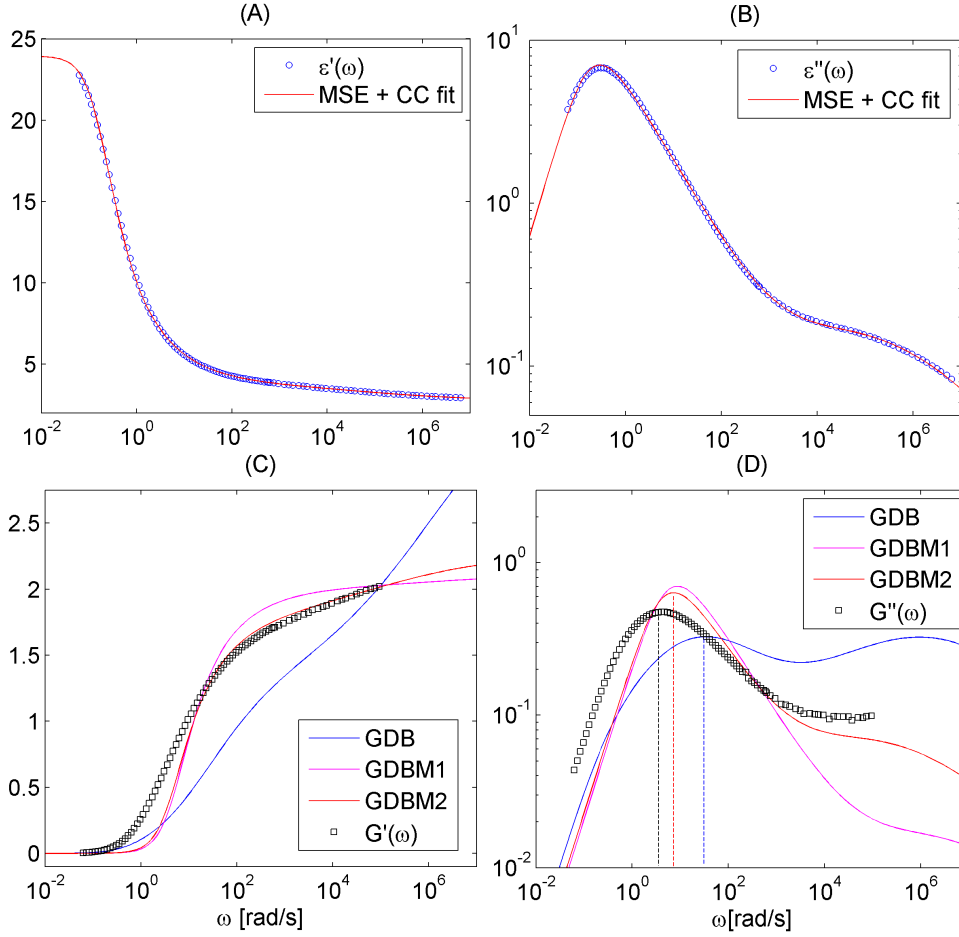


Figure 6.7: **(A)** and **(B)** show, respectively, the real and the imaginary parts (circles) of the measured dielectric response of TPG at $T = 194.0$ K ($T_g = 190$ K). The red line is the fitting with an MSE function plus a CC function (Equation (6.41)). **(C)** and **(D)** show, respectively, the real and the imaginary parts of the measured dynamic shear modulus of TPG at $T = 194.0$ K (squares). The blue line is the $G(\omega)$ predicted by the GDB model, the purple line is the $G(\omega)$ predicted by the GDBM1 model and the red line is the $G(\omega)$ predicted by the GDBM2 model. The vertical dashed lines indicates the shear loss peak positions of the measured $G(\omega)$ and of the $G(\omega)$ predicted by the models.

processes are well separated. In Figure 6.7(A) and (B) we show the measured real and imaginary part of the dielectric susceptibility of TPG at $T = 194.0$ K fitted by a combination of the MSE and of the CC function (6.41). The fitting function (6.41) describes well the measured $\epsilon(\omega)$. In Figure 6.7(B) and (C) we report the measured dynamic shear modulus (real and imaginary part) of TPG at $T = 194.0$ K and we compare it with the predictions of the GDB, of the GDBM1 and of the GDBM2 models. The amplitudes of the two predicted $G(\omega)$ and the values of n are set as described above for DC704 and PPE (Table 6.3). The GDB model in this case predicts again a deformed mechanical spectrum that is dominated by its high-frequency components. In particular the GDB model fails in predicting $G(\omega)$ even on a qualitative level, giving a mechanical beta relaxation that is intense as the alpha. The loss peak position of $G(\omega)$ predicted by the GDB model is about one order of magnitude larger than the measured one. Differently the GDBM1 gives a mechanical loss peak position only about a factor two larger than the measured one. Nevertheless the shape of the shear alpha process given by the GDBM1 model is still a little too narrow than the measured one. Moreover the magnitude of the mechanical beta process is underestimated by the GDBM1 model. In this respect the GDBM2 model gives a more satisfying description of the full $G(\omega)$ with a more accurate estimate of the intensity of the shear beta process.

In conclusion we have presented a new version of the GDB model, the GDBM model, that is modified to account for the heterogeneous dynamics. The GDBM model is inspired by the qualitative analogy between the original GDB model and the SER. In the cases examined here the GDBM model allows for a considerable improvement in the prediction of the shear modulus with respect to the GDB model. The shape of the dynamic shear modulus obtained from the GDBM model is significantly better than the one given by the GDB model especially for those liquids with a large dielectric susceptibility. Moreover the shear loss peak position predicted by the GDBM model improves in precision by almost one order of magnitude with respect to the GDB model for those liquids with intense dielectric response. We have also shown that the GDBM model can be used in two alternative ways when we want to describe spectra showing a clear beta process. In this case the GDBM model works better if we assume that the beta relaxation is intrinsically non-Debye as suggested by some arguments inspired by the studies on the multi-point susceptibilities. This is an interesting insight since a clear understanding of the heterogeneous properties of the beta process is still lacking. Certainly more work can be done to clarify if the GDBM model can be further improved. For example the Clausius Mossotti approximation connecting the rotational polarization coefficient to the dielectric susceptibility could be changed by choosing an alternative description of the local field. As discussed in Ref.s [71, 73] this choice has practically no effect on the quality of the predictions of the GDB model, but it could be that an alternative local field improves the prediction of the GDBM model, this is expected in particular for those liquids having a intense molecular dipole moment. From a more general point of view it is interesting to notice that thinking of the dynamics of a supercooled liquid in terms of dynamical heterogeneities is not only a purely theoretical exercise. The modeling described in this section indicates that this is a fruitful concept also when applied to problems of practical importance such as the indirect measurement of the shear-mechanical properties of a supercooled liquid from

the simpler measurement of its dielectric properties.

Chapter 7

Outlook

In this chapter we illustrate the perspectives of the studies presented in the thesis. We focus on the open questions that may indicate new ways to follow in future numerical and experimental studies.

7.1 Shear-Mechanical Beta Relaxation

As discussed in Chapter 2, in Paper I and in Paper II when the beta relaxation is seen the dielectric spectrum it is also seen in the shear modulus. Nevertheless in most cases the mechanical beta peak lies at high frequencies, above the highest frequency that can be probed via the PSG technique (~ 10 kHz). This is a limitation for studying the features shear beta process. The issue could be solved by slightly modifying the geometry of the transducer. Indeed one could use smaller piezo-ceramics shifting the accessible dynamic range to higher frequencies. Another possibility is to study the evolution of the beta relaxation in the glassy regime. In this condition the dielectric beta process generally shows a much more pronounced temperature dependence in its relaxation time. It is expected that, in this condition, also the mechanical beta moves to lower frequency making possible a better experimental characterization its shape and temperature dependence.

7.2 Experimental Studies of the Off-Equilibrium Dynamics

In Chapter 3 and in Paper III we illustrate an experiment for studying the off-equilibrium fluctuation-dissipation relation (FDR) in an aging colloidal suspension. This experiment could be, in principle, performed on a molecular glassy system. In the literature we can find some measurement of the depolarized light scattering correlation function of supercooled liquids (see for example Ref. [182]). Moreover it was shown that it is possible to obtain Kerr effect response measurement in supercooled liquids (see Ref. [183]). The FDR could be studied by combining these optical measurements with a temperature-controlling system allowing for a fast cooling of the liquid in the glassy regime. Recently a device optimized for a very fast temperature change of the system was developed in our group [59]. Certainly such an experiment would be challenging but it seems a promising route to follow in the experimental study of the FDR.

7.3 Numerical Studies of the Off-Equilibrium Dynamics

As discussed in Chapter 4 and in Paper IV the effective temperature T_{eff} found from the FDR has some remarkable scaling properties in strongly correlating liquids (SCLs). Moreover we have shown that in a strongly correlating liquid T_{eff} individuates the equilibrium inherent states that the system visits in aging. This scenario is found to breakdown for non-SCL systems. In this context it would be interesting to understand more precisely why an off-equilibrium thermalizing SCL system has to age through equilibrium states. Moreover it should be studied more in detail if underlying liquid-to-liquid transitions play a role in destroying this simple aging behavior. Computer simulations could provide a useful insight in this context.

In Chapter 4 we have also pointed out that a quite striking correlation exists between the non-ergodicity factor and the violation factor of an SCL glassy system. We have also mentioned that a similar situation is found in some spin systems where the correlation expresses some interesting properties of the landscape of the system. To understand if the same structure of the landscape is present in a glassy SCL system we may measure in computer simulations the multiplicity of the trapping inherent states and the overlap of the configurations belonging to the same state. Suitable operative methods for finding the multiplicity of the inherent states have been proposed in the literature [184, 185, 186]. Moreover an overlap function for the density field can be defined as done in Ref.s [187, 188]. These investigations could give very detailed information on the structure of the landscape of SCL systems.

7.4 Experimental Investigation of The Multi-Point Susceptibilities

In Chapter 5 and in Paper V we have seen how to determine indirectly the multi-point susceptibilities in experiments. We have also shown that in general the shear and dielectric three-point susceptibilities are different. Nevertheless we have found that the amplitudes of these dielectric and mechanical high-order correlations grow proportionally upon cooling for several supercooled liquids. We mentioned that this picture seems to be confirmed also by other dynamic response measurements. This fact has to be established more firmly by a more accurate analysis but, if confirmed, it opens some fundamental questions. Why do all the dynamic susceptibilities grow proportionally upon cooling? Is there a unique underlying physical mechanism that drives the growth of these dynamic correlations? More experimental, numerical, and theoretical work is certainly needed to answer these questions.

In Chapter 5 we have also described a new experiment for the direct measurement of the four-point susceptibility making use of photon correlation spectroscopy techniques. The experiment is based on the combined use of heterodyne and homodyne dynamic light scattering techniques. Moreover the experiment employs small scattering volumes to enhance the dynamic fluctuations. The experiment was applied for determining the four-point susceptibility of an aging colloidal suspension. We have mentioned that a similar approach could be used in the experimental determination of the four-point susceptibility in molecular supercooled and glassy systems provided that the focused beam

has nanometric size. With some advanced optics focused X-rays with ~ 10 nm beam waist have been obtained (see for example Ref. [165]). Moreover X-ray photon-correlation spectroscopy XPCS has been applied successfully to the study of some supercooled polymer liquid (see Ref. [189]). The use of XPCS in small scattering volume seems to be a promising route to follow in the challenging experimental studies of the multi-point susceptibilities.

7.5 Modeling The Connection of Shear and Dielectric Response

In Chapter 6 we have introduced a new model for connecting the shear and the dielectric response of a supercooled liquid based on an heterogeneous description of the dynamics. This new model (GDBM) is a modification of the Gemant-DiMarzio-Bishop (GDB) model. The GDBM model is found to work significantly better than the GDB model in predicting the shape and the mechanical loss-peak position of the shear modulus from the measured dielectric susceptibility. Nevertheless the agreement between the predicted shear modulus and the measured one is still far from being perfect. As mentioned in Chapter 6 the quality of the GDBM model could be improved by using more sophisticated expression for the local field.

Bibliography

- [1] Angell C. A. Perspective on The Glass-Transition. *Journal of Physics Reports and Chemistry of Solids*, 49(8):863–871, 1988.
- [2] MD Ediger, CA Angell, and SR Nagel. Supercooled liquids and glasses. *Journal of Physical Chemistry*, 100(31):13200–13212, AUG 1 1996.
- [3] Angell C.A. and Ngai K.L., McKenna G.B., McMillan P.F., Martin S.W. Relaxation in glassforming liquids and amorphous solids. *Journal of Applied Physics*, 88(6):3113–3157, SEP 15 2000.
- [4] Dyre J. C. Colloquium: The glass transition and elastic models of glass-forming liquids. *Reviews of Modern Physics*, 78(3):953, Jul-Sep 2006.
- [5] Steven A. Kivelson and Gilles Tarjus. In search of a theory of supercooled liquids. *NATURE MATERIALS*, 7(11):831–833, NOV 2008.
- [6] Cavagna A. Supercooled liquids for pedestrians. *Physics Reports*, 476(4-6):51 – 124, 2009.
- [7] S. U. Dzhaliilo and K. I. Rzaev. On Phenomenon Of Selenium Vitrification. *Physica Status Solidi*, 20(1):261, 1967.
- [8] R Richert and CA Angell. Dynamics of glass-forming liquids. V. On the link between molecular dynamics and configurational entropy. *Journal of Chemical Physics*, 108(21):9016–9026, JUN 1 1998.
- [9] A. P. Sokolov, E. Rossler, A. Kisliuk, and D. Quitmann. Dynamics of Strong and Fragile Glass Formers - Differences and Correlation with Low-Temperature Properties. *Physical Review Letters*, 71(13):2062–2065, SEP 27 1993.
- [10] S. N. Yannopoulos and G.N. Papatheodorou. Critical experimental facts pertaining to models and associated universalities for low-frequency Raman scattering in inorganic glass formers. *Physical Review B*, 62(6):3728–3734, AUG 1 2000.
- [11] T. Scopigno, G. Ruocco, F. Sette, and G. Monaco. Is the fragility of a liquid embedded in the properties of its glass? *Science*, 302(5646):849–852, OCT 31 2003.
- [12] Buchenau U. and Wischnewski, A. Fragility and compressibility at the glass transition. *Physical Review B*, 70(9):, SEP 2004.

BIBLIOGRAPHY

- [13] Giordano V. M. Monaco G. Frick B. Alba-Simionesco C. Niss K., Dalle-Ferrier C. Glassy properties and viscous slowing down: An analysis of the correlation between nonergodicity factor and fragility. *Journal of Chemical Physics*, 129:194513, 2008.
- [14] Christensen T. Dyre J. C., Olsen N. B. Local elastic expansion model for viscous-flow activation energies of glass-forming molecular liquids. *Physical Review B*, 53(5):2171–2174, FEB 1 1996.
- [15] Bohmer R., K. L. Ngai, C.A. Angell, and D. J. Plazek. Nonexponential Relaxations in Strong and Fragile Glass Formers. *Journal of Chemical Physics*, 99(5):4201–4209, SEP 1 1993.
- [16] Alba-Simionesco C. Salient properties of glassforming liquids close to the glass transition. *Comptes Rendus de L'Academie des Sciences Serie IV Physique Astrophysique*, 2(2):203–216, MAR 2001.
- [17] Feynman R. P. *Statistical Mechanics: A Set of Lectures*. Academic, 1972.
- [18] Landau L. D. and Lifshitz E. M. *Statistical Physics*. Butterworth-Heinemann, 1980.
- [19] Jean-Pierre Hansen and Ian R. McDonald. *Theory of Simple Liquids*. Academic Press, 1990.
- [20] Crisanti A. and F Ritort. Violation of the fluctuation-dissipation theorem in glassy systems: basic notions and the numerical evidence. *Journal of Physics A-Mathematical and General*, 36(21):R181–R290, MAY 30 2003.
- [21] Cugliandolo L. F. *Slow Relaxations and nonequilibrium dynamics in condensed matter, Course 7: Dynamics of Glassy Systems*. Springer Berlin / Heidelberg, 2004.
- [22] J Kurchan. In and out of equilibrium. *Nature*, 433(7023):222–225, JAN 20 2005.
- [23] Chamon C. and Cugliandolo L. F. Fluctuations in glassy systems. *Journal of Statistical Mechanics-Theory and Experiment*, 2007.
- [24] Umberto Marini Bettolo Marconi, Andrea Puglisi, Lamberto Rondoni, and Angelo Vulpiani. Fluctuation-dissipation: Response theory in statistical physics. *Physics Reports-Review Section of Physics Letters*, 461(4-6):111–195, JUN 2008.
- [25] MM Hurley and P Harrowell. Kinetic Structure of a 2-Dimensional Liquid. *Physical Review E*, 52(2):1694–1698, AUG 1995.
- [26] Bennemann C. and Donati, C and Baschnagel, J and Glotzer, SC. Growing range of correlated motion in a polymer melt on cooling towards the glass transition. *Nature*, 399(6733):246–249, MAY 20 1999.
- [27] C Donati, S Franz, SC Glotzer, and G Parisi. Theory of non-linear susceptibility and correlation length in glasses and liquids. *Journal of Non-Crystalline Solids*, 307:215–224, SEP 2002.

-
- [28] S Whitelam, L Berthier, and JP Garrahan. Dynamic criticality in glass-forming liquids. *Physical Review Letters*, 92(18), MAY 7 2004.
- [29] Heuer A. Feng H. Schmidt-Rohr K. Tracht U., Wilhelm M. and Spiess H. W. Length scale of dynamic heterogeneities at the glass transition determined by multidimensional nuclear magnetic resonance. *Physical Review Letters*, 81:2727, 1997.
- [30] M.D. Ediger. Spatially heterogeneous dynamics in supercooled liquids. *Annu Rev Phys Chem.*, 51:99–128, 2000.
- [31] Vidal Russell E. and Israeloff N. E. Direct observation of molecular cooperativity near the glass transition. *Nature*, 408:695, 2000.
- [32] Levitt A. C.-Schofield A. Weitz D. A.. Weeks E. R., Crocker J. C. Three-dimensional direct imaging of structural relaxation near the colloidal glass transition. *Science*, 287:627, 2000.
- [33] Vanden Bout D. A. Deschenes L. A. Single-molecule studies of heterogeneous dynamics in polymer melts near the glass transition. *Science*, 292:255, 2001.
- [34] Berthier L. and Biroli G., Bouchaud J.-P., Cipelletti L., El Masri D., L'Hote D., Ladieu F., Pierno M. Direct Experimental Evidence of a Growing Length Scale Accompanying the Glass Transition. *Science*, 310:1797, 2005.
- [35] Berthier L. and Biroli G., Bouchaud J.-B., et al. Spontaneous and induced dynamic fluctuations in glass formers. I. General results and dependence on ensemble and dynamics. *Journal of Chemical Physics*, 126:184503, 2007.
- [36] Berthier L. and Biroli G, Bouchaud JP, et al. Spontaneous and induced dynamic correlations in glass formers. II. Model calculations and comparison to numerical simulation. *Journal of Chemical Physics*, 126:184504, 2007.
- [37] Alba-Simionesco C et al. Dalle-Ferrier C, Thibierge C. Spatial correlations in the dynamics of glassforming liquids: Experimental determination of their temperature dependence. *Physical Review E*, 76:041510, 2007.
- [38] L'Hote D Ladieu F, Thibierge C. An experimental search for dynamic heterogeneities in molecular glass formers. *Journal of Physics Condensed-Matter*, 19:205138, 2007.
- [39] Capaccioli S and Ruocco G, Zamponi F. Dynamically correlated regions and configurational entropy in supercooled liquids. *Journal of Physical Chemistry B*, 112:10652, 2008.
- [40] J.D. Ferry. *Viscoelastic Properties of Polymers*. Wiley, New York, 1980.
- [41] M. Feigelman J. Kurchan J. Dalibard M. E. Cates, J. L. Barrat. *Structural Relaxation and Rheology of Soft Condensed Matter*, EDP Sciences, Les Ulis vol. 75. Springer-Verlag, Berlin, 2003.

BIBLIOGRAPHY

- [42] Christensen T., Olsen N. B. A rheometer for the measurement of a high shear modulus covering more than seven decades of frequency below 50 khz. *Review of Scientific Instruments*, 66:5019, 1995.
- [43] Larsen E. H. Olsen N. B. Pedersen I. H. Rasmussen T. Dyre J. C. Igarashi B., Christensen T. A cryostat and temperature control system optimized for measuring relaxations of glass-forming liquids. *Review of Scientific Instruments*, 79:045105, 2008.
- [44] Larsen E. H. Olsen N. B. Pedersen I. H. Rasmussen T. Dyre J. C. Igarashi B., Christensen T. An impedance-measurement setup optimized for measuring relaxations of glass-forming liquids. *Review of Scientific Instruments*, 79:045106, 2008.
- [45] T. A. Litovitz. Temperature dependence of the viscosity of associated liquids. *Journal of Chemical Physics*, 7:1088, 1952.
- [46] Barlow A. J. and Lamb J. The visco-elastic behaviour of lubricating oils under cyclic shearing stress. *Proceedings of The Royal Society A*, 253:52, 1959.
- [47] Barlow A. J. and Lamb J., Matheson A. J. Viscous behaviour of supercooled liquids. *Proceedings of The Royal Society A*, 292:322, 1966.
- [48] G Harrison. *The Dynamic Properties of Supercooled Liquids*. Academic, New York, 1976.
- [49] Bassler, H. Viscous flow in supercooled liquids analyzed in terms of transport theory for random media with energetic disorder. *Physical Review Letters*, 58:767, 1987.
- [50] Avramov I. Viscosity in disordered media. *Journal of Non-Crystalline Solids*, 351:3163, 2005.
- [51] H. Vogel. Das temperaturabhängigkeitsgesetz der viskosität von flüssigkeiten. *Physikalische Zeitschrift*, 22:645, 1921.
- [52] G.S. Fulcher. Analysis of recent measurements of the viscosity of glasses. *Journal of The American Ceramic Society*, 8:339, 1925.
- [53] G. Tammann. Glasses as supercooled liquids. *Journal of The Society of Glass Technology*, 9:166, 1925.
- [54] Olsen N. B. Dyre J. C. Hecksher T., Nielsen A. I. Little evidence for dynamic divergences in ultraviscous molecular liquids. *Nature Physics*, 4:737, 2008.
- [55] Olsen N. B. Dyre J. C. Landscape equivalent of the shoving model. *Physical Review E*, 69:042501, 2004.
- [56] Negami S. Havriliak S. A complex plane analysis of alpha-dispersions in some polymer systems. *Journal of Polymer Science Part C-Polymer Symposium*, 14PC:99, 1966.

-
- [57] Negami S. Havriliak S. A complex plane representation of dielectric and mechanical relaxation processes in some polymers. *Polymer*, 8:161, 1967.
- [58] Olsen N. B. Dyre J. C. Niss K. Saglanmak N., Nielsen A. I. An electrical circuit model of the alpha-beta merging seen in dielectric relaxation of ultraviscous liquids. *The Journal of Chemical Physics*, 132:024503, 2010.
- [59] Niss K. Hecksher T., Olsen N. B. and Dyre J. C. Physical ageing studied by a device allowing for rapid thermal equilibration. arXiv:0811.0994, 2010.
- [60] Boue P. Morfin I., Lindner P. Temperature and shear rate dependence of small angle neutron scattering from semidilute polymer solutions. *Macromolecules*, 32:7208, 1999.
- [61] Li R. Z. Time-temperature superposition method for glass transition temperature of plastic materials. *Materials Science and Engineering A*, 278:36, 2000.
- [62] Perusich S. McBreaty M. Dielectric rheological measurements of molten polymers. *Polymer Engineering and Science*, 40:201, 2000.
- [63] Kudoh H. et al. Miyano Y., Nakada M. Prediction of tensile fatigue life for unidirectional cfrp. *Journal of Composite Materials*, 34:538, 2000.
- [64] Christensen T. Olsen N. B. and Dyre J. C. Time-temperature superposition in viscous liquids. *Physical Review Letters*, 86:1271, 2001.
- [65] Goldstein M. Johari G.P. Viscous liquids and glass transition .2. secondary relaxations in glasses of rigid molecules. *Journal of Chemical Physics*, 53:2372, 1970.
- [66] Olsen N. B. Scaling of beta-relaxation in the equilibrium liquid state of sorbitol. *Journal of Non-Crystalline Solids*, 235:399, 1998.
- [67] Ngai K.L. Correlation between the secondary beta-relaxation time at t-g with the kohlrausch exponent of the primary alpha relaxation or the fragility of glass-forming materials. *Physical Review E*, 57:7346, 1998.
- [68] Roland C.M. Leon C., Ngai K.L. Relationship between the primary and secondary dielectric relaxation processes in propylene glycol and its oligomers. *Journal of Chemical Physics*, 110:11585, 1999.
- [69] Richert R. Wagner H. Dielectric beta relaxations in the glassy state of salol? *Journal of Chemical Physics*, 110:11660, 1999.
- [70] Lunkenheimer P. et al. Schneider U., Brand R. Excess wing in the dielectric loss of glass formers: A johari-goldstein beta relaxation? *Physical Review Letters*, 84:5560, 2000.
- [71] K. Niss and B. Jakobsen. Dielectric and shear mechanical relaxation in glass forming liquids. Master's thesis, Department of Mathematics and Physics IMFUFA, Roskilde University,, 2003.

BIBLIOGRAPHY

- [72] Olsen N. B. Jakobsen B., Niss K. Dielectric and shear mechanical alpha and beta relaxations in seven glass-forming liquids. *The Journal of Chemical Physics*, 123:234511, 2005.
- [73] Olsen N. B. Niss K., Jakobsen B. Dielectric and shear mechanical relaxations in glass-forming liquids: A test of the gemant-dimarzio-bishop model. *The Journal of Chemical Physics*, 123:234510., 2005.
- [74] Dyre J. C. A model for the generic alpha relaxation of viscous liquids. *Europhysics Letters*, 71:646, 2005.
- [75] Dyre J. C. Solidity of viscous liquids. iv. density fluctuations. *Physical Review E*, 74:021502, 2006.
- [76] Jakobsen B. Niss K. Olsen N. B. Richert R. Dyre J.C. Nielsen A. I., Christensen T. Prevalence of approximate \sqrt{t} relaxation for the dielectric α process in viscous organic liquids. *Journal of Chemical Physics*, 130:154508, 2009.
- [77] C. J. F. B'ottcher and P. Bordewijk. *Theory of Electric Polarization II: Dielectrics in Time-Dependent Fields*. Elsevier, New York, 1980.
- [78] Cole R. H. Davidson D. W. Dielectric relaxation induced glycerol, propylene glycol, and normal-propanol. *Journal of Chemical Physics*, 19:1484, 1951.
- [79] Cole R. H. and Davidson D. W. High frequency dispersion in normal-propanol. *Journal of Chemical Physics*, 20:1389, 1952.
- [80] McDuffie G. E. Litovitz T. A. Comparison of dielectric and mechanical relaxation in associated liquids. *Journal of Chemical Physics*, 39:729, 1963.
- [81] McDuffie G. E. Kono R., Litovitz T. A. Comparison of dielectric and mechanical relaxation processes in glycerol-n-propanol mixtures. *Journal of Chemical Physics*, 45:1790, 1966.
- [82] Parisi G. Off-equilibrium fluctuation-dissipation relation in fragile glasses. *Physical Review Letters*, 79:3660, 1997.
- [83] Barrat J.L. and Kob W. Fluctuation-dissipation ratio in an aging Lennard-Jones glass. *Europhysics Letters*, 46:637, 1999.
- [84] Parisi G. et al. Di Leonardo R., Angelani L. Off-equilibrium effective temperature in monatomic lennard-jones glass. *Physical Review Letters*, 84:6054, 2000.
- [85] Diezemann G. Aging in a free-energy landscape model for glassy relaxation. *Journal of Chemical Physics*, 123:204510, 2005.
- [86] Chandler D. Jack R.L., Hagan M.F. Fluctuation-dissipation ratios in the dynamics of self-assembly. *Physical Review E*, 76:21119, 2007.
- [87] Takano M. Hayashi K. Violation of the fluctuation-dissipation theorem in a protein system. *Biophysical Journal*, 93:895, 2007.

-
- [88] Cugliandolo L.E. Loi D., Mossa S. Effective temperature of active matter. *Physical Review E*, 77:51111, 2008.
- [89] Alba M. and Hammann J., Ocio M., Refregier P., Bouchiat H. Spin-glass dynamics from magnetic noise, relaxation, and susceptibility measurements. *Journal Applied Physics*, 61:3683, 1987.
- [90] Ocio M. Refregier P. Measurement of spontaneous magnetic fluctuations. *Revue de Physique Appliquee*, 22:367, 1987.
- [91] Bouchiat H., Experimental studies of the spin glass dynamics: towards a better understanding. *Physica A*, 163:284, 1990.
- [92] Herisson D. and Ocio M. Fluctuation-dissipation ratio of a spin glass in the aging regime. *Physical Review Letters*, 88:257202, 2002.
- [93] Grigera T. S. and Israeloff N. E. Observation of fluctuation-dissipation-theorem violations in a structural glass. *Physical Review Letters*, 83:5038, 1999.
- [94] Buisson L. and Ciliberto S. Off equilibrium fluctuations in a polymer glass. *Physica D: Nonlinear Phenomena*, 204:1, 2005.
- [95] Sprik R. Kroon M., Wegdam G.H. Dynamic light scattering studies on the sol-gel transition of a suspension of anisotropic colloidal particles. *Physical Review E*, 54:6541, 1996.
- [96] Van Damme H. et al. Mourchid A., Lecolier E. On viscoelastic, birefringent, and swelling properties of laponite clay suspensions: Revisited phase diagram. *Langmuir*, 14:4718, 1998.
- [97] Munch J P. et al. Knaebel A., Bellour M. Aging behavior of laponite clay particle suspensions. *Europhysics Letters*, 52:73, 2000.
- [98] Mourchid A. et al. Levitz P., Lecolier E. Liquid-solid transition of laponite suspensions at very low ionic strength: Long-range electrostatic stabilisation of anisotropic colloids. *Europhysics Letters*, 49:672, 2000.
- [99] Ruocco G. Ruzicka B., Zulian L. Routes to gelation in a clay suspension. *Physical Review Letters*, 93:258301, 2004.
- [100] Bandyopadhyay R. and Liang D., Yardimci H., et al. Evolution of particle-scale dynamics in an aging clay suspension. *Physical Review Letters*, 93:228302, 2004.
- [101] Bonn D. Jabbari-Farouji S., Wegdam G.H. Gels and glasses in a single system: Evidence for an intricate free-energy landscape of glassy materials. *Physical Review Letters*, 99:65701, 2007.
- [102] Reverdy G. Mousty C. Blankespoor R. Gautier A. Labbe P., Brahimia B. and Degrand C. Possible analytical application of laponite clay modified electrodes. *Journal of Electroanalytical Chemistry*, 379:103, 1994.

- [103] Galez C. et al. Teyssier J., Le Dantec R. Lithium iodate nanocrystals in laponite matrix for nonlinear optical applications. *Applied Physics Letters*, 85:710, 2004.
- [104] Boucenna I. and Royon L., and Colinart P. Effect of laponite clay particles on thermal and rheological properties of pluronic triblock copolymer. *Journal of Thermal Analysis and Calorimetry*, 98:119, 2009.
- [105] Ghofraniha N. and Zamponi F. Conti C., Ruocco G. Time-dependent nonlinear optical susceptibility of an out-of-equilibrium soft material. *Physical Review Letters*, 102:038303, 2009.
- [106] Petrosyan A. et al. Joubaud S., Percier B. Aging and effective temperatures near a critical point. *Physical Review Letters*, 102:130601, 2009.
- [107] Israeloff N.E. Oukris H. Nanoscale non-equilibrium dynamics and the fluctuation-dissipation relation in an ageing polymer glass. *Nature Physics*, 6:70, 2010.
- [108] Berne B. J., and Pecora R. *Dynamic Light Scattering with Applications to Chemistry Biology and Physics*. Dover Publications Inc., 1975.
- [109] van de Hulst H. C. *Light Scattering by Small Particles*. Dover Publications Inc., 1982.
- [110] Johnson C. S. and Gabriel D. A. *Laser Light Scattering*. Dover Publications Inc., 1995.
- [111] Xu R. *Particle Characterization: Light Scattering Methods*. Springer, 2001.
- [112] Dejardin J.-L. *Dynamic Kerr Effect: The Use and Limits of the Smoluchowski Equation and Nonlinear Inertial Responses*. World Scientific Publishing Company, 1995.
- [113] Shen Y. R. *The Principles of Nonlinear Optics*. Wiley-Interscience, 2002.
- [114] Boyd R. W. *Nonlinear Optics, Third Edition*. Academic Press, 2008.
- [115] Schroder T.B. et al. Pedersen U.R., Bailey N.P. Strong pressure-energy correlations in van der waals liquids. *Physical Review Letters*, 100:15701, 2008.
- [116] Schroder T.B. et al. Pedersen U.R., Christensen T. Feasibility of a single-parameter description of equilibrium viscous liquid dynamics. *Physical Review E*, 77:11201, 2008.
- [117] Bailey N.P. and Pedersen U.R., Gnan N., et al. Pressure-energy correlations in liquids. I. Results from computer simulations. *Journal of Chemical Physics*, 129:184507, 2008.
- [118] Bailey N.P. and Pedersen U.R., Gnan N., et al. Pressure-energy correlations in liquids. II. Analysis and consequences. *Journal of Chemical Physics*, 129:184508, 2008.

-
- [119] Pedersen U.R. et al. Schroder T.B., Bailey N.P. Pressure-energy correlations in liquids. iii. statistical mechanics and thermodynamics of liquids with hidden scale invariance. *Journal of Chemical Physics*, 131:234503, 2009.
- [120] Pedersen U.R. et al. Gnan N., Schroder T.B. Pressure-energy correlations in liquids. iv. "isomorphs" in liquid phase diagrams. *Journal of Chemical Physics*, 131:234504, 2009.
- [121] Andersen H.C. Kob W. Scaling behavior in the beta-relaxation regime of a supercooled lennard-jones mixture. *Physcal Review Letters*, 73:1376–1379, 1994.
- [122] Berthier L. and Kob W. The Monte Carlo dynamics of a binary Lennard-Jones glass-forming mixture. *Journal of Physics-Condensed Matter*, 19:205130, 2007.
- [123] Berthier L. Efficient measurement of linear susceptibilities in molecular simulations: Application to aging supercooled liquids. *Physcal Review Letters*, 98:220601, 2007.
- [124] Odagaki T. Van Hoang V. Glasses of simple liquids with double-well interaction potential. *Physica B-Condensed Matter*, 403:3910, 2008.
- [125] Rosenbluth M. N. Teller A. H. Metropoplis N., Rosenbluth A. W. and Teller E. Equation of state calculations by fast computing machines. *Journal of Chemical Physics*, 21:1087, 1953.
- [126] Allen M. P., and Tildesley D. J. *Computer Simulation of Liquids*. Oxford University Press, 1989.
- [127] Stillinger F. H. A topographic view of supercooled liquid and glass formation. *Science*, 267:1935, 1995.
- [128] Dyre J. C. Schroeder T. B., Sastry S. and Glotzer S. C. Crossover to potential energy landscape dominated dynamics in a model glass-forming liquid. *Journal of Chemical Physics*, 22:9834, 2000.
- [129] Sciortino F. and Tartaglia P. Extension of the fluctuation-dissipation theorem to the physical aging of a model glass-forming liquid. *Physcal Review Letters*, 86:107, 2001.
- [130] Sastry S. and Angell C. A. Liquid-liquid phase transition in supercooled silicon. *Nature Materials*, 2:739, 2003.
- [131] Kurita R. and Tanaka h. Critical-like phenomena associated with liquid-liquid transition in a molecular liquid. *Science*, 306:845, 2004.
- [132] Beaucage P. and Mousseau N. Liquid-liquid phase transition in Stillinger-Weber silicon. *Journal of Physics: Condensed Matter*, 17:2269, 2005.
- [133] Sciortino F. Liquid-liquid transitions in one-component systems. *Journal of Physics: Condensed Matter*, 17:V7, 2005.

BIBLIOGRAPHY

- [134] Bellissent-Funel M.-C. Zanotti J.-M. and Chen S.-H. Experimental evidence of a liquid-liquid transition in interfacial water. *Europhysics Letters*, 71:91, 2005.
- [135] Kurita R. et al. Microscopic structural evolution during the liquid-liquid transition in triphenyl phosphite. *Journal of Physics: Condensed Matter*, 19:152101, 2007.
- [136] Turnbull D. and Fisher J. C. Rate of nucleation in condensed systems. *Journal of Chemical Physics*, 17:71, 1949.
- [137] Turnbull D. Under what conditions can a glass be formed? *Contemporary Physics*, 10:473, 1969.
- [138] Granasy L. Weinberg M. C., Poisl W. H. Crystal growth and classical nucleation theory. *Comptes Rendus Chimie*, 5:765, 2002.
- [139] Derrida B.,. An exactly solvable model of disordered systems. *Physical Review B*, 24:26132626, 1981.
- [140] Gross D. J. and Mezard M. The simplest spin glass. *Nuclear Physics B*, 240:431, 1984.
- [141] Kanter I. Gross D. J. and Sopolinsky H. Mean-field theory of the potts glass. *Physical Review Letters*, 55:304307, 1985.
- [142] Goldbardt P. and Sherrington D. Replica theory of the uniaxial quadrupolar glass. *Journal of Physics C*, 18:1923, 1985.
- [143] Gardner E. Spin glasses with p-spin interactions. *Nuclear Physics B*, 257:747, 1985.
- [144] Latz A. Kim B. The dynamics of the spherical p-spin model: From microscopic to asymptotic. *Europhysics Letters*, 53:660, 2001.
- [145] Castellani T. and Cavagna A. Spin-glass theory for pedestrians. *Journal of Statistical Mechanics: Theory and Experiment*, 05:05012, 2005.
- [146] Thirumalai D. Kirkpatrick T.R. Dynamics of the structural glass-transition and theory p-spin-interaction spin-glass model. *Physical Review Letters*, 58:2091, 1987.
- [147] Wolynes P. G. Kirkpatrick T.R. Connections between some kinetic and equilibrium theories of the glass-transition. *Physical Review A*, 35:3072, 1987.
- [148] and Wolynes P. G. Kirkpatrick T.R., Thirumalai D. Scaling concepts for the dynamics of viscous-liquids near an ideal glassy state. *Physical Review A*, 40:1045, 1989.
- [149] Wolynes P.G. Xia X.Y. Fragilities of liquids predicted from the random first order transition theory of glasses. *Proceedings of The National Academy of Sciences of The United States of America*, 97:2990, 2000.

-
- [150] Wolynes P.G. Xia X.Y. Microscopic theory of heterogeneity and non-exponential relaxations in supercooled liquids. *Physical Review Letters*, 86:5526, 2001.
- [151] Wolynes P.G. Eastwood M.P. Droplets and the configurational entropy crisis for random first-order transitions. *Europhysics Letters*, 60:587, 2002.
- [152] Wolynes P.G. Lubchenko V. Theory of structural glasses and supercooled liquids. *Annual Review of Physical Chemistry*, 58:235, 2007.
- [153] Crisanti A. and Sommers H.-J. The spherical p-spin interaction spin glass model: The statics. *Zeitschrift fur Physik B*, 87:341, 1992.
- [154] Horner H. Crisanti A. and Sommers H.-J. The spherical p-spin interaction spin glass model: The dynamics. *Zeitschrift fur Physik B*, 92:257, 1993.
- [155] Nielsen J. K. and Dyre J. C. Fluctuation-dissipation theorem for frequency-dependent specific heat. *Physical Review B*, 54:15754, 1996.
- [156] Abramowitz, M. and Stegun, I. A. *Handbook of Mathematical Functions with Formulas, Graphs, and Mathematical Tables*, 9th printing. Dover, 1972.
- [157] Arfken, G. *Mathematical Methods for Physicists*, 3rd ed. Academic Press, 1985.
- [158] Christensen T. The frequency-dependence of the specific-heat at the glass-transition. *Journal de Physique*, 46:635, 1985.
- [159] Jakobsen B. and Christensen T. Olsen N. B. Frequency dependent specific heat from thermal effusion in spherical geometry. arXiv:0809.4617v1 [cond-mat.soft], 2008.
- [160] Christensen T. and Olsen N. B. Determination of the frequency-dependent bulk modulus of glycerol using a piezoelectric spherical shell. *Physical Review B*, 49:15396, 1994.
- [161] Bauer C. and Christensen T. Richert R., Boehmer R. Dynamic thermal expansivity near the glass transition. *Journal of Non-Crystalline Solids*, 262:276, 2000.
- [162] Li T. Kogelnik, H. and. Laser beams and resonators. *Applied Optics*, 5:1550, 1966.
- [163] A. E. Siegman. *Lasers*. University Science Books, 1986.
- [164] P. A. Belanger. Beam propagation and the abcd ray matrices. *Optics Letters*, 16:196, 1991.
- [165] H. C. Kang and Liu C. et al. Maser J., Stephenson G. B. Nanometer linear focusing of hard x rays by a multilayer laue lens. *Physical Review Letters*, 96:127401, 2006.
- [166] E. Roessler. Indications for a change of diffusion mechanism in supercooled liquids. *Physical Review Letters*, 65:1595, 1990.

BIBLIOGRAPHY

- [167] I. Chang and et al. Fujara F., Geil B. Translational and rotational molecular motion in supercooled liquids studied by nmr and forced rayleigh scattering. *Journal of Non-Crystalline Solids*, 248:172, 1994.
- [168] M.T. Cicerone and Ediger M.D. Enhanced translation of probe molecules in supercooled o-terphenyl: Signature of spatially heterogeneous dynamics? *Journal of Chemical Physics*, 104:7210, 1996.
- [169] A Gemant. The conception of a complex viscosity and its application to dielectrics. *Transactions of The Faraday Society*, 31:1582, 1935.
- [170] and Bishop M. DiMarzio, E.A. Connection between the macroscopic electric and mechanical susceptibilities. *Journal of Chemical Physics*, 60:3802, 1974.
- [171] R. P. Feynman. *The Feynman Lectures on Physics, Volume II*. Addison Wesley, 1965.
- [172] K. Z. Markov. *Elementary Micromechanics of Heterogeneous Media, Chapter 1: Heterogeneous Media: Modelling and Simulation*. Birkhauser, 1999.
- [173] M. P. Hughes. Ac electrokinetics: Applications for nanotechnology. *Nanotechnology*, 11:124, 2000.
- [174] B. Schiener, Loidl A. Boehmer, R., and Chamberlin R. V. Nonresonant spectral hole burning in the slow dielectric response of supercooled liquids. *Science*, 274:752, 1996.
- [175] L. F. Cugliandolo and J. L. Iguain. Hole-burning experiments within solvable glassy models. *Physcal Review Letters*, 85:3448, 2000.
- [176] G. Diezemann and R. Boehmer. Comment on "hole-burning experiments within glassy models with infinite range interactions". *Physcal Review Letters*, 87:129602, 2001.
- [177] l.F. Cugliandolo and J. L. Iguain. Reply to "comment on 'hole-burning experiments within glassy models with infinite range interactions' ". *Physcal Review Letters*, 87:129603, 2001.
- [178] A. Bello, Laredo E., and M. Grimau. Distribution of relaxation times from dielectric spectroscopy using monte carlo simulated annealing: Application to α -pvdf. *Physcal Review B*, 60:12764, 1999.
- [179] K.S. Cole and R.H. Cole. Dispersion and absorption in dielectrics - i alternating current characteristics. *Journal of Chemical Physics*, 9:341, 1941.
- [180] K.S. Cole and R.H. Cole. Dispersion and absorption in dielectrics - ii direct current characteristics. *Journal of Chemical Physics*, 10:98, 1942.
- [181] J. C. Dyre and N. B. Olsen. Minimal model for beta relaxation in viscous liquids. *Physcal Review Letters*, 91:155703, 2003.

-
- [182] E. A. Pavlatou and Papatheodorou G. N. Yannopoulos S. N. Dynamics of density and orientation fluctuations in supercooled zinc halides. *The Journal of Chemical Physics B*, 101:8748, 1997.
- [183] M. Ricci and Bartolini P. et al. Wiebel, S. Time-resolved optical kerr effect experiments on supercooled benzene and test of mode-coupling theory. *Philosophical Magazine*, 84:1491, 2004.
- [184] S. Mossa, La Nave E., and et al. Stanley, H. E. Dynamics and configurational entropy in the lewis-wahnstrom model for supercooled orthoterphenyl. *Physical Review E*, 65:041205, 2002.
- [185] I. Saika-Voivod, F. Sciortino, and P. H. Poole. Free energy and configurational entropy of liquid silica: Fragile-to-strong crossover and polyamorphism. *Physical Review E*, 69:41503, 2004.
- [186] L. Angelani and Tartaglia P. Foffi G., Sciortino F. Diffusivity and configurational entropy maxima in short-range attractive colloids. *Journal of Physics: Condensed Matter*, 17:L113, 2005.
- [187] S. Franz and G. Parisi. Effective potentials in glassy systems. *Philosophical Magazine B*, 77:239, 1998.
- [188] S. Franz and Parisi G. Donati, C. On dynamical correlations in supercooled liquids. *Philosophical Magazine B*, 79:1827, 1999.
- [189] Y. Chushkin and and Madsen A. Caronna, C. Low-frequency elastic behavior of a supercooled liquid. *Europhysics Letters*, 83:36001, 2008.

Papers

Supercooled Liquid Dynamics Studied via Shear-Mechanical Spectroscopy

Claudio Maggi,* Bo Jakobsen, Tage Christensen, Niels Boye Olsen, and Jeppe C. Dyre

DNRF Centre “Glass and Time”, IMFUFA, Department of Sciences, Roskilde University, Postbox 260, DK-4000 Roskilde, Denmark

Received: June 10, 2008; Revised Manuscript Received: October 2, 2008

We report dynamical shear-modulus measurements for five glass-forming liquids (pentaphenyltrimethyltrisiloxane, diethyl phthalate, dibutyl phthalate, 1,2-propanediol, and *m*-touluidine). The shear-mechanical spectra are obtained by the piezoelectric shear-modulus gauge (PSG) method. This technique allows one to measure the shear modulus (10^5 – 10^{10} Pa) of the liquid within a frequency range from 1 mHz to 10 kHz. We analyze the frequency-dependent response functions to investigate whether time–temperature superposition (TTS) is obeyed. We also study the shear-modulus loss-peak position and its high-frequency part. It has been suggested that when TTS applies, the high-frequency side of the imaginary part of the dielectric response decreases like a power law of the frequency with an exponent $-1/2$. This conjecture is analyzed on the basis of the shear mechanical data. We find that TTS is obeyed for pentaphenyltrimethyltrisiloxane and in 1,2-propanediol while in the remaining liquids evidence of a mechanical β process is found. Although the high-frequency power law behavior $\omega^{-\alpha}$ of the shear loss may approach a limiting value of $\alpha = 0.5$ when lowering the temperature, we find that the exponent lies systematically above this value (around 0.4). For the two liquids without β relaxation (pentaphenyltrimethyltrisiloxane and 1,2-propanediol) we also test the shoving model prediction, according to which the relaxation time activation energy is proportional to the instantaneous shear modulus. We find that the data are well described by this model.

I. Introduction

The nature of the relaxation processes taking place in supercooled liquids approaching the glass transition has been a major subject of study for a number of years. Understanding how the different response functions are connected in such systems is still a fundamental goal to reach. It is not clear whether the various observables display some universal features approaching the glass transition. Although dielectric spectroscopy is the most common experimental tool, a more detailed characterization of their behavior can be obtained by measuring different quantities, like the *shear modulus*, that are important from a practical as well as theoretical point of view. Although this dynamic variable can be measured above $\sim 10^2$ Hz with conventional techniques, high-frequency data are scarce in the literature.

Motivated by these reasons, we employed the piezoelectric shear-modulus gauge (PSG)¹ method to measure the shear modulus of five glass-forming liquids. This technique allows us to measure the dynamic shear modulus of the supercooled liquids just above the glass transition where it takes values between 0.1 MPa and 10 GPa. By means of the PSG technique we can easily observe the α relaxation process in the shear response. The frequency range of the technique is wide (10^{-3} – 10^4 Hz), and we also observe a *mechanical* Johari–Goldstein β relaxation.² As shown before³ indeed, this technique is sensitive to the secondary process, and we find evidence of the presence of a shear β relaxation^{3–5} in some of the mechanical spectra reported here.

In section II we describe the experiment performed and the liquids studied reporting the frequency-resolved mechanical spectra. In section III we report the main findings of our study; in this section we present the analyzed data showing the

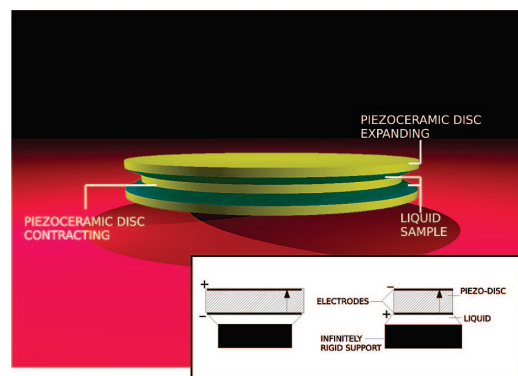


Figure 1. Pictorial representation of the shear transducer (PSG) during its expansion–contraction. The liquid sandwiched between the discs clamps their movement, inducing a measurable change in the piezoelectric capacitance of the disc system. The shear modulus can be deduced from this electrical capacitance. Inset: the one-disc equivalent system of the PSG. The applied electric field causes an expansion or a contraction depending on the polarization of the disc (represented by the arrow). See ref 1 for more details.

temperature dependence of the shear-mechanical α relaxation frequency and a test of some conjectures and models about the dynamics. Finally, we draw some general conclusions in section IV.

II. Experiment

The piezoelectric shear-modulus gauge (PSG) method is based on the piezoelectric properties of the material that composes the measuring device. The piezoelectric transducer is formed by three discs made of a special ceramic compound⁶

* Corresponding author. E-mail: cmaggi@ruc.dk.

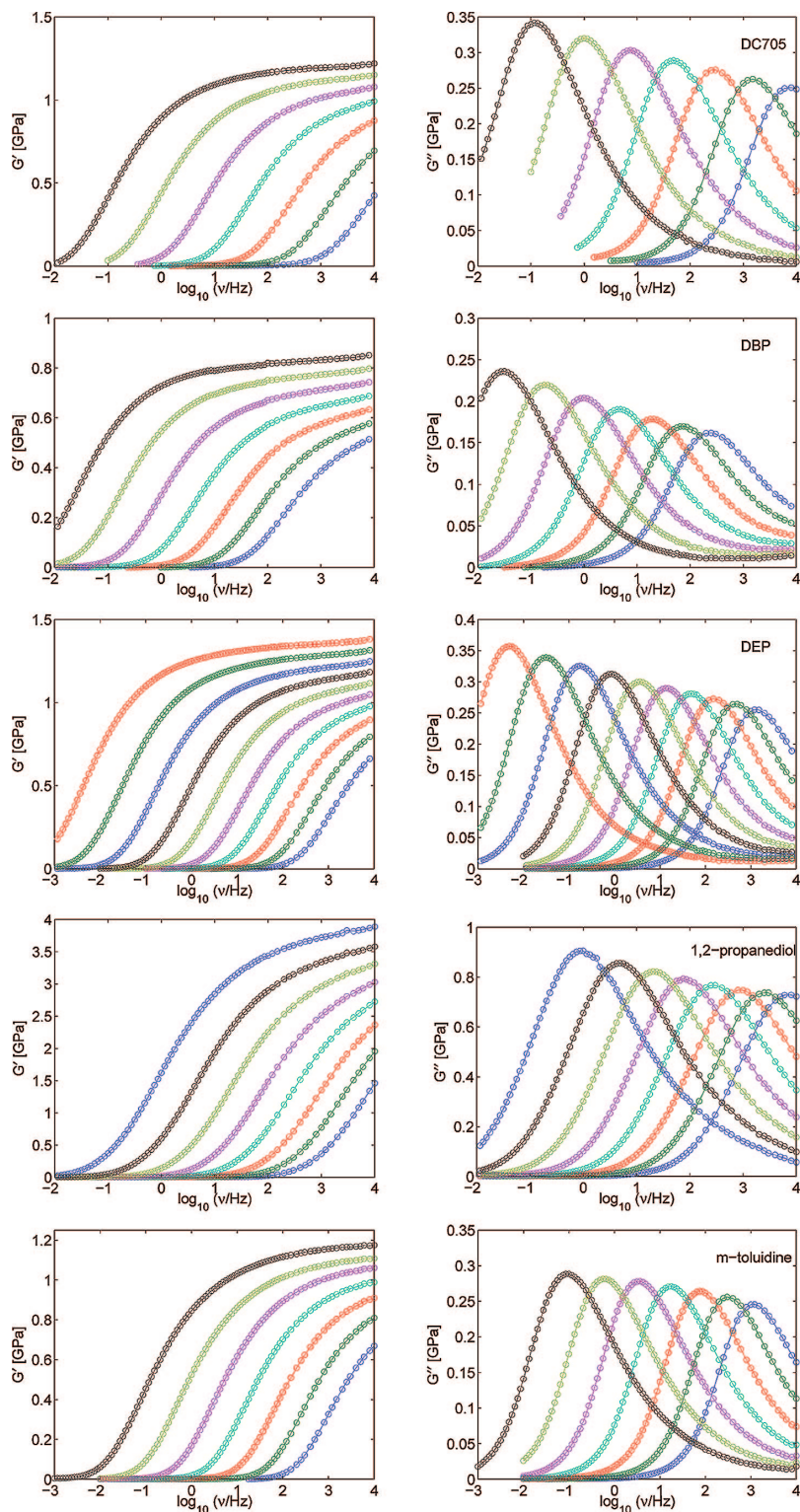


Figure 2. Real (left) and imaginary (right) part of the shear response of the liquids studied. (From top to bottom) spectra of DC705 taken at the temperatures (from right to left): 249, 246, 243, 240, 237, 234, and 231 K; of DBP at 188, 186, 184, 182, 180, 178, and 176 K; of DEP at 199, 197, 195, 193, 191, 189, 187, 185, 183, and 181 K; of 1,2-propanediol at 195, 192, 189, 186, 183, 180, 177, 173, and 171 K; and of *m*-toluidine at 198, 196, 194, 192, 190, 188, and 186 K.

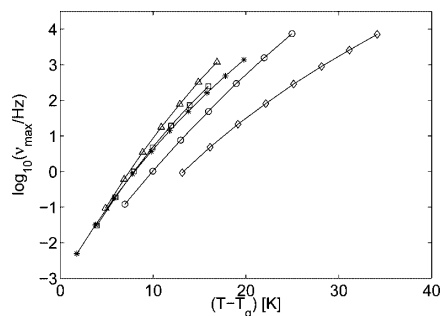


Figure 3. Frequency of the mechanical α peak as a function of the temperature for DC705 (\circ , $T_g = 224.0$ K), DBP (\square , $T_g = 172.3$ K), DEP ($*$, $T_g = 179.5$ K), 1,2-propanediol (\diamond , $T_g = 157.8$ K), and *m*-toluidine (\triangle , $T_g = 181$ K).

that has a pronounced piezoelectric effect (see Figure 1). The working principle of the PSG is illustrated in the inset of Figure 1 where the one disc equivalent of the three-disc system is shown. The ceramic disc is covered with a silver layer on both faces constituting the electrodes. When a voltage is applied, each disc expands or contracts depending on its intrinsic polarization and on the direction of the acting electric field. The electric capacitance of the disc depends on its strain state so that if a material is partially clamping its motion, the measured capacitance will be lower than that of the free moving disc. Measuring accurately this electrical capacitance,⁷ we can obtain the stiffness of the medium adhering to the disc. In other words, we can convert the electric impedance into the shear modulus knowing the exact relationship between the two.¹ The three-disc geometry, used in the experiment (main panel of Figure 1), is employed to reduce unwanted effect like the bending motion that would be present in a one-disc device. The interested reader can find details about the technique in ref 1.

The measurements are performed cooling the liquids via a home-built closed-cycle cryostat.⁸ This has an absolute uncertainty on the temperature that is less than 0.2 K and a temperature stability better than 2 mK.

The liquids studied are the following: pentaphenyltrimethyltrisiloxane (DC705), dibutyl phthalate (DBP), diethyl phthalate (DEP), 1,2-propanediol, and *m*-touluidine. The DC705 is a diffusion-pump oil from Dow Corning; all the other liquids were acquired from Sigma-Aldrich. No filtration or purification of the samples was performed before the measurement.

All mechanical spectra are reported in Figure 2. Here the real part G' and the imaginary part G'' of the complex shear modulus $G(\nu, T)$ are presented.⁹ The reactive and the absorptive part of the shear response of the liquids studied are measured at several temperatures.

For the shear loss peak of the DC705 there is a clearly defined shear α process that shifts to lower frequencies as the temperature decreases. We have found no sign of a shear β relaxation in this liquid. This is also confirmed by the fact that the curve maintains the same shape, lowering the temperature as discussed below. We will see also that the high-frequency side of the shear-mechanical spectrum shows a pretty constant slope.

The shear response of DBP clearly shows a β relaxation. The shape of the imaginary part of the response function is strongly deformed at high temperatures where the α process is merged with the β . When the temperature is low enough, the high-frequency tail of the response functions shows a pronounced increase, signaling an emerging β relaxation. Unfortunately, the β loss peak lies at much higher frequencies than the upper limit

of our device. The dielectric β process of this liquid has been observed¹⁰ to be around 10^6 Hz in a temperature window similar to the one of our mechanical experiment. This is consistent with the fact that the β relaxation is outside the PSG dynamical range since the shear-loss peak frequency is generally higher than the dielectric one³ (usually the two peaks are within the same decade). For future studies on this liquid the upper frequency limit of the PSG could possibly be increased by slightly modifying the transducer geometry.

Evidence of a secondary loss peak is also found in the mechanical response of the DEP. The dielectric β relaxation process in DEP has been the subject of an accurate investigation in connection with the behavior of the entropy in the supercooled and in the glass state,¹¹ raising fundamental questions about the nature of fast molecular motions in ultraviscous liquids. Very recently, this dielectric β process has been shown to be intimately related to the results of positron annihilation lifetime spectroscopy.¹² We note that in those dielectric measurements the β loss peak is found at about 2×10^4 Hz at $T = 179$ K, consistent with the fact that mechanically this process is above the upper limit of the PSG. We shall see in section III that when the shear loss is plotted on a logarithmic scale, the low-frequency tail of the β relaxation is more clearly visible.

The spectra taken for 1,2-propanediol are characterized by an high shear modulus, and no signature of β relaxation is found. This hydrogen-bonded liquid has recently been studied in dielectric experiments and compared to polymers differing in chain length and in the number of OH groups.¹³ These dielectric experiments did not reveal a visible β process, and a temperature-independent Cole–Davidson stretching parameter was found. These findings are fully in agreement with our shear spectra since the shape of the response function is very weakly temperature dependent as it will be stressed in the following.

Rather interesting mechanical spectra are found for *m*-toluidine. A weak, but nonzero, high-frequency tail of the loss response can be noted in Figure 2. This may hint to the existence of a shear β relaxation at frequencies around 1 MHz, consistent with recent broadband dielectric experiments performed on this liquid¹⁴ where a β relaxation process could be resolved, but only in the glassy regime where the relaxation frequency reaches a value around 1 kHz at about 130 K. This could be a range in which this β process could start to be detected mechanically.¹⁵

Finally, we mention that we attempted to measure the frequency-resolved shear modulus also for 1,3-propanediol and for propylene carbonate. An anomalous shear response was found for these two liquids, however, signaling a probable crystallization.

III. Discussion

The first information that can be extracted from our measurement is the α process loss peak frequency ν_{\max} . This has been deduced from the imaginary part through a simple unbiased method. We fitted the closest six points to the maximum of $\log(G''/GPa)$ as a function of $\log(\nu/Hz)$ with a second-order polynomial to identify the maximum G''_{\max} and the corresponding frequency ν_{\max} . These loss-peak frequencies are reported in Figure 3 as a function of the scaled temperature $(T - T_g)$. Here we define T_g as the temperature where the $\nu_{\max} = 1$ mHz. T_g is identified by a linear extrapolation of the last three points of $\log(\nu/Hz)$ as a function of T .

Time–temperature superposition (TTS) is a property of the α process appearing in the susceptibilities of some supercooled liquids expressing the fact that the shape of the response function remains the same when the system is cooled. When TTS applies,

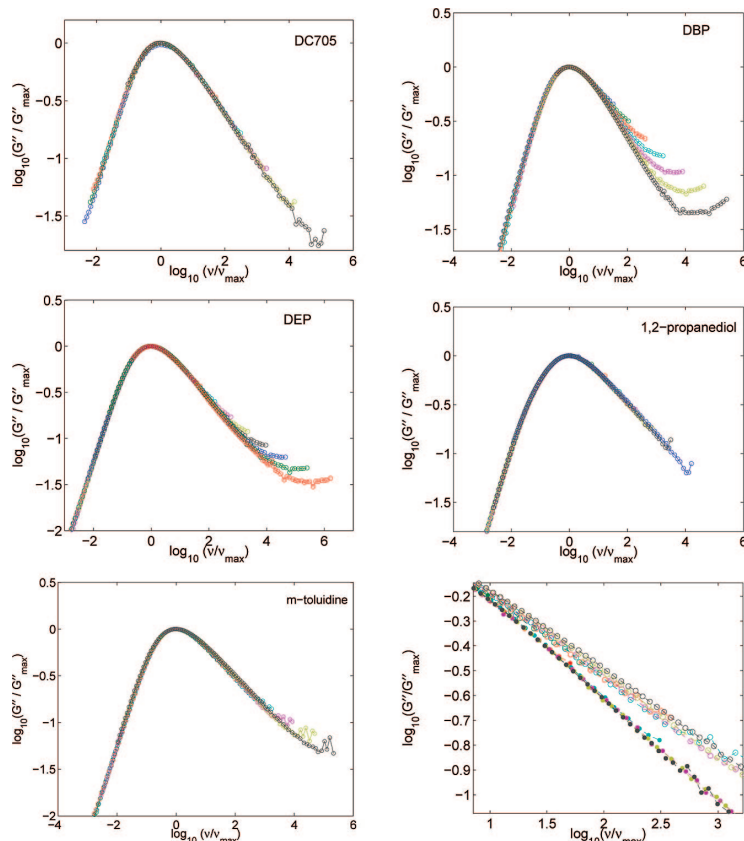


Figure 4. Shear loss G'' of liquids studied scaled by the maximum loss G''_{\max} as a function of the frequency ν divided by the frequency of the peak ν_{\max} (see also Figure 2): DC705, DBP, DEP, 1,2-propanediol, and *m*-toluidine. In the right-bottom panel we show a comparison between the scaled spectra of DC705 (full line, full symbols) and *m*-toluidine (dashed line, open symbols) on a smaller scale.

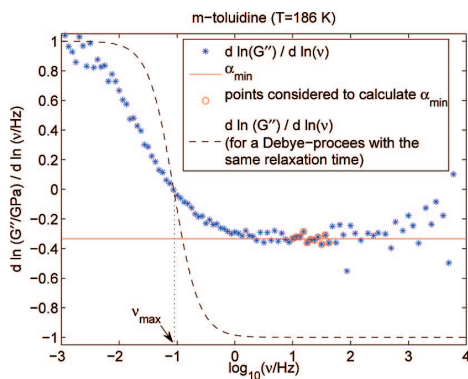


Figure 5. Representation of the procedure used to find the minimum logarithmic slope α_{\min} . In this figure we report the analysis of the mechanical spectrum of *m*-toluidine at $T = 186$ K. The derivative of $\log(G''/\text{GPa})$ with respect to $\log(\nu/\text{Hz})$ is plotted as a function of the frequency (stars). Some points are selected (red circles), and their average is taken to calculate α_{\min} (red line). Note that a Debye-like mechanical process with the same relaxation time would have a sharper drop of the α parameter reaching -1 at high frequencies.

the response is only shifting its characteristic time and its amplitude if we cool the liquid. Mathematically speaking, the generic response χ can be rewritten as $\chi(\nu, T) = A(T)\Phi(\nu/\nu_{\max}(T))$, where $\nu_{\max}(T)$ is a characteristic frequency depending

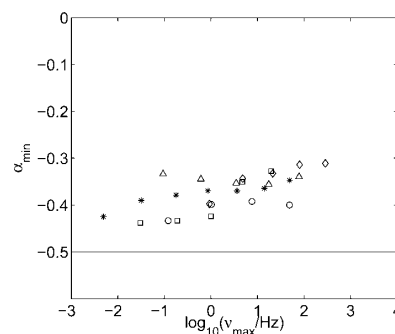


Figure 6. Minimum value of the logarithmic slope ($\alpha = d \ln G''/d \ln \nu$) for the liquids studied: DC705 (\circ), DBP (\square), DEP ($*$), 1,2-propanediol (\diamond), *m*-toluidine (\triangle).

on T . Having found the two parameters G''_{\max} and ν_{\max} at every given temperature, it is rather easy to check whether TTS applies for a given liquid.

In Figure 4 we report the imaginary part of the shear modulus divided by G''_{\max} as a function of ν/ν_{\max} . This plot underlines that for some of the liquids (DC705 and 1,2-propanediol) the shape of the α process remains constant, lowering T . This is not the case for DBP and DEP where the curves are detaching at high frequencies. The lack of TTS is clearly related to the presence of a β peak; indeed, the logarithmic scale used in this

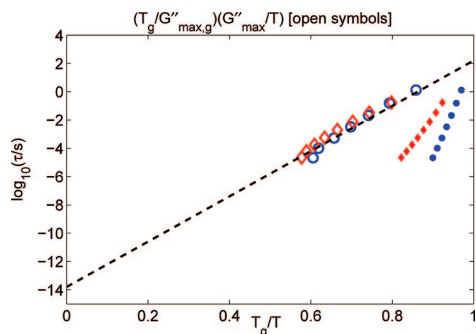


Figure 7. Characteristic time $\tau = 1/\nu_{\max}$ of the shear loss as a function of the scaled temperature T/T_g (full symbols) and as a function of $x = (T_g/G''_{\max,g})(T/G''_{\max})$ (open symbols) for the liquids in which TTS applies: DC705 (\circ , $T_g = 224.0$ K) and 1,2-propanediol (\diamond , $T_g = 157.8$ K). The dashed line is an exponential function with prefactor $\tau_0 = 10^{-14}$ s and taking the value $\tau = (2\pi 10^3)^{-1} \approx 150$ s for $x = 1$ (no free parameters are adjusted in this function).

plot makes the low-frequency tail of the secondary process more visible. For *m*-toluidine the situation is ambiguous. Indeed for this liquid TTS seems to apply, but if we look at the high-frequency end on a smaller scale (Figure 4, right-bottom) there is a sensitive difference between the curves. In this figure we report also the scaled spectra of DC705 that satisfy TTS on the small scale for an easier comparison. We also note that the dielectric strength of the secondary relaxation reported for *m*-toluidine¹⁴ is rather low while in the shear-mechanical spectra it seems to be more intense in comparison with the α process. This is another important feature of our mechanical measurement: a weak dielectric secondary process is *magnified* in the shear response.^{4,5}

An interesting feature of the spectra of 1,2-propanediol is underlined by the TTS plot in Figure 4. The portion of the spectrum at frequencies lower than ν_{\max} (i.e., at $\nu/\nu_{\max} \leq 1$) is slightly deformed. The shape of this response function is reproducible, and it seems to be almost temperature-independent in the temperature range explored in our experiment. This “shoulder” could be considered a peculiar feature of the mechanical relaxation of 1,2-propanediol since it is not found in dielectric spectra (see for example ref 13). Note that an additional process (with similar shape) close to the α relaxation is found in the case of tripropylene glycol in high-pressure conditions (see ref 16). Further studies of the dielectric relaxation of 1,2-propanediol at high pressure would be needed to better understand the origin of the shape of its mechanical response.

We want to stress again that, from our study, the lack of TTS seems to be intrinsically related to the presence of a secondary mechanical process. All the liquids studied here that show the β relaxation (as also confirmed by the dielectric measurements cited in section II) display a clear temperature dependence in the shape of the mechanical response function. Anyway, it is not generally clear how the presence of the β relaxation is related to the nature of a specific liquid. The understanding of the validity of TTS in some supercooled liquids requires the understanding of one of the most puzzling phenomena of ultraviscous liquids and glasses that is the secondary relaxation process.

It has been suggested from empirical observations^{17,18} that when TTS applies, the high-frequency decay of the dielectric loss is characterized by a power-law behavior ν^α with exponent $\alpha = -1/2$. A theoretical explanation for this power-law dependence of the dielectric response has been proposed,

assuming the dominance of long-wavelength fluctuations.^{19–21} We have tested this conjecture for the mechanical response, finding the minimum value of the logarithmic derivative of G'' , i.e. $\alpha_{\min} = [d \ln G''/d \ln \nu]_{\min}$. It has to be noted that the extraction of this information is much more complicated for the shear loss than the dielectric response. This is due to the fact that the shear response is generally affected by a higher noise level than dielectric. An example of the procedure followed to extract α_{\min} is reported in Figure 5 for the mechanical response of *m*-toluidine at $T = 186$ K. When α is plotted as a function of the frequency, a minimum can be identified within some data points. The average of these points is taken as the α_{\min} . Note that a Debye process would have a characteristic behavior of the logarithmic slope showing a sudden drop of α at the relaxation frequency ν_{\max} .

In Figure 6 we report the value of α_{\min} as a function of the loss peak frequency for the temperatures where the minimum of the derivative of the logarithm was well-defined. We note that even if the behavior of this quantity for the liquids studied is compatible with a limiting $\alpha = -1/2$ at low temperatures, the data seem to lie systematically above the -0.5 line. We stress also that it is easy to expect that a $\nu^{-1/2}$ behavior in the shear loss is disturbed more when a β relaxation is present since its intensity is enhanced in the mechanical spectrum compared to the dielectric.

Finally, we remark that the parameter α_{\min} is not expected to monotonically decrease in a wider temperature range. Indeed, at higher temperatures the shape of the shear response should recover a simpler Debye-like shape where the stretching parameters (the KKW β parameter for example) come close to unity.²² The relaxation frequencies belonging to this high-temperature regime are currently outside the dynamical window of the PSG technique.²³

To conclude the analysis of our data, we want to present a comparison between the mechanical spectral features and a simple phenomenological model for the dynamics of supercooled liquids. The shoving model²⁴ is based on the assumption that the relaxation in the supercooled liquid takes place with a local volume increase and that the activation energy is mainly elastic energy spent to shove aside the surrounding of the rearranging molecules. As has been reported, this model can be derived estimating the barrier height in a classical energy landscape approach.²⁵

The shoving model predicts that the relaxation time is related to the infinite-frequency shear modulus G_∞ by the equation

$$\ln(\tau) = \ln \tau_0 + V_c G_\infty(T)/T \quad (1)$$

where V_c is a characteristic volume in a relaxation process (V_c is assumed temperature independent) and τ_0^{-1} is the phonon-frequency ($\tau_0 \approx 10^{-14}$ s). The determination of G_∞ is not necessary to test the model if TTS applies; indeed, if this property holds, we can write

$$G_\infty(T) \propto G''_{\max}(T) \quad (2)$$

since the constant factor A determining the amplitude of the complex response in $\chi(\nu, T) = A(T)\Phi(\nu/\nu_{\max}(T))$ is the same for the real and the imaginary part Φ' and Φ'' . Note that this proportionality does not apply when TTS does not hold. For example, in a case where the β relaxation is present the value of G_∞ is modified by the secondary process, and a more complicated fitting procedure would be needed to estimate the

value of the infinite-frequency shear modulus. On the other hand, when TTS is satisfied, we can write the simple equation (using eq 2 in eq 1)

$$\log(\tau) = \log \tau_0 + BG''_{\max}(T)/T \quad (3)$$

where B is a constant factor. Equation 3 represents the prediction of the shoving model when TTS also applies: the logarithm of the relaxation time is a linear function of the quantity $G''_{\max}(T)/T$. This is tested in Figure 7 for the liquids in which time-temperature superposition is found to hold (DC705 and 1,2-propanediol). In this figure the relaxation time (defined as $\tau = (2\pi\nu_{\max})^{-1}$) is reported as a function of $1/T$ and as a function of G''_{\max}/T . To report all the data in the same plot, the abscissa has been normalized to the unity as T_g/T and as $x = (T_g/G''_{\max,g})(G''_{\max}/T)$. Note that here we find $G''_{\max,g}$ through a linear extrapolation of the last values G''_{\max} to T_g previously identified to give $\nu_{\max}(T_g) = 10^{-3}$ Hz (corresponding to $\tau(T_g) = (2\pi 10^3)^{-1} \approx 150$ s).

The dashed line in Figure 7 represents the shoving model prediction (no adjustable parameters are used in this function) ending, at high temperature, at the physically reasonable prefactor 10^{-14} s.

IV. Conclusion

We have reported shear-mechanical spectra of five glass-forming liquids close to T_g . Via the PSG¹ technique, we have investigated the behavior of the mechanical α process and found evidence of the presence of a mechanical β relaxation in dibutyl phthalate, diethyl phthalate, and *m*-toluidine. Time-temperature superposition for the mechanical susceptibility is found to hold for the liquids without signature of β process (pentaphenyltrimethyltrisiloxane and 1,2-propanediol). The conjecture originally developed for the dielectric response that, when TTS applies, a $\nu^{-1/2}$ decay is found for the high-frequency part of the loss is checked for the shear response. We find that the data are consistent with a limiting $\nu^{-1/2}$ low-temperature behavior although the minimum slopes are systematically higher than -0.5 . The shoving model has been tested for the two liquids without β relaxation, finding that it well describes the experimental data.

Acknowledgment. The Center for Viscous Liquid Dynamics "Glass and Time" is sponsored by The Danish National Research Foundation (DNRF).

References and Notes

- (1) Christensen, T.; Olsen, N. B. *Rev. Sci. Instrum.* **1995**, *66*, 5019.
- (2) Johari, G. P.; Goldstein, M. *J. Chem. Phys.* **1970**, *53*, 2372.
- (3) Jakobsen, B.; Niss, K.; Olsen, N. B. *J. Chem. Phys.* **2005**, *123*, 234511.
- (4) Jakobsen, B.; Maggi, C.; Christensen, T.; Dyre, J. C. *J. Chem. Phys.* **129**, 184502.
- (5) Niss, K.; Jakobsen, B.; Olsen, N. B. *J. Chem. Phys.* **2005**, *123*, 234510.
- (6) The piezoelectric ceramic is PZ26 produced by FerroPerm (Denmark).
- (7) Igarashi, B.; Christensen, T.; et al. *Rev. Sci. Instrum.* **2008**, *79*, 045106.
- (8) Igarashi, B.; Christensen, T.; et al. *Rev. Sci. Instrum.* **2008**, *79*, 045105.
- (9) All the shear-mechanical spectra reported in this work are available in the "Glass and Time: Data repository" found online at <http://glass.ruc.dk/> data.
- (10) Dixon, P. K.; Wu, L.; Nagel, S. R.; Williams, B. D.; Carini, J. P. *Phys. Rev. Lett.* **1990**, *65*, 1108.
- (11) Power, G.; Vij, J. K.; Johari, G. P. *J. Chem. Phys.* **2006**, *124*, 044513.
- (12) Bartos, J.; Alegria, A.; Sausa, O.; et al. *Phys. Rev. E* **2007**, *76*, 031503.
- (13) de Francesco, L.; Cutroni, M.; Mandanici, A. *Philos. Mag. B* **2002**, *82*, 5-625.
- (14) Mandanici, A.; Cutroni, M.; Richert, R. *J. Chem. Phys.* **2005**, *122*, 084508.
- (15) Note that a number of problems could be present in such low-temperature measurements. There is the possibility of damaging the piezo-discs because of the sandwiched glass contracting; nevertheless, unknown memory effects could be induced in piezo-ceramics lowering repetitively their temperature when the stresses are not fully relaxed.
- (16) Prevosto, D.; Capaccioli, S.; Lucchesi, M.; et al. *J. Chem. Phys.* **2005**, *122*, 061102.
- (17) Olsen, N. B.; Christensen, T.; Dyre, J. C. *Phys. Rev. Lett.* **2001**, *86*, 1271.
- (18) Nielsen, A. I.; Christensen, T.; Jakobsen, B.; et al. arXiv:0811.1116v1.
- (19) Dyre, J. C. *Europhys. Lett.* **2005**, *71*, 646.
- (20) Dyre, J. C. *Phys. Rev. E* **2006**, *74*, 021502.
- (21) Dyre, J. C. *Phys. Rev. E* **2006**, *76*, 041508.
- (22) Trachenko, K.; Roland, C. M.; Casalini, R. *J. Phys. Chem. B* **2008**, *112*, 5111.
- (23) The high-frequency limit of the PSG technique (10 kHz) is set by the geometrical and material properties of the piezo-electric discs. Above this frequency the response of the measuring device is dominated by the intrinsic resonances of the piezo-ceramics (see ref 1).
- (24) (a) Dyre, J. C.; Olsen, N. B.; Christensen, T. *Phys. Rev. B* **1996**, *53*, 2171. (b) Olsen, N. B.; Dyre, J. C.; Christensen, T. *Phys. Rev. Lett.* **1998**, *81*, 1031. (c) Dyre, J. C. *Rev. Mod. Phys.* **2006**, *78*, 953.
- (25) Dyre, J. C.; Olsen, N. B. *Phys. Rev. E* **2004**, *69*, 042501.

JP805097R

Investigation of the shear-mechanical and dielectric relaxation processes in two monoalcohols close to the glass transition

Bo Jakobsen,^{a)} Claudio Maggi, Tage Christensen, and Jeppe C. Dyre

DNRF Centre "Glass and Time," IMFUFA, Department of Sciences, Roskilde University, Postbox 260, DK-4000 Roskilde, Denmark

(Received 29 May 2008; accepted 3 October 2008; published online 10 November 2008)

Shear-mechanical and dielectric measurements on the two monohydroxy (monoalcohol) molecular glass formers 2-ethyl-1-hexanol and 2-butanol close to the glass-transition temperature are presented. The shear-mechanical data are obtained using the piezoelectric shear-modulus gauge method covering frequencies from 1 mHz to 10 kHz. The shear-mechanical relaxation spectra show two processes, which follow the typical scenario of a structural (alpha) relaxation and an additional (Johari-Goldstein) beta relaxation. The dielectric relaxation spectra are dominated by a Debye-type peak with an additional non-Debye peak visible. This Debye-type relaxation is a common feature peculiar to monoalcohols. The time scale of the non-Debye dielectric relaxation process is shown to correspond to the mechanical structural (alpha) relaxation. Glass-transition temperatures and fragilities are reported based on the mechanical alpha relaxation and the dielectric Debye-type process, showing that the two glass-transition temperatures differ by approximately 10 K and that the fragility based on the Debye-type process is a factor of 2 smaller than the structural fragility. If a mechanical signature of the Debye-type relaxation exists in these liquids, its relaxation strength is at most 1% and 3% of the full relaxation strength of 2-butanol and 2-ethyl-1-hexanol, respectively. These findings support the notion that it is the non-Debye dielectric relaxation process that corresponds to the structural alpha relaxation in the liquid. © 2008 American Institute of Physics. [DOI: 10.1063/1.3007988]

I. INTRODUCTION

A class of often investigated glass-forming liquids is the hydrogen-bonding liquids, among which the alcohols are a much studied subclass (for a compilation of references to classical results prior to 1980 see Ref. 1, Sec. IX-c.1). Alcohols are normally classified into those containing one hydroxyl group (the monoalcohols) and those with two or more hydroxyl groups.

During the 1950s it was observed that the main relaxation in most monoalcohols, contrary to the main relaxation in other liquids, can be represented by a single relaxation time—they follow the Debye prediction.² It was further realized that additional relaxation processes exist at frequencies above the main Debye-type relaxation. One additional process is normally observed, but in some cases two processes can be resolved (see, e.g., Ref. 3). Comparisons between mechanical and dielectric measurements^{4,5} further showed that when the main dielectric relaxation is of Debye-type its time scale is separated from the mechanical time scale, but no explanation was given for this. It was further discussed to what extent the Debye-type process corresponds to the mechanical relaxation, as, e.g., stated by Johari and Goldstein⁶ discussing the importance of mechanical measurements near the glass-transition temperature; “such a study can answer an important question: whether or not the same molecular motions are involved in the volume, shear, and dielectric relaxation of H-bonded liquids.”

During the past decade a number of studies^{7–19} (see below for details) have indicated that the low-frequency Debye-type peak is decoupled from the mechanical relaxation and that the non-Debye dielectric peak at higher frequencies reflects the structural alpha relaxation. In this paper we shall term the two lowest frequency dielectric relaxations the Debye-type relaxation and the alpha relaxation, respectively. This scenario offers an explanation for the earlier observations and it gives the possibility that the behavior of monoalcohols follows that of other glass formers, except for the existence of the Debye-type dielectric peak.

Two classes of arguments are generally given for this idea: comparisons of time scales/glass-transition temperatures and the lack of a Debye-type peak in other measurement types. A large number of experiments and comparisons exists including the following: comparison with calorimetric measurements,^{7,8} comparison with photon correlation spectroscopy probing the density-density correlations,⁹ comparison with the time scale found from viscosity data,^{9,13} analysis of the alpha-beta relaxation,¹⁰ solvation dynamics probing mechanical relaxation of the liquid,¹¹ dielectric and calorimetric investigation of mixtures of monoalcohols with other substances,^{12,14–16} frequency-dependent specific heat measurements,¹⁷ systematic comparison to differential scanning calorimetry measurements¹⁸ and dielectric studies of mixtures.¹⁹ Except for the early ultrasonic-based measurements^{4,20} no direct comparison, to the best of our knowledge, of the macroscopic mechanical relaxation spectra and dielectric relaxation spectra of monoalcohols exists.

^{a)}Electronic mail: boj@ruc.dk.

Such measurements directly reveal if the non-Debye relaxation mode seen in dielectrics is in accordance with the shear-mechanical structural α relaxation. Shear-mechanical relaxation data are, furthermore, generally a good complement to dielectric data,²¹ and such investigations can also explore to what extent a shear-mechanical Debye-type relaxation exists.

In this study we present shear-mechanical investigations in the temperature range down to the glass-transition temperature together with complementary dielectric spectroscopy investigation to allow for direct comparison.

The two liquids studied are 2-butanol and 2-ethyl-1-hexanol. The reason for not studying simple normal alcohols like ethanol is that such systems easily crystallize. The chosen systems represent two ways of introducing steric hindrances in the system, hence improving the glass-forming ability. Both liquids have been investigated earlier. For early results on 2-butanol see, e.g., Refs. 22 and 23 and for 2-ethyl-1-hexanol see, e.g., Refs. 8, 12, 17, 18, 24, and 25.

II. EXPERIMENTAL

The measurements were performed using a custom-built setup.^{26–28} The temperature is controlled by a custom-built cryostat with temperature fluctuations smaller than 2 mK (see Ref. 27 for details on the cryostat). The same cryostat was used for all measurements, thus ensuring equal temperatures and directly comparable results. The electrical signals were measured using a HP 3458A multimeter in connection with a custom-built frequency generator in the frequency range of 10^{-3} – 10^2 Hz and an Agilent 4284A LCR meter in the frequency range of 10^2 – 10^6 Hz (see Ref. 28 for details on the electrical setup).

The shear-mechanical relaxation data were obtained using the piezoelectric shear modulus gauge method.²⁶ This method has a wide frequency range (up to 10^{-3} – 10^4 Hz) and is optimized for measuring moduli in the range of MPa–GPa, corresponding to typical moduli of liquids close to the glass-transition temperature. The dielectric data were obtained using a multilayered gold-plated capacitor with a empty capacitance of 95 pF.

2-ethyl-1-hexanol ($\geq 99.6\%$, CAS number 104–76–7) and 2-butanol (99.5%, CAS number 78–92–2, racemic mixture) were acquired from Aldrich and used as received. To ensure that the samples did not change characteristics (e.g., due to absorption of water), dielectric measurements were performed on the newly opened bottles and repeated at the end of the studies. For both liquids the only observable changes were in the unimportant low-frequency contributions from conduction.

The raw data²⁹ obtained consist of frequency ν , scans of the complex dielectric constant $\epsilon(\nu)$, and the complex shear modulus $G(\nu)$. Each scan was taken at constant temperature in thermal equilibrium, stepping down in temperature.

Equilibrium was ensured by repeating some of the frequency scans on reheating the sample from the lowest temperature. Repetition of parts of the shear-mechanical measurements showed that the uncertainty on the overall absolute level of the shear modulus is rather large in the case

of 2-ethyl-1-hexanol ($\approx 20\%$); it is much better for 2-butanol. The influence of this experimental uncertainty on the position of the loss peaks is, however, minor (at most ± 0.1 decade).

III. RESULTS AND DISCUSSIONS

A selection of the obtained dielectric spectra is shown in Fig. 1, represented as the dielectric loss as a function of frequency [minus the imaginary part of the complex dielectric constant $-\epsilon(\nu)''$]. The dielectric data are further illustrated in Fig. 2 as a Nyquist plot at a representative temperature. The dielectric spectrum follows the general pattern for monoalcohols with a dominant Debye-type relaxation and a minor second relaxation—the alpha relaxation.

A common way (e.g., Refs. 3, 9, 13, 19, 22, and 23) to separate the minor alpha process and possible Johari–Goldstein beta processes from the Debye-type relaxation process is to assume additivity of the processes in the dielectric susceptibility (corresponding to statistical independent dipole-moment fluctuations of the two processes). This is done either by fitting a sum of a Debye function and a Havriliak–Negami function (and possibly a Cole–Cole function for the beta process) or by subtracting the fit of a Debye function from the raw data (most common in elder studies, e.g., Ref. 3).

In this paper we assume additivity of the processes³⁰ and subtract the Debye function in order to analyze the residual, this procedure is illustrated in Fig. 3. The fit to the Debye function is also shown in the Nyquist plot in Fig. 2, illustrating the quality of the fit with respect to both real and imaginary parts of the dominant dielectric relaxation process.

A selection of the shear-mechanical data is shown in Fig. 1 as mechanical loss $G''(\nu)$, as function of frequency. Figure 2, furthermore, shows the shear-mechanical relaxation spectra illustrated as a Nyquist plot at a typical temperature. The general pattern for liquids close to the glass-transition temperature is observed, with a pronounced non-Debye alpha relaxation and a smaller Johari–Goldstein beta relaxation. The beta relaxation is much stronger in the shear-mechanical relaxation spectrum than in the dielectric spectrum for these liquids (the existence of a dielectric beta relaxation for these systems has been reported in the literature^{8,23}), consistent with previous observation on molecular liquids²¹ and the Gemant–DiMarzio–Bishop model.³¹

A. Temperature dependence of the dynamics

To analyze the time scales associated with the observed processes and their temperature dependences, the loss-peak frequencies (ν_p) were determined. These are shown in Fig. 4. For the alpha process in the shear-mechanical data and the Debye-type process in the dielectric data, they were determined directly from the raw data. For the alpha relaxation in the dielectric data the loss peak was found after subtracting the Debye function. To ensure consistency in the analysis, the dielectric alpha loss peak was only calculated at temperatures where the loss peak of the Debye-type relaxation was observed.

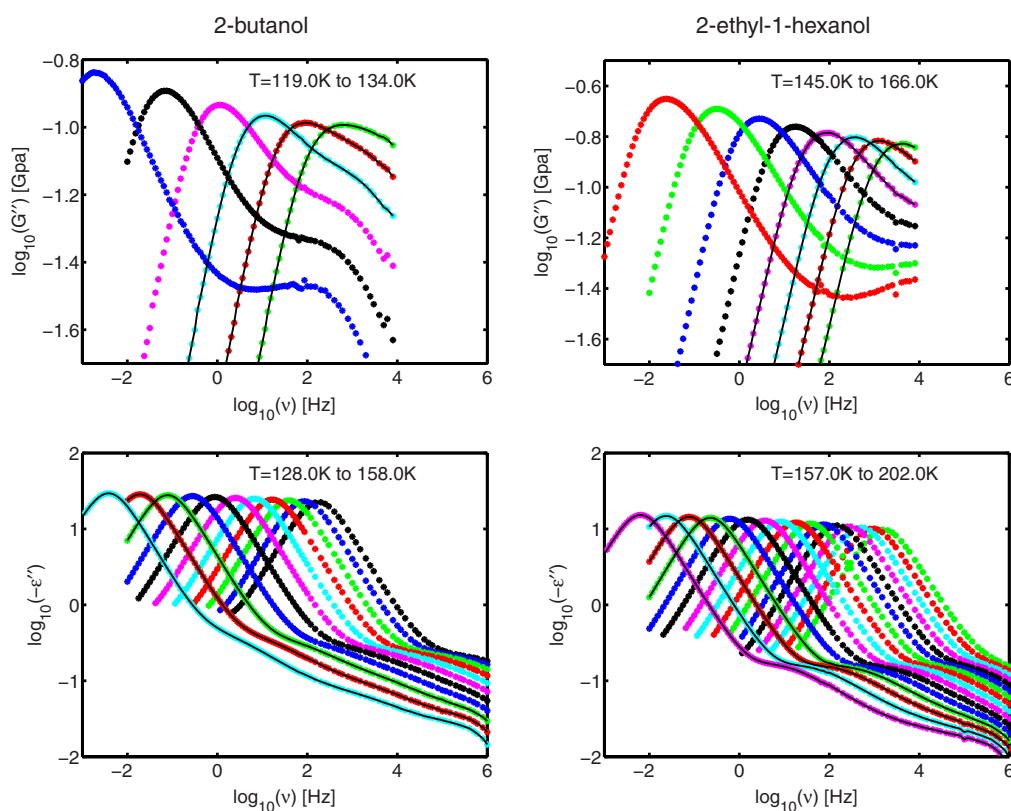


FIG. 1. (Color online) Selected dielectric and shear-mechanical spectra for the two liquids (the full data set is available online, see Ref. 29). Temperature intervals are indicated and the step size is 3 K. Temperatures that are highlighted by a full line through the points exist for both dielectric and shear-mechanical measurements, this is only the case in a limited temperature interval, where an overlap exists between the high temperature shear data and low temperature dielectric data. Top: shear-mechanical loss as function of frequency. Bottom: dielectric loss as function of frequency. To enhance readability of the figure, the dielectric spectra have been truncated at low frequencies, at around the onset of the contribution from conduction.

The dielectric alpha-peak frequency closely follows the peak frequency of the shear-mechanical alpha process. This is further illustrated in the lower part of Fig. 4, where the “decoupling” index [defined as $\log_{10}(\nu_{p,G}/\nu_{p,\epsilon})$] is shown for the dielectric processes (Debye-type and alpha process) relative to the mechanical alpha process. The mechanical and dielectric alpha-time scales are separated by approximately 1 decade in frequency, whereas the mechanical alpha and the dielectric Debye-type processes are separated by four orders of magnitude in frequency. The separation between the loss-peak positions can also directly be seen in Fig. 1 for the temperatures where both shear-mechanical and dielectric data exist (indicated by full lines). The separation between the shear-mechanical and dielectric alpha processes is in agreement with previous comparisons of the shear-mechanical and dielectric alpha time scale.^{4,5,21,32–36} From Fig. 1 it can be seen that the mechanical beta relaxation may influence the loss-peak position of the shear-mechanical alpha relaxation at high temperatures. From, e.g., Ref. 21 we know that such influences only change the decoupling index between the shear mechanic and dielectric alpha relaxations slightly; such an effect can, therefore, not disturb the general

observations. It is further noticeable that no changes can be observed in the temperature dependence of the shear-mechanical relaxation time around the temperature where the Debye-type process falls out of equilibrium on the time scale of the experiment.

The glass-transition temperature(s) was determined from the loss-peak frequencies³⁷ as the temperature where $\nu_{p,\epsilon} = 10^{-2}$ Hz. The numbers for the dielectric Debye-type relaxation and the shear-mechanical alpha relaxation are given in Table I. The huge separation in time scale between the two processes results in a separation of T_g of 10 K for 2-butanol and 14 K for 2-ethyl-1-hexanol.

Based on the loss-peak frequencies an Angell plot was constructed, as shown in Fig. 5. The two substances show a remarkable similarity in the temperature dependence of the characteristic time when plotted this way. The dielectric alpha process, furthermore, closely follows the tendencies of the mechanical alpha process.

The fragility index $m = [(d \log_{10} 1/\nu_{p,\epsilon}) / (dT_g/T)]|_{T=T_g}$ (Refs. 38–40) is reported in Table I. A clear difference is seen between the fragility index if defined from the dielectric Debye-type process or from the mechanical alpha process.

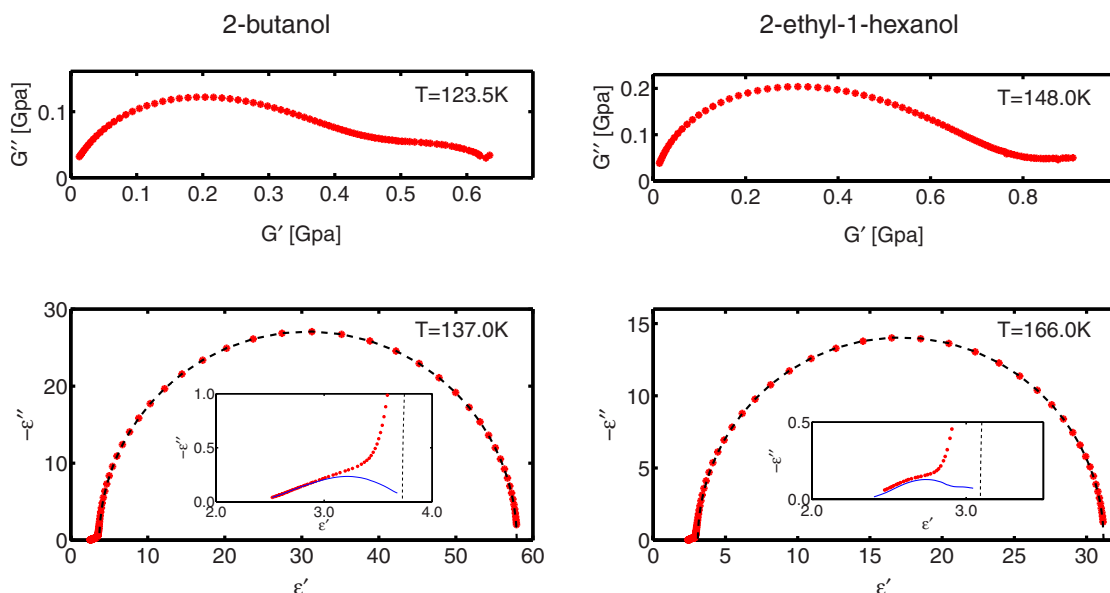


FIG. 2. (Color online) Typical dielectric and shear-mechanical spectra for the two liquids, represented as Nyquist plots. Top: shear-mechanical spectra. Bottom: dielectric spectra (the inset shows a zoom on the high frequency foot point). Lines indicate the separation of the dielectric data into a Debye-like process (dashed lines) and an alpha-relaxation process (full lines), see Fig. 3 for full explanation.

The Debye-type process leads to a classification of the liquid as much stronger than the mechanical alpha relaxation.

The difference in temperature dependence of the Debye-type process and the structural relaxation will lead to a merging of the two processes at low temperatures, if the trend continue. This is of course close to impossible to test experimentally as the relaxation times at such low temperatures become very long. The possibility of a low temperature merge of the Debye-type process and the structural alpha

process has been discussed earlier in Refs. 19 and 41. The idea is further supported by the compilation of data presented in Ref. 13; the data generally show a decrease in the difference between the loss-peak frequency of the dielectric Debye-type relaxation and dielectric alpha relaxation with decreasing temperature.

B. Spectral shape

The spectral shape of the shear-mechanical alpha peak was characterized by calculation of the minimum slope in a log-log plot, as shown on Fig. 6. Similar data have been reported for shear-mechanical relaxation studies on other systems by our group^{21,42} based on the ideas presented in Ref. 43. In comparing to these previous results, it is observed that the two liquids follow the general trend of liquids with a mechanical beta relaxation. The minimum slope is in the range from -0.3 to -0.4 close to T_g , still decreasing upon cooling (most prominent for 2-butanol), possibly toward -0.5 as conjectured in Refs. 44–46. This shows that the mechanical alpha-relaxation spectra, hence the mechanical relaxation processes, are similar to what is generally observed for glass-forming liquids.

C. Limits on a mechanical Debye-type process

A small low-frequency peak was observed in the raw data obtained by the shear-mechanical transducer. Closer investigations, however, showed that this was not a mechanical signal of the Debye-type process, but a “spillover effect” of the large dielectric signal. This effect is caused by wetting of the edges of the piezoceramic disks in the transducer and the

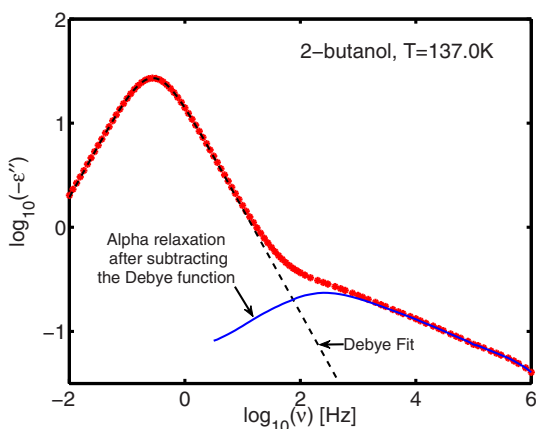


FIG. 3. (Color online) Illustration of the procedure used for separating the alpha relaxation from the Debye-type relaxation. The data shown are the dielectric loss spectrum for 2-butanol at $T=137$ K. Points are measured data, dashed line is a fit of the main relaxation to a Debye function $\epsilon = [\Delta\epsilon_D / (1 + i\omega\tau)] + \epsilon_{D,\infty}$, and the full line the residual after subtracting the Debye function from the measured data (representing the alpha-relaxation process).

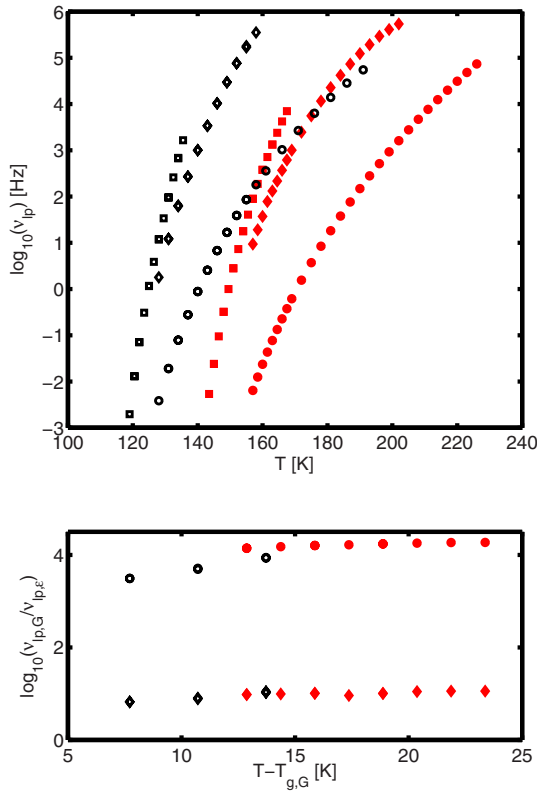


FIG. 4. (Color online) Top: loss-peak positions for the different processes evaluated for the two investigated systems (repeated measurements exist at some temperatures). Bottom: the decoupling index $[\log_{10}(\nu_{ip,G}/\nu_{ip,\epsilon})]$ for the dielectric alpha and Debye-type process relative to the mechanical alpha process. (□) Shear-mechanical alpha relaxation. (○) Dielectric Debye-type relaxation. (◇) Dielectric alpha relaxation. Open symbols: 2-butanol. Closed symbols: 2-ethyl-1-hexanol.

large dielectric strength of the investigated systems; it is equivalent to sometimes observed conduction contributions in the raw data.

We can, of course, not entirely exclude that a mechanical

TABLE I. Glass-transition temperature (T_g) and fragility (m) for the dielectric Debye-type process ($\epsilon_{\text{Debye-type}}$) and mechanical alpha process (G_{alpha}). The glass-transition temperature is defined from the loss-peak frequencies as $\nu_{ip}(T_g) = 10^{-2}$ Hz.

	T_g		m	
	G_{alpha}	$\epsilon_{\text{Debye-type}}$	G_{alpha}	$\epsilon_{\text{Debye-type}}$
2-butanol	120 K ^a	130 K	63	29
2-ethyl-1-hexanol	144 K ^b	158 K ^c	60 ^d	30 ^e

^aIn accordance with calorimetric T_g of 120.3 K from Ref. 23.

^bIn accordance with calorimetric T_g of 145.9 K from Ref. 18 and of 148.9 K from Ref. 8, and dielectric alpha-relaxation T_g of 144.0 K from Ref. 18.

^cIn accordance with the value of 155.0 K reported in Ref. 18, and 154.0 K reported in Ref. 8 [using $\nu_{ip}(T_g) = 10^{-3}$ Hz as definition of T_g].

^dComparable to the value of 70 reported in Ref. 18 on the basis of dielectric data.

^eIn accordance with the value of 27.0 reported in Ref. 8.

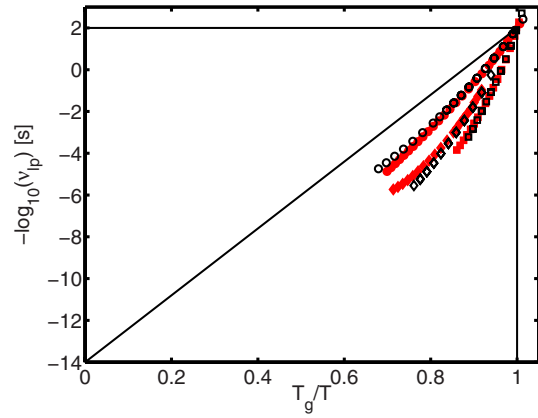


FIG. 5. (Color online) Angell fragility plot based on loss-peak positions. (Symbols as in Fig. 4.) The vertical and horizontal lines define the glass transition, the diagonal line corresponds to Arrhenius behavior. T_g for the mechanical alpha relaxation and dielectric Debye-type relaxation is as given in Table I. For the dielectric alpha relaxation, T_g from the mechanical alpha relaxation was used. The reason for this is that the data do not allow for direct determination of the T_g for the dielectric alpha relaxation without extensive extrapolation, and that the two temperatures normally are not too different due to the small decoupling between the processes.

signal is hiding below this dielectric spillover signal, but we are able to put limits on the maximal relaxation strength. In the case of 2-butanol the signal was partly eliminated by a correction procedure using data from a mechanically empty but still wetted transducer. From the resulting shear-mechanical spectra one can conclude that a shear-mechanical relaxation process corresponding to the Debye-type process in the dielectrics must have a relaxation strength below 5 MPa (corresponding to at most 1% of the full relaxation strength) if it exists. In the case of 2-ethyl-1-hexanol the raw data show that a mechanical Debye-type relaxation process must have a strength below 30 MPa (corresponding to at most 3% of the full relaxation strength).

IV. SUMMARY AND CONCLUSIONS

Two monoalcohols (2-butanol and 2-ethyl-1-hexanol) were investigated by conventional dielectric spectroscopy and broadband shear-mechanical spectroscopy in the temperature range down to the glass-transition temperature. In the dielectric spectrum a low-frequency Debye-type process is dominant, as is generally observed for monoalcohols. The second relaxation process observed was mathematically separated from the Debye-type relaxation by assuming additivity of the processes in the dielectric susceptibility. Loss-peak positions were found for the two processes.

Viewed from the shear-mechanical perspective, the liquids behave as generic glass formers. Besides a clear non-Debye alpha relaxation, a minor Johari–Goldstein beta relaxation is observed. The loss-peak positions of the alpha process were determined.

The time scale of the mechanical alpha relaxation is clearly non-Arrhenius with a fragility index of ≈ 60 for both

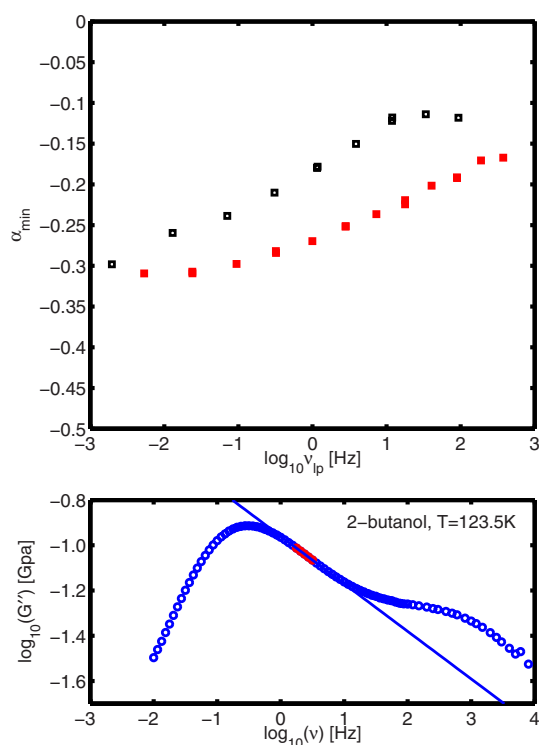


FIG. 6. (Color online) Top: minimum slope of the alpha-peak (α_{\min}) in a log-log plot of G'' as a function of frequency, plotted against the loss-peak frequency (repeated measurements exist at some temperatures). Open symbols: 2-butanol. Closed symbols: 2-ethyl-1-hexanol. Bottom: illustration of the minimum slope in a log-log plot of G'' as a function of frequency. The slope of the relaxation curve is found for all frequencies by pointwise differentiation, and from this a frequency range of minimum slope is determined. The reported minimum slope is an average over the slope in this frequency range. In the figure the frequency range of minimum slope is marked by closed circles, and the full line goes through a central point in this frequency range and has a slope equal to the found minimum slope.

liquids. The Debye-type dielectric relaxation has a much different temperature dependence, with a fragility index of ≈ 30 for both liquids.

The time scale of the dielectric alpha relaxation follows closely that of the mechanical alpha relaxation. The two processes are separated by roughly 1 decade of frequency, consistent with what is usually observed for the separation of mechanical and dielectric alpha relaxations. The Debye-type process is separated from the mechanical alpha relaxation by roughly 4 decades (depending on temperature). The temperature dependence of the mechanical relaxation time seems to be unaffected by the falling out of equilibrium of the dielectric Debye-type process.

The possibility that the Debye-type relaxation process has a mechanical signature can still not be ruled out, but the present results show that if it exists one has to use measurement methods specialized for rather soft systems to look for it. If the Debye-type process has a mechanical signature, it must have a relaxation strength below 1% and 3% of the full relaxation strength for 2-butanol and 2-ethyl-1-hexanol, respectively.

These observations support the existing idea^{7–19} that the “minor” non-Debye peak observed by dielectric spectroscopy is the structural alpha relaxation, and that the major Debye-type relaxation is *something else*. Any explanation on the dielectric Debye-type relaxation should be able to explain why no significant signature is observed in either mechanical or calorimetric studies.¹⁷

ACKNOWLEDGMENTS

We are grateful to Niels Boye Olsen for inspiring this work and Kristine Niss for contributing with interesting comments and questions. This work was supported by the Danish National Research Foundation’s (DNRF) center for viscous liquid dynamics “Glass and Time.”

- ¹C. J. F. Böttcher and P. Bordewijk, *Theory of Electric Polarization II: Dielectrics in Time-Dependent Fields*, 2nd ed. (Elsevier, New York, 1980).
- ²D. W. Davidson and R. H. Cole, *J. Chem. Phys.* **19**, 1484 (1951).
- ³R. H. Cole and D. W. Davidson, *J. Chem. Phys.* **20**, 1389 (1952).
- ⁴R. Kono, T. A. Litovitz, and G. E. McDuffie, *J. Chem. Phys.* **45**, 1790 (1966).
- ⁵T. A. Litovitz and G. E. McDuffie, *J. Chem. Phys.* **39**, 729 (1963).
- ⁶G. P. Johari and M. Goldstein, *J. Chem. Phys.* **55**, 4245 (1971).
- ⁷S. S. N. Murthy, *Mol. Phys.* **87**, 691 (1996).
- ⁸S. S. N. Murthy, *J. Phys. Chem.* **100**, 8508 (1996).
- ⁹C. Hansen, F. Stickel, T. Berger, R. Richert, and E. W. Fischer, *J. Chem. Phys.* **107**, 1086 (1997).
- ¹⁰A. Kudlik, C. Tschirwitz, S. Benkhof, T. Blochowicz, and E. Rössler, *Europhys. Lett.* **40**, 649 (1997).
- ¹¹H. Wendt and R. Richert, *J. Phys. Chem. A* **102**, 5775 (1998).
- ¹²S. S. N. Murthy and M. Tyagi, *J. Chem. Phys.* **117**, 3837 (2002).
- ¹³L. M. Wang and R. Richert, *J. Chem. Phys.* **121**, 11170 (2004).
- ¹⁴L. M. Wang and R. Richert, *J. Phys. Chem. B* **109**, 11091 (2005).
- ¹⁵L. M. Wang and R. Richert, *J. Phys. Chem. B* **109**, 8767 (2005).
- ¹⁶L. M. Wang, S. Shahriari, and R. Richert, *J. Phys. Chem. B* **109**, 23255 (2005).
- ¹⁷H. Huth, L. M. Wang, C. Schick, and R. Richert, *J. Chem. Phys.* **126**, 104503 (2007).
- ¹⁸L. M. Wang, Y. Tian, R. Liu, and R. Richert, *J. Chem. Phys.* **128**, 084503 (2008).
- ¹⁹T. El Goresy and R. Böhmer, *J. Chem. Phys.* **128**, 154520 (2008).
- ²⁰T. Lyon and T. A. Litovitz, *J. Appl. Phys.* **27**, 179 (1956).
- ²¹B. Jakobsen, K. Niss, and N. B. Olsen, *J. Chem. Phys.* **123**, 234511 (2005).
- ²²W. Dannhauser and R. H. Cole, *J. Chem. Phys.* **23**, 1762 (1955).
- ²³S. S. N. Murthy and S. K. Nayak, *J. Chem. Phys.* **99**, 5362 (1993).
- ²⁴R. Wemelle, C. R. Hebd. Seances Acad. Sci. **244**, 775 (1957).
- ²⁵A. Bondeau, G. Noyel, and J. Huck, C. R. Seances Acad. Sci., Ser. C **286**, 273 (1978).
- ²⁶T. Christensen and N. B. Olsen, *Rev. Sci. Instrum.* **66**, 5019 (1995).
- ²⁷B. Igarashi, T. Christensen, E. H. Larsen, N. B. Olsen, I. H. Pedersen, T. Rasmussen, and J. C. Dyre, *Rev. Sci. Instrum.* **79**, 045105 (2008).
- ²⁸B. Igarashi, T. Christensen, E. H. Larsen, N. B. Olsen, I. H. Pedersen, T. Rasmussen, and J. C. Dyre, *Rev. Sci. Instrum.* **79**, 045106 (2008).
- ²⁹The full raw data sets [$G(\nu)$ and $\epsilon(\nu)$ at the investigated temperatures] can be obtained from the “Glass and Time: Data repository,” found online at <http://glass.ruc.dk/data>.
- ³⁰The problem with such approach is discussed in the context of the merging of the alpha and beta process in Ref. 47.
- ³¹K. Niss, B. Jakobsen, and N. B. Olsen, *J. Chem. Phys.* **123**, 234510 (2005).
- ³²N. Menon, S. R. Nagel, and D. C. Venerus, *Phys. Rev. Lett.* **73**, 963 (1994).
- ³³T. Christensen and N. B. Olsen, *J. Non-Cryst. Solids* **172-174**, 357 (1994).
- ³⁴R. Zorn, F. I. Mopsik, G. B. McKenna, L. Willner, and D. Richter, *J. Chem. Phys.* **107**, 3645 (1997).
- ³⁵R. D. Deegan, R. L. Leheny, N. Menon, S. R. Nagel, and D. C. Venerus, *J. Phys. Chem. B* **103**, 4066 (1999).

- ³⁶K. Schröter and E. Donth, *J. Chem. Phys.* **113**, 9101 (2000).
- ³⁷A loss-peak position of 10^{-2} Hz corresponds to a relaxation time of ≈ 10 s, a factor of 10 smaller than the often used 100 s. The choice of relaxation time at the glass-transition temperature is always somewhat arbitrary, and will of course influence the reported glass-transition temperatures. 10^{-2} Hz has the advantage that equilibrium points close to and even below T_g , and are easily accessible, leading to a more precise determination of T_g .
- ³⁸D. J. Plazek and K. L. Ngai, *Macromolecules* **24**, 1222 (1991).
- ³⁹R. Böhmer and C. A. Angell, *Phys. Rev. B* **45**, 10091 (1992).
- ⁴⁰R. Böhmer, K. L. Ngai, C. A. Angell, and D. J. Plazek, *J. Chem. Phys.* **99**, 4201 (1993).
- ⁴¹O. E. Kalinovskaya and J. K. Vij, *J. Chem. Phys.* **112**, 3262 (2000).
- ⁴²C. Maggi, B. Jakobsen, T. Christensen, N. B. Olsen, and J. C. Dyre, *J. Phys. Chem. B* (in press).
- ⁴³N. B. Olsen, T. Christensen, and J. C. Dyre, *Phys. Rev. Lett.* **86**, 1271 (2001).
- ⁴⁴J. C. Dyre, *Europhys. Lett.* **71**, 646 (2005).
- ⁴⁵J. C. Dyre, *Phys. Rev. E* **74**, 021502 (2006).
- ⁴⁶J. C. Dyre, *Phys. Rev. E* **76**, 041508 (2007).
- ⁴⁷N. Sağlanmak, K. Niss, A. I. Nielsen, J. C. Dyre, and N. B. Olsen (unpublished).

Generalized fluctuation-dissipation relation and effective temperature in off-equilibrium colloids

Claudio Maggi,^{1,*} Roberto Di Leonardo,² Jeppe C. Dyre,¹ and Giancarlo Ruocco^{3,2}

¹*DNRF Centre “Glass and Time,” IMFUFA, Department of Sciences, Roskilde University, P.O. Box 260, DK-4000, Roskilde, Denmark*

²*Research Center “Soft,” INFN-CNR, c/o Department of Physics, “Sapienza” University of Rome, Italy*

³*Department of Physics, “Sapienza” University of Rome, Piazzale Aldo Moro 5, I-00185 Rome, Italy*

(Received 27 November 2009; revised manuscript received 22 January 2010; published 9 March 2010)

The *fluctuation-dissipation theorem* (FDT), a fundamental result of equilibrium statistical physics, can be violated when a system is taken out of equilibrium. A generalization of FDT has been theoretically proposed for out-of-equilibrium systems; the kinetic temperature entering the *fluctuation-dissipation relation* (FDR) is substituted by a time-scale-dependent effective temperature. We combine the measurements of the correlation function of the rotational dynamics of colloidal particles obtained via dynamic light scattering with those of the birefringence response to study the generalized FDR in an off-equilibrium Laponite suspension undergoing aging. (i) We find that the FDT is strongly violated in the early stage of the aging process and is gradually recovered as the aging time increases and (ii) we determine the aging-time evolution of the effective temperature, comparing our results with those of previous experiments.

DOI: 10.1103/PhysRevB.81.104201

PACS number(s): 05.40.-a, 05.45.-a, 05.70.Ln, 47.50.-d

I. INTRODUCTION

The study of the dynamics in nonequilibrium systems is an intriguing and fascinating area of modern physics. There is an obvious interest in the off-equilibrium regime as condensed matter is often found far from ideal equilibrium condition where “things keep happening on all time scales.”¹ A particular class of systems where the out-of-equilibrium status occurs naturally are the so-called glass-forming systems. These systems include, for example, disordered spin systems close to the spin-glass transition, supercooled molecular liquids, and jamming colloidal solutions. In general, the dynamics of these systems is extremely sensitive to change in external parameters so that, when they are a little cooled or densified, the time required to reestablish equilibrium can grow enormously or become infinite (the system never reaches the final equilibrium state). In these situations, an off-equilibrium regime is entered. In this, the average quantities becomes time dependent and the correlation and response functions depend on two times; in this regime the system is *aging*.

Correlation functions and response functions are the basic quantities through which one probes the dynamics of a system in many-body statistical physics. These functions are closely related in equilibrium by the *fluctuation-dissipation theorem* (FDT). The FDT (Ref. 2) establishes a relationship between the correlation function $C_{AB}(t) = \langle A(0)B(t) \rangle$ of the spontaneous equilibrium fluctuations of the dynamic variables A and B and the response function $\chi_{AB}(t) = \langle A(t) \rangle / h$, describing the change in the average value of A due to an infinitesimal external field h that is coupled to the variable B in the perturbation Hamiltonian,

$$\chi_{AB}(t) = \beta [C_{AB}(0) - C_{AB}(t)]. \quad (1)$$

Here $\beta = 1/k_B T$, where T is the kinetic temperature of the system and A and B are variables that have zero mean in the unperturbed case. In this formulation of the FDT, the field h introduces a contribution $\delta H = -hB$ to the system Hamiltonian, which is switched on instantaneously at $t=0$ and kept

constant for $t > 0$ as a Heaviside step function. In the following, we will refer to autocorrelation function ($B=A$) and drop the label AA in $C_{AA}(t)$ and $\chi_{AA}(t)$.

Out of equilibrium, the system is *nonstationary* and *time-translational invariance* is lost. The correlation and the response become two-times quantities depending also on the *aging time* t_w : $C = C(t_w, t_w + t)$, $\chi = \chi(t_w, t_w + t)$, and the FDT [Eq. (1)] is not expected to hold. The importance of extending the theorem to the nonequilibrium regime has led to the *generalized fluctuation-dissipation relation* (GFDR).³⁻⁵

The generalization of the FDT proposed by Kurchan and Cugliandolo^{6,7} in the early 1990s can be expressed as follows:

$$\chi(t_w, t_w + t) = \beta \int_{t_w+t}^{t_w} ds X(t_w, s) \partial_s C(t_w, s), \quad (2)$$

where for short times t (i.e., $t/t_w \ll 1$), this equation reduces to the FDT [Eq. (1)] and the system is said to be in a *quasi-equilibrium state*; for intermediate t ($t/t_w \approx 1$), the violation function $X(t_w, t)$ quantifies the deviation of the GFDR from the FDT; finally, when $t/t_w \gg 1$, the function X depends on t_w and s only through the function C . The violation function can also be interpreted^{8,9} in terms of an *effective temperature* $T_{eff} = T/X$. The latter has complicated behavior for intermediate t values, but in the long- t regime it assumes a value that depends only on the waiting time t_w and one can think of it as “waiting-time-dependent effective temperature.”

The GFDR in out-of-equilibrium systems has been studied theoretically and through computer simulations in spin glasses^{10,11} and in models for glassy dynamics.¹² Later, off-equilibrium molecular-dynamics simulations have given the possibility to perform the same analysis on structural glasses.¹³⁻¹⁵ Recently, the generalized relation has also been investigated in more exotic systems, such as in the simulations for a glassy protein,¹⁶ in self-assembling processes of viral capsids formation and of sticky disks crystallization,¹⁷ and in active systems composed of self-propelled particles.¹⁸

On the other hand, few experiments have studied the GFDR.^{19–24} Experiments in structural glasses are difficult because it is necessary to simultaneously measure a correlation function of a given variable and the associated response function, and all this in a systems that is *instantaneously* brought out of equilibrium. These difficulties are relaxed in the case of colloidal glasses (or gels or jams) because the associated time scales are much longer and fall easily in the experimentally accessible window.

In this paper, we report an experimental investigation of the generalized FDR in a colloidal systems composed of a water suspension of clay platelets (Laponite), which is *off-equilibrium* when it ages toward the final arrested state (gel or glass, depending on the clay concentration²⁵).

We emphasize that the FDT violation and the effective temperature in these colloidal solution are object of intense debate since the results published so far are controversial (see, for example, Refs. 21–24 and 26). Indeed, previous works on off-equilibrium Laponite suspensions have reported contradicting results in studying the GFDR. Dielectric spectroscopy combined with spontaneous polarization-noise measurements have revealed very high effective temperatures characterizing the low-frequency part of the spectra. This effective temperature was found to decrease with the aging time.

Later a new series of experiments employed microrheology to measure the effective temperature of these colloidal systems. These experiments studied the Brownian motion of probe particles added to the Laponite solution. The results of these experiments are rather contradicting. Abou *et al.*²⁶ observed an effective temperature evolving nonmonotonically as a function of the aging time. T_{eff} was found to increase from the bath temperature T , reach a maximum and return to T for long times. In contrast, the results of Ref. 22 by Jabbari-Farouji *et al.* indicated that no significant deviation from the FDT takes place over a wide frequency range. These conclusions were later confirmed by Jop *et al.*²⁴ Finally, the experiments of Greinert *et al.*²³ measured an effective temperature increasing with aging time.

We want to stress that none of these works studied directly the degrees of freedom of the colloidal Laponite disks. Indeed, the dielectric techniques are mostly sensitive to the strong polarization signal from the solvent molecules and to the effect of ionic conduction at low frequencies. In the microrheological measurements, some large trapped probe particles (typically $\sim 1 \mu\text{m}$ diameter) are used to study the off-equilibrium dynamics of the system. In contrast, our experiment is selective in measuring the dynamics of specific degrees of freedom of the Laponite disks (as will be clear in the following). Our correlation and response optical measurements (Secs. III and IV) are sensitive only to the (rotational) motion of the colloids that we are interested in. Moreover, we emphasize that, in principle, is also possible that different observables give different values of the FDT violation and therefore of the effective temperature. Our experiment is a fully time-resolved experiment.

II. OFF-EQUILIBRIUM SAMPLE

A solution, prepared by stirring the Laponite powder with water, evolves toward an arrested state on a time scale that

spans the ranges hours to months when kept at room temperature and pressure. Even low-concentration aqueous solutions of this colloid, as the one used in our experiment ($\sim 1\%$ Laponite weight fraction), show strong aging of their light-scattering correlation function.²⁷ Due to the long (with respect to the experimental time scale and to the decorrelation time) aging process of the systems, one can approximate the different measure of fluctuations and response as obtained in a sequence of steady out of equilibrium states.

The anisotropic shape of the clay disk makes it possible to study its reorientation dynamics via the response and the correlation function. Laponite particles dissolved in water have the form of flat cylinders with a diameter of 25 nm and thickness of about 1 nm. Laponite colloidal particles are good scatterers of visible light and this allow us to rapidly measure the autocorrelation function of the scattered field.

In this work we study the reorientational dynamics of the asymmetric clay platelets, looking at the orientational *correlation functions* via depolarized dynamic light scattering and at the corresponding *response function* via the electric field induced birefringence. Measuring both $C=C(t_w, t_w+t)$ and $\chi=\chi(t_w, t_w+t)$ at different waiting time during the (days long) aging process, we find that FDT is strongly violated in the early stage of the aging process and is gradually recovered as the aging time increases. Moreover, from the parametric $C-\chi$ plot (the so-called “FDT plot”), we determine the effective temperature and follow its evolution from the high values ($T_{eff}/T \approx 5$) pertaining to young systems toward the equilibrium ($T_{eff}/T=1$) attained at long waiting time. Our findings confirm the generalization of the FDT to off-equilibrium systems proposed by Cugliandolo and Kurchan 15 years ago.

III. CORRELATION FUNCTION

In a dynamic light-scattering experiment one measures the correlation function of the optical field scattered by the sample. The scattered field can be directly related to the translational and rotational motion of the anisotropic colloids suspended in the solvent.²⁸ The colloids’ rotations are related to the second-rank tensor of the optical susceptibility. Specifically, in the VH (depolarized) scattering geometry one measures the autocorrelation function of a variable that depends on the platelet’s orientation,

$$A(t) = \sum_i P_2\{\cos[\theta_i(t)]\}, \quad (3)$$

where $P_2(x)=(3x^2-1)/2$ is the second-order Legendre polynomial, θ_i is the angle formed by the symmetry axes of the i th particle with the polarization vector of the incident field, and the sum is extended over the particles contained in the scattering volume.²⁸ This results holds exactly only if the time scale of the rotational dynamics is much faster than the translational one. This assumption was confirmed by comparing the VV (polarized) and VH (depolarized) photon-correlation spectroscopy (PCS) at different waiting times and clay concentration.²⁹ The autocorrelation function of A was measured using the VH geometry via PCS. Several autocorrelation functions have been measured during the aging pro-

cess of the sample with a time resolution ($1 \mu\text{s}$) dictated by the detector (photomultiplier) response. Note that the time is set to zero at the instant at which we stop stirring the colloidal suspension.

IV. RESPONSE FUNCTION

If one applies an external field that tends to align the particles, the system due to the anisotropic platelet's polarizability becomes birefringent.^{30,31} If the aligning field is a dc (or low frequency) electric field (Kerr effect), the degree of rotation of a linearly polarized laser beam is proportional to the square of the electric field via a coefficient that is proportional to A [Eq. (3)]. Therefore, the (time-dependent) Kerr response to the switch on of an electric field is proportional to the desired response function (i.e., the response conjugated to the correlation function measured in depolarized PCS). For selected values of the waiting times, the time-resolved response functions and the corresponding correlation functions were measured during the aging process of the Laponite solution. The length of the electric pulses produced sets the dynamic window of our experiment to about 1 ms.

Note that the relaxation time τ of these functions is always much smaller than the typical waiting time ($\tau \ll t_w$). This means that the time-resolved correlation and response are well-defined quantities although the system is aging. In addition, if any FDT violation can be detected, we expect to find it on a time scale comparable to the relaxation time ($t/\tau \geq 1$) (Fig. 1).

V. RESULTS AND DISCUSSION

Examples of the measured quantities are shown in the left panel of Fig. 2. The correlation function and the response function are reported as functions of t for different aging times t_w .³² For short t , the FDT holds while we can see a clear deviation from the FDT for long t where χ/β does not overlap with $1-C$ [$C(t)$ is normalized to $C(0)=1$]. When $\chi(t_w, t_w+t)/\beta$ is parametrically plotted against $C(t_w, t_w+t)$ using t as a parameter (FDT plot), the departure from the $1-C$ line becomes evident (see the right panel of Fig. 2). The deviation from the behavior expected from the FDT reduces its importance as t_w grows, and the time where $T\chi$ and C detaches from each other moves to longer t [see also Fig. 3(a) where the interested region of the FDT plot has been expanded]. In order to quantify this deviation, we introduced a linear fit to the longer-time points in the FDT plot. The slopes (m) of these lines are a measure of the effective temperature, $1/m = T_{eff}/T$.

The t_w dependence of T_{eff} is reported in Fig. 3(b). T_{eff} decreases as t_w increases. The linear fit to the long- t region of the FDT plot also defines a characteristic value of the correlation C where the FDT breaks down, the so-called Edwards-Anderson value q ; this quantity is reported as a function of t_w in Fig. 3(c). Finally, the quantity q , defined via $C(t_0)=q$, identifies a characteristic time t_0 that mark the "starting time" of the violation. t_0 is found to move to higher values as the aging time increases [Fig. 3(d)]. It is interesting to compare t_0 to the relaxation times τ of the response and the

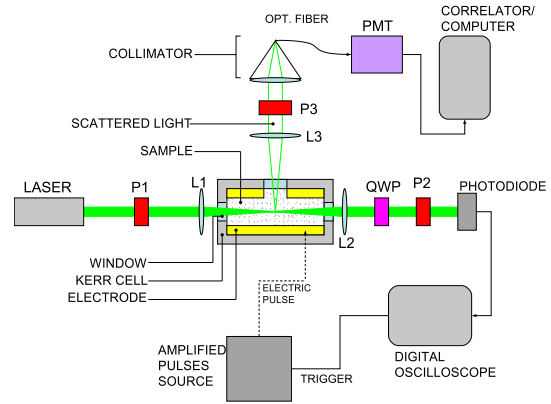


FIG. 1. (Color online) Sketch of the experimental setup (see Ref. 29 for more details). The laser's radiation ($\lambda=532 \text{ nm}$) is polarized by the polarizer P1 and focused by the lens L1 at the center of the cell containing the sample. The scattered light is collected by the lens L3 and selected by the polarizer P3 (orthogonal to P1). A photomultiplier tube (PMT) detects the scattered photons. When no electric pulse is applied to the cell, the output of the PMT is acquired by a computer equipped with a custom digital correlator, this measures and stores the correlation function. The Kerr cell containing the sample is provided by two electrodes connected to a source of amplified electric pulses. The forward-scattered light (rotated by the electrically stimulated sample) is collected by the lens L2 and passes through a quarter-wave plate and the polarizer P2 (orthogonal to P1). The transmitted light is detected by a photodiode connected to a digital oscilloscope. This is triggered by the source of electric pulse measuring and storing the Kerr-response function.

correlation. We find τ fitting the correlation and the response with stretched exponentials of the form $\exp[-(t/\tau)^\beta]$ and $(1-a \exp[-(t/\tau)^\beta])$, respectively. The response ages faster than the correlation, almost reaching the same relaxation time for the longest t_w .

It is important to emphasize that in all models investigated so far for studying the GFDR, the relaxation time grows roughly as the waiting time, $\tau \sim t_w$. The aging process that we study experimentally here does not obey this simple scaling. Indeed, the off-equilibrium (aging time-dependent) relaxation time measured is several orders of magnitude shorter than the typical values of t_w . Nevertheless, our results show that the different time scales (the one where the dynamics is at the equilibrium and the one where that is out of the equilibrium) are set by the aging time t_w . Indeed, the $\tau(t_w)$ that grows as the sample ages marks the transition from the regime where the FDT holds to another where the FDT is violated.

Finally, we mention that these results show a qualitative behavior that is similar to the one found in dielectric measurements (performed in the frequency domain). T_{eff} is equal to the bath temperature for short times (at high frequency) while it is higher than T for long times (at low frequency). In addition, the time scale for the deviation of T_{eff} from T increases as t_w increases (the frequency at which the FDT is violated shifts to lower frequencies).

Although these similarities are intriguing, we stress that some profound differences are also found. First, the relevant

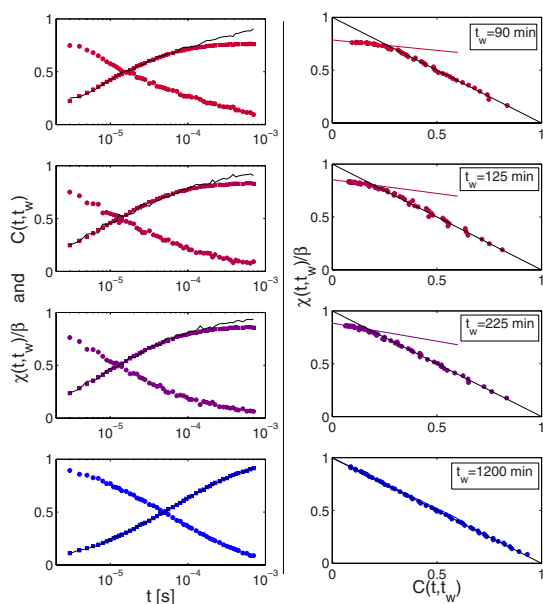


FIG. 2. (Color online) (Left) Normalized time-correlation function (\circ) and response function (\square) measured at different aging times (from top to bottom: $t_w=90, 125, 225, 1200$ min), the solid line represents $1 - C$. Note that $1 - C$ deviates from χ/β when the FDT is violated. The importance of this deviation reduces as t_w increases. (Right) Response function vs correlation function measured at different aging times (\circ). The black line represents the expectation of the FDT while the color lines represent the linear fits to the points in the off-equilibrium section of the FDT plot. It can be appreciated how these points corresponding to long-time gradually approach the FDT as the aging time increases, for the longest waiting time the fitting line overlaps almost perfectly with the prediction of the FDT (see Fig. 3 for a comparison of the FDT plots at different aging times).

time scales detected are very different. In our experiment, the deviation from the FDT is found at times between 0.1 and 1 ms (i.e., at frequencies between 10 and 1 kHz). In the studies based on the dielectric response, the violation of the FDT was detected at much lower frequencies (between 10 and 1 Hz). Second, the effective temperature found from dielectric measurements was extremely high (orders of magnitude higher than the bath temperature) while we measure a T_{eff} at most a factor 5 higher than T . Note that our measurements

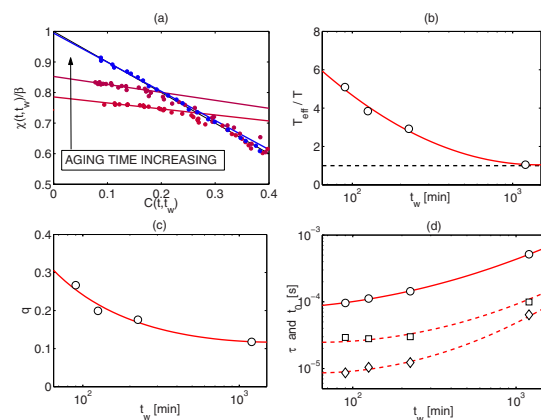


FIG. 3. (Color online) (a) The interesting region of the FDT plots for different aging times: $t_w=90, 125, 1200$ min (cf. Fig. 2, right panel). (b) The inverse slope of the long-time points of the FDT plot (see Fig. 2) as a function of the aging time (the full line is a guide for the eye). This parameter can be interpreted as an effective temperature and it is found to reduce to the bath temperature as the aging time increases. (c) Waiting-time dependence of the Edwards-Anderson parameter, the characteristic value of the correlation function at which the FDT breaks down. (d) Evolution with t_w of the characteristic time at which the FDT is violated (\circ), together with the relaxation time of the correlation function (\square) and of the response (\diamond). The characteristic time for the FDT violation t_o increases as t_w grows followed by the two relaxation times.

(as the dielectric measurement) give a different result with respect to the various findings obtained via the microrheological measurement mentioned in Sec. I.

In conclusion, by measuring the autocorrelation function of a given variable and the response function of the same quantity in an off-equilibrium (aging) colloidal suspension in the route to the arrested state, we have investigated the generalized fluctuation-dissipation relation. The GFDR applies to the present experiment in the following sense: for short-time scales the FDT is fulfilled, while for long times a clear violation is observed. The characteristic time at which the violation is seen, is always slightly above the aging-time-dependent relaxation time of the measured response and correlation function. Moreover, we observe that the deviation from the standard FDT reduces gradually as the aging time increases and the arrested phase is approached.

*cmaggi@ruc.dk

¹R. P. Feynman, *Statistical Mechanics: A Set of Lectures*, edited by Jacob Shaham (Academic, New York, 1972).

²See, for example, the textbooks: J.-P. Hansen and I. R. McDonald, *Theory of Simple Liquids*, 3rd ed. (Academic, New York, 2006), Chap. 7; L. D. Landau and E. M. Lifshitz, *Statistical Physics* (Butterworth-Heinemann, Oxford, 1980), Vol. 5;

D. Chandler, *Introduction to Modern Statistical Mechanics* (Oxford University Press, New York, 1987).

³A. Crisanti and R. Ritort, *J. Phys. A* **36**, R181 (2003).

⁴U. M. Marconi, A. Puglisi, L. Rondoni, and A. Vulpiani, *Phys. Rep.* **461**, 111 (2008).

⁵L. F. Cugliandolo, *Slow Relaxations and Nonequilibrium Dynamics in Condensed Matter* (Springer, Berlin/Heidelberg,

- 2004).
- ⁶L. F. Cugliandolo and J. Kurchan, Phys. Rev. Lett. **71**, 173 (1993).
- ⁷L. F. Cugliandolo and J. Kurchan, J. Phys. A **27**, 5749 (1994).
- ⁸L. F. Cugliandolo, J. Kurchan, and L. Peliti, Phys. Rev. E **55**, 3898 (1997).
- ⁹A. Garriga and F. Ritort, Eur. Phys. J. B **20**, 105 (2001); **21**, 115 (2001).
- ¹⁰M. Mézard, G. Parisi, and M. A. Virasoro, *Spin Glass Theory and Beyond* (World Scientific, Singapore, 1987).
- ¹¹*Spin Glasses and Random Fields*, edited by A. P. Young (World Scientific, Singapore, 2000).
- ¹²G. Diezemann, J. Chem. Phys. **123**, 204510 (2005).
- ¹³G. Parisi, Phys. Rev. Lett. **79**, 3660 (1997).
- ¹⁴J. L. Barrat and W. Kob, Europhys. Lett. **46**, 637 (1999).
- ¹⁵R. Di Leonardo, L. Angelani, G. Parisi, and G. Ruocco, Phys. Rev. Lett. **84**, 6054 (2000).
- ¹⁶K. Hayashi and M. Takano, Biophys. J. **93**, 895 (2007).
- ¹⁷R. L. Jack, M. F. Hagan, and D. Chandler, Phys. Rev. E **76**, 021119 (2007).
- ¹⁸D. Loi, S. Mossa, and L. F. Cugliandolo, Phys. Rev. E **77**, 051111 (2008).
- ¹⁹D. Herisson and M. Ocio, Phys. Rev. Lett. **88**, 257202 (2002).
- ²⁰T. S. Grigera and N. E. Israeloff, Phys. Rev. Lett. **83**, 5038 (1999).
- ²¹L. Bellon, S. Ciliberto, and C. Laroche, Europhys. Lett. **53**, 511 (2001).
- ²²S. Jabbari-Farouji, D. Mizuno, M. Atakhorrami, F. C. MacKintosh, C. F. Schmidt, E. Eiser, G. H. Wegdam, and D. Bonn, Phys. Rev. Lett. **98**, 108302 (2007).
- ²³N. Greinert, T. Wood, and P. Bartlett, Phys. Rev. Lett. **97**, 265702 (2006).
- ²⁴P. Jop, A. Petrosyan, and S. Ciliberto, Philos. Mag. **88**, 4205 (2008).
- ²⁵B. Ruzicka, L. Zulian, R. Angelini, M. Sztucki, A. Moussaid, and G. Ruocco, Phys. Rev. E **77**, 020402(R) (2008).
- ²⁶B. Abou and F. Gallet, Phys. Rev. Lett. **93**, 160603 (2004).
- ²⁷B. Ruzicka, L. Zulian, and G. Ruocco, Langmuir **22**, 1106 (2006).
- ²⁸B. Berne and R. Pecora, *Dynamic Light Scattering* (Plenum, New York, 1985).
- ²⁹See supplementary material at <http://link.aps.org/supplemental/10.1103/PhysRevB.81.104201> for preliminary tests verifying the assumption that the rotational dynamics is much faster than the translational one, and tests the linearity of the response function.
- ³⁰R. W. Boyd, *Nonlinear Optics* (Academic, San Diego, 2003).
- ³¹E. Hecht, *Optics*, 4th ed. (Addison-Wesley, Reading, 2001).
- ³²Here $t_w=0$ is set as the time in which we stop stirring the prepared Laponite suspension. Note that the first measurement of T_{eff} is taken at $t_w=90$ min but we expect T_{eff} at $t_w=0$ to be quite similar to $T_{eff}(t_w=90$ min) since the correlation and response change extremely slowly at the beginning of the aging process.

Predicting the Effective Temperature of a Glass

Nicoletta Gnan,* Claudio Maggi, Thomas B. Schröder, and Jeppe C. Dyre

DNRF Center “Glass and Time,” IMFUFA, Department of Sciences, Roskilde University, P.O. Box 260, DK-4000 Roskilde, Denmark
(Received 23 December 2009; published 24 March 2010)

We explain the findings by Di Leonardo *et al.* [Phys. Rev. Lett. **84**, 6054 (2000)] that the effective temperature of a Lennard-Jones glass depends only on the final density in the volume and/or temperature jump that produces the glass. This is not only a property of the Lennard-Jones liquid, but a feature of all strongly correlating liquids. For such liquids data from a single quench simulation provide enough information to predict the effective temperature of any glass produced by jumping from an equilibrium state. This prediction is validated by simulations of the Kob-Andersen binary Lennard-Jones liquid and shown not to apply for the nonstrongly correlating monatomic Lennard-Jones Gaussian liquid.

DOI: 10.1103/PhysRevLett.104.125902

PACS numbers: 65.20.-w

Condensed matter is frequently found in out-of-equilibrium states. For example, for systems like supercooled liquids, dense colloids, spin systems, etc., the (off-equilibrium) glass state occurs naturally after cooling or compression from a state of thermal equilibrium. An effective temperature describes the nonequilibrium properties of a glass, and the possibility of connecting the effective temperature with the observed violation of the fluctuation-dissipation theorem (FDT) [1] has opened new ways of inquiry [2–6]. In 2000, Di Leonardo *et al.* [5] studied the off-equilibrium dynamics of the single-component Lennard-Jones (LJ) liquid (with a small many-body term added to the potential to prevent crystallization). This system was subjected to sudden temperature decreases at constant density (quenches) as well as to sudden density increases at constant temperature (crunches). From the violation of the FDT, the effective temperature was determined. Surprisingly, it was observed that the effective temperature T_{eff} is independent of the particular path in the temperature-density plane crossing the glass transition line: T_{eff} depends only on the final density. In this Letter we demonstrate that the findings of Di Leonardo *et al.* hold generally for strongly correlating liquids (defined below). We further argue and demonstrate that—for this class of liquids—from a single quench simulation one can predict the effective temperature for any off-equilibrium jump.

Reference [7] documented the existence of a large class of liquids characterized by strong correlations between virial ($W \equiv pV - Nk_B T$) and potential energy (U) thermal equilibrium fluctuations at fixed volume, $\Delta W(t) \cong \gamma \Delta U(t)$. Strongly correlating liquids have a hidden (approximate) scale invariance, which implies that they inherit many—but not all—of the scaling properties of liquids interacting via inverse power-law potentials. Strongly correlating liquids include van der Waals-type liquids but not, e.g., hydrogen-bonding liquids. Strongly correlating liquids have curves in their phase diagrams—“isomorphs”—along which several static and dynamic prop-

erties are invariant [8]. These invariants derive from the fact that two microscopic configurations of two isomorphic state points, which scale into one another, to a good approximation have identical canonical probabilities. If the density is denoted by ρ , an isomorph is given by $\rho^\gamma/T = \text{const}$. The exponent γ —which may be slightly state-point dependent—can be calculated from equilibrium fluctuations at one state point or from a single quench simulation utilizing the relation between the relaxing averages, $\langle W(t) \rangle \cong \gamma \langle U(t) \rangle + W_0$.

Because the canonical probabilities of scaled configurations belonging to the same isomorph are identical, a jump between two isomorphic state points takes the system instantaneously to equilibrium [property (i)][8]. Moreover, jumps from isomorphic state points to the same final state point show identical aging behavior [property (ii)] [8]. In view of these properties the results of Di Leonardo *et al.* [5] may be understood as follows. A crunch from density ρ_1 to density ρ_2 can be ideally decomposed into two parts (Fig. 1): First, the system jumps instantaneously from its initial state to the corresponding isomorphic state at the final density (i.e., the state which has the same ρ^γ/T as the initial state); see Fig. 1. This is an equilibrium state [8]. Thereafter the system at constant density begins to approach the equilibrium state defined by the temperature. If the crunch is made to a state with very high density, the thermalization takes an extremely long time and the effective temperature may be determined from the FDT violation as detailed below. In this way any crunch corresponds to a quench to the final density with the same relaxation pattern. In particular, these two transformations should have identical FDT violation factors and identical effective temperatures.

These arguments should apply to any strongly correlating liquid, not just the single-component LJ system. To confirm this we simulated the Kob-Andersen binary Lennard-Jones (KABLJ) liquid [9,10]. Following Di Leonardo *et al.* [5] we subjected the KABLJ liquid to a number of instantaneous quenches and crunches and

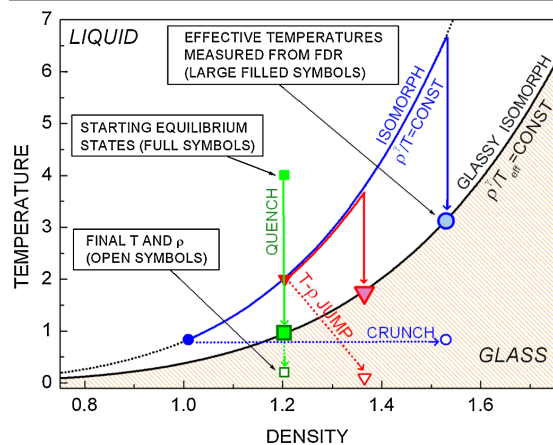


FIG. 1 (color online). Patterns followed by the KABLJ liquid in different off-equilibrium density and/or temperature jumps. Consider, for example, the case of a crunch (horizontal dotted line), where the system is densified at constant temperature. This transformation is equivalent to a quench (right-most vertical line) from an isomorph state point having the final density of the crunch. Thus the T_{eff} (large filled circle) is identical for these transformations. In all processes represented here the liquid undergoes a glass transition characterized by an effective temperature that can be measured from the fluctuation-dissipation relation (FDR) Eq. (1). T_{eff} versus (final) density constitutes an isomorph, as discussed later in the text.

calculated the effective temperatures from the fluctuation-dissipation relation (FDR). Recall that for off-equilibrium systems the FDR in $k_B = 1$ units is [11–15]

$$T \partial_{t'} \chi(t, t') = -X(t, t') \partial_{t'} C(t, t'). \quad (1)$$

Here $C = \langle A(t)B(t') \rangle$ is the correlation function of the variables A and B in the unperturbed situation, the perturbing contribution to the Hamiltonian is $\delta H = -\epsilon B$, $\chi(t, t') = \langle A(t) \rangle / \epsilon |_{\epsilon \rightarrow 0}$ is the response of A to the perturbation applied at time $t' < t$, and X is the FDT violation factor. This is unity at short times $(t - t')/t' \ll 1$, while $X < 1$ in the long-time limit $(t - t')/t' \gg 1$. We chose as dynamic variables $A_{\mathbf{k}}(t) = N^{-1} \sum_j \eta_j \cos[\mathbf{k} \cdot \mathbf{r}_j(t)]$ and $B_{\mathbf{k}}(t) = 2NA_{\mathbf{k}}(t)$, where the sum is extended to all N particles of the system and $\eta_j = \pm 1$ is a random variable with zero mean. With this choice the correlation function $C(t, t')$ is the self-intermediate scattering function.

For quenches to low enough temperatures, at long times an effective temperature of the slow degrees of freedom is associated with the FDT violation factor: $T_{\text{eff}} = T/X$ [12–16]. The effective temperature reflects the slow structural rearrangements in the sense that the aging system behaves as if it were thermalized at T_{eff} [16]. We obtained X by calculating the correlation function and the response function in the nonequilibrium regime by means of $X = X(t) = -T \partial_{t'} \chi(t, t') / \partial C(t, t')$, which applies at long times (note

that the correct X is found by taking this derivative at fixed t , not at fixed t' [17]).

Recently Berthier introduced a new method for calculating the response without applying an external field for an off-equilibrium Monte Carlo simulation of the KABLJ [17]. Using his procedure Fig. 2 shows the FD plots for the KABLJ liquid during a number of temperature-density jumps. In Fig. 2 we test the construction of equivalent crunches and quenches argued above: a crunch and a quench from initially isomorphous states (i.e., with the same ρ^2/T) to the same final T and ρ (red circles and red squares). Clearly the crunch overlaps well with the quench; in fact, they follow the same aging pattern. The exponent γ was estimated by a linear fit of the parameter plot $\langle W(t) \rangle$ vs $\langle U(t) \rangle$ when the system is relaxing after a temperature jump from $T = 2.55$ to $T = 0.3192$ at fixed $\rho = 1.264$. The resulting value is $\gamma = 5.01$ (for details, refer to Ref. [10]). Figure 3 shows the linear relation that connects $\langle W(t) \rangle$ and $\langle U(t) \rangle$ during two “isomorphous” quenches.

Identical responses and correlations do not only appear when a strongly correlating liquid is taken from two isomorphous states to the same state point. Supplementing properties (i) and (ii), strongly correlating liquids have a

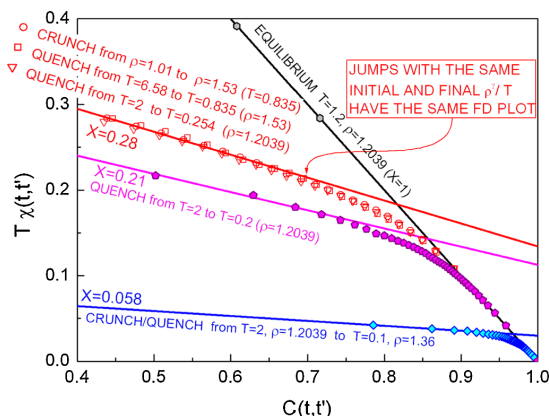


FIG. 2 (color online). Response versus correlation function for several density or temperature jumps for the KABLJ liquid. All FD plots have fixed $t = 10^4$ (Monte Carlo steps) and t' varying from 10^3 to 10^4 . All functions plotted here have the same reduced \mathbf{k} -vector (referring to the final density) and the same reduced microscopic time. In the crunch (○) we set $|\mathbf{k}| = 7.81$ corresponding to the reduced \mathbf{k} -vector $|\bar{\mathbf{k}}| = 6.78$ (see Ref. [10] for details). The crunch (○) overlaps very well with the quench (□) that takes the system from an initial state isomorphous to the one of the crunch to the same final state. Note also the good superposition of the additional quench (▽) that takes the system from a state isomorphous to the initial state of (○) to a state isomorphous to the final one of (○). The full lines have the slopes predicted from the density-scaling relation Eq. (2) for T_{eff} .

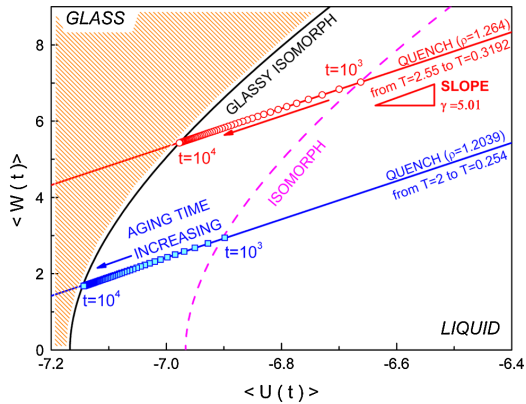


FIG. 3 (color online). Average virial versus potential energy per particle during aging in two quenches for the KABLJ liquid. These quenches were performed between states with same initial and final ρ^γ/T . At each time the off-equilibrium states are connected by an isomorph (e.g., the dashed line). In these two jumps the FDT violation factor X should be identical. The slope of the $\langle W(t) \rangle$ vs $\langle U(t) \rangle$ plot is γ . The analytical equation used for drawing the isomorphs in the W - U plot here is reported in Ref. [20].

third interesting aging property (iii): For two jumps $(T_1, \rho_1) \rightarrow (T_2, \rho_2)$ and $(T_3, \rho_3) \rightarrow (T_4, \rho_4)$ between mutually isomorphic initial and final states (i.e., $\rho_1^\gamma/T_1 = \rho_3^\gamma/T_3$ and $\rho_2^\gamma/T_2 = \rho_4^\gamma/T_4$), the systems follow the same path in configuration space in reduced units [10] because the dynamical equations governing the evolution of the particle trajectories are identical in reduced units. Accordingly, the responses and correlations of two such jumps must be identical in reduced units. In Fig. 2 we show the reduced unit C and χ of a quench between initial and final states that are isomorphic, respectively, to the initial and final states of the crunch described above (red triangles). The overlap between the functions is good. Figure 3 shows the variables $\langle W(t) \rangle$ vs $\langle U(t) \rangle$ in two such isomorphic jumps; they are connected by an isomorph at each time during the relaxation.

A further consequence of property (iii) is the following. Because the reduced-unit evolution is the same for the system in the two jumps, their FDR violation factors must also be identical, $X_2 = X_4$. Combining this equation with $\rho_2^\gamma/T_2 = \rho_4^\gamma/T_4$ and expressing X via the effective temperature, we find $\rho_2^\gamma/T_{\text{eff},2} = \rho_4^\gamma/T_{\text{eff},4}$, i.e.,

$$\rho^\gamma/T_{\text{eff}} = \text{const.} \quad (2)$$

This equation identifies the glass transition curve in the (T, ρ) plane defined in terms of the FDR effective temperature with an isomorph. This is consistent with the findings of Ref. [5] and the standard way of defining the glass transition, because the standard glass line in the (T, ρ) plane is located where the equilibrium relaxation

time reaches a certain (high) value of order the inverse cooling rate. For strongly correlating liquids an isomorph is also an ‘‘isochronal’’ curve along which the (reduced) relaxation time is constant [8]. Figure 2 shows the slopes predicted by Eq. (2) (lines); clearly the prediction is fulfilled.

It is well known (see, for example, Refs. [4,17]) that the effective temperature is independent of the initial and final temperature if the initial temperature is high (the system is in a warm liquid state) and if the quenching temperature is low enough (i.e., in the regime where $X = T/T_{\text{eff}}$ with constant T_{eff}). Consequently, Eq. (2) predicts the effective temperatures for all possible jumps ending at density ρ . The exponent γ and the constant may both be calculated from the results of one single aging simulation. In Fig. 4 we compare T_{eff} identified from several crunches and quenches (not only involving isomorphic initial and final state points) with the prediction of Eq. (2). The agreement is very good.

The above discussed simple aging properties are only expected to apply for liquids with isomorphs, i.e., strongly correlating liquids. To validate this we simulated the non-equilibrium dynamics of the monatomic Lennard-Jones Gaussian (MLJG) model [18]. The pair potential of the MLJG has an additional Gaussian attractive well compared to the LJ liquid (see the inset of Fig. 5); details about the model’s potential and its glassy behavior can be found in Ref. [18]. The MLJG liquid has WU fluctuations which correlate less than 2% at the state points studied here. As is clear from Fig. 5, two jumps to the same final density lead to quite different effective temperatures. Thus, this system provides a counterexample to the observation by

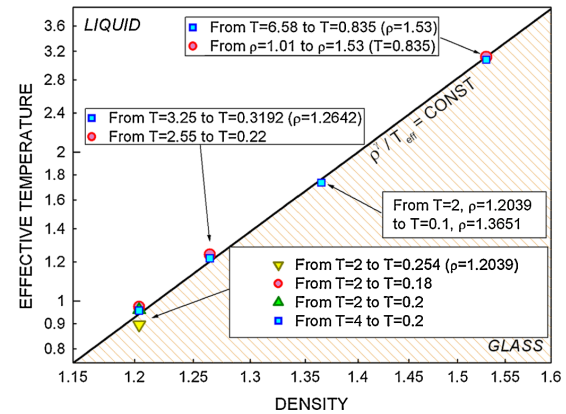


FIG. 4 (color online). Effective temperature as a function of density in several crunch and/or quenches (in double log scale) for the KABLJ liquid. The effective temperature is computed from the violation factor: $T/T_{\text{eff}} = X = -T\partial\chi(t, t')/\partial C(t, t')|_t$. The scaling exponent γ is computed from potential energy-virial relaxation (see Fig. 3) as described in the text. The full line is the prediction of the density scaling equation (2) for T_{eff} .

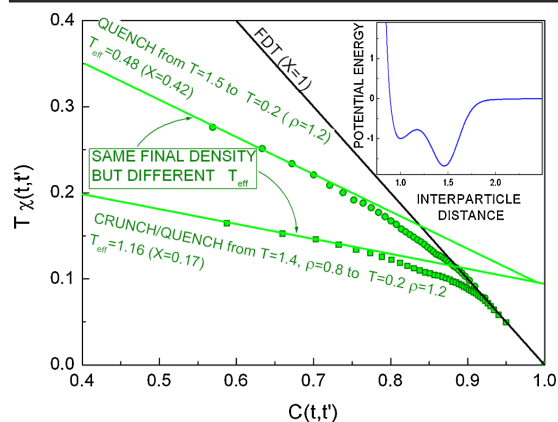


FIG. 5 (color online). FD plot for two jumps of the MLJG liquid ending at same final density and temperature. The potential defining this model is shown in the inset. In this case the two effective temperatures are very different.

Di Leonardo *et al.* [5] that the effective temperature depends only on the final density.

We also investigated the relation between the inherent state energies in aging and at equilibrium for the KABLJ and the MLJG liquids (see Ref. [10] for more details). Only for the strongly correlating liquid KABLJ can one interpret T_{eff} as an indicator of which part of the energy landscape is visited during aging, confirming a suggestion by Sciortino and Tartaglia in [19].

In conclusion, the existence of isomorphs for strongly correlating liquids explains the previously reported result [5] for the LJ liquid that the effective temperature depends only on the final density of any jump (when temperature and density are the externally controlled variables). We presented simulations of the aging dynamics of another strongly correlating liquid, the KABLJ liquid, as well as simulations of aging of a liquid without strong virial or potential energy correlations (the MLJG liquid). For strongly correlating liquids it is always possible to produce equivalent density or temperature transformations connected by the density-scaling relation. Moreover, for this class of liquids the effective temperature satisfies the density-scaling equation (2). Since the exponent γ and the constant of Eq. (2) may both be identified from a single quench simulation, the implication is that for a strongly

correlating liquid the effective temperature of an arbitrary glass may be calculated from the results of a single jump simulation.

The center for viscous liquid dynamics *Glass and Time* is sponsored by the Danish National Research Foundation (DNRF).

*ngnan@ruc.dk

- [1] J.-P. Hansen and I.R. Mc-Donald, *Theory of Simple Liquids* (Academic, New York, 2006).
- [2] G. Parisi, Phys. Rev. Lett. **79**, 3660 (1997).
- [3] M. Sellitto, Eur. Phys. J. B **4**, 135 (1998).
- [4] W. Kob and J.L. Barrat, Europhys. Lett. **46**, 637 (1999).
- [5] R. Di Leonardo, L. Angelani, G. Parisi, and G. Ruocco, Phys. Rev. Lett. **84**, 6054 (2000).
- [6] R.L. Jack, M.F. Hagan, and D. Chandler, Phys. Rev. E **76**, 021119 (2007).
- [7] U.R. Pedersen *et al.*, Phys. Rev. Lett. **100**, 015701 (2008); Phys. Rev. E **77**, 011201 (2008); N.P. Bailey *et al.*, J. Chem. Phys. **129**, 184507 (2008); **129**, 184508 (2008); T.B. Schröder *et al.*, Phys. Rev. E **80**, 041502 (2009).
- [8] N. Gnan, T.B. Schröder, U.R. Pedersen, N.P. Bailey, and J.C. Dyre, J. Chem. Phys. **131**, 234504 (2009).
- [9] W. Kob and H.C. Andersen, Phys. Rev. Lett. **73**, 1376 (1994); L. Berthier and W. Kob, J. Phys. Condens. Matter **19**, 205130 (2007).
- [10] See supplementary material at <http://link.aps.org/supplemental/10.1103/PhysRevLett.104.125902> for simulation details, definitions of the reduced units, and the study of the off-equilibrium landscape in the two systems studied.
- [11] U.M. Marconi, A. Puglisi, L. Rondoni, and A. Vulpiani, Phys. Rep. **461**, 111 (2008).
- [12] J. Kurchan, Nature (London) **433**, 222 (2005).
- [13] A. Crisanti and R. Ritort, J. Phys. A **36**, R181 (2003).
- [14] L.F. Cugliandolo, *Slow Relaxations and Nonequilibrium Dynamics in Condensed Matter*, Dynamics of Glassy Systems Course 7 (Springer, Berlin, 2004).
- [15] C. Chamon and L.F. Cugliandolo, J. Stat. Mech. (2007) P07022.
- [16] L. Leuzzi, J. Non-Cryst. Solids **355**, 686 (2009).
- [17] L. Berthier, Phys. Rev. Lett. **98**, 220601 (2007).
- [18] V. Van Hoang and T. Odagaki, Physica (Amsterdam) **403B**, 1803 (2008).
- [19] F. Sciortino and P. Tartaglia, Phys. Rev. Lett. **86**, 107 (2001).
- [20] N. Gnan *et al.*, arXiv:0905.3497v1.

Unique Dynamic Correlation Length in Supercooled Liquids

Claudio Maggi,^a Bo Jakobsen,^b and Jeppe C. Dyre^c
*DNRF Centre “Glass and Time”, IMFUFA, Department of Sciences,
 Roskilde University, Postbox 260, DK-4000 Roskilde, Denmark*
 (Dated: March 1, 2010)

We present a direct comparison of the number of dynamically correlated molecules in the shear-mechanical and dielectric relaxations of the following seven supercooled organic liquids: triphenylethylene, tetramethyl-tetraphenyl-trisiloxane, polyphenyl ether, perhydrosqualene, polybutadiene, decahydroisoquinoline, and tripropylene glycol. For each liquid we observe that the numbers of dynamically correlated molecules in the shear and in the dielectric relaxation are proportional. We show that this proportionality can be explained by the constancy of the decoupling index of the shear and dielectric relaxation times in conjunction with time-temperature superposition. Moreover the value of this proportionality constant is related to the difference in stretching of the shear and dielectric response functions. The most significant deviations from unity of this constant are found in a liquid with strong hydrogen bonds and in a polymer.

INTRODUCTION

The dynamical processes taking place in a supercooled liquid are complex. This is due to the fact that the motion of the molecules of a liquid close to the glass transition is intrinsically collective. When the liquid enters this ultra-viscous regime [1], the rearrangement of a particle involves the motion of many of its neighbors. The idea that the dynamics becomes more and more cooperative has led to searches for a growing length scale as the dynamics slow-down upon cooling. So far no standard static correlation has revealed a detectable growing correlation length arising in the supercooled phase. On the other hand, *dynamic correlations* [2] may account for the evolution of the correlation length scales involved in the glass transition. Recently Berthier, Biroli and co-workers invented a simple and powerful method to estimate the four-point susceptibility, χ_4 [3–5]. The central idea is to estimate the four-point function via a more accessible three-point function. The function χ_4 , which cannot be easily measured directly, can be approximated from the temperature evolution of any measured dynamic variable.

We can measure the frequency-dependent dielectric susceptibility, $\epsilon(\omega)$, and shear modulus, $G(\omega)$ using the same cryostat and covering overlapping temperature-frequency ranges [6–8]. The *piezo-shear-gauge* (PSG) technique [8] allows us to measure the dynamic shear modulus of a supercooled liquid close to its glass transition (where G typically assumes values between 0.1 MPa and 10 GPa) in a wide frequency range ($10^{-3} - 10^4$ Hz). In this work we extract and compare the number of dynamically correlated molecules in the structural (alpha) relaxation from two different dynamic variables: the dielectric susceptibility and the shear modulus.

	T_g [K]	m	$I(T)$	(clear) β -relaxation
TPE	249	73	3.4 – 3.5	no
DC704	211	83	3.7 – 3.9	no
PPE	245	80	3.9-3.9	no
Squalane	167	64	0.4 – 2.9	yes
PB20	176	79	3.7	yes
DHIQ	179	154	3.8 – 8.3	yes
TPG	190	65	1.4 – 3.0	yes

TABLE I: Properties of the seven liquids studied (from Refs. [9–12, 18]). T_g is the glass transition temperature, m is the Angell fragility, I is the temperature index (the values of I are reported for the highest and lowest temperature studied). The last column indicates if the liquid has or not a clear secondary β -relaxation. All the data here refer to dielectric measurements.

We analyze below dielectric and shear-dynamic data collected and published by our group [9, 11], available on-line [12]. This study focuses on seven liquids: triphenylethylene (“TPE”), tetramethyl-tetraphenyl-trisiloxane (“DC704”), polyphenyl ether (“PPE”), perhydrosqualene (“squalane”), polybutadiene (“PB20”), decahydroisoquinoline (“DHIQ”), and tripropylene glycol (“TPG”). DC704, TPE, PPE, squalane and DHIQ are molecular van der Waals bonded liquids, TPG has hydrogen bonds, and PB20 is a polymer with molecular weight of 5000 g/mol. All liquids were used as acquired. The PPE used is the Santovac®5 vacuum pump fluid, and DC704 is the Dow Corning®704 diffusion pump fluid. All the other liquids were acquired from Sigma-Aldrich. All the experimental details about these measurements can be found in Refs. [6–9].

Some properties of the liquids [9–12, 18] are reported in Table I. Here the relaxation time τ is defined by the inverse loss peak frequency and the glass transition temperature T_g is defined as the temperature where the loss-peak is located at $2\pi 10^{-3}$ rad/s. The temperature dependence of the relaxation time around T_g is expressed

^aElectronic address: cmaggi@ruc.dk

^bElectronic address: boj@ruc.dk

^cElectronic address: dyre@ruc.dk

in terms of the Angell fragility index [13–16]

$$m = \left. \frac{d \log_{10} \tau}{d(T_g/T)} \right|_{T=T_g} \quad (1)$$

The temperature dependence of activation energy is quantified via the temperature index [17, 18]

$$I(T) = \frac{d \ln \Delta E(T)}{d \ln T} \quad (2)$$

where $\Delta E(T)$ is the activation energy defined by $\tau = \tau_0 \exp(\Delta E(T)/k_B T)$. Table I reports the variation of $I(T)$ in the temperature interval studied [18]. Table I also reports presence of a clear Johari-Goldstain β -relaxation [19] in the dielectric spectrum of the liquid.

COMPARISON OF SHEAR-MECHANICAL AND DIELECTRIC RESPONSES

The studies carried out by our group [9, 11, 20, 21] focused on the temperature-dependence of the shear-mechanical and dielectric α relaxation times (indicated with τ_G and τ_ϵ , respectively). Furthermore, comparison of the shape of these two relaxation functions was presented. The main conclusions of these studies may be summarized as follows:

(i) The relaxation time of the shear modulus is generally different from that of the dielectric susceptibility at the same temperature T . The shear-mechanical relaxation is always slightly faster than the dielectric, $\tau_\epsilon(T) \geq \tau_G(T)$. Nevertheless, the shear and dielectric characteristic alpha relaxation times evolve in a rather similar way in the liquids studied when T is changed. This was discussed in detail in [9] where the *decoupling index* $\tau_\epsilon(T)/\tau_G(T)$ was reported and its insignificant temperature dependence was established ($\tau_\epsilon(T)/\tau_G(T) \simeq \text{const}$). This picture is also confirmed by other studies found in the literature [22–26].

(ii) The shear response function and the dielectric response function generally have different shapes. In liquids that do not show any detectable Johari-Goldstain β -relaxation [19] the shape of each frequency-dependent response is found to be almost temperature independent. This feature is referred as *time-temperature superposition* (TTS), and it is found to hold to a very good degree in the temperature-frequency range explored [9, 20] both for the shear and the dielectric relaxation [31].

(iii) For those liquids that have a clear beta-relaxation the alpha relaxations in the shear and dielectric spectrum seem to approach a temperature independent shape as

the temperature is lowered. This has been presented in detail in Refs. [9, 20, 21, 31] suggesting that for the alpha process alone TTS applies, while in the full spectrum TTS is lost because of the presence of the beta process.

In the following we show that (i) and (ii) imply that the shear and the dielectric numbers of dynamically correlated molecules (for the liquids without clear beta relaxation) are proportional in the temperature range studied. Moreover, the same conclusion applies if we *assume* TTS (as suggested by (iii) and also done in [29]) to hold for the alpha process in those liquids that have a secondary relaxation. To understand this link it we first briefly recall how to approximate the four-point susceptibility.

ESTIMATION OF THE NUMBER OF DYNAMICALLY CORRELATED MOLECULES

The four-point correlator can be interpreted as the variance of the dynamics around its average value. One can estimate this function from the following equation (Refs. [3–5, 27–29])

$$\chi_4(\omega, T) \simeq \frac{k_B}{c_P} \left(\frac{\partial \tilde{\chi}'(\omega, T)}{\partial \ln T} \right)^2. \quad (3)$$

In this equation $\tilde{\chi}'$ is the normalized real part of the response function and c_P is the configurational heat capacity per molecule at constant pressure. The right-hand side of Eq. (3) is an approximation of χ_4 , it actually represents a lower bound for this function. Nevertheless, this method is found to give values of the four-point susceptibility in good agreement with the actual values of χ_4 when these can be evaluated directly (for example in computer simulations) [4, 5]. The characteristic value of the four-point function (i.e., the typical number of correlated molecules in the relaxation, N_{corr}) is associated with the maximum of χ_4 ,

$$N_{\text{corr}}(T) = \max_{\omega} [\chi_4(\omega, T)]. \quad (4)$$

The maximum of this function is consistently found to close to a frequency close to the loss-peak frequency of the alpha dynamics.

The normalized response function $\tilde{\chi}'$ appearing in Eq. (3) is computed by subtracting a baseline parameter to the measured response (for example the dielectric susceptibility), subsequently dividing by the amplitude of the function [27]

$$\tilde{\chi}(\omega, T) = \frac{\chi(\omega, T) - \chi_{\infty}}{\Delta \chi}. \quad (5)$$

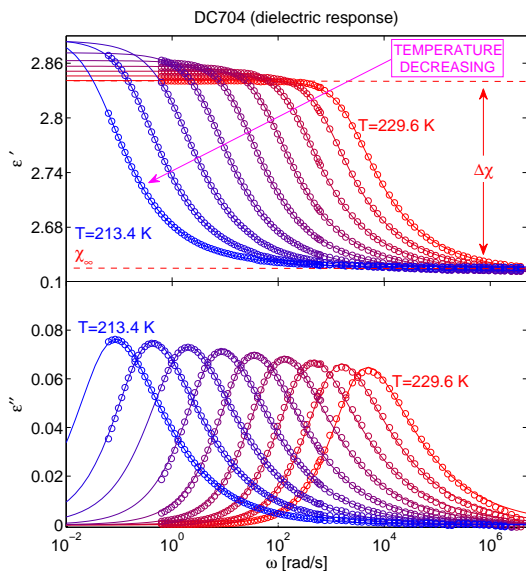


FIG. 1: Real and imaginary part (top and bottom respectively) of the dielectric response of DC704 measured at $T = 229.6, 227.6, 225.5, 223.5, 221.5, 219.5, 217.5, 215.4, 213.4$ K (open circles). The full lines are fits with the HN function Eq. (6). The amplitude $\Delta\chi$ and the baseline χ_∞ of the fitting function are shown graphically for the curve at $T = 229.6$ K.

In this work we fit all response functions with the Havriliak-Negami (HN) function [30]

$$\chi(\omega, T) = \chi_\infty + \frac{\Delta\chi}{[1 + (i\tau\omega)^\alpha]^\beta}. \quad (6)$$

The Appendix details how we introduce the assumption of TTS in the analysis of the spectra of the liquids presenting a beta process (this is done by fixing the α and β parameters of the function (6)). An example of the fitting is reported in Fig. 1 for the dielectric responses of DC704. The normalized functions are shown in the upper parts of Fig. 2.A (dielectric) and in Fig. 2.B (shear). The function χ_4 obtained from Eq. 3 is shown in Fig. 2 for the dielectric responses and the shear-mechanical response of DC704. Note that the maximum of these functions at the same temperature is located at different frequencies in the shear and the dielectric case (as is also the case for the loss peaks of the responses). Moreover, the shape of χ_4 is slightly different in the shear and in the dielectric case as discussed in detail below.

Once we have determined the maximum of χ_4 , the quantity N_{corr} can be obtained via Eq. (4). In this way two independent estimates of the number of dynamically

correlated molecules can be obtained: the number of correlated molecules in the shear relaxation N_G and in the dielectric relaxation N_ϵ . Note that for comparing these two numbers knowledge of c_P is unnecessary, being only a constant multiplicative factor in Eq. (4).

From Fig. 3 we can appreciate the growth of the shear and dielectric N_{corr} upon cooling. The minimum increase of N_ϵ is of a factor ~ 1.6 in TPE and its maximum increase is of a factor ~ 5.7 found in TPG. The relaxation times of the responses studied grow at least four orders of magnitude in all liquids.

Let us now see the form assumed by the equations (3) and (4) if TTS applies. To do this let us consider the very general expression for a (normalized) response function obeying TTS:

$$\tilde{\chi}(\omega, T) = \phi(\omega\tau(T)). \quad (7)$$

This is the case of Eq. 6 if the parameters α and β are kept constant. Differentiating the real part of Eq. (7) with respect to $\ln T$ (as in Eq. (3)) we obtain

$$\frac{\partial \phi'(\omega\tau(T))}{\partial \ln T} = \omega \frac{d\phi'(x)}{dx} \frac{\partial \tau(T)}{\partial \ln T}. \quad (8)$$

where the prime indicates the real part and we have introduced $x \equiv \omega\tau(T)$. The maximum of the function (8) can be estimated setting $\omega = \tau^{-1}$ (a minor correction term is present in the case of very large stretching [29]):

$$N_{\text{corr}} \propto \left[\max_\omega \left(\frac{\partial \phi'(\omega\tau(T))}{\ln T} \right) \right]^2 = f^2(1) \left(\frac{\partial \ln \tau(T)}{\partial \ln T} \right)^2 \quad (9)$$

where $f(x) = (d\phi'(x)/dx)$. From Eq. (9) it is clear that the growth of N is determined uniquely by the growth of the relaxation time upon cooling if TTS strictly holds. If (as stated in (i)) the decoupling index has a negligible temperature-dependence ($\tau_\epsilon(T)/\tau_G(T) \simeq \text{const}$) then

$$\left(\frac{\partial \ln \tau_\epsilon(T)}{\partial \ln T} \right)^2 \simeq \left(\frac{\partial \ln \tau_G(T)}{\partial \ln T} \right)^2. \quad (10)$$

This means that the decoupling index of the characteristic number of correlated molecules in the shear and dielectric relaxation is also constant as T is lowered:

$$\frac{N_\epsilon(T)}{N_G(T)} \simeq \text{const} \quad (11)$$

where the constant is determined by the stretching of the shear and dielectric relaxations. In other words, the growth of N_G and N_ϵ is identical upon cooling, while their difference in absolute values is set by the different (temperature independent) shape of the two response functions.

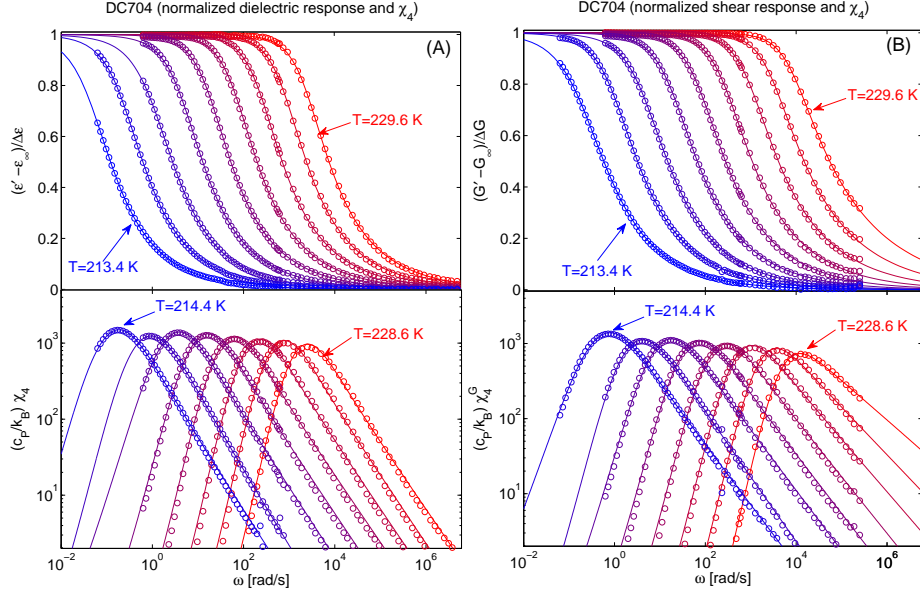


FIG. 2: **(A-Top)** Normalized real part of the dielectric response for DC704 at $T = 229.6, 227.6, 225.5, 223.5, 221.5, 219.5, 217.5, 215.4$ and 213.4 K. The full lines are the corresponding (normalized) fits to the HN functions. **(A-Bottom)** $(c_P/k_B)\chi_4 = (\partial\tilde{\chi}'(\omega, T)/\partial \ln T)^2$ for the dielectric (left) and shear (right) relaxation at $T = 228.6, 226.6, 224.5, 222.5, 220.5, 218.5, 216.4$ and 214.4 K. The full line are the corresponding $(c_P/k_B)\chi_4$ computed from the fitting HN functions. **(B)** Same as A for the shear-mechanical response

COMPARISON OF THE SHEAR AND DIELECTRIC NUMBERS OF DYNAMICALLY CORRELATED MOLECULES

The results expected from the constant decoupling index and TTS can be readily checked. Plotting $N_\epsilon(T)$ versus $N_G(T)$ as in Fig. 4 we check that these quantities approximatively differ only by a multiplicative factor in the temperature range studied for all liquids considered in this work. As seen in the inset of Fig. 4 all the data collapse onto the line $N_\epsilon \propto N_G$ if we multiply N_ϵ by the value $\langle N_G/N_\epsilon \rangle$ where the average is taken over the temperature range studied.

We test Eq. (11) directly in Fig. 5. As seen from this figure the decoupling index $N_\epsilon(T)/N_G(T)$ of the number of correlated molecules in the dielectric and shear relaxation is very weakly temperature dependent and it does not show any clear trend of a systematic increase or decrease. Note that, while $N_\epsilon(T)/N_G(T)$ stays constant, N_ϵ and N_G both grow significantly upon cooling for all liquids (see Fig. 3).

In Fig. 6 we test further the constancy of the decoupling index. Fig. 6 demonstrate the validity of Eq. (10). The equality $(\partial \ln \tau_\epsilon / \partial \ln T)^2 = (\partial \ln \tau_G / \partial \ln T)^2$

seems to hold to a good approximation as expected from $\tau_\epsilon(T)/\tau_G(T) \simeq \text{const}$.

We stress once again that the multiplicative factor between the shear and dielectric N_{corr} (i.e., the constant appearing in Eq. (11)) is determined by the shape of the shear and dielectric response. Indeed, the function $f(1)$ defined in Eq. (9) depends on the form of the relaxation functions that set $N_\epsilon/N_G \simeq [f_\epsilon(1)/f_G(1)]^2$. When the response is modelled by the HN function (6), the value of $f(1)$ depends only on the parameters α and β :

$$f(1) = -\alpha\beta \text{Re}[i^\alpha/(1+i^\alpha)^{1+\beta}]. \quad (12)$$

From Eq. (12) it is easy to understand that if the dielectric response function has approximatively the same shape as the shear-mechanical one, the constant of Eq. (11) is close to unity. This is the case of DC704 as can be seen from Figs. 5 and 7.A for which Eq. (12) gives consistently $N_\epsilon/N_G \simeq [f_\epsilon(1)/f_G(1)]^2 \simeq 1.35$ using the values α and β obtained from the fitting.

If the dynamic shear modulus is instead much broader than the dielectric response (as shown in Fig. 7.B for TPG), N_ϵ/N_G is significantly larger than unity (as seen

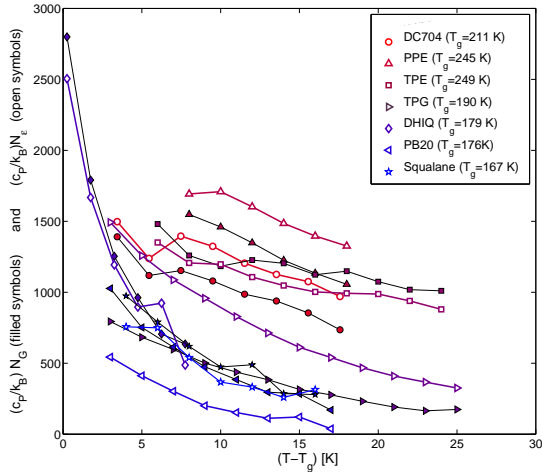


FIG. 3: The quantity $(c_p/k_B)N_{\text{corr}}$ for shear (filled symbols) and dielectric (open symbols) as a function of $(T - T_g)$ for the liquids studied (see legend). T_g is the glass transition temperature for the dielectric relaxation from Ref. [9] (see legend and Table I).

in Fig. 5). Also for this liquid we can check that the value of this ratio is consistent with the equations given above obtaining $N_e/N_G \simeq 1.97$.

Finally we want to stress that the stretching of the relaxation function does not only significantly affect N_{corr} , but also the full shape of the function $\chi_4(\omega)$ as calculated from Eq. (3). This is illustrated in Fig. 8. If the stretching of the shear and dielectric response functions is similar as in DC704 (see Fig. 7.A), N_e/N_G is close to one, but also the shapes of $\chi_4^G(\omega)$ and $\chi_4^e(\omega)$ are quite similar as seen in Fig. 8.A.

If the two response functions have significantly different stretching, the corresponding four-point susceptibilities will have quite different shapes. This is the case of TPG whose dielectric response function is more “Debye-like” than the shear-mechanical one (Fig. 7.B). In this case the functions χ_4^G is clearly broader than χ_4^e as seen in Fig. 8.B.

CONCLUSIONS

We have compared the shear-mechanical and dielectric characteristic number of dynamically correlated molecules for seven supercooled liquids close to the glass transition. The number of dynamically correlated molecules in the shear-mechanical relaxation is generally different from that of the dielectric relaxation. Neverthe-

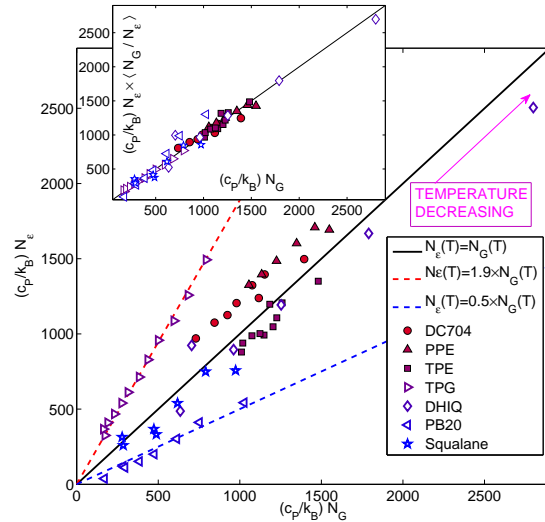


FIG. 4: Characteristic number of correlated molecules in the dielectric relaxation plotted versus the characteristic number of correlated molecules in the shear mechanical relaxation at the same temperatures for the seven glass-forming liquids (see legend). The full line indicates $N_e = N_G$ while the dashed lines represents $N_e = \lambda N_G$ (with $\lambda = 1.9$ and 0.5 respectively for the upper and the lower line). In the inset we show the data collapse on the line $N_e \propto N_G$ obtained when we multiply N_e by the value $\langle N_G/N_e \rangle$ where the average is taken over the temperature range studied.

less, these quantities are approximately proportional in the explored temperature range. For five of the seven liquids studied the ratio between the shear and dielectric characteristic number of correlated molecules is close to the unity. The most significant deviations from this unitary ratio are found in a liquid with strong hydrogen bonds and in a polymer. Finally, we showed that the difference in these absolute numbers arises from the different stretching of the dielectric and shear response functions.

Center for viscous liquid dynamics “Glass and Time” is sponsored by The Danish National Research Foundation (DNRF).

- [1] Jeppe C. Dyre *Rev. Mod. Phys.* **78**, 953 (2006).
- [2] M. D. Ediger *Annu. Rev. Phys. Chem.* **51**, 99 (2000).
- [3] L. Berthier, G. Biroli, J.-P. Bouchaud, et al. *Science* **310**, 1797 (2005).
- [4] L. Berthier, G. Biroli, J.-P. Bouchaud, et al. *J. Chem. Phys.* **126** 184503 (2007).
- [5] L. Berthier, G. Biroli, J.-P. Bouchaud, et al. *J. Chem. Phys.* **126** 184504 (2007).

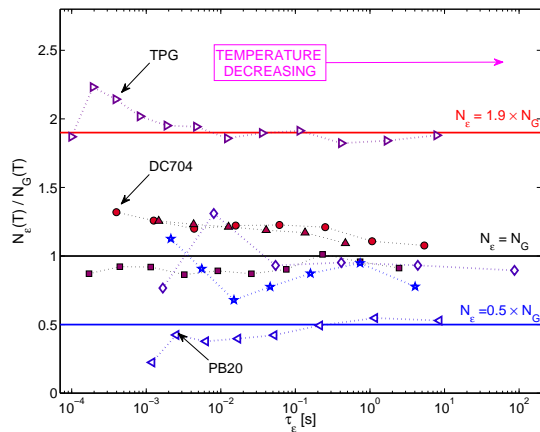


FIG. 5: Ratio between the characteristic number of dynamically correlated molecules in the shear and in the dielectric relaxation at the same temperature as a function of the (dielectric) relaxation time for different liquids (same symbols as in Fig. 4). The full lines represent $N_\epsilon = \lambda N_G$ with $\lambda = 1.9, 1.0, 0.5$ respectively from top to bottom.

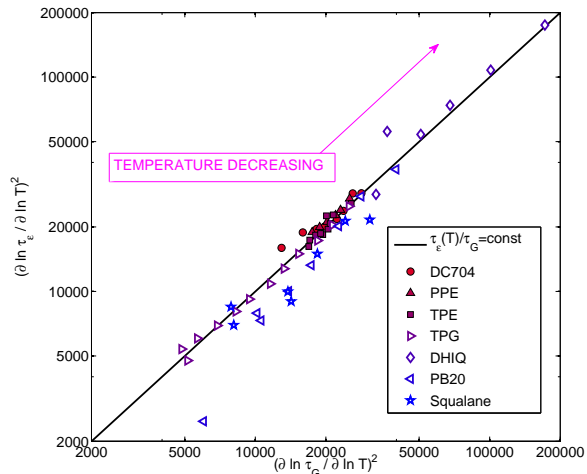


FIG. 6: $(\partial \ln \tau_\epsilon / \partial \ln T)^2$ plotted versus $(\partial \ln \tau_G / \partial \ln T)^2$ for the seven liquids (see legend). The full line represents $(\partial \ln \tau_\epsilon / \partial \ln T)^2 = (\partial \ln \tau_G / \partial \ln T)^2$ (Eq. 10).

- [6] B. Igarashi, T. Christensen, E. H. Larsen et al., *Rev. Sci. Instrum.* **79**, 045105 (2008).
- [7] B. Igarashi, T. Christensen, E. H. Larsen et al., *Rev. Sci. Instrum.* **79**, 045106 (2008).
- [8] T. Christensen and N. B. Olsen, *Rev. Sci. Instrum.* **66**, 5019 (1995).
- [9] B. Jakobsen, K. Niss and N. B. Olsen *J. Chem. Phys.* **123**, 234511 (2005).
- [10] K. Niss and B. Jakobsen, MS thesis, Department of Mathematics and Physics IMFUFA, Roskilde University, 2003.
- [11] K. Niss, B. Jakobsen and N. B. Olsen *J. Chem. Phys.* **123**, 234510 (2005).
- [12] All the shear-mechanical and dielectric spectra analyzed in this work together with more recent data [20, 21] are available in the ‘‘Glass and Time: Data repository’’ found online at <http://glass.ruc.dk/data>.
- [13] D. J. Plazek and K. L. Ngai, *Macromolecules* **24**, 1222 (1991).
- [14] R. Böhmer and C. A. Angell, *Phys. Rev. B* **45**, 10091 (1992).
- [15] R. Böhmer, K. L. Ngai, C. A. Angell, and D. J. Plazek, *J. Chem. Phys.* **99**, 4201 (1993).
- [16] R. Richert and C.A. Angell. *J. Chem. Phys.* **108** (21) 9016, (1998).
- [17] Dyre, J. C. and Olsen N. B. *Phys. Rev. B* **69**, 042501 (2004).
- [18] Tina Hecksher, Alben I. Nielsen, Niels Boye Olsen, Jeppe C. Dyre *Nature Phys.* **4**, 737 (2008)
- [19] G. P. Johari and M. Goldstein, *J. Chem. Phys.* **53**, 2372 (1970).
- [20] C. Maggi, B. Jakobsen, T. Christensen et al. *J. Phys. Chem. B* **112** 16320 (2008).
- [21] B. Jakobsen, C. Maggi, T. Christensen et al. *J. Chem. Phys.* **129** 184502 (2008).
- [22] N. Menon, S. R. Nagel, and D. C. Venerus, *Phys. Rev. Lett.* **73**, 963 (1994).
- [23] Claus F. Behrens, Tine G. Christiansen, Tage Christensen, Jeppe C. Dyre, and Niels B. Olsen *Phys. Rev. Lett.* **76**, 1553 (1996).
- [24] R. Zorn, F. I. Mopsik, G. B. McKenna, L. Willner, and D. Richter, *J. Chem. Phys.* **107**, 3645 (1997).
- [25] R. D. Deegan, R. L. Leheny, N. Menon, S. R. Nagel, and D. C. Venerus, *J. Phys. Chem. B* **103**, 4066 (1999).
- [26] K. Schröter and E. Donth, *J. Chem. Phys.* **113**, 9101 (2000).
- [27] F. Ladiou, C. Thibierge and D. L’Hôte *J. Phys.: Condens. Matter* **19** 205138 (2007).
- [28] C. Dalle-Ferrier, C. Thibierge, C. Alba-Simionesco et al. *Phys. Rev. E* **76** 041510 (2007).
- [29] S. Capaccioli, G. Ruocco and F. Zamponi *J. Phys. Chem. B* **112**, 10652 (2008).
- [30] S. Havriliak and S. Negami *Polymer* **8** 161 (1967)
- [31] A. I. Nielsen, T. Christensen, B. Jakobsen, et al *J. Chem. Phys.* **130**, 154508 (2009)

APPENDIX: Analysis details

Note that, although we consider the real part of $\tilde{\chi}$ when computing the four-point susceptibility, we fit simultaneously the real and imaginary part with Eq. (6). This is done minimizing the (generalized) residual χ^2 for a complex variable x , i.e.: $\chi^2 = \sum_j (x_{exp}^j - x_{th}^j)^* \cdot (x_{exp}^j - x_{th}^j)$ where the star indicates the complex conjugate.

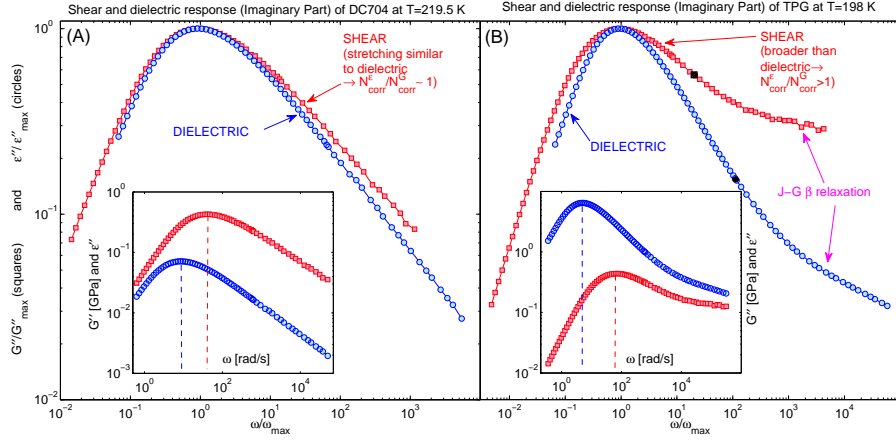


FIG. 7: **(A)** Comparison of (normalized) imaginary part of the shear and dielectric response function of DC704 at the same temperature $T = 219.5$ K (main panel). The amplitude of the functions is normalized to the loss maxima (ϵ''_{\max} and G''_{\max}) and they are plotted vs ω/ω_{\max} for an easier comparison of the shapes. In the inset we show the two susceptibilities as they are measured. **(B)** Same as (A) for TPG at $T = 198$ K. The black symbols indicate the last point included in the fitting (see Appendix).

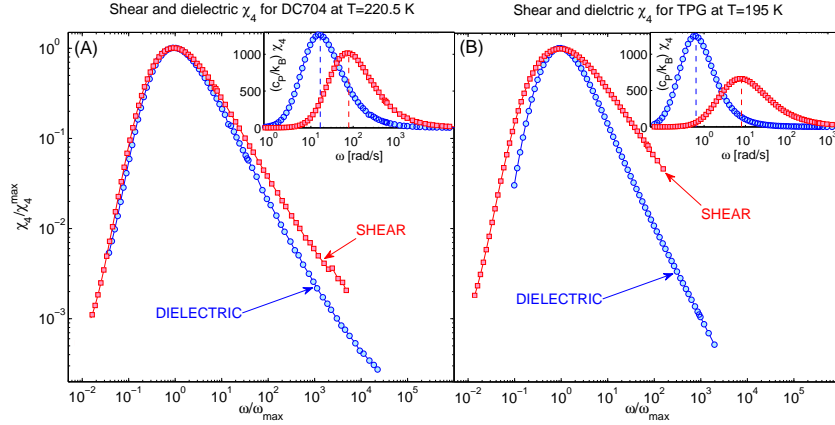


FIG. 8: **(A)** Comparison of the shear and dielectric four-point susceptibility of DC704 at the same temperature $T = 220.5$ K (main panel). The amplitude of each function is normalized to the maximum (χ_4^{\max}) and it is plotted vs ω/ω_{\max} for an easier comparison of the shapes. In the inset we show χ_4^G and χ_4^ϵ calculated from Eq. 3. **(B)** same as (A) for TPG at $T = 195$ K.

A further remark on the computation of χ_4 is that Eq. (3) involves the derivative with respect to the temperature that is, in practice, performed as finite difference. After obtaining the normalized curves we consider two successive functions measured at different temperatures T_1 and $T_2 (< T_1)$. Each frequency scan of a response function is carried in a way that each curve has points

in the same frequencies. The derivative appearing in Eq. (3) is then computed, at the single frequency, as follows:

$$\left[\frac{\partial \bar{\chi}'(\omega, T)}{\partial \ln T} \right]_{T=(T_1+T_2)/2} \simeq \frac{\bar{\chi}'(\omega, T_1) - \bar{\chi}'(\omega, T_2)}{\ln T_1 - \ln T_2}$$

Here we illustrate how we introduce the assumption

of TTS in the analysis of the spectra of the liquids presenting a secondary relaxation process (as TPG, DHIQ, Squalane and PB20). This is done by fixing the stretching parameters in (6) for the fitting in the following way.

First we fit the spectrum at the lowest temperatures (with free stretching parameters) where the secondary process is well separated from the α relaxation. We exclude from this fit some of the high frequency data (affected by the secondary relaxation). To select which data to remove from the minimization we plot the logarithmic derivative of the imaginary part of the response (that is $\alpha = \partial \ln \chi'' / \partial \ln \omega$) that shows a minimum α_{min} at the frequency ω_{min} where the α process meets the secondary relaxation. The frequencies larger than this ω_{min} are not considered in the fitting.

Once the parameters are found from this low-temperature spectrum they are fixed to fit all the other spectra up to high temperature. In those fits we also exclude the high frequency points from the computation in the same way illustrated above.

When this procedure is completed χ_4 is estimated from the obtained fitting functions. All the liquids with a secondary process have been treated in this way. Note that analyzing the data in this manner we are implicitly assuming TTS. A final remark is that if we compute χ_4 from the original (normalized) relaxation function, instead that from the fitting functions, we find a relative difference between the heights of the maxima only of a few percents.